Initiation of smouldering combustion in biomass

Houzhi Wang

A thesis submitted in fulfilment of the requirements for the degree of Doctor of Philosophy

in the

School of Mechanical Engineering

Tuesday 29th May, 2018

Declaration

I, Houzhi WANG, certify that this thesis titled, 'Initiation of smouldering combustion in biomass' contains no material which has been accepted for the award of any other degree or diploma in my name, in any university or other tertiary institution and, to the best of my knowledge and belief, contains no material previously published or written by another person, except where due reference has been made in the text. In addition, I certify that no part of this work will, in the future, be used in a submission in my name, for any other degree or diploma in any university or other tertiary institution without the prior approval of The University of Adelaide and where applicable, any partner institution responsible for the joint-award of this degree.

I acknowledge that copyright of published works contained within this thesis resides with the copyright holder(s) of those works.

I also give permission for the digital version of my thesis to be made available on the web, via the University's digital research repository, the Library Search and also through web search engines, unless permission has been granted by the University to restrict access for a period of time.

I acknowledge the support I have received for my research through the provision of an Australian Government Research Training Program Scholarship.

Houzhi Wang

Signed: _____

Date: Tuesday 29th May, 2018

"A single (smouldering) spark can start a prairie fire."

Mao Zedong

THE UNIVERSITY OF ADELAIDE

Abstract

Faculty of Engineering, Computer and Mathematical Sciences
School of Mechanical Engineering

Initiation of smouldering combustion in biomass

Houzhi Wang

Submitted for the degree of Doctor of Philosophy

Wildfires are naturally occurring phenomena that result in significant and catastrophic damage. Due to climate change, there has been a significant increase in the frequency, severity, and extent of wildfires. Therefore, there is a growing need to mitigate wildfire risk. In order to help mitigate the risk of wildfires, greater understanding is required. One particular gap in knowledge is the impact of smouldering combustion of potential fuel on wildfires. This thesis focuses on combustion of fuel beds in wildfires. Specifically, the thesis targets smouldering combustion. Smouldering combustion is a common type of combustion regime in wildfires and hazard reduction burning (a wildfire mitigation measure). Smouldering is a slow and low-temperature form of combustion, which shows no flame. Smouldering is a serious hazard because of its low ignition temperature, which makes it particularly relevant to fire initiation and spread. Smouldering plays a vital role in wildfires, as many forest biomass fuels such as grass, leaves and coarse woody debris are prone to smoulder. Most previous studies of smouldering combustion have only been carried out on polyurethane foam, due to its importance for residential fires. However, smouldering has been scarcely investigated from the point of view of wildfires. For example, smouldering combustion of forest fuel is scarcely studied. Hence, the project aims to develop a greater understanding of the initiation of smouldering combustion in biomass under different conditions with an emphasis on wildfire.

Locating smouldering combustion in wildfires and hazard reduction burning is difficult and time-consuming, as there is no effective method to identify the initiation of smouldering combustion in biomass fuel beds. It is critical to know

when and where smouldering combustion in a biomass fuel bed starts, as smouldering combustion could transition to flaming combustion under certain conditions. Radiation is one of the important heat transfer mechanisms in wildfires; however, there are few studies on smouldering combustion in biomass fuel beds started by external radiant heat flux. Although oxidiser flow rate and oxygen concentration have significant influences on the propagation of smouldering front, their effects on the initiation of smouldering combustion in biomass fuels are not well understood. Hence, the effects of oxidiser flow rate and oxygen concentration on the initiation of smouldering combustion are investigated. Fuels in a forest are diverse, and it is essential to have a better understanding of what effects forest fuels have on smouldering combustion. Thus, the effects of plant species and plant parts on the initiation of smouldering in biomass fuel beds are also investigated. Within this framework, the work presented in this thesis can be split into two main topics:

1. Conditions required to initiate smouldering combustion in biomass fuel beds

The required radiant heat flux and air flow rate for the initiation of smouldering and flaming combustion in a biomass fuel bed are investigated in an experimental testing rig. This investigation identifies and quantifies smouldering and flaming combustion in a biomass fuel bed based on the measurements of temperature, product gas concentration and mass change, and the required radiant heat flux and air flow rate for the initiation of smouldering and flaming combustion are determined. The effects of heating time and oxygen concentration on the initiation of radiation-aided and self-sustained smouldering combustion are investigated in the same testing rig. In this experimental study, the differences between radiation-aided and self-sustained smouldering combustion are characterised based on the measurements of temperature, product gas concentration and mass change, and the required heating time and oxygen concentration for radiation-aided and self-sustained smouldering combustion are determined.

2. Factors that influence smouldering combustion in biomass fuel beds

The results from the first topic reveal that oxygen availability has significant effects on the initiation of smouldering combustion in a biomass fuel bed. The air permeability of a biomass fuel bed determines oxygen availability in that fuel bed. Hence, the air permeability of natural forest fuel beds is investigated in an air permeability testing rig. In this study, the air permeability of natural forest fuel

beds is determined using experimental and theoretical methods. A comparison between the experimental and theoretical methods is made. The effects of *Eucalyptus* species and plant parts on smouldering combustion are also investigated. In this study, the different plant parts from different *Eucalyptus* species are characterised based on the results of the thermogravimetric and ultimate analyses. The results of this study show that the differences among the different plant parts from different *Eucalyptus* can be characterised and quantified based on the results of the thermogravimetric and ultimate analyses. It is also found that *Eucalyptus* species and plant parts have significant effects on smouldering combustion.

Although this thesis covers a series of experimental studies of the initiation of smouldering combustion in biomass fuel beds. There are still many important factors to be considered. For examples, the thesis focuses on small-scale laboratory experiments to better understand the fundamental studies of smouldering combustion of biomass. However, the real-world conditions could be much more complex. For example, forest fuel beds are composed with fuel particles with various sizes and shapes. These factors also have effects on smouldering combustion.

Acknowledgements

This thesis would not have been possible without the guidance, support, inspiration and the encouragement from many people and organisations. Hence, I would like to gratefully acknowledge the efforts, aids and support of all the people who have made a contribution towards this thesis. In particular, I would like to thank:

Dr Paul Medwell from the University of Adelaide who kept me on track, pointed out my shortcomings, provided the needed guidance, shared his experiences and set a good example of an independent researcher for me. (Paul, it has been a period of intense learning, not only in the scientific perspective, but also on a personal level. I would not be able to make it without your guidance and encouragement.);

Dr Philip van Eyk from the University of Adelaide who taught me so much about solid combustion and gasification, and his encouragement when I was down. (Philip, thank you for telling me that '*PhD is a marathon, not a sprint*'. These words indeed helped me get through the difficult times in my PhD.);

Dr Cristian Birzer from the University of Adelaide who shared his experience, knowledge and supported me throughout the journey. (Cris, thank you for sharing your experiences which inspired me to discover the research topics of my thesis.);

Dr Zhao Feng Tian from the University of Adelaide who provided support and inspiration (Zhao, thank you for all your suggestions and ideas throughout my PhD.);

Dr Malcolm Possell from the University of Sydney who provided much support and input to this project, particularly from an interdisciplinary point of view. (Malcolm, I am blissful to have you as my supervisor. Your support, patience and encouragement are greatly appreciated.);

Dr Tina Bell from the University of Sydney who brought me into the field of hazard reduction burning, enlightened and encouraged me. (Tina, this research would have been more difficult without your assistance.);

I would also like to give thanks to Dr Peijun Guo, Dr Xue Dong, Dr Yang Chen, Dr Zhiwei Sun, Dr Daniel Lane, Dr Woei Saw, Dr Xiao Chen, Dr Chenxi Li, and Ms Yibo Yang for their enlightening discussions, to Mr. Marc Simpson for his

assistance throughout the experimental campaigns, to my S324b office mates, Ms Amy Lewis, Mr. Shen Long, Mr. Orddom Leav, Mr. Francesco Larizza, Mr. Kae Ken Foo, Mr. Dominic Davis, Mr. Eshodarar Sureshkumar, Mr. Sammuel Sobey, Mr. David Haydon, for making me feel at home. Many thanks to Ms Alison-Jane Hunter for the wonderful writing workshops which truly helped me a lot.

This research has been undertaken with the support of the Bushfire and Natural Hazard Cooperative Research Centre which is gratefully acknowledged.

Finally, I would like to thank my parents, Jianwei Wang and Yanmei Li, who provided strong emotional and financial support during my PhD.

Contents

List of Figures

List of Tables

Abbreviations

AIC	**A**ustralian **I**nstitute of **C**riminology
BCWS	**B**ritish **C**olumbia **W**ildfire **S**ervice
CFD	**C**omputational **F**luid **D**ynamics
CRC	**C**ooperative **R**esearch **C**entre
CCD	**C**harge-**C**oupled **D**evice
DEWNR	**D**epartment of **E**nvironment, **W**ater and **N**atural **R**esources
HRB	**H**azard **R**eduction **B**urning
ICA	**I**nsurance **C**ouncil of **A**ustralia
WUI	**W**ildland **U**rban **I**nterface

Chapter 1

Introduction

1.1 Research Motivation

1.1.1 Importance of This Research

Australia is a wildfire-prone country, and wildfires have been a part of the Australian ecosystems for more than 65 million years [Cary et al., 2012]. Wildfires have significant impacts on the economy, society and environment [White et al., 2006]. The annual economic cost of wildfires in Australia is approximately 100 million Australian dollars [Gayler et al., 2001]. In some of the most severe wildfires, such as Black Tuesday (A$610 million), Ash Wednesday (A$1.796 billion) and Black Saturday (A$1.266 billion), the economic losses were much more significant [Insurance Council of Australia, 2013]. Wildfires are not only a burning issue in Australia, but they are also a global issue. In 2017 alone, devastating wildfires in Southern Europe and America caused more than 170 fatalities, an economic loss of over 20 billion U.S. dollars and at least 3,000,000 hectares of land were burned [British Columbia Wildfire Service, 2017, California Fire Service, 2017, Riquier, 2017]. Wildfires also create many social problems, such as the death of family members, social disruption and trauma [Clayer et al., 1985, Freeman and Freeman, 2010]. Moreover, wildfires cause atmospheric pollution, contamination of

water resources and increasing greenhouse emissions [Chen et al., 2006, Hennessy et al., 2005, Johnston et al., 2011, White et al., 2006]. To reduce and control the impacts of wildfires, it is important to better understand the initiation and spread of wildfires.

Numerous studies have argued that climate change is already increasing the likelihood of wildfires, as climate change makes hot days hotter and heat waves more frequent and longer [Hennessy et al., 2005, Lucas et al., 2007, Murphy and Timbal, 2008, Poumadere et al., 2005]. Wildfires also contribute to climate change because of the high emission of greenhouse gases [Bagamsah, 2005, Beer and Williams, 1995]. Thus, it is a vicious circle. More importantly, authorities may not be ready for the increasing severity and frequency of extreme wildfire conditions. Therefore, it is important to better understand the initiation and spread of wildfires, which could be beneficial for wildfire management.

Fire is natural to wildland environments and plays irreplaceable roles in ecosystems [Biswell, 1999]. For example, fires in many ecosystems are responsible for ecological renewal and vitality [Berry and Sitters, 2015, DellaSala and Hanson, 2015]. Moreover, fire has been an essential part of the Earth system since the Silurian Period (∼450 million years ago) [Glasspool and Scott, 2013]. Therefore, it is not wise to avoid wildfires, as the elimination of wildfires may eventually lead to a serious ecological problem. However, it is also difficult and costly to combat wildfires, especially the extreme and large-scale ones. Hence, wildfire mitigation is becoming increasingly important. There are three ways of mitigating the risk of wildfires: mechanical clearing, chemical treatment, and hazard reduction burning [Bidwell et al., 2002]. The overall purpose of these three different measures is to mitigate the risk of massive uncontrolled wildfires by reducing fuel loads. Mechanical clearing and chemical treatment are more suitable for small-scale treatments, as these two measures are costlier than hazard reduction burning. Hazard reduction burning, also known as prescribed burn, has been the most effective way to control the severity of wildfires [Stephens, 1998, Van Wagtendonk, 1996]. In recent years, hazard reduction burning has been applied more widely and frequently as a land management tool; however, more burning is required to reduce the chance and risk

of large-scale wildfires [Arno, 1996, Mutch, 1994, USDI and USDA, 1995, Wright and Bailey, 1982].

Wildfires can be divided into three stages: pre-fire, during fire and post-fire [Miller and Yool, 2002]. Smouldering combustion can occur in these three stages. Most fires start as a smouldering fire, because smouldering combustion normally requires less energy for ignition than flaming combustion [Rein et al., 2008]. Smouldering combustion is a slow and low-temperature form of combustion process, which shows no flame. In the post-fire stage, smouldering combustion poses a fire hazard, as smouldering combustion lasts for a long period of time and can spontaneously turn into flaming combustion under certain conditions [Bar-Ilan et al., 2005, Chao and Wang, 2001, Hadden et al., 2014]. Therefore, smouldering combustion is an important factor in the initiation and development of a wildfire. Similarly, smouldering is also a common type of combustion process in hazard reduction burning. After a hazard reduction burn has been completed, a mopping-up operation is necessary to ensure that all smouldering fires are extinguished [Biswell, 1999]. Smouldering combustion is one of the biggest challenges in hazard reduction burning, because it requires less energy to ignite and can therefore lead to undesirably fast fire spread. Hence, more research is required to develop a better understanding of the initiation of smouldering combustion.

1.1.2 Significance of This Research

The focus of wildfire control is shifting from combating to managing, as it is increasingly apparent that wildfires are inevitable, part of natural ecosystems, and the risk of wildfires can be controlled through proper management measures. It is widely recognised that the most effective and economical way to reduce the risk of wildfires is through hazard reduction burning [Arno, 1996, Frost, 1999, Mutch, 1994, USDI and USDA, 1995, Walstad and Radosevich, 1990]. Hazard reduction burning has often been used by land managers and relevant government departments to mitigate wildfire as well as manage wildlands and forestry.The overall aim of this research is to provide a better understanding of the required

conditions to initiate smouldering combustion in wildfires and hazard reduction burning. This knowledge is essential to improve the ability of predicting and locating smouldering combustion. Hence, the potential end users of this project will be the ones who are in charge of combating wildfires, planning and conducting hazard reduction burning.

It is known that smouldering combustion is a common form of combustion process in wildfires and hazard reduction burning. Smouldering combustion poses a potential fire hazard in wildfires and hazard reduction burning. Hence, smouldering combustion must be extinguished from the fire safety perspective. However, it is difficult and time-consuming to locate smouldering combustion in wildfires and hazard reduction burning. The reason is that the lack of understanding of the initiation of smouldering combustion in wildfires and hazard reduction burning greatly limit the ability of locating and predicting the initiation of smouldering combustion. Therefore, this research focuses on the initiation of smouldering combustion in biomass, which is relevant to wildfires and hazard reduction burning. This project aims to develop a better understanding of how smouldering combustion is initiated in the biomass fuel bed and the required conditions for the initiation of smouldering combustion in the fuel bed. This is because locating smouldering combustion is the necessary prerequisite to suppressing smouldering combustion. Hence, it is important to know under what conditions, smouldering combustion can be initiated. The outcomes of this research project provide knowledge that can help enhance the ability to locate and predict the initiation of smouldering in biomass fuel beds.

1.2 Research Background

Smouldering combustion is sustained by the heat evolved when oxygen directly reacts at the surface of condensed-phase fuels; it is normally a slow and low-temperature form of combustion [Ohlemiller, 2002]. Smouldering combustion

occurs in a wide range of materials, such as biomass, coal and charring polymer. Materials prone to smouldering are typically porous and form a significant amount of char when heated. Smouldering combustion occurs in many various fire incidents, such as residential fires, wildfires, landfill fires, mine fires and spacecraft fires. Despite the importance of smouldering, knowledge of the fundamental science behind the phenomenon is limited. In this section, an overview of the current understanding on smouldering combustion is summarised.

1.2.1 Research on Smouldering Combustion

Smouldering combustion is a serious fire hazard. From the point of view of ignition, smouldering can be initiated by weak heat sources ($\sim$6 kW$\cdot$m^{-2}), while flaming ignition typically requires fluxes of 20 kW$\cdot$m^{-2} or higher [McAllister, 2013]. Once ignited, smouldering can last for a long period of time, often days or weeks [Svensen et al., 2003]. Smouldering typically produces more toxic gases, such as carbon monoxide, than flaming combustion, which has been proven to contribute more than 25 % of the residential fire fatalities in the United States [Hall, 2003]. Smouldering combustion may also undergo a sudden transition to flaming combustion, which is a more destructive hazard because of its rate of spread. Smouldering combustion is one of the important combustion regimes in many fire hazards.

When referring to smouldering, it is important to understand the differences between smouldering and other non-flaming reactions which involve external heat flux, such as gasification and thermal decomposition. Gasification and thermal decomposition typically involve little or no oxidation reactions and hence are endothermic; while smouldering involves both endothermic and exothermic reactions [Ohlemiller, 2002]. If smouldering reactions are self-sustained, then the reactions are the driving force for the smouldering. Char oxidation is typically the principal heat source in self-sustained smouldering; therefore, any material that forms char during thermal decomposition has the potential for smouldering combustion [Anca-Couce et al., 2012, Hadden, 2011, Ohlemiller, 2002, Palmer, 1957]. There

are two types of smouldering ignition, aided and self-sustained smouldering ignitions [Anderson et al., 2000]. An aided smouldering ignition will be extinguished if the external heat source is removed. For a self-sustained smouldering ignition, smouldering combustion can still propagate without any external heat source.

Smouldering is a branch of solid fuel combustion, and is distinctly different from flaming combustion. Smouldering combustion is a typical heterogeneous combustion in which the combustion reaction involves species in two phases: solid and gaseous reactions [Puri, 1993], whereas flaming combustion typically occurs in the gas phase. The other differences between smouldering and flaming combustion include temperature, spread rate, toxic gas and particulate matter production. The characteristic temperature and heat released during smouldering are lower than in flaming combustion [Ohlemiller, 2002]. Due to these characteristics, the propagating rate of smouldering is slow ($\sim$0.08 mm$\cdot$s^{-1}) compared with fire spread ($\sim$2.6 mm$\cdot$s^{-1}) [Anca-Couce et al., 2012, Chen et al., 1996, Li et al., 2014]. Additionally, smouldering produces more particulate matter and toxic gases, such as carbon monoxide, than flaming combustion, because it is typically incomplete combustion. Figure 1.1 shows the fundamental steps from virgin solid fuel to self-sustained smouldering combustion or transition to flaming combustion. The transition from smouldering to flaming can be defined as a spontaneous gas-phase ignition of combustible gases which includes pyrolysate. Pyrolysate is generated when large molecules (solid fuel) break apart [Babrauskas, 2003]. The transition occurs when critical conditions are met. The critical conditions include the flammability of the gas mixture, and a net excess of heat released by strong solid phase oxidation reactions [Rein, 2005]. The research will focus on investigating the initiation of smouldering combustion, which includes aided and self-sustained smouldering ignitions.

1.2.2 Smouldering Combustion in Wildfires

Smouldering combustion plays an important role in wildfire initiation and spread, as many forest biomass fuels, such as grass, leaves and coarse woody debris are

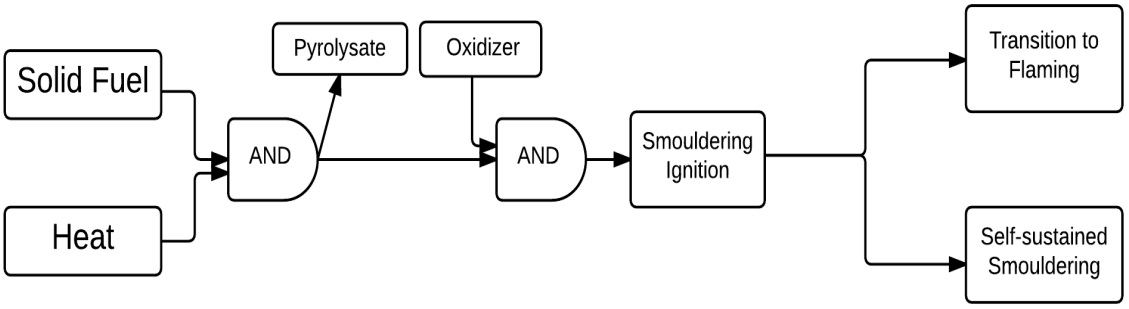

FIGURE 1.1: Flowchart for smouldering combustion (Adapted from *"Computational Model of Forward and Opposed Smoldering Combustion with Improved Chemical Kinetics"*, by Guillermo Jose Rein, 2005).

prone to smoulder during a wildfire [Hadden et al., 2014]. Smouldering combustion also has significant impacts on ecosystems. Smouldering combustion burns large amounts of biomass. While a fire front typically only burns the superficial parts of biomass, self-sustained smouldering combustion can consume the biomass almost completely. Compared with flaming combustion, smouldering combustion causes the most damage to forest ecosystems and prolongs ecosystem restoration [Hyde et al., 2011].

Solid fuel combustion with external heating typically undergoes three regimes: preheating ($\dot{Q}_{in} > \dot{Q}_{out}$ [†]), smouldering ($\dot{Q}_{in} \approx \dot{Q}_{out}$) and flaming ($\dot{Q}_{in} < \dot{Q}_{out}$). This makes smouldering important to wildfires, especially in fire front propagation, because it provides a critical pathway from virgin biomass solid fuel to flaming combustion. As biomass solid fuel is heated, it firstly undergoes a preheating stage. Water evaporation and devolatilisation occur in this stage. After the preheating stage, the combustion of biomass solid fuel will occur in one of three ways: smouldering combustion, smouldering to flaming combustion or direct flaming combustion. The conditions that lead to the three different regimes are complex, which include heat flux, oxygen concentration, fuel type, fuel depth and fuel particle size. All of these regimes involve the transport of heat and mass in the gas and solid phase. Therefore, it is necessary to identify and investigate the specific conditions which are key for the initiation of smouldering combustion.

[†] $\dot{Q}_{in}$ is the heat input rate and $\dot{Q}_{out}$ is the heat output rate

Radiation is one of the important heat transfer mechanisms, because fuels can potentially be ignited by radiant heat from flames at a distance. In most cases, the radiant heat may not directly initiate flaming combustion; but, it is sufficient to start smouldering combustion. Hence, it is necessary to develop a better understanding of smouldering combustion of biomass initiated by radiant heat. Radiant heat is chosen, because it is easier to control and quantify radiant heat compared to conduction and convection.

1.2.3 Smouldering Combustion and Its Applications

Although smouldering combustion is often stereotyped as a dangerous hazard, smouldering combustion is actually used in many fields. For instance, a smoking ceremony is an ancient custom among Indigenous Australians, that uses smouldering combustion to produce smoke [Hanssens, 2008]. This example shows that the use of smouldering combustion can be traced back to several thousand years ago. Smouldering combustion is also often used in the oil industry for oil recovery and producing biochar [Akkutlu and Yortsos, 2003, Rein, 2009]. Recently, there has been renewed interest in developing novel technologies, which are based on smouldering combustion. These technologies cover a wide range of applications, including soil remediation, humanitarian engineering, waste management and landmine detection [Pironi et al., 2009, 2011, Rein et al., 2017, Wall et al., 2015, Yerman et al., 2015].

1.3 Overview of Thesis

In this thesis, the initiation of smouldering combustion in biomass fuel beds is investigated. This thesis describes an experimental study on smouldering combustion in biomass fuel beds, which covers two main topics: 1) the conditions required for the initiation of smouldering combustion in biomass fuel beds; 2) the factors that affect smouldering combustion of biomass fuel beds. The first topic focuses

on the effects of radiant heat flux, oxidiser flow rate, oxygen concentration, and heating time on the initiation of smouldering combustion in biomass fuel beds. The second topic includes the effects of the air permeability, *Eucalyptus* species and plant parts on smouldering combustion of biomass fuel beds.

The second chapter of this thesis provides a detailed literature review on relevant topics, and research gaps and questions are identified from the literature review. Chapter 3 describes the major techniques used in this research project.

A compilation of two published and two submitted journal papers is included in Chapters 4–7. In Chapter 4, the initiation of smouldering and flaming combustion in a radiata pine fuel bed is demonstrated in an experimental testing rig. The required radiant heat flux and air flow rate for the initiation of smouldering and flaming combustion are investigated. The differences between smouldering and flaming combustion are characterised and quantified based on the measurements of temperature, product gas concentrations and mass change. The results in Chapter 4 suggest that air flow rate is a critical factor that determines the initiation of smouldering or flaming combustion in the radiata pine fuel bed. In Chapter 5, smouldering combustion of the radiata pine fuel bed is further studied. The effects of oxygen concentration and heating time on the initiation of smouldering of the radiata pine fuel bed are investigated. Radiation-aided and self-sustained smouldering combustion are demonstrated in the experimental testing rig. Radiation-aided and self-sustained smouldering combustion are characterised based on the measurements of temperature, product gas concentrations and mass change. The results in Chapter 5 suggest that oxygen concentration has significant effects on smouldering combustion in the radiata pine fuel bed. The results in Chapter 4 and 5, suggest that oxygen availability has significant effects on the initiation of smouldering combustion in a biomass fuel bed. In a real-world scenario, the air permeability of a natural forest fuel bed determines the oxygen availability in that fuel bed. Hence, an experimental study on the air permeability of natural forest fuel beds is presented in Chapter 6. Chapter 7 investigates the effects of *Eucalyptus* species and plant parts on smouldering combustion. The

differences among different plant parts from different *Eucalyptus* species are characterised based on the thermogravimetric and ultimate analyses. The results of the combustion experiment indicate that *Eucalyptus* species and plant parts have significant effects on smouldering combustion. The conclusions of this thesis are made in Chapter 8 along with some recommendations for future work.

References

I. Y. Akkutlu and Y. C. Yortsos. The dynamics of in-situ combustion fronts in porous media. *Combustion and Flame*, 134(3):229–247, 2003.

A. Anca-Couce, N. Zobel, A. Berger, and F. Behrendt. Smouldering of pine wood: Kinetics and reaction heats. *Combustion and Flame*, 159(4):1708–1719, 2012.

M. Anderson, R. Sleight, and J. Torero. Downward smolder of polyurethane foam: Ignition signatures. *Fire Safety Journal*, 35(2):131–147, 2000.

S. Arno. The seminal importance of fire in ecosystem management—impetus for this publication. *USDA Forest Service General Technical Report INT-GTR-341*, 1996.

V. Babrauskas. *Ignition handbook: principles and applications to fire safety engineering, fire investigation, risk management and forensic science*. Fire Science Publishers, Issaquah, Washington, United States, 2003.

T. T. Bagamsah. *The impact of bushfire on carbon and nutrient stocks as well as albedo in the savanna of northern Ghana*. PhD thesis, University of Bonn, 2005.

A. Bar-Ilan, O. Putzeys, G. Rein, A. C. Fernandez-Pello, and D. L. Urban. Transition from forward smoldering to flaming in small polyurethane foam samples. *Proceedings of the Combustion Institute*, 30(2):2295–2302, 2005.

T. Beer and A. Williams. Estimating Australian forest fire danger under conditions of doubled carbon dioxide concentrations. *Climatic change*, 29(2):169–188, 1995.

L. E. Berry and H. Sitters. Chapter 8 - regional case studies: Southeast australia, sub-saharan africa, central europe, and boreal canada. In D. A. DellaSala and C. T. Hanson, editors, *The Ecological Importance of Mixed-Severity Fires*, pages 210 – 264. Elsevier, 2015. ISBN 978-0-12-802749-3.

T. G. Bidwell, J. R. Weir, and D. M. Engle. *Eastern Redcedar Control and Management: Best Management Practices to Restore Oklahoma's Ecosystems*. Division

of Agricultural Sciences and Natural Resources, Oklahoma State University, 2002.

H. H. Biswell. *Prescribed burning in California wildlands vegetation management*. University of California Press, Oakland, California, United States, 1999.

British Columbia Wildfire Service. Current wildfire statistics, December 2017. URL `http://bcfireinfo.for.gov.bc.ca/hprScripts/WildfireNews/Statistics.asp`. Last accessed on 30/January/2018.

California Fire Service. Wildfire statistics by CA FIRE, December 2017. URL `http://cdfdata.fire.ca.gov/incidents/incidents_stats?year=2017`. Last accessed on 30/January/2018.

G. J. Cary, R. A. Bradstock, A. M. Gill, and R. J. Williams. *Global change and fire regimes in Australia*. CSIRO Publishing: Collingwood, VIC, Australia, 2012.

C. Y. H. Chao and J. Wang. Transition from smoldering to flaming combustion of horizontally oriented flexible polyurethane foam with natural convection. *Combustion and Flame*, 127(4):2252–2264, 2001.

L. Chen, K. Verrall, and S. Tong. Air particulate pollution due to bushfires and respiratory hospital admissions in Brisbane, Australia. *International journal of environmental health research*, 16(03):181–191, 2006.

Y. Chen, V. Motevalli, and M. Delichatsios. Horizontal flame spread on ship compartment surfaces. Technical report, Worcester Polytechnic Institute, 1996.

J. R. Clayer, C. Bookless-Pratz, A. McFarlane, S. A. H. Commission, et al. The health and social impact of the Ash Wednesday bushfires: a survey of the twelve months following the bushfires of February 1983. *Disaster management*, page 1, 1985.

D. A. DellaSala and C. T. Hanson. Preface. In D. A. DellaSala and C. T. Hanson, editors, *The Ecological Importance of Mixed-Severity Fires*, pages xxiii – xxxviii. Elsevier, 2015. ISBN 978-0-12-802749-3.

M. Freeman and A. Freeman. Bonding over bushfires: Social networks in action. In *IEEE International Symposium on Technology and Society (ISTAS)*, pages 419–426. IEEE, 2010.

E. Frost. The scientific basis for managing fire and fuels in national-forest roadless areas. Technical Report 201, World Wildlife Fund. CFR 64 No 201, Ashland, 1999.

D. Gayler, M. Chilvers, J. Abrahams, A. Coghlan, P. Koob, A. Kuslap, T. Casinader, J. Schneider, R. Brown, P. Gabriel, I. Gauntlett, P. Buckle, L. Galloway, G. Hoffman, C. Henri, C. Kilby, and L. Amiel. Economic costs of natural disasters in Australia. Technical report, Bureau of Transport Economics, Canberra, Australia, 2001.

I. J. Glasspool and A. C. Scott. *Identifying Past Fire Events*, chapter 10, pages 177–206. John Wiley & Sons, 2013. ISBN 9781118529539.

R. Hadden. *Smouldering and self-sustaining reactions in solids: an experimental approach*. PhD thesis, The University of Edinburgh, 2011.

R. Hadden, A. Alkatib, G. Rein, and J. L. Torero. Radiant ignition of polyurethane foam: the effect of sample size. *Fire Technology*, 50(3):673–691, 2014.

J. R. Hall. *The smoking-material fire problem*. National Fire Protection Association, Quincy, Massachusetts, United States, 2003.

L. Hanssens. Clusters of suicide: The need for a comprehensive postvention response to sorrow in indigenous communities in the northern territory. *Aboriginal and Islander Health Worker Journal*, 32(2):25, 2008.

K. Hennessy, C. Lucas, N. Nicholls, J. Bathols, R. Suppiah, and J. Ricketts. Climate change impacts on fire-weather in south-east australia. Technical report, Climate Impacts Group, CSIRO Atmospheric Research and the Australian Government Bureau of Meteorology, Aspendale, 2005.

J. C. Hyde, A. M. Smith, R. D. Ottmar, E. C. Alvarado, and P. Morgan. The combustion of sound and rotten coarse woody debris: a review. *International Journal of Wildland Fire*, 20(2):163–174, 2011.

Insurance Council of Australia. Historical disaster statistics., 2013. URL `http://www.insurancecouncil.com.au/industry-statistics-data/disasterstatistics/historical-disaster-statistics`. Last accessed on 5/October/2017.

F. Johnston, I. Hanigan, S. Henderson, G. Morgan, and D. Bowman. Extreme air pollution events from bushfires and dust storms and their association with mortality in Sydney, Australia 1994–2007. *Environmental research*, 111(6):811–816, 2011.

B. Li, H. Pang, J. Xing, B. Wang, C. Liu, K. McAdam, and J. Xie. Effect of reduced ignition propensity paper bands on cigarette burning temperatures. *Thermochimica Acta*, 579:93–99, 2014.

C. Lucas, K. Hennessy, G. Mills, and J. Bathols. Bushfire weather in southeast Australia: recent trends and projected climate change impacts. Technical report, The Bushfire CRC and Australian Bureau of Meteorology, 2007. Consultancy report prepared for the Climate Institute of Australia.

S. McAllister. Critical mass flux for flaming ignition of wet wood. *Fire Safety Journal*, 61:200–206, 2013.

J. D. Miller and S. R. Yool. Mapping forest post-fire canopy consumption in several overstory types using multi-temporal Landsat TM and ETM data. *Remote Sensing of Environment*, 82(2):481–496, 2002.

B. F. Murphy and B. Timbal. A review of recent climate variability and climate change in southeastern Australia. *International journal of Climatology*, 28(7): 859–879, 2008.

R. W. Mutch. Fighting fire with prescribed fire: a return to ecosystem health. *Journal of forestry (USA)*, 1994.

T. Ohlemiller. Chapter 9: Smoldering combustion. *SFPE Handbook of Fire Protection Engineering, 3rd ed., National Fire Protection Association, Quincy, Massachusetts*, 2002.

K. Palmer. Smouldering combustion in dusts and fibrous materials. *Combustion and Flame*, 1(2):129 – 154, 1957.

P. Pironi, C. Switzer, G. Rein, A. Fuentes, J. I. Gerhard, and J. L. Torero. Small-scale forward smouldering experiments for remediation of coal tar in inert media. *Proceedings of the Combustion Institute*, 32(2):1957–1964, 2009.

P. Pironi, C. Switzer, J. I. Gerhard, G. Rein, and J. L. Torero. Self-sustaining smoldering combustion for NAPL remediation: laboratory evaluation of process sensitivity to key parameters. *Environmental Science and Technology*, 45(7): 2980–2986, 2011.

M. Poumadere, C. Mays, S. Le Mer, and R. Blong. The 2003 heat wave in France: dangerous climate change here and now. *Risk Analysis*, 25(6):1483–1494, 2005.

I. K. Puri. *Environmental implications of combustion processes*. CRC Press, 1993.

G. Rein. *Computational Model of Forward and Opposed Smoldering Combustion with Improved Chemical Kinetics*. PhD thesis, University of California Berkeley, Dec 2005.

G. Rein. Smouldering combustion phenomena in science and technology. *International Review of Chemical Engineering*, 1:3–18, 2009.

G. Rein, J. Garcia, A. Simeoni, V. Tihay, and L. Ferrat. Smouldering natural fires: comparison of burning dynamics in boreal peat and mediterranean humus. *WIT Transaction on Ecology and the Environment*, 119:183–192, 2008.

G. Rein, X. Huang, F. Restuccia, and T. McArdle. Detection of landmines in peat soils by controlled smouldering combustion: Experimental proof of concept of o-revealer. *Experimental Thermal and Fluid Science*, 88:632–638, 2017.

A. Riquier. California wildfires could mean over $27 billion in damages to homes, December 2017. URL `https://www.marketwatch.com/story/california-wildfires-could-mean-over-27-billion-in-damages-to-homes-corelogic-says-2017-12-08`. Last accessed on 30/January/2018.

S. L. Stephens. Evaluation of the effects of silvicultural and fuels treatments on potential fire behaviour in Sierra Nevada mixed-conifer forests. *Forest Ecology and Management*, 105(1):21–35, 1998.

H. Svensen, D. K. Dysthe, E. H. Bandlien, S. Sacko, H. Coulibaly, and S. Planke. Subsurface combustion in Mali: Refutation of the active volcanism hypothesis in West Africa. *Geology*, 31(7):581–584, 2003.

USDI and USDA. Federal wildland fire management and policy and program review final report, 1995. URL `http://www.forestsandrangelands.gov/strategy/documents/foundational/1995_fed_wildland_fire_policy_program_report.pdf`. Last accessed on 30/January/2018.

J. W. Van Wagtendonk. Use of a deterministic fire growth model to test fuel treatments. In *Sierra Nevada ecosystem project, final report to congress*, volume 2, pages 1155–1166, 1996.

H. Wall, J. Gerhard, I. Fabris, D. Cormier, Y.-L. Cheng, J. L. Torero, et al. Investigation of self-sustaining smouldering of faeces: key parameters and scaling effects. In *Dynamic Ecolibrium: Sustainable Engineering Society Conference (SENG 2015)*, page 113. Engineers Australia, 2015.

J. D. Walstad and S. R. Radosevich. *Natural and prescribed fire in Pacific Northwest forests*. Oregon State Univ Pr, 1990.

I. White, A. Wade, M. Worthy, N. Mueller, T. M. Daniell, and R. Wasson. The vulnerability of water supply catchments to bushfires: impacts of the January 2003 wildfires on the Australian Capital Territory. *Australian Journal of Water Resources*, 10(2):179, 2006.

H. A. Wright and A. W. Bailey. *Fire ecology: United States and southern Canada*. John Wiley & Sons, 1982.

L. Yerman, H. Wall, J. L. Torero, J. I. Gerhard, I. Fabris, D. Cormier, Y.-L. Cheng, et al. Self-sustaining smouldering combustion of faeces as treatment and disinfection method. In *Asia Pacific Confederation of Chemical Engineering Congress 2015: APCChE 2015, incorporating CHEMECA 2015*, page 2677. Engineers Australia, 2015.

Chapter 2

Literature Review

2.1 Fundamentals of Smouldering Combustion

Smouldering combustion can be initiated in two ways: self-heating and external heating. For self-heating, the heat which supports smouldering combustion is mainly generated by exothermic reactions. The phenomenon of spontaneous ignition normally occurs in large masses of material, and ignition begins deep inside the material [Drysdale, 2011]. Spontaneous ignition occurs when exothermic reactions can provide enough heat to overcome heat losses. The material that is prone to spontaneous ignition is porous to allow air to permeate through, and it produces char when undergoing thermal decomposition [Drysdale, 2011]. The high permeability allows air to reach the ignition location and provide sufficient oxygen for the subsequent oxidation reactions. The majority of the heat generated is from the char oxidation. Hence, the yield of char is a requirement. In the case of external heating, the heat from an external source can be transferred by three mechanisms, namely are conduction, convection and radiation [Bowes and Britain, 1984]. Previous research in smouldering combustion has typically focused on smouldering combustion initiated by conduction or convection heat transfer mechanisms, because the majority of the work is for residential fires, where radiation may be less important than the other heating mechanisms. Radiation

has significant effects on fire initiation and spread in wildfires, as it is one of the major heat transfer mechanisms in wildfires; however, there are only few studies on smouldering combustion started by external radiant heating [Morandini et al., 2013, Sullivan et al., 2003, Weber, 1989].

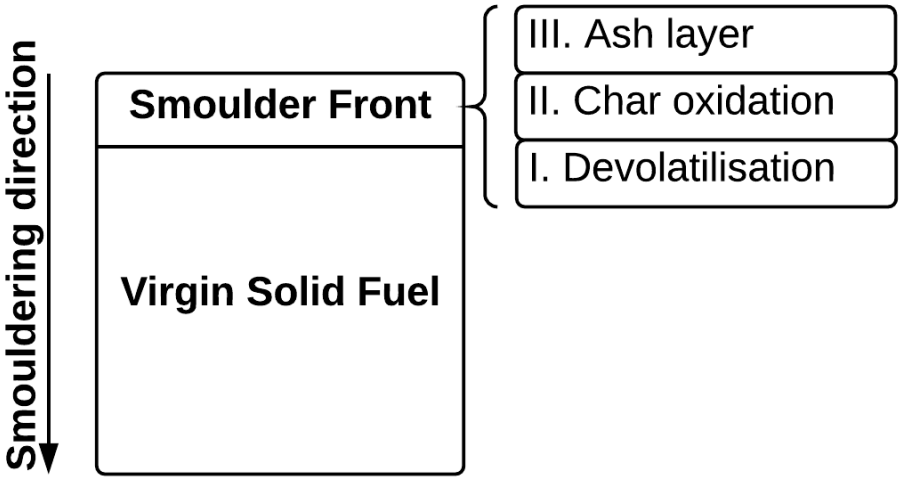

FIGURE 2.1: Structure of a smouldering front. Adapted from Rein [2009].

The smoulder front consists of three distinct zones, which are shown in Figure 2.1 [Moussa et al., 1977, Rein, 2009]. The first zone (Zone I) is also referred to as the devolatilisation zone, where fast temperature rise, smoke generation and thermal decomposition occur; Zone II is a char combustion zone in which the temperature reaches a maximum value, the evolution of the smoke stops and char starts to combust; highly porous residual char and ash can be found in Zone III, where the temperature decreases slowly [Drysdale, 2011, Moussa et al., 1977].

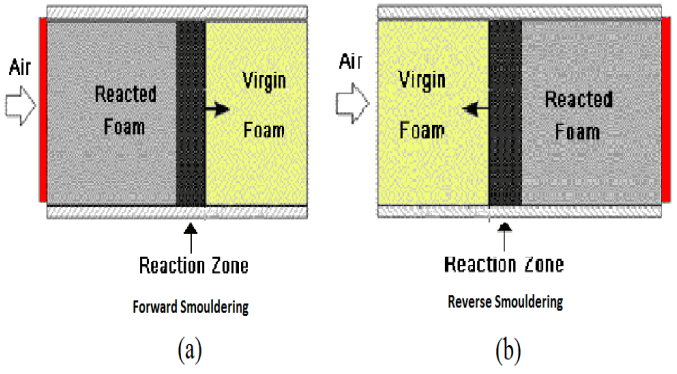

FIGURE 2.2: Smouldering propagation configurations in one-dimension. [Rein, 2009].

Smouldering front can propagate in either a forward or a reverse direction, depending on its propagation relative to the direction of oxidiser flow. In the forward smouldering propagation (Figure 2.2a), the reaction front propagates in the same direction as the oxidiser; in reverse smouldering propagation (Figure 2.2b), the reaction front propagates in the opposite direction [Torero and Fernandez-Pello, 1996]. As reported by Ohlemiller [2002], the relative direction of airflow has significant effects on smouldering propagation rate and the peak temperature, because it determines the convective transport mechanisms and chemical reactions [Ohlemiller and Lucca, 1983]. In the forward configuration, the oxidiser flows through the ash and char residual layer, reacts at the smoulder front and then flows through the virgin solid fuel. As the oxidiser reaches the end of the smoulder front, it promotes the char oxidation and oxygen consumption. The oxidiser passes through the smoulder front, the oxygen concentration in the oxidiser becomes low due to the oxidation reactions. At the same time, the oxidiser also preheats the virgin solid fuel by convection before the smoulder front arrives [Rein, 2005]. In the opposed configuration, the oxidiser flows through the virgin solid fuel and reacts at the smoulder front. In this configuration, the oxidizer passes through the smouldering front and transport heat to the char left behind the front [Rein, 2005].

Smouldering combustion typically involves two major chemical processes: devolatilisation and oxidation. The devolatilisation stage is defined as an endothermic process where carbonaceous charcoal, volatile gases and tar are produced through the thermal degradation of solid fuel without reaction with oxygen [Koppejan and Van Loo, 2012]. Devolatilisation reactions usually takes place at temperatures above 200 °C, subsequent heating above the temperature increases the devolatilisation rate [Rein, 2009].

$$Solid\ fuel \xrightarrow{Heating} Char(s) + Volatiles(g) + Tar(s) \tag{2.1}$$

The yield of volatile gases and its composition can be affected by many factors, including heating rate, initial and final temperature, reaction time, particle size,

fuel type and pressure [Basu, 2006]. The majority of volatile matter is not oxidised in smouldering combustion.

The oxidation of char normally occurs when the temperature is above 300 °C [Rein, 2009]. The char oxidation reaction provides the majority of heat which supports the propagation of smouldering front. Self-sustained smouldering combustion is also dependent of the char oxidation reaction because the char oxidation is the main heat input. The products of char oxidation are mainly carbon monoxide and carbon dioxide. The CO/CO_2 ratio increases with decreasing oxygen concentration; therefore, more carbon dioxide is formed where the oxygen concentration is high and more carbon monoxide where the oxygen supply is limited [Rein, 2005]. For example, in a natural convection downward smouldering, the CO/CO_2 ratio increases as the smoulder front propagates into the deep layer of solid fuel. The char oxidation can also be facilitated by the increase in surface area and alkali metal impurities which catalyse the reaction [Ohlemiller, 2002].

2.2 Smouldering Ignition

There are three types of solid fuel ignition: smouldering, smouldering to flaming and direct flaming [Babrauskas, 2003]. Smouldering ignition is often referred to as the onset of surface combustion, and flaming ignition is the gas-phase combustion. Smouldering ignition is not a phenomenon with a clear definition [Bilbao et al., 2001]. In other words, smouldering ignition is difficult to detect or predict, because it normally does not have obvious indications, such as a visible flame, high temperature or high product gas emission [Beyler et al., 2014, Kashiwagi and Nambu, 1992, Krause et al., 2006]. In order to better understand smouldering ignition, it is important to define and understand the indication of smouldering ignition, the key parameters to identify smouldering ignition and the controlling parameters of smouldering ignition.

Three stages are identified in the smouldering ignition process: preheating, aided smouldering combustion and self-sustained smouldering combustion. The

elimination of external heating in the preheating stage will lead to no ignition. In the case of no ignition, mass loss rate and gas emission are negligible.

Moisture in solid fuels can exist in two different forms: as free water within the pores of the solid fuel, and as bound water which is absorbed to the interior surface structure of the fuel [Borman and Ragland, 1998]. Moisture content is an important fuel characteristic, which influences the combustion behaviour, the adiabatic temperature of combustion and the volume of flue gas produced per energy unit [Koppejan and Van Loo, 2012]. For example, wet biomass fuels require a longer residence time for water evaporation process before devolatilisation and oxidation occur. The water evaporation rate is affected by heat, air flow and atmospheric pressure [Ortiz-Molina et al., 1979, Torero and Fernandez-Pello, 1996, Torero et al., 1993]. The evaporation of water is an endothermic process, therefore it absorbs heat which decreases the temperature rise rate. The elimination of heat supply during this stage will lead to extinction. After the drying of solid fuel is completed, the temperature continues to rise in the presence of heating, the solid fuel begins to decompose, releasing volatiles [Borman and Ragland, 1998]. As the volatiles flow out of the solid fuel through the pores, external oxygen cannot penetrate into the particle, and therefore devolatilisation takes place. As evident from Table 2.1, the devolatilisation temperature varies in different solid fuels. Devolatilisation is an endothermic reaction, therefore devolatilisation suppresses smouldering combustion. Large quantities of volatiles are released during the devolatilisation stage, which can be indicated by the increase of mass loss rate [Simmons and Ragland, 1986].

TABLE 2.1: Devolatilisation temperatures for solid fuels [Borman and Ragland, 1998]

Fuel	**Devolatilisation temperature (°C)**
Lignite coal	300
Hemicellulose	225
Cellulose	325
Lignin	300

After devolatilisation is completed, char remains. Char is highly porous; for example, the porosity of wood char is up to 90 % [Borman and Ragland,

1998]. After solid fuel (char) stops releasing volatiles, external oxygen is then able to diffuse through the pores into the char particles. Char oxidation is affected by both the rate of the carbon–oxygen reactions and the diffusion rate of oxygen. The carbon–oxygen reaction depends on many factors, including oxygen concentration, gas temperature, particle size and porosity [Borman and Ragland, 1998].

2.3 Transition from Smouldering to Flaming Combustion

Smouldering combustion is an important element in many fire events because it can transition to flaming combustion under certain conditions. For example, undetected smouldering combustion in wildfires and hazard reduction burning could re-ignite flaming combustion that was thought extinguished [Cochrane and Schulze, 1998]. Therefore, it is vital to develop a better understanding of the transition from smouldering to flaming combustion. The research to date has tended to focus on the mechanism of the transition from smouldering to flaming combustion.

Smouldering combustion can only transition to flaming combustion if two critical conditions, namely the flow rate of volatiles and the presence of an ignition source, are met [Drysdale, 2011]. Firstly, smouldering combustion has to produce sufficient volatile matters, which mix with the surrounding air to create a combustible mixture. Then, the combustible mixture will be ignited if an ignition source presents. The transition will never happen if the flow rate of volatiles does not reach a certain level. In other words, flammable mixtures of air and volatiles are essential for the transition to flaming combustion. To increase the yield of volatile matter, the temperature of the devolatilisation layer has to be increased. The temperature of the devolatilisation layer can be increased by increasing oxygen availability in the char combustion layer. It has been demonstrated that the smouldering-to-flaming transition can be initiated by increasing air flow velocity [Ohlemiller, 1990, Ohlemiller and Rogers, 1978, Torero and Fernandez-Pello,

1995]. Once the flow rate of volatiles reaches a certain level, the transition will be triggered if an ignition source is present. In previous research, the smouldering to flaming transition is often initiated by piloted ignition [Putzeys et al., 2006, 2008], while char combustion is the ignition source in the case of the spontaneous transition [Aldushin et al., 2006].

The transition from smouldering to flaming combustion is influenced by many factors, such as oxygen concentration, oxidiser flow rate, volatile matter and external heat input [Bar-Ilan et al., 2005, Putzeys et al., 2006, 2008]. The configurations of the experiments, such as the orientation of the fuel sample and, the mode of smouldering combustion, i.e. forward or reverse smouldering combustion, also influence the latter transition to flaming. Previous research has also shown that a buoyancy-induced flow is a prerequisite of the transition in a fuel bed, because the flow promotes the oxidation of char and enhances the temperature and the yield of flammable pyrolysis products [Ohlemiller, 1990, Torero and Fernandez-Pello, 1995]. In these experiments, the air was free to enter through the lower face of the fuel bed. However, this configuration is not the case in forest fuel beds.

Most of the previous studies on the transition from smouldering to flaming combustion focused on building materials, such as polyurethane foam [Bar-Ilan et al., 2005, Chao and Wang, 2001, Ortiz-Molina et al., 1979, Putzeys et al., 2006, 2007, 2008, Stephen et al., 1996]. Previous research of the transition from smouldering to flaming combustion in biomass fuel beds has been performed [Fernandez-Pello et al., 2015, Hagen et al., 2015, Wang et al., 2017]. In these studies, smouldering combustion was initiated by conduction. Radiation is also an important heat transfer mechanism in wildfires [Linn et al., 2002]. However, there are a few studies that focus on the transition from smouldering to flaming combustion in biomass fuel beds by radiation.

Besides the limited understanding of the transition from smouldering to flaming in wildfires and hazard reduction burning, the initiation of smouldering combustion in wildfires and hazard reduction burning is still not well understood. Smouldering combustion is a prerequisite for the transition to flaming. A better

understanding of the initiation of smouldering combustion is essential, as it will provide more information about the possible physical location of the smouldering to flaming transition and the critical parameters that affect the transition.

2.4 Indications of Smouldering Ignition

The initiation of smouldering combustion has received less attention than the propagation of smouldering combustion [Drysdale, 2011]. It is difficult to know whether smouldering combustion is initiated or not, as the indications of smouldering combustion are not fully quantified. The initiation of smouldering combustion can be divided into aided smouldering ignition and true ignition (the initiation of self-sustained smouldering) based on the dependence of external heating. During the aided ignition stage, the reaction is typically close to the surface of fuel layer which is exposed to external heating. Therefore, the heat losses are high and the ignition is dominated by the external heat flux—the ignition will cease without the external heat input. The heat released by exothermic reactions during aided ignition cannot balance the heat losses; hence the smouldering combustion is not self-sustained. It has been demonstrated that temporal and spatial temperature profiles and mass-loss profile can be used to identify and characterise aided ignition and true ignition [Anderson et al., 2000, Hadden et al., 2014]. For example, the onset of strong exothermic reactions can be observed in the results of temperature profiles.

Mass-loss profile has been demonstrated experimentally for indicating the three stages of smouldering ignition, namely the warm-up stage (no ignition), the aided ignition, and the self-sustained ignition. The experimental results suggest that the average mass-loss rate during the aided ignition stage is slightly higher than the warm-up stage; the average mass-loss rate during the self-sustained smouldering ignition stage is approximately two times higher than the aided ignition stage [Anderson et al., 2000]. Hence, the mass-loss profile can be used as an indication of the initiation of smouldering combustion. It should be noted that

the solid fuel used in the past experiments is polyurethane foam, as the focus has largely been on residential fires; however, this methodology has not been applied to biomass fuel, which is the focus of the current research project. Furthermore, the results of mass loss profile cannot be applied in wildfires, as it is difficult to take mass-loss measurements of smouldering samples in real-world situations due to limited measuring capacity and high external disturbances. Therefore, other measurement types are still needed to help indicate the initiation of smouldering combustion of biomass fuel.

Smouldering ignition can be determined when the surface temperature of the sample is greater than the surface temperature of an inert insulator which has a lower thermal inertia than the sample [Boonmee and Quintiere, 2002]. The temperature difference indicates the endothermic reactions, because a material with higher thermal inertia will have a lower surface temperature under the same level of heat flux. The major drawback of this approach is that the char formed during the smouldering combustion has many different properties from the original solid fuel, such as density, thermal conductivity, specific heat, absorptivity and heat transfer coefficient, whereas the inert insulator only represents the properties of original solid fuel. Alternatively, glowing ignition is often used to indicate the onset of smouldering combustion [Boonmee and Quintiere, 2005, He et al., 2006, 2014]. The glowing ignition is a visual observation, and therefore it is subjective. Although several studies have indicated that ignition for smouldering can be characterized by temperature change, mass-loss rates and visual observation, little attention has been paid to product gas concentration. Therefore, it may be possible to develop a new approach which characterizes smouldering ignition based on the product gas concentration.

2.5 Controlling Parameters

Smouldering combustion can be affected by many factors, such as ambient temperature, the duration of heating, oxidiser flow rate, oxygen concentration and fuel

type and properties [Badr and Karim, 1992, Hadden and Rein, 2011, Martin, 1965, Swann et al., 2008]. Previous work suggests that two main parameters, external heat flux and the duration of the exposure, control ignition [Badr and Karim, 1992, Hadden and Rein, 2011, Martin, 1965, Swann et al., 2008]. Kinbara et al. [1967] presented an approximate theory of smouldering combustion where they assumed that: 1) smouldering occurs when the sample reached ignition temperature; 2) the rate of heat generation in the smouldering zone is governed by oxygen availability.

The results obtained by Kim and Hwang [1996] suggest that the minimum hot-surface ignition temperature decreases as the thickness of the solid fuel layer increases. This is because an increase in the solid fuel layer thickness decreases the heat loss through the fuel layer, which causes a decrease in the heat input needed for ignition. The decreased heat input leads to a lower hot-surface ignition temperature [El-Sayed and Khass, 2013, He et al., 2009]. Bilbao et al. [2001] suggested the critical temperature for smouldering ignition is a function of radiant heat flux and showed that the critical temperature increases with increasing heat flux. The reason is that the increasing heat flux increases the yield of volatiles, and causes the oxygen concentration to be lower at the surface of sample [Bilbao et al., 2001]. The low oxygen concentration inhibits the char oxidization on the surface of the sample; hence higher ignition temperature is needed for smouldering. Ohlemiller [1985] investigated the effects of heat source geometry on ignition temperature and argues the important factor that causing the difference in the minimum ignition temperature, is the heat loss rate and heat generation per unit volume from the hottest layers of heat sources.

Smouldering combustion can be initiated by self-heating or external heating. There is much research on smouldering combustion initiated by external heating, mostly conduction [Anthenien and Fernandez-Pello, 1998, El-Sayed and Khass, 2013, Hagen et al., 2013, Palmer, 1957] and convection [Anez et al., 2015, Carvalho et al., 2002]. There has been relatively less research on smouldering combustion by radiation, while the majority of these studies focus on polyurethane foam, due to its importance in residential fires [Anderson et al., 2000, Bar-Ilan et al., 2005, Hadden et al., 2014]. These studies investigated the effects of radiant heat

flux and sample size on the initiation of smouldering combustion in polyurethane foam. Radiant heat flux from the fire front is one of the major heat transfer mechanisms which preheats biomass fuel. Smouldering combustion of biomass can be initiated if the radiant heat flux reaches a certain level in a wildfire. In some cases, smouldering combustion could be initiated by the radiation emitted by a fire front from a long distance. The lack of understanding of smouldering combustion of biomass initiated by radiation increases the difficulty of predicting the initiation of smouldering combustion in wildfires.

Smouldering combustion can continue at low oxygen concentrations, as low as 10 percent [Belcher and McElwain, 2008, Hadden et al., 2013]. Therefore, smouldering front can propagate deep in a fuel bed. For example, smouldering combustion often occurs in the duff layer, where the oxygen availability is limited [Hardy et al., 2001]. This increases the difficulties of detecting and smothering smouldering combustion in a fuel bed because it can continue to burn beneath the surface and out of sight. There have been a few studies on the oxygen concentration that is required to extinguish smouldering combustion in peat [Hadden, 2011, Hadden et al., 2013, Huang and Rein, 2016]; however, it is still not clear that the minimum oxygen concentration required for self-sustained smouldering combustion in biomass. Similar research has previously been conducted by Hadden [2011] and Hadden et al. [2013] on the effects of oxygen concentration on the smouldering combustion of peat. It has been experimentally demonstrated that smouldering combustion of peat can only be initiated when the oxygen concentration is above a critical value (10 % for peat) [Hadden, 2011, Hadden et al., 2013]. However, there is a lack of understanding of what effects oxygen concentration has on the initiation of smouldering combustion in biomass. It was found that oxygen concentration does not have a significant effect on the minimum heating time for radiation-aided smouldering [Walther et al., 2000]. However, the effect of oxygen concentration on the minimum heating times for self-sustained smouldering combustion is still unclear. Moreover, past research on aided and self-sustained smouldering is based on polyurethane foam and peat [Hadden, 2011, Ortiz-Molina et al., 1979, Walther

et al., 2000]. There is a paucity of research on the effect of oxygen concentration on the initiation of radiation-aided and self-sustained smouldering of biomass.

Fuel beds account for a large percentage of fuel in forests [Biswell, 1999] and are especially important for hazard reduction burning, as most of the fuel reduction is from them [Knapp et al., 2005]. Modelling of their combustion needs to consider two different combustion regimes: smouldering and flaming. The combustion regime of a fuel bed can be controlled by oxygen availability [Hadden et al., 2011, Huang and Rein, 2016, Santoni et al., 2014], which is affected by the fuel bed's air permeability. The air permeability of a fuel bed, which can be considered a porous medium, characterises the ease with which air can pass through it. It is critical to have a better understanding of the air permeability of the forest fuel bed. Previous studies of the air permeability of biomass have been only performed on regular-shaped particles, such as pine needles and soy straw; which reveals a strong dependence of particle shape on the air permeability [Erić et al., 2011, Santoni et al., 2014]. However, the fuel particles in forest fuel beds are diverse in size and shape, and therefore no such data are available in the literature. Hence, there is a need to investigate the effects of the size and type of the forest fuel bed particles on the air permeability..

One of the challenges of developing an understanding of smouldering combustion in wildfires and hazard reduction burning is the fuel of smouldering combustion. The fuels in wildfires are diverse because of the diversity of plant genera and species, as well as their plant parts. Gill and Moore [1996] conducted a series of experiments to investigate the ignition delay time of Australian native plants leaves, and the results of that study show that plant genera and species have a significant effect on the ignition delay time due to the differences in surface to volume ratio. It was also found that the volatile content of fuel could affect the ignition delay time [Mutch, 1964]. These previous studies have demonstrated that plant genera, species and parts could influence the ignition of fuel. However, there is a lack of understanding of the effects of plant genera, species and parts on smouldering combustion.

Eucalyptus, one of the most widespread genera of native plants in Australia, has always played a central part in Australian wildfires. Not only does it contribute the majority of fuel for wildfires, but it is also highly combustible due to its high content of volatile oil. There are more than 800 species of *Eucalyptus*. Different *Eucalyptus* species have different chemical and physical properties. The differences in the properties will have effects on the combustion process. In a *Eucalyptus* forest, the accumulation of fuel, such as leaves, barks and twigs, builds up a fuel bed for fire events. The different plant parts (leaf, bark and twig) behave differently in a fire event because of their different physical and chemical properties. In wildfires and hazard reduction burning, smouldering combustion often occurs in fuel beds. Hence, it is essential to understand the effects of *Eucalyptus* species and plant parts on smouldering combustion.

2.6 Modelling of Smouldering Combustion

Research on modelling of smouldering combustion has become popular, because it is not only a cost-effective alternative to experiments, but it can also provide additional insight that is not possible from experiments [Rein, 2005]. Current research on modelling smouldering reaction is focussed on two main themes: smouldering propagating rate and ignition delay time. The majority of the existing models on smouldering combustion in the literature mainly covers three types of fuel: polyurethane foam, timber and cellulose. The chemical kinetics mechanisms of the models for these three types of fuel are normally based on five–step kinetics (polyurethane foam), three–step kinetics (cellulose) and the time to the smouldering ignition in timber as a function of heat flux [Bilbao et al., 2001, Rein, 2009]. Most of the models of smouldering combustion are based on materials that have simple chemical components, such as cellulose and polyurethane foam. However, the chemical components of fuels in a forest are very diverse and complex. Hence, more research is needed to develop a better understanding of smouldering combustion of different fuels with an emphasis of wildfires and hazard reduction burning.

Ohlemiller [1985] conducted some pioneering studies on developing the modelling of smouldering combustion, providing the governing equations of smouldering combustion, including gas/solid mass conservation equations, gas momentum equation, gas species conservation equation, and condensed-phase species conservation equation. Rein et al. [2007] developed a one-dimensional, transient model for smouldering combustion in polyurethane foam under forced flow condition including five steps kinetics, and the model can be used to predict the temporal and spatial temperature for both forward and opposed smouldering propagation. The forward and opposed forced flow smouldering of polyurethane foam model was developed for predicting the propagating velocity in polyurethane foam [Torero and Fernandez-Pello, 1996, Torero et al., 1993]. Mukunda et al. [2007] developed a model on the smouldering rate of incense sticks as a function of ambient oxygen content. Ohlemiller [1986] mentioned that gas-phase oxidation, oxidative polymer degradation and char oxidation are critical in smouldering ignition and propagation; therefore they must be included in a smouldering reaction model. Kashiwagi [1973] developed a model on smouldering ignition delay time that includes the effects of gas phase reaction and a finite value of the absorption coefficient of the solid fuel. Many models of smouldering combustion focus on the propagation of smouldering combustion; while, there has been relatively less research on modelling the initiation of smouldering combustion.

Smouldering is an essential element in wildfires as it plays vital roles in fire initiation and spread; however, smouldering combustion has been considered in only a few wildfire models [Kourtz and O'Regan, 1971, Kourtz et al., 1977]. The propagation and size of smouldering fires were modelled in these wildfire models. Kourtz et al. [1992] developed a model of predicting the chance of smouldering combustion caused by lighting. Overall, the majority of previous research on wildfire models does not take into account the initiation of smouldering combustion. Previous research has demonstrated that the initiation of smouldering combustion in forest fuel beds by conduction [Fernandez-Pello et al., 2015, Wang et al., 2017]. These studies only cover the case when smouldering combustion is initiated by a hot-particle. However, smouldering combustion can be initiated by many different

ways in wildfires, such as lighting and radiation from fires. Hence, the initiation of smouldering of biomass with an emphasis of wildfires deserves more research, especially from the experimental perspective.

2.7 Research Gaps

Smouldering combustion is a common type of combustion regime that often occurs in fire events. Smouldering combustion is considered to be a potential hazard, as it is capable of reigniting fires which were deemed extinguished. Smouldering combustion not only plays important roles in wildfire initiation and spread, but the suppression of smouldering combustion is also a key element to a successful hazard reduction burning. Devastating wildfires are becoming the 'new normal'. Hence, a better understanding on smouldering of biomass fuel beds is essential to the solution to the increased risk of wildfires. The following research gaps have been identified from the aforementioned literature review.

- The first research gap is that there is no effective method to identify the initiation of smouldering combustion for biomass fuel. It is critical to know when smouldering combustion starts, as it will be beneficial to find and extinguish smouldering combustion before it turns to flaming combustion.
- Radiant heat flux from the fire front is one of the major heat transfer mechanisms which preheats biomass fuel. Smouldering combustion of biomass can be initiated, if the radiant heat flux reaches a certain level in a wildfire. In the literature, only limited studies have been carried out on smouldering combustion of biomass started by radiant heat flux. More importantly, the majority of these studies focus on polyurethane foam, due to its importance in residential fires. However, there has been relatively little literature published on smouldering combustion of biomass initiated by radiant heat flux.

- It has been demonstrated that flow condition and oxygen concentration have significant effects on the rate of smouldering propagation. However, little has been reported on the effects of flow condition and oxygen concentration on the initiation of smouldering combustion of biomass fuel. The third research gap is therefore the effects of flow condition and oxygen concentration on the initiation of smouldering combustion are not well understood.

- *Eucalyptus* is an essential element in Australian wildfires. Different *Eucalyptus* species have different chemical and physical properties. The differences in the properties will have effects on the combustion process. In a *Eucalyptus* forest, the accumulation of fuel, such as leaves, barks and twigs, builds up a fuel bed for fire events. The different plant parts (leaf, bark and twig) behave differently in a fire event because of their different physical and chemical properties. Smouldering combustion often occurs in fuel beds. However, the effects of *Eucalyptus* and plant parts on smouldering combustion is not clear.

2.8 Research Aims and Questions

The motivation of this research project is to investigate the smouldering combustion of biomass because of its importance in wildfires. To develop this understanding, four research aims have been identified from the research gaps listed in Section 2.7. Each of these aims maps to a research question. The overall aim of the research project is to identify the initiation of smouldering combustion in biomass fuel beds and determine the effects of the controlling parameters, including radiant heat flux, oxidiser flow rate, heating time, oxygen concentration, *Eucalyptus* species and plant parts on the initiation of smouldering combustion. Based on the research aims, multiple research questions are raised.

Research Aim 1

- To identify a method which can identify the initiation of smouldering combustion in biomass.

Research Questions

What metrics are appropriate for identifying the initiation of smouldering combustion in biomass fuel? And, how will they be measured?

- To investigate the required conditions, including radiant heat flux and air flow rate, for the initiation of smouldering and flaming combustion in biomass fuel beds.

  Research Question

  What are the interactive effects of radiant heat flux and air flow rate on the initiation of smouldering and flaming combustion in biomass fuel beds?

Research Aim 2

- To investigate the effects of heating time and oxygen concentration on the initiation of radiation-aided and self-sustained smouldering combustion.

  Research Questions

  What are the interactive effects of heating rate and oxygen concentration on the initiation of radiation-aided and self-sustained smouldering combustion?

- To investigate the differences between radiation-aided and self-sustained smouldering combustion.

  Research Question

  What are the differences between radiation-aided and self-sustained smouldering combustion in terms of temperature, product gas concentration and mass change?

Research Aim 3

- To investigate the air permeability of natural forest fuel beds as well as the characterisation of natural forest fuel beds.

Research Questions

What is the air permeability of natural forest fuel beds? How to determine the air permeability of natural forest fuel beds?

Research Aim 4

- To investigate the effects of *Eucalyptus* species and plant parts on smouldering combustion.

  Research Question

  What are the effects of *Eucalyptus* species and plant parts on the initiation of smouldering combustion?

- To characterise the different plant parts from different *Eucalyptus* species based on the physical and chemical properties.

  Research Questions

  Will *Eucalyptus* species and plant parts have effects on their physical and chemical properties? How will these differences in the properties have effects on smouldering combustion?

References

A. Aldushin, A. Bayliss, and B. Matkowsky. On the transition from smoldering to flaming. *Combustion and Flame*, 145(3):579–606, 2006.

H. E. Anderson. Aids to determining fuel models for estimating fire behavior. Technical report, USDA Forest Service, Intermountain Forest and Range Experiment Station, 1982.

M. Anderson, R. Sleight, and J. Torero. Downward smolder of polyurethane foam: Ignition signatures. *Fire Safety Journal*, 35(2):131–147, 2000.

N. F. Anez, J. G. Torrent, L. M. Pejic, and C. G. Olmedo. Detection of incipient self-ignition process in solid fuels through gas emissions methodology. *Journal of Loss Prevention in the Process Industries*, 36:343–351, 2015.

R. Anthenien and A. Fernandez-Pello. A study of forward smolder ignition of polyurethane foam. In *Proceedings of the Combustion Institute*, volume 27, pages 2683–2690, 1998.

V. Babrauskas. *Ignition handbook: principles and applications to fire safety engineering, fire investigation, risk management and forensic science*. Fire Science Publishers, Issaquah, Washington, United States, 2003.

O. Badr and G. Karim. Experimental study of self-ignition and smoldering of moist cellulosic materials. *Journal of Energy Resources Technology*, 114(2):146–151, 1992.

A. Bar-Ilan, O. Putzeys, G. Rein, A. C. Fernandez-Pello, and D. L. Urban. Transition from forward smoldering to flaming in small polyurethane foam samples. *Proceedings of the Combustion Institute*, 30(2):2295–2302, 2005.

P. Basu. *Combustion and gasification in fluidized beds*. CRC press, 2006.

C. Belcher and J. McElwain. Limits for combustion in low O2 redefine paleoatmospheric predictions for the Mesozoic. *Science*, 321(5893):1197–1200, 2008.

C. Beyler, J. Dinaburg, and C. Mealy. Development of test methods for assessing the fire hazards of landscaping mulch. *Fire Technology*, 50(1):39–60, 2014.

R. Bilbao, J. Mastral, M. Aldea, J. Ceamanos, M. Betran, and J. Lana. Experimental and theoretical study of the ignition and smoldering of wood including convective effects. *Combustion and Flame*, 126(1):1363–1372, 2001.

H. H. Biswell. *Prescribed burning in California wildlands vegetation management*. University of California Press, Oakland, California, United States, 1999.

N. Boonmee and J. Quintiere. Glowing and flaming autoignition of wood. *Proceedings of the Combustion Institute*, 29(1):289–295, 2002.

N. Boonmee and J. Quintiere. Glowing ignition of wood: The onset of surface combustion. *Proceedings of the Combustion Institute*, 30 II:2303–2310, 2005.

G. L. Borman and K. W. Ragland. *Combustion engineering*. McGraw-Hill New York, 1998.

P. Bowes and G. Britain. *Self-heating: evaluating and controlling the hazards*. Department of the Environment, Building Research Establishment, 1984.

E. R. Carvalho, C. A. G. Veras, and J. A. Carvalho Jr. Experimental investigation of smouldering in biomass. *Biomass and Bioenergy*, 22(4):283–294, 2002.

C. Y. H. Chao and J. Wang. Transition from smoldering to flaming combustion of horizontally oriented flexible polyurethane foam with natural convection. *Combustion and Flame*, 127(4):2252–2264, 2001.

M. A. Cochrane and M. D. Schulze. Forest fires in the Brazilian Amazon. *Conservation Biology*, 12(5):948–950, 1998.

D. Drysdale. *An introduction to fire dynamics*. John Wiley & Sons, 2011.

S. El-Sayed and T. Khass. Smoldering combustion of rice husk dusts on a hot surface. *Combustion, Explosion, and Shock Waves*, 49(2):159–166, 2013.

A. Erić, D. Dakić, S. Nemoda, M. Komatina, and B. Repić. Experimental method for determining forchheimer equation coefficients related to flow of air through the bales of soy straw. *International Journal of heat and mass transfer*, 54 (19-20):4300–4306, 2011.

A. Fernandez-Pello, C. Lautenberger, D. Rich, C. Zak, J. Urban, R. Hadden, S. Scott, and S. Fereres. Spot fire ignition of natural fuel beds by hot metal particles, embers, and sparks. *Combustion science and technology*, 187(1-2): 269–295, 2015.

A. M. Gill and P. H. Moore. *Ignitibility of leaves of Australian plants*, volume 34. CSIRO Canberra, 1996.

R. Hadden. *Smouldering and self-sustaining reactions in solids: an experimental approach*. PhD thesis, The University of Edinburgh, 2011.

R. Hadden and G. Rein. Chapter 18 - burning and water suppression of smoldering coal fires in small-scale laboratory experiments. In G. B. Stracher, A. Prakash, and E. V. Sokol, editors, *Coal and Peat Fires: A Global Perspective*, pages 317 – 326. Elsevier, Amsterdam, 2011. ISBN 978-0-444-52858-2.

R. Hadden, A. Alkatib, G. Rein, and J. L. Torero. Radiant ignition of polyurethane foam: the effect of sample size. *Fire Technology*, 50(3):673–691, 2014.

R. M. Hadden, S. Scott, C. Lautenberger, and A. C. Fernandez-Pello. Ignition of combustible fuel beds by hot particles: an experimental and theoretical study. *Fire technology*, 47(2):341–355, 2011.

R. M. Hadden, G. Rein, and C. M. Belcher. Study of the competing chemical reactions in the initiation and spread of smouldering combustion in peat. *Proceedings of the Combustion Institute*, 34(2):2547–2553, 2013.

B. C. Hagen, V. Frette, G. Kleppe, and B. J. Arntzen. Effects of heat flux scenarios on smoldering in cotton. *Fire Safety Journal*, 61:144–159, 2013.

B. C. Hagen, V. Frette, G. Kleppe, and B. J. Arntzen. Transition from smoldering to flaming fire in short cotton samples with asymmetrical boundary conditions. *Fire Safety Journal*, 71:69–78, 2015.

C. C. Hardy, R. D. Ottmar, J. L. Peterson, J. E. Core, and P. Seamon. Smoke management guide for prescribed and wildland fire: 2001 edition. *PMS 420-2. NFES 1279. Boise, ID: National Wildfire Coordination Group. 226 p*, 2001.

F. He, W. Yi, and X. Bai. Investigation on caloric requirement of biomass pyrolysis using TG-DSC analyzer. *Energy Conversion and Management*, 47(15-16):2461–2469, 2006.

F. He, W. Yi, and J. Zha. Measurement of the heat of smoldering combustion in straws and stalks by means of simultaneous thermal analysis. *Biomass and Bioenergy*, 33(1):130–136, 2009.

F. He, W. Yi, Y. Li, J. Zha, and B. Luo. Effects of fuel properties on the natural downward smoldering of piled biomass powder: Experimental investigation. *Biomass and Bioenergy*, 67:288–296, 2014.

X. Huang and G. Rein. Interactions of earth's atmospheric oxygen and fuel moisture in smouldering wildfires. *Science of the Total Environment*, 572:1440–1446, 2016.

T. Kashiwagi. A radiative ignition model of a solid fuel. *Combustion Science and Technology*, 8(5-6):225–236, 1973.

T. Kashiwagi and H. Nambu. Global kinetic constants for thermal oxidative degradation of a cellulosic paper. *Combustion and Flame*, 88(3-4):345–368, 1992.

H. M. Kim and C. Hwang. Heating and ignition of combustible dust layers on a hot surface: Influence of layer shrinkage. *Combustion and Flame*, 105(4):471–485, 1996.

T. Kinbara, H. Endo, and S. Sega. Downward propagation of smoldering combustion through solid materials. In *Proceedings of the Combustion Institute*, volume 11, pages 525–531, 1967.

E. E. Knapp, J. E. Keeley, E. A. Ballenger, and T. J. Brennan. Fuel reduction and coarse woody debris dynamics with early season and late season prescribed fire in a Sierra Nevada mixed conifer forest. *Forest Ecology and Management*, 208(1-3):383–397, 2005.

J. Koppejan and S. Van Loo. *The handbook of biomass combustion and co-firing*. Routledge, 2012.

P. Kourtz and W. G. O'Regan. A model a small forest fire... to simulate burned and burning areas for use in a detection model. *Forest Science*, 17(2):163–169, 1971.

P. Kourtz, S. Nozaki, W. G. O'Regan, et al. Forest fires in the computer: a model to predict the perimeter location of a forest fire. 1977.

P. Kourtz, B. Todd, et al. Predicting the daily occurrence of lightning-caused forest fires. In *Central Region Fire Weather Committee Scientific and Technical Seminar*, page 37, 1992.

U. Krause, M. Schmidt, and C. Lohrer. A numerical model to simulate smouldering fires in bulk materials and dust deposits. *Journal of Loss Prevention in the Process Industries*, 19(23):218 – 226, 2006.

R. Linn, J. Reisner, J. J. Colman, and J. Winterkamp. Studying wildfire behavior using firetec. *International journal of wildland fire*, 11(4):233–246, 2002.

S. Martin. Diffusion-controlled ignition of cellulosic materials by intense radiant energy. In *Proceedings of the Combustion Institute*, volume 10, pages 877–896, 1965.

F. Morandini, Y. Perez-Ramirez, V. Tihay, P.-A. Santoni, and T. Barboni. Radiant, convective and heat release characterization of vegetation fire. *International Journal of Thermal Sciences*, 70:83–91, 2013.

N. A. Moussa, T. Toong, and C. Garris. Mechanism of smoldering of cellulosic materials. In *Proceedings of the Combustion Institute*, volume 16, pages 1447–1457, 1977.

H. Mukunda, J. Basani, H. Shravan, and B. Philip. Smoldering combustion of incense sticks: experiments and modeling. *Combustion Science and Technology*, 179(6):1113–1129, 2007.

R. W. Mutch. Ignition delay of ponderosa pine needles and sphagnum moss. *Journal of Chemical Technology and Biotechnology*, 14(7):271–275, 1964.

T. Ohlemiller. *Smoldering combustion.* Center for Fire Research, 1986.

T. Ohlemiller. Chapter 9: Smoldering combustion. *SFPE Handbook of Fire Protection Engineering, 3rd ed., National Fire Protection Association, Quincy, Massachusetts*, 2002.

T. Ohlemiller and D. Lucca. An experimental comparison of forward and reverse smolder propagation in permeable fuel beds. *Combustion and Flame*, 54(13): 131 – 147, 1983. ISSN 0010-2180.

T. J. Ohlemiller. Modeling of smoldering combustion propagation. *Progress in Energy and Combustion Science*, 11(4):277–310, 1985.

T. J. Ohlemiller. Forced smolder propagation and the transition to flaming in cellulosic insulation. *Combustion and Flame*, 81(3-4):354–365, 1990.

T. J. Ohlemiller and F. E. Rogers. Survey of several factors influencing smoldering combustion in flexible and rigid polymer foams. *Journal of fire and flammability*, 9(4):489–509, 1978.

M. G. Ortiz-Molina, T.-Y. Toong, N. A. Moussa, and G. C. Tesoro. Smoldering combustion of flexible polyurethane foams and its transition to flaming or extinguishment. In *Proceedings of the Combustion Institute*, volume 17, pages 1191–1200, 1979.

K. Palmer. Smouldering combustion in dusts and fibrous materials. *Combustion and Flame*, 1(2):129 – 154, 1957.

O. Putzeys, G. Rein, A. Fernandez-Pello, and D. Urban. Piloted ignition to flaming in smoldering polyurethane foam. volume 18, pages 13747–13755, 2006.

O. Putzeys, A. Bar-Ilan, G. Rein, A. C. Fernandez-Pello, and D. L. Urban. The role of secondary char oxidation in the transition from smoldering to flaming. *Proceedings of the Combustion Institute*, 31(2):2669–2676, 2007.

O. M. Putzeys, A. C. Fernandez-Pello, G. Rein, and D. L. Urban. The piloted transition to flaming in smoldering fire retarded and non-fire retarded polyurethane foam. *Fire and Materials*, 32(8):485–499, 2008.

G. Rein. *Computational Model of Forward and Opposed Smoldering Combustion with Improved Chemical Kinetics*. PhD thesis, University of California Berkeley, Dec 2005.

G. Rein. Smouldering combustion phenomena in science and technology. *International Review of Chemical Engineering*, 1:3–18, 2009.

G. Rein, A. C. Fernandez-Pello, and D. L. Urban. Computational model of forward and opposed smoldering combustion in microgravity. *Proceedings of the Combustion Institute*, 31(2):2677–2684, 2007.

P. Santoni, P. Bartoli, A. Simeoni, and J. Torero. Bulk and particle properties of pine needle fuel beds–influence on combustion. *International Journal of Wildland Fire*, 23(8):1076–1086, 2014.

W. W. Simmons and K. W. Ragland. Burning rate of millimeter sized wood particles in a furnace. *Combustion Science and Technology*, 46(1-2):1–15, 1986.

D. T. Stephen, A. Carlo, F. Nde-Pello, and K. Miyasaka. Controlling mechanisms in the transition from smoldering to flaming of flexible polyurethane foam. In *Proceedings of the Combustion Institute*, volume 26, pages 1505–1513. Elsevier, 1996.

A. Sullivan, P. Ellis, and I. Knight. A review of radiant heat flux models used in bushfire applications. *International Journal of Wildland Fire*, 12(1):101–110, 2003.

J. Swann, J. Hartman, and C. Beyler. Study of radiant smoldering ignition of plywood subjected to prolonged heating using the cone calorimeter, TGA, and DSC. *Fire Safety Science*, 9:155–166, 2008.

J. Torero and A. Fernandez-Pello. Forward smolder of polyurethane foam in a forced air flow. *Combustion and Flame*, 106(1-2):89–109, 1996.

J. Torero, A. Fernandez-Pello, and M. Kitano. Opposed forced flow smoldering of polyurethane foam. *Combustion Science and Technology*, 91(1-3):95–117, 1993.

J. L. Torero and A. Fernandez-Pello. Natural convection smolder of polyurethane foam, upward propagation. *Fire Safety Journal*, 24(1):35–52, 1995.

D. C. Walther, R. A. Anthenien, and A. Fernandez-Pello. Smolder ignition of polyurethane foam: effect of oxygen concentration. *Fire Safety Journal*, 34(4): 343–359, 2000.

S. Wang, X. Huang, H. Chen, and N. Liu. Interaction between flaming and smouldering in hot-particle ignition of forest fuels and effects of moisture and wind. *International Journal of Wildland Fire*, 26(1):71–81, 2017.

R. Weber. Analytical models for fire spread due to radiation. *Combustion and Flame*, 78(3-4):398–408, 1989.

Chapter 3

Methodology

The experimental and numerical techniques and methodologies used in this project are described in this chapter. To achieve the aims stated in Section 2.8, a combustion testing rig and an air permeability testing rig have been designed and developed.

3.1 Combustion Testing Rig

3.1.1 Overview of Rig

To achieve the first and second research aims stated in Section 2.8, an experimental testing rig has been designed and developed. The pictorial representation of the experimental combustion testing rig in Figure 3.1 shows that it is composed of four main parts: an infrared heater, a combustion reactor, thermocouples, and a laboratory balance. The combustion reactor is made of stainless steel. The heat loss through the reactor wall to ambient was estimated and the heat loss to the reactor walls is approximately 13 % of the heat generated by exothermic reactions. This amount of heat loss will reduce the temperatures near the walls, but is sufficiently low to consider the reactor close to one dimensional. In addition, the focus of this study is to distinguish the different combustion regimes based

on thermocouples placed along the centerline of the reactor, where the effects of the heat loss are minimal. Figure 3.2 is a more detailed schematic diagram of the experimental setup for the combustion experiment. An infrared heat lamp is placed above the combustion reactor to ignite the fuel sample through radiant heat. Multiple thermocouples installed at different locations inside the combustion reactor are used to measure the temporal and spatial temperature changes in the reactor. A laboratory balance with a maximum total loaded mass of 610 g and a precision of ±0.01 g is used to measure the mass change of the fuel sample. Additionally, a heat shield made of aluminium was used to protect the balance from the radiant heat.

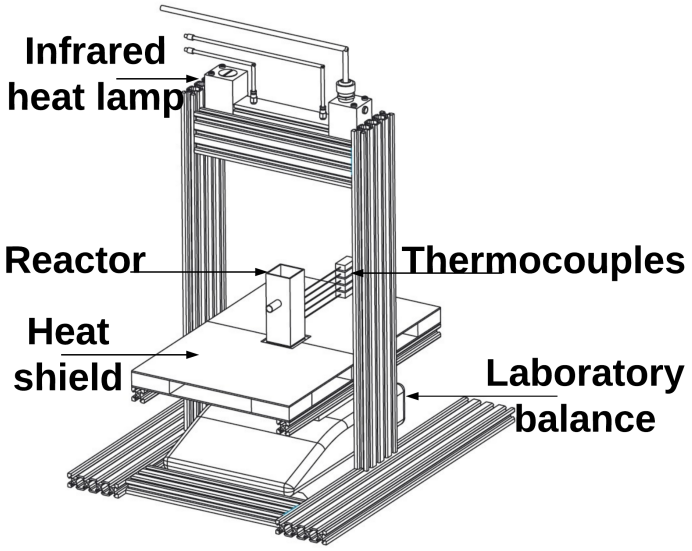

FIGURE 3.1: Pictorial representation of the experimental setup for the combustion experiment

3.1.2 Temperature Measurements

The temperature of the fuel bed is monitored with five sheathed 1.5 mm diameter Type-K thermocouples. One of the research objectives is to determine the time and the location of smouldering ignition. The thermocouples are used to measure the temperatures above the fuel bed (FB) and within the fuel bed (TC1-4). The thermocouples are located into the reactor perpendicular to the incident radiant heat flux. The first thermocouple (FB) is installed ∼7 mm above the surface of

the fuel bed to measure the gas-phase temperature above the fuel bed. The second thermocouple (TC1) is buried in the fuel bed, 3 mm beneath the surface of the fuel bed, and the distance between adjacent thermocouples is 10 mm. Temperature data is recorded at 1 Hz using a thermocouple data logger (Pico Technology USB TC-08 Data Logger). Therefore, temporal and spatial (depth) temperature profiles can be obtained. Based on the temporal and spatial temperature profiles, the time and the position of the exothermic reaction can be observed. However, the temperature profiles are not enough to indicate the initiation of smouldering combustion and hence more information, such as mass loss rate and product gas concentration are required to indicate smouldering ignition. More details are discussed in Chapter 4 and 5.

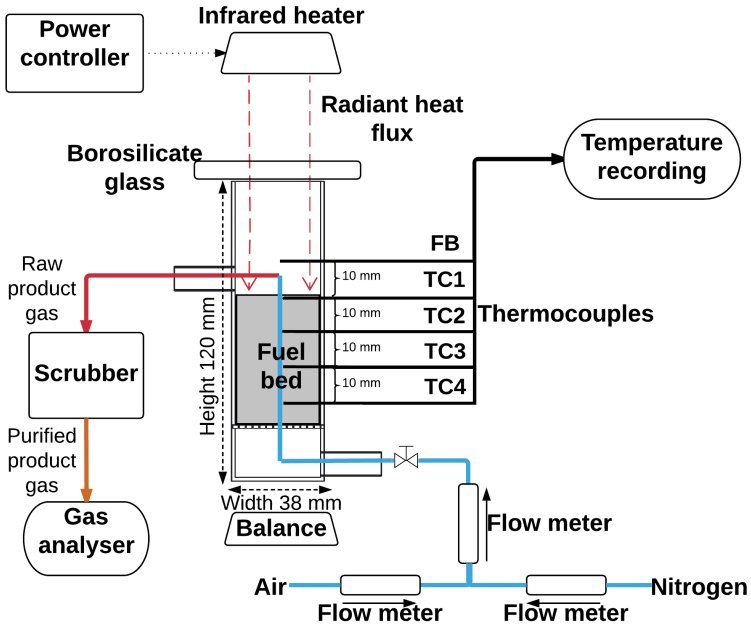

FIGURE 3.2: Schematic diagram of the experimental setup for the combustion experiment

3.1.3 Radiant Heat Flux

Radiant heat flux is an important parameter in the combustion experiment, as it provides the necessary heat for the initiation of combustion processes. A radiant heat lamp (model 5306B, Research Inc., Eden Prairie, MN, United States) is used to generate radiant heat flux in the combustion experiment. Hence, it is important

to measure the level and spatial distribution of the radiant heat flux generated by the heat lamp. In this study, a water-cooled heat flux sensor is used to measure the radiant heat flux level in a small area; while the spatial radiant heat flux distribution is determined using an indirect flux measurement method based on a CCD camera.

The radiant heat flux sensor measures the irradiance incident upon the sensing area. The sensor is capable of measuring the irradiance with wavelengths from 300 to 3000 nm [Hukseflux, 2016], which covers most (∼91%*) of the spectrum of the radiation heat flux generated by the infrared heat lamp. When measuring the irradiance, the radiation source is perpendicular to the surface of the sensing area. After the irradiance reaches the sensing area, it will be absorbed by the black coating. Then, the irradiance is converted to heat. The heat will flow through the internal thermopile sensor, and the thermopile sensor will generate a voltage signal that is proportional to the level of the incoming irradiance [Hukseflux, 2016]. The radiant heat flux level can then be determined based on the measured voltage using Equation 3.1 [Hukseflux, 2016].

$$\phi = U/S + \sigma \cdot (T + 273.15)^4 \tag{3.1}$$

where, ϕ represents the level of the incoming irradiance in $\mathrm{W{\cdot}m^{-2}}$, U is the measured voltage, S is the sensitivity factor, σ represents the Stefan-Boltzmann constant, 5.67 $\times 10^{-8}$ $\mathrm{W{\cdot}m^{-2}{\cdot}K^{-4}}$, and T is the temperature of the sensor in °C.

Although the heat flux sensor can provide direct measurements of the radiant heat flux level, the measurement of the sensor only represents the average heat flux level in a small area (∼78.5 $\mathrm{mm^2}$) [Hukseflux, 2016]. An indirect heat flux measurement method is used to measure spatial heat flux distribution over the entire area illuminated by the lamp. The indirect heat flux measurement method (Figure 3.3), uses a Lambertian reflector and a CCD camera (D200, Nikon Corporation, Tokyo, Japan). Firstly, a customised grid is placed on the Lambertian reflector. Secondly, the CCD camera records an image without turning on the

*This value is calculated based on the spectra output of the lamp [ResearchInc., 2010].

radiant heat source. Then, the customised grid is removed, and the heat source is turned on. After that, the CCD camera is used to record another image. Finally, the Lambertian reflector is removed, and the heat flux sensor measures the irradiance. The theory behind the indirect heat flux measurement is that each pixel of the image records the luminous intensity at that point. It is assumed that there is a positive correlation between luminous intensity and radiant heat flux [Ballestrín, 2001]. Hence, a map of heat flux distribution can be plotted with the ratio of luminous intensity to heat flux level. The role of the customised grid is used as a reference, so the dimensions of the image can be later corrected based on the reference. The processing of recorded images applies a two-dimension transformation to the images based on the customised grid. An example of the spatial radiant heat flux distribution is shown in Figure 3.4. The spatial heat flux distribution suggests that the infrared heat lamp is capable of providing uniformly distributed radiation in an approximate square cross-section of 45 mm × 45 mm.

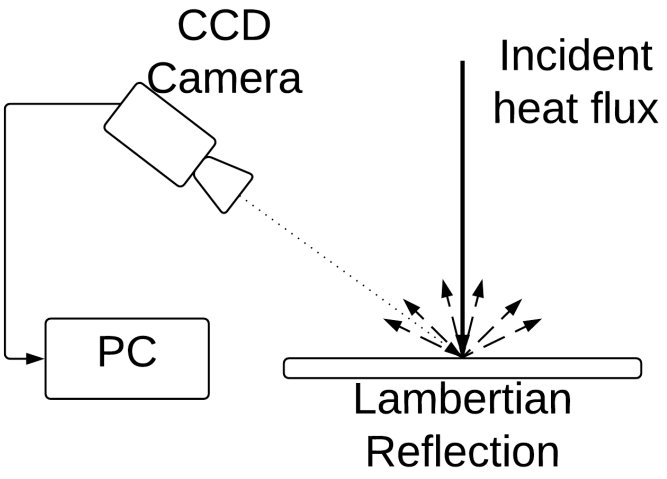

FIGURE 3.3: Schematic diagram of the experimental setup for the determination of the distribution of radiant heat flux

3.1.4 Mass Change Measurements

It has been demonstrated that the mass loss rates during the stages of smouldering combustion are variable. For example, the mass-loss rate during smouldering ignition is roughly five times the mass-loss rate during pyrolysis [Anderson et al., 2000]. A laboratory balance (GX-600, A&D Ltd., Tokyo, Japan) is introduced

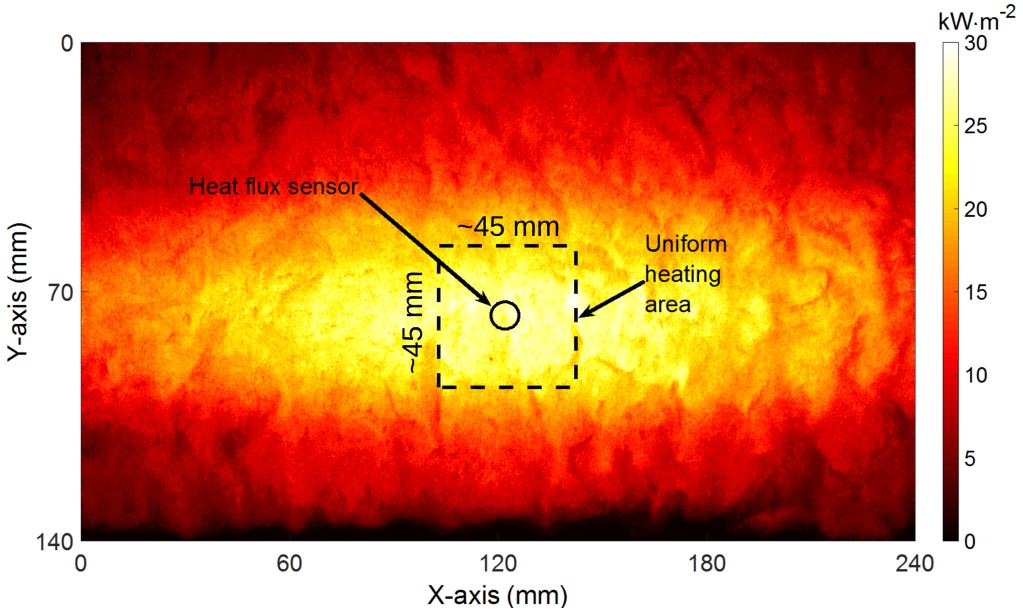

FIGURE 3.4: Spatial radiant heat flux distribution

to measure the mass-loss rate during the experiment. The results obtained by Anderson et al. [2000] suggest that the average mass-loss rate during the initiation of smouldering combustion is between 0.4 $g{\cdot}m^{-2}{\cdot}s^{-1}$ and 1.2 $g{\cdot}m^{-2}{\cdot}s^{-1}$. The reactor has a square cross-section of 1444 mm^2, and therefore the mass loss rate of fuel during the initiation of smouldering combustion could be between 0.002 $g{\cdot}s^{-1}$ to 0.01 $g{\cdot}s^{-1}$. Therefore, the resolution of the laboratory balance needs to be high enough to detect the minor mass change. The resolution of the laboratory balance (GX-600, A&D Ltd., Tokyo, Japan) is 0.001 gram, which meets the requirement. The laboratory balance can be connected to a computer and record data automatically. The laboratory balance is quite sensitive to ambient temperature changes. As fuel is heated, the balance needs to be carefully protected to minimise the influence of the ambient temperature changes. As shown in Figure 3.2, a thermal insulation layer is located between the balance and the external heater to reduce the radiation heat transfer. The reactor is placed on thermal insulation foam to reduce the conduction heat transfer from the reactor to the balance. The mass-loss profile may have some other limits, such as low measuring capacity and highly sensitive to the external disturbances. Hence, other measurements are still needed to help indicate the initiation of smouldering combustion of biomass fuel. Mass loss profile can be used to help justify and determine the accuracies of the

measurements.

3.1.5 Gas Analyser

As mentioned previously, mass-loss profile itself is not enough to indicate the initiation of smouldering combustion of biomass in practice. Previous research has demonstrated that the product gases from smouldering combustion and flaming combustion are quite different. As discussed in Chapter 2, the product gas content could be used to indicate the initiation of smouldering combustion. Hence, a gas analyser is connected to the output of the combustion reactor, which measures carbon monoxide (CO), carbon dioxide (CO_2), methane (CH_4), hydrogen (H_2) and oxygen (O_2) in the product gas. The measurements of oxygen, carbon monoxide and carbon dioxide can be used to indicate oxidisation and devolatilisation reactions. For example, the ratio of carbon monoxide and carbon dioxide was used to characterise smouldering and flaming combustion. However, the measurements of carbon monoxide and carbon dioxide cannot provide sufficient information about devolatilisation reactions, as devolatilisation is an important stage in smouldering combustion. Hence, methane and hydrogen were measured to characterise devolatilisation reactions. From preliminary tests, the flow rate of the input air has to be at least 7 $g{\cdot}min^{-1}$ in order to avoid the entrainment of ambient air into the top of the reactor. However, based on the results of the preliminary tests, smouldering combustion did not occur under this flow rate, only flaming combustion was observed. Therefore, the top of the reactor is sealed with borosilicate glass. The reasons for choosing borosilicate glass are, it has high transparency (90 % for 2 mm thickness) in the short-wavelength infrared region (700 to 2500 nm) and high-temperature resistance [THORLABS, 2018]. The spectral output of the radiant heat lamp is within the short-wavelength infrared region (1000 to 1500 nm) [ResearchInc., 2010]. It was also found that the gas analyser has different delay times for the sensors. Therefore, the delay times of the sensors as well as the mean flow-through time were taken into account (based on the sampling rate of the gas

analyser and the volume of the connecting tube between the gas analyser and the outlet of the reactor).

3.1.6 Gas Scrubber

The product gas stream was directly sampled from the reactor. The product gas stream contains a large amount of heavy hydrocarbons, which must be scrubbed to prevent erroneous gas concentration measurements and to prevent damage to the gas analyser. A wet scrubber was implemented to remove the heavy hydrocarbons, as shown in Figure 3.5. The scrubber consists of a series of 75 mL test tubes, containing ethanol (labelled A–C), empty (labelled D), and activated carbon (labelled E and F), and submerged in a bath of ethylene glycol at -5 °C. The gases from the reactor pass through ethanol, which is sufficiently stable and an efficient hydrocarbon solvent [Perez and Cortez, 1997]. Testing confirmed that the test gases were not dissolved in the ethanol, consistent with previous studies [Abraham et al., 1998, Tokunaga, 1975]. Whilst the ethanol performed well at scrubbing the heavy hydrocarbons, a small amount of ethanol vapour was released into the gas stream, which was then captured by activated carbon [Bansal and Goyal, 2005, El-Sharkawy et al., 2008]. The variation in the input oxidiser flow rate does not have a significant effect on the effectiveness of the scrubbing process. The sampling rate of the gas analyser has more impact on the scrubbing process than the input oxidiser flow rate. The sampling rate of the gas analyser is constant during the experiments. Hence, the effect of the sampling rate on the effectiveness of the scrubbing process is minimal.

3.2 Air Permeability Testing Rig

The air permeability of a fuel bed has significant effects on the combustion within that fuel bed, as the air permeability determines the oxygen availability within that fuel bed. Hence, it is essential to gain a better understanding of the air

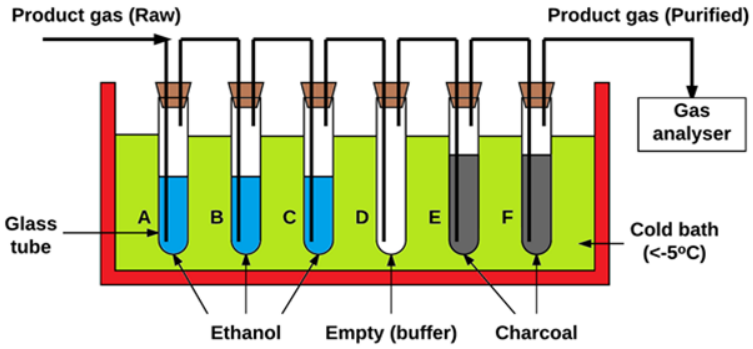

FIGURE 3.5: Schematic diagram of gas scrubber system used to remove heavy hydrocarbons from the product gas.

permeability of a fuel bed. An air permeability testing rig has been designed to determine the air permeability of a fuel bed by measuring the pressure drop across the fuel bed. The experimental testing rig consists of three parts: a permeability testing rig, an air supply system and a manometer (Model 9565, TSI Inc., Shoreview, United States). The air permeability testing rig has top and bottom sections (Figure 3.6). There is a dual inlet and a bed of ceramic beads in the bottom section to obtain uniform flow through the fuel bed. Fuel bed samples were loaded in the top section of the air permeability testing rig. The input air flow in this study was supplied by an air compressor, and the moisture in the input air flow was removed by a dehumidifier before introducing into the air permeability testing rig.

The input air flow rate was varied from 50.5 to 404 $g{\cdot}m^{-2}{\cdot}s^{-1}$, with a 50.5 $g{\cdot}m^{-2}{\cdot}s^{-1}$ increment. Below the lower limit (50.5 $g{\cdot}m^{-2}{\cdot}s^{-1}$), the error in the pressure drop measurement significantly increases due to the range of the manometer. Above the upper limit (404 $g{\cdot}m^{-2}{\cdot}s^{-1}$), the bed becomes fluidised. The pressure drop across the fuel bed (Figure 3.6) was measured using the manometer through the holes on the rig. Prior to each experiment, fuel material was weighed and loaded into the rig. The fuel material was carefully loaded to create an unconsolidated fuel bed; this is to ensure the consistency throughout the fuel bed. The pressure drop across the fuel bed was based on a 60-second averaging period, with a 1 Hz sampling frequency. All fuel bed samples were classified and sieved to homogenise the fuel samples. All experiments were repeated three times to determine the uncertainty of measurements.

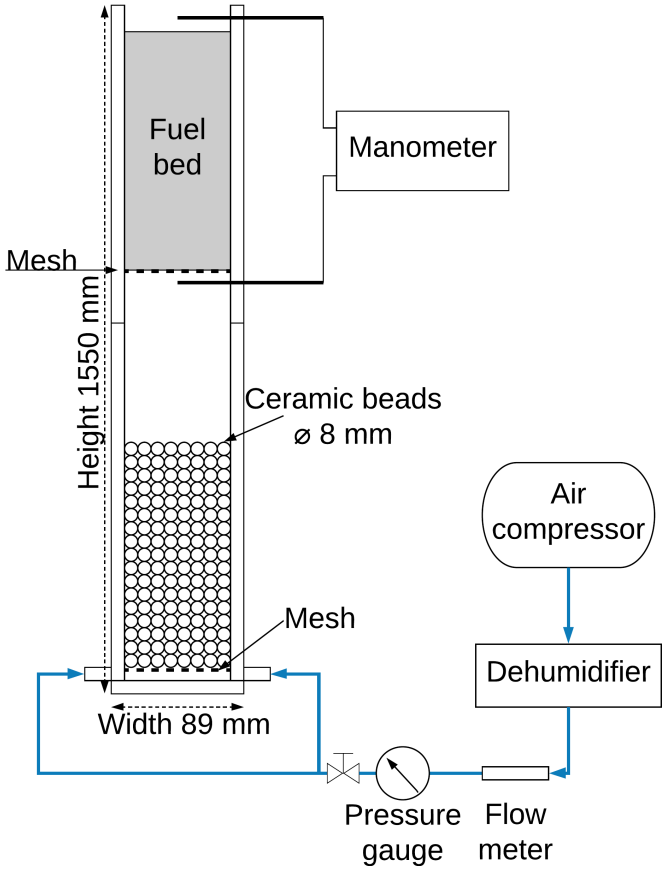

FIGURE 3.6: Schematic diagram of the experimental setup for the air permeability experiment

3.2.1 Calculation of Fluid Permeability

The air permeability of a porous medium can be determined from either the pressure gradient or from the fuel bed/particle properties. In this study, both methods are used to determine the air permeability of different porous media (For more details, please refer to Chapter 6). A schematic diagram outlining how the air permeability was determined in this study is summarised in Figure 3.7.

The pressure gradient method is an empirical approach that does not need any information about the particle properties such as particle size. For the pressure gradient method, the air permeability was directly determined from the measured pressure gradient using Darcy's Law (Section 3.2.1.1) for the Darcian flow regime, while the Forchheimer equation (Section 3.2.1.2) was used to determine the air permeability and the Forchheimer coefficient within the non-Darcian flow regime.

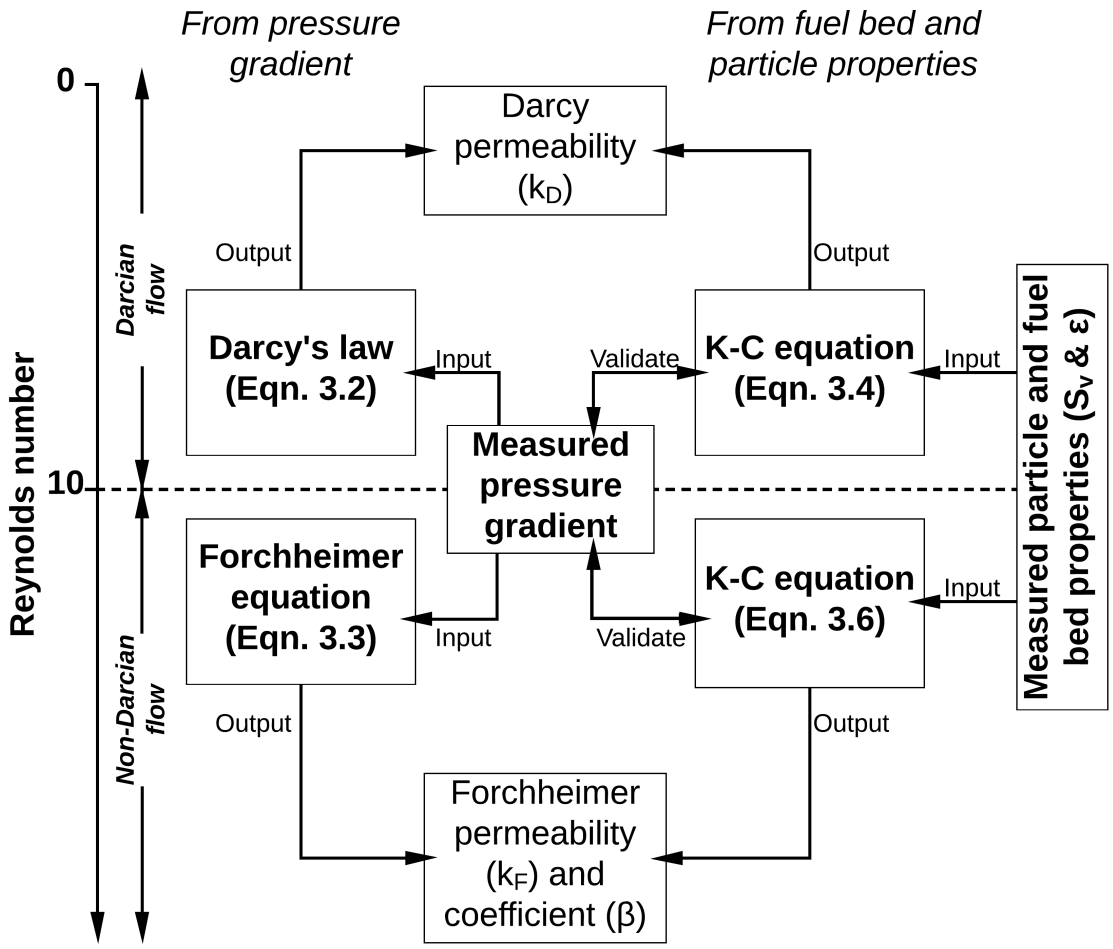

FIGURE 3.7: Schematic diagram for determining the air permeability of a fuel bed.

It should be noted that Darcy's Law is only applicable in the Darcian flow regime, namely when the Reynolds number, $Re_d < 10$ [Chapman, 2012, Hassanizadeh and Gray, 1987, Sukop et al., 2013]. Here, $Re_d = \rho \cdot U_0 \cdot d/\mu$, where U_0 is superficial velocity and d is the average particle diameter [Sobieski and Trykozko, 2014]. For non-Darcian flow ($Re_d > 10$), the Forchheimer equation may be used.

For the fuel bed/particle properties method, the specific area of particles (S_v) and the porosity (ε) of fuel bed were measured to calculate the pressure gradient and the air permeability using the Kozeny-Carman equation (Section 3.2.1.3). The calculated pressure gradient was compared with the measured pressure gradient to validate the Kozeny-Carman equation. Similar research has been conducted on the air permeability of pine needle fuel beds and the air permeability of fuel

bed was calculated using Darcy's Law and the Kozeny-Carman equation [Santoni et al., 2014]. However, both Darcy's Law and the Kozeny-Carman equation (Equation 3.4) can only be applied when $Re_d < 10$ [Hassanizadeh and Gray, 1987]. This is because, as the air flow velocity increases, the experimental results do not match with Darcy's law due to inertial effects.

To overcome the discrepancy between experimental results and Darcy's law, Forchheimer (1901) has suggested adding a kinetic energy term to Darcy's Law. In this study, for the cases with $Re_d > 10$, the air permeability was calculated using the Forchheimer equation. To calculate the air permeability of fuel bed using the Forchheimer equation, the pressure drop across fuel bed is required. The pressure drop can either be measured through experiment or calculated using the function of pressure gradient and the superficial air velocity. Similarly, the Kozeny-Carman equation can be modified to account for non-Darcian flow (Equation 3.6).

3.2.1.1 Darcy's Law

Permeability (isotropic permeability in this study) can be determined by using Darcy's Law (Equation 3.2) from the pressure gradient and the superficial velocity. Darcy's Law is only valid for Darcian flow, i.e. $Re_d < 10$.

$$\frac{\Delta P}{L} = \frac{\mu}{k_D} U_0 \tag{3.2}$$

where, Δ P is the total pressure drop across the fuel bed [Pa]; L is the length of the fuel bed [m]; μ is dynamic viscosity [Pa·s]; k_D is air permeability of the fuel bed [m^2] (subscript D indicates Darcian flows) and U_0 is superficial velocity [$m \cdot s^{-1}$].

Equation 3.2 shows that the pressure drop of Darcian flows through a porous medium is proportional to the fluid dynamic viscosity and velocity. The pressure drop of Darcian flows through a porous medium is mainly attributed to the skin friction of the porous medium wall surfaces in the porous voids (particle surfaces of the fuel bed in this study).

3.2.1.2 Forchheimer Equation

The air permeability through a porous medium in a non-Darcian flow ($\mathrm{Re}_d > 10$) can be determined from the Forchheimer equation (Equation 3.3). The difference between the Forchheimer equation (Equation 3.3) and Darcy's Law (Equation 3.2) is that the Forchheimer equation includes an additional term to incorporate the importance of kinetic energy loss due to inertial effects in non-Darcian flows. When the flow velocity increases, the pressure drop due to inertial effects increases and needs to be considered when Re_d is larger than 10. As a result, the relationship between the superficial velocity and the pressure gradient is a quadratic function in non-Darcian flows. The air permeability determined through the Forchheimer equation in this paper is referred to as the Forchheimer permeability (k_F), to distinguish it from the permeability from Darcy's Law (k_D). To characterise a porous medium in non-Darcian flow, the Forchheimer permeability (k_F) and the Forchheimer coefficient (β) are required.

$$\frac{\Delta P}{L} = \frac{\mu}{k_F} U_0 + \beta \cdot \rho \cdot U_0^2 \tag{3.3}$$

where, Δ P is the total pressure drop across the fuel bed [Pa]; L is the length of the fuel bed [m]; μ is dynamic viscosity [Pa·s]; k_F is air permeability of the fuel bed [m^2] (subscript F indicates non-Darcian flows); β is Forchheimer coefficient [m^{-1}]; ρ is the density of air [kg·m^{-3}] and U_0 is superficial velocity [m·s^{-1}].

The air permeability can be determined by either Darcy's Law or the Forchheimer equation, depending on the flow regime. These methods require the experimental data of the pressure gradient and the superficial velocity, which means that a similar experiment has to be conducted before using Darcy's Law or the Forchheimer equation.

3.2.1.3 Kozeny-Carman Equation

For flows through unconsolidated beds of fuel particles, the pressure gradient can be calculated from the particle and fuel bed properties using the Kozeny-Carman equation (Equation 3.4 and 3.6) [Holdich, 2002]. Equation 3.4 is for Darcian flows, while Equation 3.6 is for non-Darcian flows. In the non-Darcian flow condition, a modified Reynolds number, Re_1, (Equation 3.11) is required to calculate the friction factor term, $\frac{R}{\rho \cdot U^2}$ (Equation 3.10). Within the Darcian flow regime, the air permeability can be calculated by rearranging the Kozeny-Carman equation, i.e. Equation 3.5. In the non-Darcian flow condition, the air permeability and the Forchheimer coefficient can be calculated by Equation 3.8 and 3.9.

$$\frac{\Delta P}{L} = \mu \left(\frac{K(1-\varepsilon)^2 S_V^2}{\varepsilon^3} \right) U_0 \tag{3.4}$$

where, ΔP is the total pressure drop across the fuel bed [Pa]; L is the length of the fuel bed [m]; μ is dynamic viscosity [Pa·s]; K is Kozeny constant; ε is porosity of fuel bed and S_V is specific surface area per unit volume [m^{-1}]. From Equation 3.4, the air permeability can be calculated using the following equation based on Equation 3.2:

$$k_{KC} = k_D = \frac{\varepsilon^3}{K(1-\varepsilon)^2 S_V^2} \tag{3.5}$$

where, k_{KC} is the air permeability calculated through the Kozeny-Carman equation; ε is porosity of fuel bed; K is Kozeny constant and S_V is specific surface area per unit volume [m^{-1}]. For non-Darcian flows, the following equation can be used to calculate the pressure drop across the fuel bed.

$$\frac{\Delta P}{L} = \left(\frac{R}{\rho U^2} \right) \frac{S_V(1-\varepsilon)\rho U_0^2}{\varepsilon^3} \tag{3.6}$$

where, ΔP is the total pressure drop across the fuel bed [Pa]; L is the length of the fuel bed [m]; R is drag force on the particle surface [N]; ρ is the density of air [kg·m^{-3}]; U is interstitial velocity [m·s^{-1}]; S_V is specific surface area per unit

volume [m^{-1}]; ε is porosity of fuel bed and U_0 is superficial velocity [$m{\cdot}s^{-1}$]. By substituting the Carman correlation (Equation 3.10) into the friction factor, $\frac{R}{\rho \cdot U^2}$ in Equation 3.6, Equation 3.7 shows Equation 3.6 in Forchheimer form:

$$\frac{\Delta P}{L} = \frac{5(1-\varepsilon)^2 S_V^2}{\varepsilon^3}\mu U_0 + \left[\frac{0.4(1-\varepsilon)^{1.1} S_V^{1.1} \mu^{0.1}}{\rho^{0.1}\varepsilon^3 U_0}\right]\rho U_0^2 \tag{3.7}$$

where, ΔP is the total pressure drop across the fuel bed [Pa]; L is the length of the fuel bed [m]; ε is porosity of fuel bed; S_V is specific surface area per unit volume [m^{-1}]; μ is dynamic viscosity [Pa·s]; U_0 is superficial velocity [$m{\cdot}s^{-1}$] and ρ is the density of air [$kg{\cdot}m^{-3}$]. From Equation 3.7, the air permeability and the Forchheimer coefficient can be calculated using the following equations based on Equation 3.3:

$$k_{KC} = k_F = \frac{\varepsilon^3}{5(1-\varepsilon)^2 S_V^2} \tag{3.8}$$

$$\beta = \frac{0.4(1-\varepsilon)^{1.1} S_V^{1.1} \mu^{0.1}}{\rho^{0.1}\varepsilon^3 U_0} \tag{3.9}$$

where, k_{KC} is the air permeability calculated through the Kozeny-Carman equation; ε is porosity of fuel bed; S_V is specific surface area per unit volume [m^{-1}]; β is Forchheimer coefficient [m^{-1}]; ρ is the density of air [$kg{\cdot}m^{-3}$]; μ is dynamic viscosity [Pa·s] and U_0 is superficial velocity [$m{\cdot}s^{-1}$]. For non-Darcian flows, the friction factor can be represented using the Carman correlation (Equation 3.10) and the friction can be represented as a function of the modified Reynolds number [Carman, 1956, Holdich, 2002].

$$\frac{R}{\rho U^2} = \frac{5}{Re_1} + \frac{0.4}{Re_1^{0.1}} \tag{3.10}$$

where, R is drag force on the particle surface [N]; ρ is the density of air [$kg{\cdot}m^{-3}$]; U is interstitial velocity [m·s-1] and Re_1 is modified Reynolds number. The modified Reynolds number is calculated using Equation 3.11.

$$Re_1 = \frac{\rho U_0}{(1-\varepsilon)S_V \mu} \tag{3.11}$$

where, Re_1 is modified Reynolds number; ρ is the density of air [kg·m^{-3}]; U_0 is superficial velocity [m·s^{-1}]; ε is porosity of fuel bed; S_V is specific surface area per unit volume [m^{-1}] and μ is dynamic viscosity [Pa·s].

3.3 Fuels

3.3.1 Fuel Selection

Wildfires are fuelled by an enormous variety of forest vegetation. Fuel is an essential element of combustion. Therefore, there is a strong link between forest vegetation and wildfires. In this thesis, *Pinus* and *Eucalyptus* trees are chosen as the fuels for the combustion experiments. In Chapter 4 and 5, combustion of radiata pine is studied. The reason for choosing radiata pine is because it is not only one of the most widely planted tree species, but it is also highly combustible. More importantly, the plantations of radiata pine can be found in many wildfire-prone regions, such as southern California, southern Europe and southeast Australia. Hence, it is critical to develop a better understanding of combustion of radiata pine.

Australia is one of the most wildfire-prone countries in the world, and the southeast is the worst region in Australia in terms of wildfire severity. This dangerous feature of southeast Australia is mainly because the forests of southeast Australian contain a large quantity of *Eucalyptus* trees. *Eucalyptus* trees are highly flammable due to a high content of combustible oils. Hence, Chapter 7 focuses on four common *Eucalyptus* species in southeast Australia: two smooth barks (*Eucalyptus* camaldulensis and *Eucalyptus* fasciculosa) and two stringybarks (*Eucalyptus* baxteri and *Eucalyptus* obliqua).

3.3.2 Fuel Preparation

To reduce variability between samples, all the fuel samples used in this research were pulverised using a cutting mill (SM100, Retsch, Inc, Düsseldorf, Germany). All the pulverised fuel samples were then sieved to further homogenise the fuel samples. Later, all the sieved fuel samples were dried in an oven at 105 ^{o}C for 24 h [Sluiter et al., 2008]. After drying the fuel samples, the fuel samples were stored in an air-tight container, and desiccants were also placed in the container to reduce the moisture content inside the container. All the fuel samples were carefully loaded into the combustion reactor and the air permeability reactor to create an unconsolidated fuel bed; this is to ensure the consistency throughout the fuel bed. The density of fuel beds ranged from 82 to 196.8 kg·m^{-3}, depending on the fuel samples.

3.3.3 Fuel Properties

The characterisation of fuel samples is an essential part of the studies. All of the fuel samples are characterised based on the physical and chemical properties. The physical property is mainly based on the air permeability of fuel samples. The chemical properties include thermogravimetric analysis, ultimate analysis and calorific value analysis.

3.3.3.1 Proximate Analysis

Proximate analysis were conducted for all fuel samples in the current study to determine the content of the following compositions:

- **Moisture**

  The moisture content in the fuel samples was determined by drying the pulverised samples in a thermogravimetric analyser (TGA/DSC 2, Mettler Toledo, Greifensee, Switzerland) at 105 ^{o}C. The moisture content is calculated

using Equation 3.12.

$$Moisture = \frac{W_i - W_{dry}}{W_i} \tag{3.12}$$

where, W_i is the initial weight of sample, and W_{dry} is the weight of the dried sample.

- **Volatile Matter**

  The volatile matter content in the fuel samples was determined by heating the dried sample in the thermogravimetry analyser at high temperature (∼600 ^oC) in the absence of oxygen. The weight loss is due to the release of volatile matter. The remaining sample is char, which includes fixed carbon and ash. The volatile matter content in dry basis is calculated using Equation 3.13.

$$Volatile\ matter = \frac{W_{dry} - W_{VM}}{W_{dry}} \tag{3.13}$$

  where, W_{dry} is the weight of the dried sample, and W_{VM} is the weight after the complete release of volatile matter.

- **Fixed Carbon/Ash**

  The fixed carbon content in the fuel samples was determined by heating the remaining fuel sample in the thermogravimetry analyser at the same at high temperature (∼600 ^oC) with an externally supplied oxidising agent. At the end of this stage, the remaining residue is defined as ash. The contents of fixed carbon and ash in dry basis is calculated using Equation 3.13 and 3.15

$$Fixed\ carbon = \frac{W_{dry} - W_{VM} - W_{ash}}{W_{dry}} \tag{3.14}$$

$$Ash = \frac{W_{ash}}{W_{dry}} \tag{3.15}$$

  where, W_{dry} is the weight of the dried sample, W_{VM} is the weight after the complete release of volatile matter, and W_{ash} is the weight of the remaining residue (ash).

The thermogravimetric analysis was repeated three times for all the samples to ensure verifiable repeatability. The results (Appendix C) show that the repeatability of the measurements was high, with a variability of less than 1 %.

3.3.3.2 Carbohydrate and Lignin Analysis

Cellulose, hemicellulose and lignin are the three main constituents of plants [Gaur and Reed, 1995, Koppejan and Van Loo, 2012]. Carbohydrate and lignin composition analysis was used to determine the percentage of the three major components, namely, cellulose, hemicellulose and lignin, in each fuel sample. The theory of the carbohydrates and lignin composition analysis is based on the assumption that a mechanical mixture of materials would give a thermogram from the TGA that would be the arithmetic sum of the proportional quantities of each component [Gaur and Reed, 1995]. The results in Figure 3.8 show that the three major components, namely, cellulose, hemicellulose and lignin, have distinctive peak derivative thermogravimetric (DTG) rates and the temperatures at which these peak rates occur. These differences in the peak DTG rate and the temperature at which the peak rates occur will make it easier to separate these three components from a thermogram.

It has been proved that a mechanical mixture of materials would give a thermogram from the TGA that would be the arithmetic sum of the proportional quantities of each component [Gaur and Reed, 1995]. Figure 3.8 also shows that the peak DTG values of cellulose, hemicellulose and lignin occur at different temperatures. Hence, the interaction among cellulose, hemicellulose and lignin should not have a significant effect on the carbohydrate and lignin analysis.

The thermogravimetric analyses of cellulose, hemicellulose and lignin were conducted in the same thermogravimetric analyser using the same method as for

the fuel samples. Then, it is assumed that the fuel sample is composed of five components, namely, cellulose, hemicellulose, lignin, protein and ash (Equation 3.16):

$$Cellulose(\%) + Hemicellulose(\%) + Lignin(\%) + Protein(\%) + Ash(\%) = 100(\%) \tag{3.16}$$

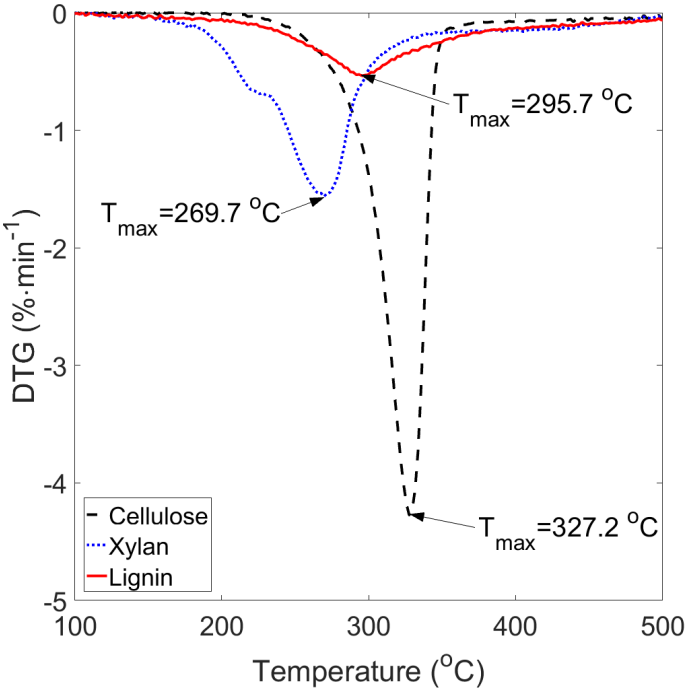

FIGURE 3.8: Derivative thermogravimetric analyses (DTG) of the devolatilisation of starch, cellulose, hemicellulose (xylan) and lignin at a heating rate of 2 K·min^{-1}. This figure is generated using the data from the author.

The percentage of protein was estimated based on the nitrogen content from the ultimate analysis using the Kjeldahl method [Maclean et al., 2003]. The ash content is based on the results of the proximate analysis. Protein and ash were assumed constant across the temperature range of the thermogravimetric analysis. Protein is assumed constant due to two reasons. Firstly, protein is not a major chemical component in the fuel samples. Secondly, unlike cellulose, hemicellulose and lignin, it is difficult to find a reference protein which can be used to present the protein of the fuel samples. Hence, the method of the carbohydrates and lignin composition analysis is to find mixtures of cellulose, hemicellulose and lignin, whose derivative thermogravimetric curves match with those of the fuel samples. Figure 3.9 shows how a three compositions mixture can be simplified and represented by an arithmetic sum of three compositions' thermograms. The proportions of

the three components is determined from curve-fitting to the thermogram of the *Eucalyptus* fuel samples.

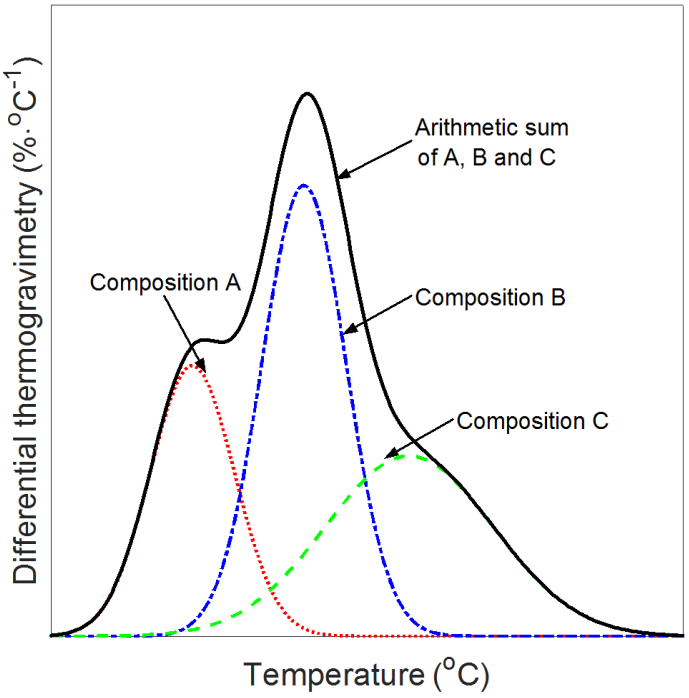

FIGURE 3.9: An illustration of the arithmetic sum of three compositions

3.3.3.3 Ultimate Analysis

Ultimate analysis was conducted to determine the elemental composition, including carbon, hydrogen, nitrogen and oxygen of the fuel samples. Ultimate analysis was conducted with an elemental analyser (2400 CHNS/O Series II System, Perkin Elmer, Waltham, Massachusetts, United States). Based on the results of ultimate analysis, the higher heating value and the protein content can be estimated. The higher heating value (HHV) is estimated using Equation 3.17 [Koppejan and Van Loo, 2012]. The higher heating value of all the fuel samples was also measured using an oxygen bomb calorimeter (6400 Automatic Isoperibol Calorimeter; Parr Instrument Company, Moline IL).

$$HHV = 0.3491 \cdot Y_C + 1.178 \cdot Y_H - 0.0151 \cdot Y_N - 0.1034 \cdot Y_O - 0.0211 \cdot Y_{ash} \quad (3.17)$$

where Y_C is the mass fraction of carbon; Y_H of hydrogen; Y_N of nitrogen; Y_O of oxygen; Y_{ash} of ash, and HHV reported in MJ·kg^{-1}.

The protein content is calculated using the Kjeldahl method (Equation 3.18).

$$Protein(\%) = Nitrogen(\%) \times 6.25 \tag{3.18}$$

where, the nitrogen content is from the results of the ultimate analysis.

References

M. H. Abraham, G. S. Whiting, W. J. Shuely, and R. M. Doherty. The solubility of gases and vapours in ethanol—the connection between gaseous solubility and water-solvent partition. *Canadian Journal of Chemistry*, 76(6):703–709, 1998.

M. Anderson, R. Sleight, and J. Torero. Downward smolder of polyurethane foam: Ignition signatures. *Fire Safety Journal*, 35(2):131–147, 2000.

J. Ballestrín. Direct heat-flux measurement system (mdf) for solar central receiver evaluation. Technical report, Centro de Investigaciones Energeticas Medioambientales y Tecnologicas (CIEMAT), 2001.

R. C. Bansal and M. Goyal. *Activated carbon adsorption*. CRC press, 2005.

P. C. Carman. *Flow of gases through porous media*. Academic press, 1956.

R. E. Chapman. *Geology and water: an introduction to fluid mechanics for geologists*, volume 1. Springer Science & Business Media, 2012.

I. El-Sharkawy, B. Saha, S. Koyama, J. He, K. Ng, and C. Yap. Experimental investigation on activated carbon–ethanol pair for solar powered adsorption cooling applications. *International Journal of Refrigeration*, 31(8):1407–1413, 2008.

S. Gaur and T. B. Reed. An atlas of thermal data for biomass and other fuels. Technical report, National Renewable Energy Lab., Golden, CO (United States), 1995.

S. M. Hassanizadeh and W. G. Gray. High velocity flow in porous media. *Transport in Porous Media*, 2(6):521–531, 1987.

R. G. Holdich. *Fundamentals of particle technology*. Midland Information Technology and Publishing, 2002.

Hukseflux. USER MANUAL SBG01: Water cooled heat flux sensor, 2016. URL `https://www.hukseflux.com/sites/default/files/product_manual/SBG01_manual_v1722.pdf`. Last accessed on 5/October/2017.

J. Koppejan and S. Van Loo. *The handbook of biomass combustion and co-firing*. Routledge, 2012.

W. Maclean, J. Harnly, J. Chen, S. Chevassus-Agnes, G. Gilani, G. Livesey, and P. Warwick. Food energy–methods of analysis and conversion factors. In *Food and Agriculture Organization of the United Nations Technical Workshop Report*, volume 77, 2003.

L. B. Perez and L. Cortez. Potential for the use of pyrolytic tar from bagasse in industry. *Biomass and Bioenergy*, 12(5):363–366, 1997.

ResearchInc. LampIR Data Sheet, 2010. URL `http://www.pcscontrols.com/sites/default/files/LampIR%20Data%20Sheet.pdf`. Last accessed on 20/January/2018.

P. Santoni, P. Bartoli, A. Simeoni, and J. Torero. Bulk and particle properties of pine needle fuel beds–influence on combustion. *International Journal of Wildland Fire*, 23(8):1076–1086, 2014.

A. Sluiter, B. Hames, D. Hyman, C. Payne, R. Ruiz, C. Scarlata, J. Sluiter, D. Templeton, and J. Wolfe. Determination of total solids in biomass and total dissolved solids in liquid process samples. *National Renewable Energy Laboratory, Golden, CO, NREL Technical Report No. NREL/TP-510-42621*, pages 1–6, 2008.

W. Sobieski and A. Trykozko. Darcy's and Forchheimer's laws in practice: Part 1 The experiment. *Technical Sciences*, 17(4):321–335, 2014.

M. C. Sukop, H. Huang, P. F. Alvarez, E. A. Variano, and K. J. Cunningham. Evaluation of permeability and non-Darcy flow in vuggy macroporous limestone aquifer samples with lattice Boltzmann methods. *Water Resources Research*, 49 (1):216–230, 2013.

THORLABS. Borosilicate glass transmission (2 mm thick), 2018. URL `https://www.thorlabs.com/newgrouppage9.cfm?objectgroup_ID=1470`. Last accessed on 20/January/2018.

J. Tokunaga. Solubilities of oxygen, nitrogen, and carbon dioxide in aqueous alcohol solutions. *Journal of Chemical and Engineering Data*, 20(1):41–46, 1975.

Chapter 4

Identification and Quantitative Analysis of Smoldering and Flaming Combustion of Radiata Pine

Statement of Authorship

Title of Paper	Identification and quantitative analysis of smoldering and flaming combustion of radiata pine.
Publication Status	☑ Published ☐ Accepted for Publication ☐ Submitted for Publication ☐ Unpublished and Unsubmitted w ork w ritten in manuscript style
Publication Details	Wang, H., van Eyk, P., Medwell, P., Birzer, C., Tian, Z., & Possell, M. (2016). Identification and Quantitative Analysis of Smoldering and Flaming Combustion of Radiata Pine. *Energy and Fuels*, 30(9), 7666-7677.

Principal Author

Name of Principal Author (Candidate)	Houzhi Wang
Contribution to the Paper	I conducted a thorough literature review, and identified the research gaps of the papers. After discussion with my supervisors, a detailed research methodology and experimental plan were decided. According to the plan, I designed and developed an experiment testing rig. I tested and calibrated the testing rig. A fuel was selected for this study. I prepared the fuel samples for the experiments. I did preliminary experiments using the testing rig. I discussed the preliminary experiments with my supervisors; then, I modified the testing rig based on feedback from my supervisors. I set up the experiments. I conducted all the experiments and collected experimental data independently. I processed, analysed and interpreted all the experimental data. I performed an analysis of the experimental results, and the analysis was presented in text or figures by me. I interpreted data, wrote the manuscript. I also acted as the corresponding author, and responded to the reviewers' and the editor's comments and recommendations.
Overall percentage (%)	75
Certification:	This paper reports on original research I conducted during the period of my Higher Degree by Research candidature and is not subject to any obligations or contractual agreements with a third party that would constrain its inclusion in this thesis. I am the primary author of this paper.
Signature	Date: 15/Jan/2018

Co-Author Contributions

By signing the Statement of Authorship, each author certifies that:

i. the candidate's stated contribution to the publication is accurate (as detailed above);

ii. permission is granted for the candidate in include the publication in the thesis; and

iii. the sum of all co-author contributions is equal to 100% less the candidate's stated contribution.

Name of Co-Author	Philip van Eyk
Contribution to the Paper	This co-author provided feedback, supervised development of work, helped in data interpretation and manuscript evaluation.
Signature	Date: 19/Jan/2018

Name of Co-Author	Paul Medwell		
Contribution to the Paper	This co-author provided feedback, supervised development of work, helped in data interpretation and manuscript evaluation.		
Signature		Date	18-JAN-2018

Name of Co-Author	Cristian Birzer		
Contribution to the Paper	This co-author provided feedback, supervised development of work, helped in data interpretation and manuscript evaluation.		
Signature		Date	19 Jan 2018

Name of Co-Author	Zhao Feng Tian		
Contribution to the Paper	This co-author provided feedback, supervised development of work, helped in data interpretation and manuscript evaluation.		
Signature		Date	18/01/2018

Name of Co-Author	Malcolm Possell		
Contribution to the Paper	This co-author provided feedback, supervised development of work, helped in data interpretation and manuscript evaluation.		
Signature		Date	19/01/2018

Please cut and paste additional co-author panels here as required.

energy&fuels

Article

pubs.acs.org/EF

Identification and Quantitative Analysis of Smoldering and Flaming Combustion of Radiata Pine

Houzhi Wang,*[,†,‡] Philip J. van Eyk,[§] Paul R. Medwell,[†] Cristian H. Birzer,[†] Zhao F. Tian,[†] and Malcolm Possell[∥,‡]

[†]School of Mechanical Engineering, The University of Adelaide, Adelaide, SA 5005, Australia

[‡]Bushfire and Natural Hazards CRC, Melbourne, VIC 3002, Australia

[§]School of Chemical Engineering, The University of Adelaide, Adelaide, SA 5005, Australia

[∥]Faculty of Agriculture and Environment, The University of Sydney, Sydney, NSW 2006, Australia

Supporting Information

ABSTRACT: Smoldering combustion is an important combustion process in wildfires; however, there are fewer experimental studies recorded in the literature in comparison with flaming combustion. An experimental study was conducted to characterize the initiation of smoldering and flaming combustion of biomass using temporal and spatial temperature profiles, mass loss profiles, and gas analyses. The results show that the peak temperature, temperature rise rate, and average mass loss rate of flaming combustion are much higher than those of smoldering combustion. The results on the ratio of CO to CO_2 for flaming and smoldering combustion show good agreement with the data reported in the literature. The results also show that smoldering combustion can be initiated only under a low air flow; for the experimental apparatus used, this corresponded to flow velocity of $\leq$38.1 mm·s^{-1}. A combustion progress pathway diagram was developed that describes the stages of smoldering and flaming combustion of a single dry biomass particle. An analysis of combustion kinetic parameters (activation energy and pre-exponential factor) and an energy balance analysis were also conducted to understand the differences between smoldering and flaming combustion.

1. INTRODUCTION

Wildfires are uncontrolled fire events, which are a global issue.[1−4] To date, the majority of research on wildfires focuses on "fires" that exhibit a flaming regime of combustion. However, there is another form of combustion, termed smoldering combustion, which is also ubiquitous in wildfires.[5−9]

Smoldering combustion is a slow, low-temperature, nonflaming form of combustion that is sustained by the heat evolved when oxygen directly reacts at the surface of a condensed-phase fuel.[10] Many fires start as smoldering combustion because it normally requires less energy for ignition than flaming combustion.[11,12] Most studies of smoldering combustion have been carried out only on polyurethane foam, which is important for residential fires. However, the initiation of smoldering combustion in biomass has scarcely been investigated.

Wildfires can be divided into three stages: prefire, during fire, and postfire. Smoldering combustion occurs in both the pre- and postfire stages.[13] In wildfires, a large amount of radiation is emitted from fire fronts; the radiation could potentially initiate smoldering combustion a long distance from the fire front. Once ignited, smoldering combustion is a serious hazard because it lasts for a long period of time and can suddenly lead to flaming combustion under certain conditions. The lack of research on smoldering ignition and its propagation in biomass limits the ability to make accurate predictions of the initiation of smoldering combustion in wildfires.

There are two types of solid-fuel ignition: smoldering and flaming. Smoldering ignition is the onset of surface combustion of solid particle, and flaming ignition is the gas-phase combustion of volatile gases.[14] Three stages have been identified in the smoldering ignition process, namely, preheating, aided smoldering ignition, and self-sustained smoldering ignition.[15] During preheating, water evaporation occurs, and thus, the mass loss rate and gas emission are minimal. If the heat source is removed in this stage, no ignition will occur. In the next stage, aided smoldering ignition, net exothermic reactions start to occur but are not sufficient to completely sustain combustion. If the external heat source is removed in this stage, the smoldering combustion will decay and extinguish. In the third stage, self-sustained smoldering ignition, smoldering is independent of the external heat source, and exothermic reactions maintain combustion. Smoldering ignition is not a phenomenon with a clear definition. It is difficult to detect or predict smoldering ignition because it normally does not have obvious indications, such as a visible flame, high temperature, and high product gas emission.[16]

There are several approaches to characterize the initiation of smoldering and flaming combustion. Temperature change is one of the most common methods used to identify the initiation of combustion processes, as ignition normally accompanies a strong increase in temperature due to the

Received: February 6, 2016
Revised: July 27, 2016
Published: July 28, 2016

DOI: 10.1021/acs.energyfuels.6b00314
Energy Fuels 2016, 30, 7666−7677

onset of exothermic reactions. It has been suggested that temporal temperature profiles can be a good indicator of the onset of strong exothermic reactions; however, the onset of exothermic reactions does not necessarily signify the initiation of smoldering or flaming combustion. Hence, it is difficult to reliably distinguish the initiation of smoldering and flaming combustion by using only the temperature profiles.

It has been demonstrated that smoldering ignition can be divided into three stages on the basis of mass loss profiles;[15] however, mass loss profiles have little real-world application since it is difficult to take mass loss measurements of smoldering samples outside of the laboratory because of limited measuring capacity and high external disturbances. This highlights the need for an alternative indicator to distinguish the initiation of smoldering and flaming combustion of biomass fuel.

It has been suggested that the concentrations of product gases could be used to distinguish the initiation of smoldering and flaming combustion.[17] However, the concentrations of product gases depend on many factors, including the fuel type, oxygen concentration, and experimental apparatus. Furthermore, data on the product gas concentrations in biomass fuel are still limited, and as yet smoldering and flaming combustion regimes cannot be accurately characterized by the product gas concentrations alone. Hence, in comparison with the temperature and mass loss profiles, gas analysis could be a promising method of identifying the initiation of smoldering.

The purpose of this study is to characterize the smoldering and flaming regimes in the combustion of biomass, since smoldering combustion has scarcely been quantitatively defined or compared with flaming combustion in biomass fuel. Although smoldering combustion has been widely studied, the understanding of the initiation of smoldering combustion still relies on observations of phenomena, such as smoke and glowing char, rather than quantitative characterization.[18] This lack of understanding increases the difficulty of predicting and detecting the initiation of smoldering combustion. Hence, it is important to know what the indications of smoldering combustion are and how to quantify them. The experiments reported in this study are designed to characterize smoldering and flaming combustion using temporal and spatial temperature profiles, mass loss profiles, and gas analyses and to determine the required conditions, air flow velocities, and radiant heat flux levels for the smoldering and flaming combustion regimes.

2. METHODOLOGY

2.1. Experimental Apparatus. The experimental testing rig consisted of four main parts: an infrared heater, a smoldering reactor, thermocouples, and a laboratory balance (Figure 1). An infrared heat lamp (model 5306B, Research Inc., Eden Prairie, MN, United States) was placed above the smoldering reactor to heat the testing sample. Multiple thermocouples were installed to measure the temporal and spatial temperature changes in the reactor. A laboratory balance (GX-600, A&D Ltd., Tokyo, Japan) with a maximum total loaded mass of 610 g and a precision of ±0.01 g was used to measure the mass of the testing sample during the experiment. The combined weight of the reactor (211 g) and the biomass sample was below the maximum load of the balance. Additionally, a heat shield made of aluminum was used to protect the balance from the radiation. The experimental apparatus was designed to initiate smoldering and flaming

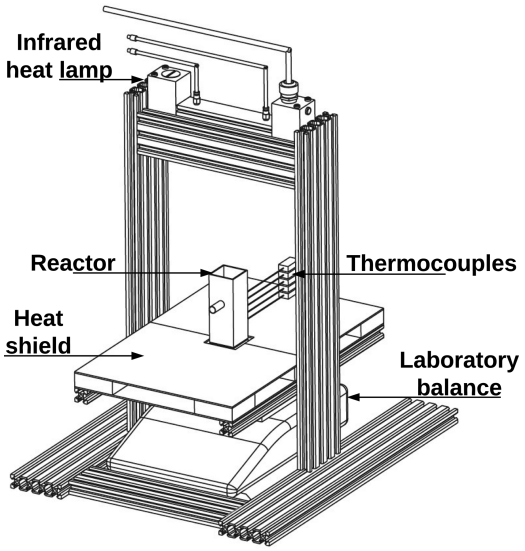

Figure 1. Experimental testing rig.

combustion under different presetting conditions, including radiant heat flux and air flow velocity.

2.2. Smoldering Reactor. A perspective view of the smoldering reactor is shown in Figure 2. The reactor has an air

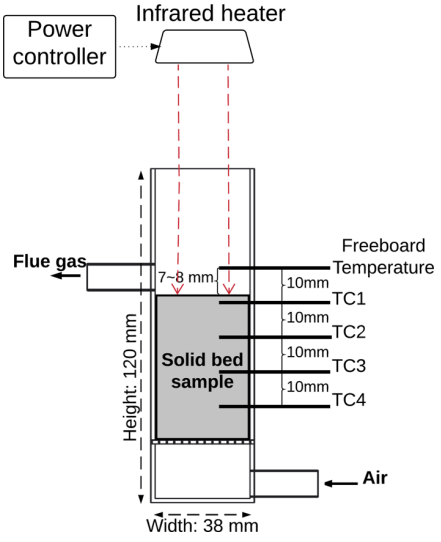

Figure 2. Schematic diagram of the experimental testing rig.

input near the bottom, a gas output for sampling the product gas, and a mesh inside to distribute the air flow and support the biomass fuel sample. The reactor has a square cross section of 1444 mm^2 and a height of 120 mm (Figure 2).

2.3. Experimental Setup. The electrical power input into the heat lamp was a controlled variable during the experiments, spanning the range from 300 to 750 W, which gives a radiant heat flux range of 5 to 27.5 $kW{\cdot}m^{-2}$ at the position of the fuel bed surface (measured with a 64-series heat flux sensor, Medtherm Corp., Huntsville, AL, United States). The irradiance of 27.5 $kW{\cdot}m^{-2}$ was selected as the maximum radiant heat flux level because it is typical of that encountered during wildfires.[19,20] The input of the reactor was connected to an air compressor. The air flow velocity was adjustable, and the

DOI: 10.1021/acs.energyfuels.6b00314
Energy Fuels 2016, 30, 7666−7677

oxygen concentration could be modified by introducing nitrogen. A gas analyzer (Testo 350, Testo AG, Lenzkirch, Germany) was connected to the output of the reactor directly and used to measure the CO, CO_2, and O_2 contents in the product gas. On the basis of the specifications of the gas analyzer, the response times for the CO sensor (40 s) and CO_2 sensor (10 s) and the transport delay (~4.6 s) were taken into account when analyzing the data.

2.4. Thermocouple Location. Five 1 mm diameter type-K thermocouples (TC-Direct) were installed in the reactor; the thermal response of the thermocouples was approximately 200 °C·s^{-1}. As shown in Figure 2, the space between adjacent thermocouples was constant (10 mm). One thermocouple was placed approximately 7−8 mm above the fuel bed (labeled "Freeboard Temperature" in Figure 2). This thermocouple measured the freeboard gas temperature above the biomass bed. One thermocouple (TC1 in Figure 2) was buried in the fuel bed, 2−3 mm beneath the fuel surface (below one pine chip particle). This thermocouple was used to measure the temperature of fuel particles that are close to the fuel bed surface.

2.5. Preparation of the Biomass Fuel. Pulverized and dried radiata pine chips were used as fuel in this study, as radiata pine is a common vegetation type. To reduce variability between samples, the pine chips were milled, sieved (2 mm < d < 3 mm, where d is the sieve mesh size) and then dried in an oven at 105 °C for 24 h, consistent with previous studies.[21] The mass of the biomass sample used in each test was 10 g. The proximate and ultimate analyses of the pine chips are shown in Table 1. The oxygen measurement in the ultimate analysis was calculated by the difference in the ash-free dry weight.

Table 1. Proximate and Ultimate Analyses of Radiata Pine Chips

proximate analysis[a] [wt %, wet basis]				ultimate analysis [wt %, dry ash-free basis]			
moist.	VM	FC	ash	C	H	O	N
3.51	80.02	16.16	0.31	51.39	6.25	42.18	0.18

[a]Abbreviations: moist., moisture; VM, volatile matter; FC, fixed carbon.

2.6. Experimental Procedures. Before the experiment started, the milled and sieved fuel was weighed and loaded into the reactor. The input air flow velocity was then set to a corresponding value, and an aluminum shutter was placed above the reactor to block the radiation. The experiments were started by first setting the corresponding radiant heat flux from the infrared heater by adjusting a Variac transformer. Once the adjustment was completed, recording of the temperature, mass change, and product gas concentrations commenced. Then the aluminum shutter was taken away, and the fuel bed was heated by the infrared heater directly. During the experiment, the testing sample was heated for 25 min or until smoldering/flaming combustion occurred. The experiments investigated the different combustion regimes under different combinations of air flow velocity and radiant heat flux. In each experiment, only one variable was changed at a time. In the first set of experiments, the flow velocity of input air was kept constant, and only the level of radiant heat flux was varied to study the effect of the radiant heat flux on the initiation of different combustion processes. The radiant heat flux level was a factor varied between 5 and 27.5 kW·m^{-2} (10 settings with a 2.5 kW·m^{-2} interval). In the second set, the radiant heat flux was kept constant, and the air flow velocity was varied to study the effect of the air flow velocity on the initiation of different combustion processes. The air flow velocity was a factor with four possible settings. The main purpose of the experiment was to investigate the range of combinations and factors that lead to different regimes of combustion processes, such as no ignition, smoldering, and flaming. For example, if no ignition occurred at a particular heat flux level and air flow velocity, then it was considered that no ignition will occur at this air flow velocity if the heat flux level is below that particular value. Hence, the experiment was not full factorial. A summary of the experimental runs is shown in Table 2.

Table 2. Summary of Experimental Runs

case	air flow velocity (mm·s^{-1})	heat flux level (kW·m^{-2})	results
1	11.5	5	no ignition
2	11.5	7.5	smoldering
3	11.5	25	smoldering
4	11.5	27.5	smoldering
5	20.8	10	no ignition
6	20.8	12.5	no ignition
7	20.8	15	no ignition
8	20.8	17.5	smoldering
9	20.8	20	smoldering
10	20.8	25	smoldering
11	20.8	27.5	flaming
12	38.1	17.5	no ignition
13	38.1	20	smoldering
14	38.1	25	flaming
15	38.1	27.5	flaming
16	55.4	20	no ignition
17	55.4	22.5	no ignition
18	55.4	25	no ignition
19	55.4	27.5	flaming

Multiple experiments under the same conditions were conducted to examine the reproducibility of the measurements. According to the results, the reproducibilities of the temperature measurement, mass loss, and gas analyses were 91%, 82%, and 87%, respectively. Although care needs to be taken in extrapolating the results of a single experiment, it is inevitable that very detailed measurements can be performed only for a limited number of cases. Also, there is substantial value in identifying what does happen in at least one case and in demonstrating an approach by which such details can be provided for other assessments.

2.7. Data Processing. A Savitzky−Golay filter was used to reduce the effect of noise on the temperature, mass loss, and gas analysis measurements. For example, the first derivatives of the temperature and gas analyses can have high noise due to the sensitivity of the sensors. Stress caused by airflow along the gas input and output lines can also cause some experimental errors in the mass change measurements.

3. RESULTS AND DISCUSSION

3.1. Smoldering Combustion. The first part of the Results shows a typical example of smoldering combustion of the pine particles in this study (case 8 in Table 2). In order to distinguish between the initiation of different combustion regimes using temperature, a thermocouple was installed above the biomass fuel bed to measure the freeboard (FB)

DOI: 10.1021/acs.energyfuels.6b00314
Energy Fuels 2016, 30, 7666−7677

temperature. Figure 3a shows that the freeboard temperature is surpassed by the TC1 temperature during the ignition period

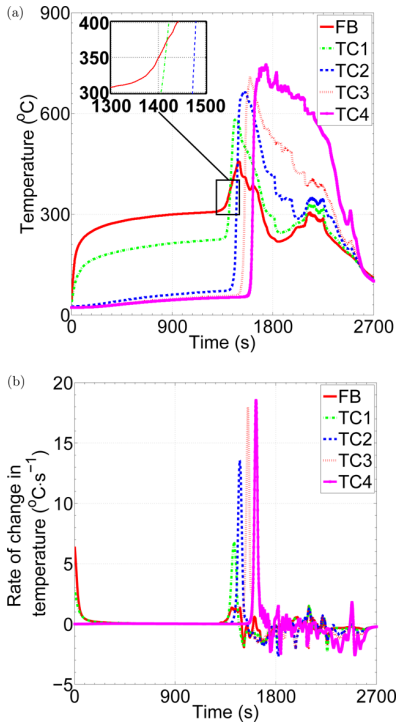

Figure 3. Temporal and spatial profiles of (a) temperature and (b) rate of temperature change for smoldering combustion (case 8, heat flux = 17.5 kW·m^{-2}, flow velocity = 20.8 mm·s^{-1}). FB denotes the freeboard thermocouple, and TC1−TC4 are the thermocouples at positions 1−4 of the reactor, respectively.

(1400 to 1500 s) and that the peak measured FB temperature (456 °C) is lower than that of TC1 (583 °C). These results indicate that strong exothermic reactions occur in the solid phase and that the exothermic reactions in the gas phase are much weaker than those in the solid phase. Figure 3b shows that the peak temperature change rate of the FB temperature (1.35 °C·s^{-1}) is much less than that of TC1 (6.7 °C·s^{-1}) and that the peak temperature change rates of TC2−TC4 are all below 20 °C·s^{-1}. Hence, there is no strong evidence to show the onset of strong exothermic reactions above the fuel bed. Although the peak temperature of smoldering combustion is known to vary with fuel type, flow conditions, and fuel moisture content, in general the peak smoldering combustion temperature can range from 550 to 840 °C.[22−24] The results in Figure 3a show that the peak measured temperatures of TC1−TC4 lie in the aforementioned temperature range. This demonstrates that this particular example (case 8 in Table 2) is smoldering combustion in terms of peak temperature.

As shown in Figure 3, both the temperatures and the temperature gradients increase as the smolder front propagates through the testing sample. This occurs because smoldering combustion preheats the reactor and reduces the heat loss from the combustion region to the reactor wall. In Figure 3a, it can be seen that the temporal temperature profile of the fourth thermocouple (TC4) shows a distinct pattern compared with the other thermocouples. In the temporal temperature profile of the other thermocouples (TC1−TC3), as a smolder front propagates through these thermocouple locations, the temperature rapidly increases and reaches the peak value, and then the temperature decreases quickly when the smolder front is away from the thermocouples. In the temporal temperature profile of the fourth thermocouple (TC4), the temperature starts to increase as the smolder front propagates past the thermocouple and reaches a peak value (750 °C). After reaching the peak temperature, the temperature decreases more slowly than those measured by the other thermocouples. During smoldering combustion, both pyrolysis and char oxidation reactions lead to shrinkage of the fuel bed,[25,26] and char accumulates in the bottom of the reactor. As the char continues to burn after the smolder front propagates past TC4, the temperature profile of TC4 is different from those of the other thermocouples. It has previously been demonstrated in a model that shrinkage of the fuel bed can have a significant effect on the temperature of smoldering combustion.[27] The effect is that the shrinkage factor (i.e., the ratio of the changes in the volumes of ash and char) reduces the rate of decrease in temperature in smoldering combustion.[27]

Figure 4 shows examples of the temporal profiles of the concentration and concentration change rate for CO_2 in

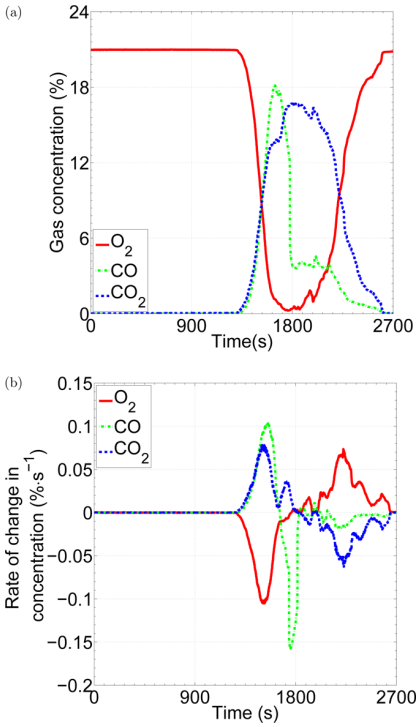

Figure 4. Temporal profiles of (a) gas concentrations and (b) rates of change of gas concentrations for smoldering combustion (case 8, heat flux = 17.5 kW·m^{-2}, flow velocity = 20.8 mm·s^{-1}).

smoldering combustion. The temporal CO_2 profile can be divided into three stages, similar to the stages in the oxygen and CO profiles. The first stage is from 1300 to 1650 s, where the concentration of CO_2 increases at a high rate; the second stage is from 1650 to 1900 s, where the CO_2 concentration is close to a peak value (~16.5%) and remains at this level during this stage; the third stage (char combustion stage) is from 1900 to 2600 s, where the CO_2 decreases gradually to zero. The results in Figure 4 also show that there is correlation between the CO_2 and oxygen concentrations. It is noteworthy that the

DOI: 10.1021/acs.energyfuels.6b00314
Energy Fuels 2016, 30, 7666−7677

concentrations of CO and CO_2 in Figure 4a are not the same in the first 1300 s. The concentration of CO actually increased from 0 to 160 ppm while the concentration of CO_2 stayed at the same level (0.05%) in the first 1300 s. The change of CO in the first 1300 s is due to the release of volatile matter from the surface of the fuel bed before the smoldering ignition.

Figure 5 shows the temporal profiles of the mass loss and the mass loss rate for the smoldering combustion. Four stages of

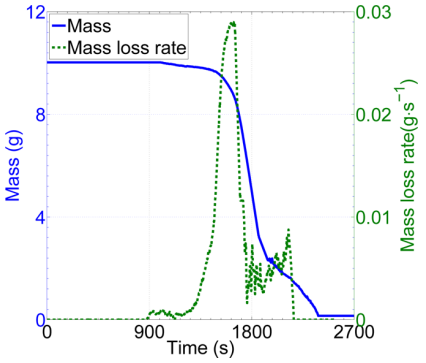

Figure 5. Temporal profiles of the mass loss and the mass loss rate for smoldering combustion (case 8, heat flux: 17.5 kW·m^{-2}; flow velocity: 20.8 mm·s^{-1}).

mass loss can be found in the smoldering combustion: (1) a zero mass loss stage (0−1400 s), (2) a low mass loss stage (1400−1700 s), (3) a high mass loss stage (1700−1950 s), and (4) a medium mass loss stage (1950−2400 s). The first stage is also called the preheating stage, and the mass loss is minimal in this stage because the fuel sample had been completely dried. In the next stage, exothermic reactions start to occur, corresponding to where the thermocouple temperatures start to increase (Figure 3a) during aided smoldering combustion. In the third stage, the mass loss rate is high and the peak mass loss rate is about 0.027 g·s^{-1}, which indicates that the fuel sample is quickly combusted by strong reactions; smoldering combustion is self-sustained in this stage. In the last stage, the mass loss rate decreases to a relatively low value (~0.005 g·s^{-1}).

The temporal profile of the ratio of CO to CO_2 is shown in Figure 6. The peak ratio of CO to CO_2 is 1.3, which occurs at 1650 s (the end of the first stage). According to the three stages in the oxygen and CO_2 concentration profiles, the ratio of CO to CO_2 is between 0.2 and 1.3 for smoldering combustion and

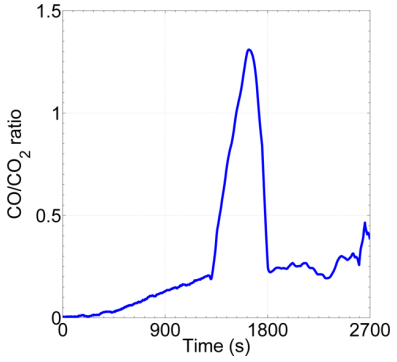

Figure 6. Temporal profile of the ratio of CO to CO_2 for smoldering combustion (case 8, heat flux = 17.5 kW·m^{-2}, flow velocity = 20.8 mm·s^{-1}).

between 0.2 and 0.5 for char combustion. While the peak CO to CO_2 ratio for smoldering combustion in this study was 1.3, the average ratio was 0.27, which is comparable to those of peat and biomass.[28−32] The difference may be because the pine chips have a higher volatile content, which can produce higher yields of CO and CO_2 during pyrolysis.

3.2. Flaming Combustion. This section shows the results of a typical example of the flaming combustion of pine chips (case 15 in Table 2). Figure 7a shows that the temperature of

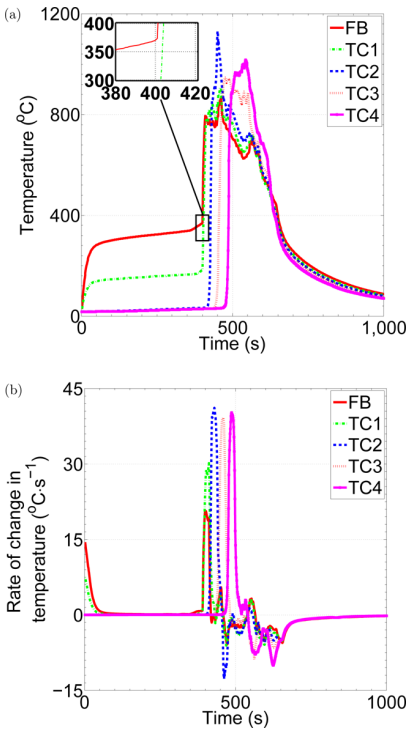

Figure 7. Temporal and spatial profiles of (a) temperature and (b) rate of temperature change for for flaming combustion (case 15, heat flux = 27.5 kW·m^{-2}, flow velocity = 38.1 mm·s^{-1}). FB denotes the freeboard thermocouple, and TC1−TC4 are the thermocouples at positions 1−4 of the reactor, respectively.

the FB thermocouple increases before the temperature of TC1. Compared with the peak freeboard temperature in smoldering combustion (456 °C), the peak freeboard temperature in flaming combustion (865 °C in this case) is much higher. This would imply that strong exothermic reactions occur in the gas phase above the fuel bed in flaming combustion. In this case, the peak temperature measured at TC2 is 1131 °C at 450 s, and the peak measured temperatures of FB and TC1 also occur at around this time (Figure 7a). These results indicate that strong exothermic reactions occur near TC2 and that the heat produced by the exothermic reactions increases the temperatures of FB and TC1, which are 20 and 10 mm away from TC2, respectively. The peak temperatures of TC1−TC4 are all above 900 °C, which are higher than the peak temperature of the smoldering combustion case (745 °C). This indicates that the exothermic reactions in this example are stronger than those in the smoldering combustion case.

Figure 7b shows that the temperature change rates of FB and TC1−TC4 range from 20.7 to 41.2 °C·s^{-1}. The peak rate of temperature increase of FB in this study (20.7 °C·s^{-1}) is higher than the peak rate of temperature increase in the smoldering

DOI: 10.1021/acs.energyfuels.6b00314
Energy Fuels 2016, 30, 7666−7677

combustion case (18.5 °C·s^{-1}) and is ∼15 times higher than that of the FB of the smoldering combustion case (1.35 °C·s^{-1}). These results indicate that the heat release in this case is much faster than that in the smoldering combustion case. The peak temperatures of smoldering and flaming combustion are 550−840 °C and 1500−1800 °C, respectively, in the literature, while the peak temperature of flaming combustion reported in this study is only 900 °C.[28,33,34] The difference is due to the fact that in this study combustion takes place inside a reactor, and the oxygen availability is limited by the air flow velocity. In the flaming combustion cases in this study, there is not enough oxygen to complete the combustion reactions. The results in Figure 8a show that oxygen is almost consumed after the ignition and that the concentration of CO is high during flaming combustion, which indicates incomplete combustion.

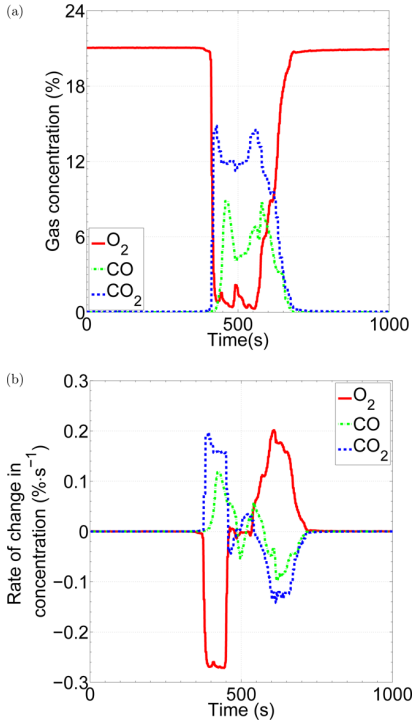

Figure 8. Temporal profiles of (a) gas concentrations and (b) rates of change of gas concentrations for flaming combustion (case 15, heat flux = 27.5 kW·m^{-2}, flow velocity = 38.1 mm·s^{-1}).

As shown in Figure 8a, the oxygen concentration starts to decrease at about 400 s and reaches a low value (∼0.5%) at 472 s. Hence, the oxygen is almost consumed in about 72 s, whereas in the smoldering combustion case it takes 410 s to reach the same low oxygen concentration (Figure 4a). This shows that the oxidation reactions in the flaming cases are stronger than those in the smoldering combustion cases. The oxidation reactions in smoldering combustion are mainly char combustion, which is in the solid phase, while the oxidation reactions in flaming combustion include both solid-phase and gas-phase reactions. Figure 8a shows that the peak concentration of CO in flaming combustion is 8.8% and that it takes about 88 s for the CO concentration to increase from zero to this peak value. In contrast, in the smoldering combustion case shown in Figure 4a, the CO concentration takes about 393 s to increase from zero to its peak concentration of 18.1%. This result indicates that some of the CO is consumed in the flaming combustion case. As shown in Figure 8b, the temporal profile of the rate of change of the CO_2 concentration is inversely correlated with that of the oxygen concentration. This indicates that the consumption of oxygen has a connection with the yield of CO_2.

Figure 9 shows the temporal profiles of the mass loss and the mass loss rate of the flaming combustion. Three stages of mass loss can be defined in the flaming combustion: (1) a zero mass loss stage (0−400 s), (2) a high mass loss stage (400−600 s), and (3) a medium mass loss stage (600−750 s). Compared with smoldering combustion, flaming combustion does not have a low mass loss stage. The mass of sample starts to decrease dramatically at 400 s, and this time also corresponds to the time of the onsets of the sudden temperature increase (Figure 7a) and the sudden oxygen concentration drop (Figure 8a). These all indicate that strong exothermic reactions accompany pyrolysis during the initiation of flaming combustion. Figure 9 shows that the peak mass loss rate of biomass fuel in flaming combustion (∼0.59 g·s^{-1}) is much higher than that in smoldering combustion (∼0.027 g·s^{-1}). The results in Figure 10 show that an increase in air flow velocity increases the time to smouldering ignition, and the mass loss rate. This is because that increasing air flow velocity increases the convective heat loss and oxygen availability. An increase in oxygen availability would promote char combustion, which leads to a higher heat release and mass loss rate. Figure 11 shows three distinct stages of flaming combustion based on the

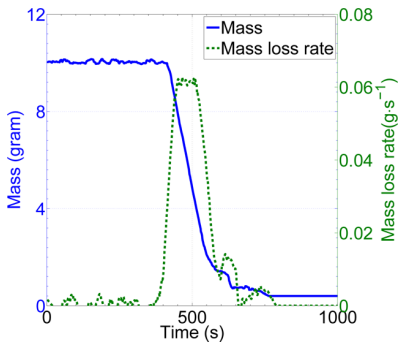

Figure 9. Temporal profiles of the mass loss and the mass loss rate for flaming combustion (case 15, heat flux = 27.5 kW·m^{-2}, flow velocity = 38.1 mm·s^{-1}).

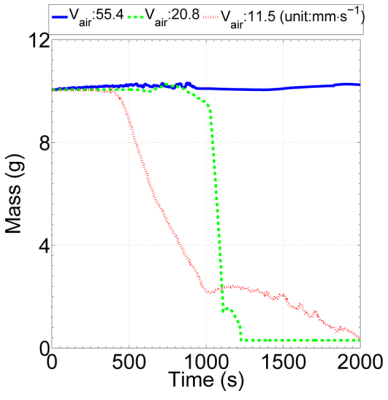

Figure 10. Effects of air flow velocity (V_{air}) on the mass of the remaining sample (heat flux = 25 kW·m^{-2}).

DOI: 10.1021/acs.energyfuels.6b00314
Energy Fuels 2016, 30, 7666−7677

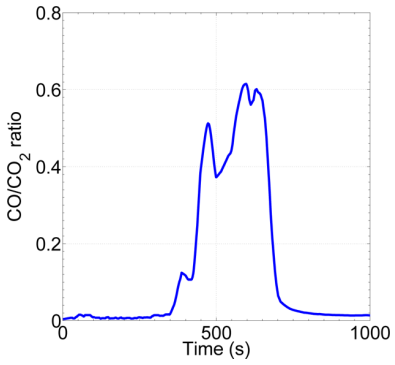

Figure 11. Temporal profile of the ratio of CO to CO_2 for flaming combustion (case 15, heat flux = 27.5 kW·m^{-2}, flow velocity = 38.1 mm·s^{-1}).

temporal profile of the ratio of CO to CO_2. In the first stage (0−350 s), the ratio of CO to CO_2 fluctuates around 0.013. In the second stage (350−800 s), the ratio of CO to CO_2 dramatically increases, reaching a peak value of 0.62 at 597 s, and then dramatically decreases to a low value of 0.02 at 800 s. In the third stage (800−1000 s), the ratio of CO to CO_2 fluctuates around 0.013. As shown in Figure 11, the temporal ratio of CO to CO_2 in flaming combustion is between 0.01 and 0.62.

3.3. Combustion Regimes of Biomass. Examples of temporal profiles of temperature for biomass under different combustion regimes are shown in Figure 12. The results in Figure 12a show the temporal profiles of the freeboard temperature of smoldering combustion under different conditions. In cases 3 and 10, in which the radiant heat flux was kept at a high value (25 kW·m^{-2}), an increase in air flow velocity slightly increased the peak FB temperature of smoldering combustion (from 520 to 580 °C). In cases 9 and 13, in which the radiant heat flux was kept at a lower value (20 kW·m^{-2}), the peak temperatures of smoldering combustion were both above 600 °C. Overall, Figure 12a shows that the air velocity does not have a significant effect on the peak FB temperature in smoldering combustion. The time to ignition is considered as a sudden increase in temperature. Figure 12a shows that an increase in air flow velocity increases the time to ignition in smoldering combustion. This is the case because an increase in air velocity increases convective heat loss.

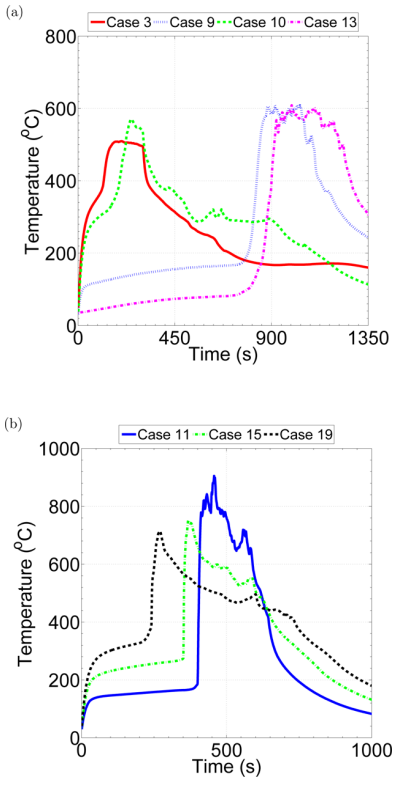

Figure 12. Comparison of temporal profiles of the freeboard temperature under (a) smoldering and (b) flaming conditions; see Table 2 for description of experimental conditions for each case.

Figure 12b shows temporal profiles of the freeboard temperature of flaming combustion under different conditions. In cases 11, 15, and 19, in which the radiant heat flux was kept constant (27.5 kW·m^{-2}), an increase in air flow velocity increased the peak FB temperature of flaming combustion. This occurred because increasing the air velocity could promote the combustion of volatile gases, releasing more heat via exothermic combustion reactions. It is noticed that an increase in air flow velocity decreases the time to ignition in flaming combustion. The results in Figure 12 indicate that the peak freeboard temperature in smoldering combustion of pine chips is normally between 500 and 600 °C, while the peak freeboard temperature in flaming combustion of pine chips is between 700 and 900 °C. This suggests that the freeboard temperature could be used as an indicator of smoldering or flaming combustion.

Figure 13 shows that the time-integrated gas concentrations for different combustion processes are different. The integrated gas concentrations are based on the periods of time when the gas concentration is above 100 ppm for CO and above 0.5% for CO_2. For the example of no ignition, the integrated gas concentration of CO is negligible, and the integrated gas concentration of CO_2 is close to zero. In smoldering combustion, the integrated gas concentration of CO (4.03%) is about 1.5 times the integrated gas concentration of CO_2 (2.74%). Overall, Figure 13 shows that the time-averaged integrated gas concentrations of CO and CO_2 in smoldering combustion are much lower than those in flaming combustion. This is the case because the time required for complete smoldering combustion is longer than that for flaming combustion for the same amount of fuel. The results also show that the time-averaged integrated gas concentration of

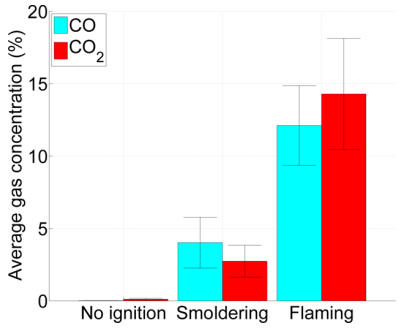

Figure 13. Comparison of the time-averaged integrated gas yields for different types of combustion. The error bars represent the average standard deviation for each combustion regime.

DOI: 10.1021/acs.energyfuels.6b00314
Energy Fuels 2016, 30, 7666−7677

CO is higher than that of CO_2 in smoldering combustion. However, in flaming combustion the time-averaged integrated gas concentration of CO is high (12.1%), although it is lower than the CO_2 concentration (14.3%). This suggests that a large amount of CO is not consumed in flaming combustion, possibly because CO produced during pyrolysis and char combustion cannot be combusted because of the low oxygen concentration experienced in this experimental setup.

Three combustion regimes of biomass combustion, including no ignition, smoldering, and flaming combustion, can be achieved by varying the air flow velocity and the radiant heat flux. The results presented in Figure 14 indicate that

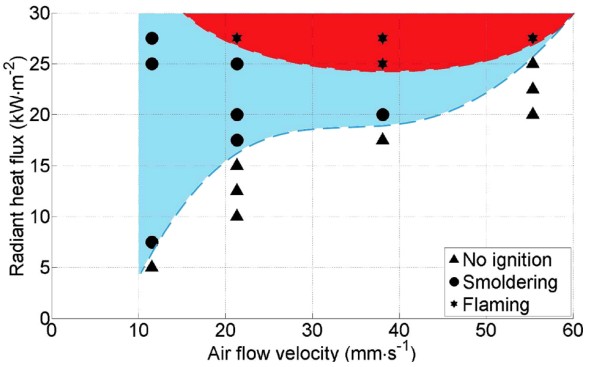

Figure 14. Interactive effects of air flow velocity and radiant heat flux on the initiation of different combustion processes. The red area indicates conditions under which flaming combustion will occur, while the blue area indicates conditions under which smoldering combustion will occur.

smoldering combustion is prone to be initiated at low air flow velocities (<40 mm·s^{-1}) while flaming combustion preferentially occurs at high air flow velocities (>40 mm·s^{-1}) under the conditions used in this experiment. However, this depends on the level of energy provided. For example, at a heat flux level of 25 kW·m^{-2}, smoldering combustion can be initiated at low flow velocities (≤20.8 mm·s^{-1}), flaming combustion at a medium flow velocity (38.1 mm·s^{-1}), and no ignition at high flow velocities (≥58.1 mm·s^{-1}).

3.4. Further Discussion and Analysis. The majority of previous studies on the gas emissions of smoldering combustion have been conducted only on polyurethane foam and peat because of their importance to residential fires and peat fires. Data on CO/CO_2 ratios of the smoldering combustion of other biomasses are still lacking. Peat is closer to biomass than to polyurethane foam. Hence, peat was chosen to compare with the results in this study. The data in Table 3 from various literature studies show that the ratio of CO to CO_2 is between 0.01 and 0.62 for flaming combustion and between 0.12 and 4 for smoldering combustion of peat. The CO/CO_2 ratio is relatively low in flaming combustion because volatile matter was combusted in flaming combustion cases as a result of high oxygen availability. Conversely, in smoldering combustion, a large amount of volatile matter is not combusted because of low oxygen availability and low temperature. Hence, the CO/CO_2 ratio is high. The CO/CO_2 ratios for smoldering and flaming combustion in the current study are relatively higher than those reported in the literature (Table 3). This is likely caused by the type of fuel and the experimental approach. According to the proximate analysis (Table 1), radiata pine has

Table 3. CO/CO_2 Ratios in Small-Scale Experiments

combustion regime	fuel type	CO/CO_2	reference
flaming	vegetable fibers	0.17−0.6	Kallonen (1985)[36]
flaming	biomass	0.01−0.6	Prager (1987)[37]
flaming	plywood	~0.02	Tsuchiya (1991)[38]
smoldering	peat	0.2−4	Arpiainen (1989)[39]
smoldering	peat	~0.3	Hadden (2011)[28]
smoldering	peat	0.3−0.9	Rein et al. (2009)[33]
smoldering	peat	0.12	Christian et al. (2003)[33]
smoldering	peat	0.19−0.28	Yokelson et al. (1997)[33]
smoldering	peat	0.12	Akagi et al. (2011)[33]
smoldering	pine chips	1.3	current work
flaming	pine chips	0.62	current work

a high percentage of volatile matter. In this study, the testing sample was combusted in a closed reactor, the combustion process was supported by the inlet air, and incomplete combustion occurs when the supply of air is limited.

A combustion progress pathway diagram (Figure 15) has been developed to help understand the different regimes of combustion in a single dry biomass particle. In smoldering combustion, the yields of CO and CO_2 are mainly from two sources: pyrolysis of the fuel and char combustion. During the fuel pyrolysis, a large amount of volatile matter, including CO and CO_2, are released, and biomass fuel is converted into char. The oxygen is not consumed in the pyrolysis stage. If the heating is ceased in this stage, no ignition will occur. The volatile matter (including CO) is not combusted in smoldering combustion because of the absence of strong gas-phase reactions. At the same time, char oxidation also produces CO and CO_2.[35] CO and CO_2 in smoldering combustion is actually a mixture of the product gases from both pyrolysis and char oxidation. The oxygen in smoldering combustion is mainly consumed by char oxidation to form CO and CO_2. In smoldering combustion, there is no strong CO oxidation because of the low oxygen availability and low temperature, leading to the high concentration of CO in the product gas. In this study, the oxygen concentration during the smoldering combustion dropped to zero, which indicates that there was insufficient oxygen for gas-phase reactions. The oxygen availability is dependent on the air flow velocity; hence, the smoldering combustion in this study could only be initiated at low air flow velocities.

In flaming combustion, three processes involve the yield of CO. First, fuel pyrolysis produces char and releases volatile matter, including CO, and char oxidation also produces CO and CO_2. The volatile matter and the product gases of char oxidation then form a combustible mixture, and flaming combustion starts once enough heat is present. In flaming combustion, CO is combusted to CO_2 via gas-phase oxidation. The conversion of CO to CO_2 in the gas-phase reactions mainly depends on the temperature, oxygen concentration, and residence time.[35] In this study, CO was not combusted because of the low temperature, low oxygen availability, and short residence time. For these reasons, the concentration of CO and the CO to CO_2 ratio in the flaming combustion cases in this study are higher than reported in the literature (Table 3). Flaming combustion requires greater oxygen availability and heat for gas-phase reactions than are required for smoldering combustion. Hence, flaming combustion in this study occurs only under high air flow velocity and high heat flux conditions.

DOI: 10.1021/acs.energyfuels.6b00314
Energy Fuels 2016, 30, 7666−7677

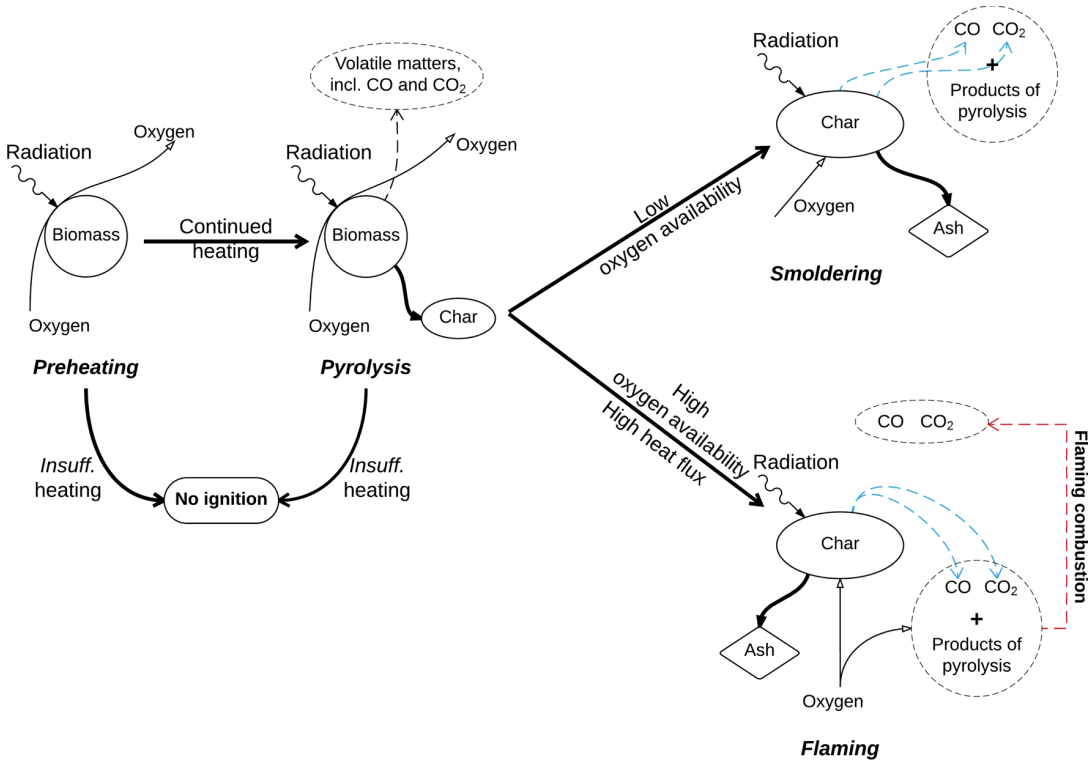

Figure 15. Combustion progress pathway diagram for smoldering/flaming combustion of a single dry biomass fuel particle.

In order to provide a better understanding of the differences between the smoldering and flaming combustion regimes, an analysis of the combustion kinetics (activation energy and pre-exponential factor) and an energy balance analysis were performed for the ignition stage. In this study, the ignition stage is the reaction of the top layer of the fuel bed at the start of combustion (see the Supporting Information for more details). The activation energy and pre-exponential factor during the ignition stage were calculated based on the global mass balance (eq 1) and the Arrhenius equation (eq 2). The rate of combustion, k, at any time t is given by

$$k(t) = -\frac{\partial W(t)}{\partial t}/(W_0 - W_f) \quad (1)$$

where $W(t)$ is the mass of the sample at time t, W_0 is the initial mass of the sample, and W_f is the final mass of the sample. The temperature dependence of k is given by the Arrhenius equation (in logarithmic form):

$$\ln(k) = \ln(A) - \frac{E_a}{RT} \quad (2)$$

By means of eq 1, the combustion rate k was calculated from the experimental mass loss versus time data. By association of the temperature of the top layer of the bed, TC1, with the combustion rate at a given time, the natural logarithm of the combustion rate was related to the reciprocal of temperature for each experimental data set. By means of eq 2, the activation energy and pre-exponential factor were then determined for each experiment. Figure 16 shows plots of $\ln(k)$ versus $1/T$ for examples of flaming and smoldering combustion. Table 4 shows the ranges of activation energy and pre-exponential factor values determined from the entire data set.

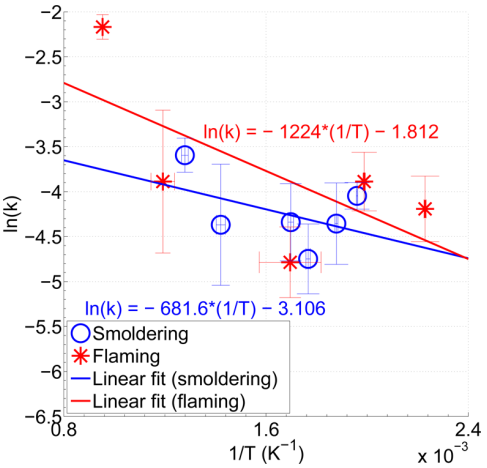

Figure 16. Arrhenius plots for examples of smoldering and flaming combustion of radiata pine (smoldering, case 8; flaming, case 15). Error bars represent the standard deviation at each point.

Table 4. Kinetic Parameters Obtained from Linear Fits of the Experimental Data for the Smoldering Cases and Flaming Cases (Activation Energies E_a in kJ·mol^{-1}, Pre-exponential Factors A in s^{-1})

parameter	smoldering	flaming
E_a	2.9−11.0	7.8−12.4
A	0.019−0.20	0.093−0.14

The evaluated activation energy for the smoldering combustion of radiata pine (2.9−11.0 kJ·mol^{-1}) is smaller than that for the pyrolysis reaction of pine sawdust reported in

DOI: 10.1021/acs.energyfuels.6b00314
Energy Fuels 2016, 30, 7666−7677

the literature (Table 5). The discrepancy between these two values is mainly a result of the fact that the pyrolysis experiment was conducted in nitrogen whereas the combustion processes in this study were conducted in air. From Figure 15 it can be seen that char and volatile matter start to combust in the presence of sufficient oxygen. The oxidation of char and volatile matter have significant effects on the evaluated activation energy. As shown in Figure 16, the combustion rate for flaming combustion is higher than that for smoldering combustion at a given temperature. From the experimental results shown in Figure 14, flaming combustion occurred only at high flow velocities (>55.4 mm·s^{-1}) and smoldering combustion occurred only at low flow velocities (<38.1 mm·s^{-1}). The temperature of the top layer of the fuel bed was assumed to be equal to the temperature of TC1, which was located 2−3 mm underneath the surface of the fuel bed. In flaming combustion cases (high flow velocities), the convectional heat loss from TC1 was higher than that in smoldering combustion cases (low flow velocities). Hence, the actual surface temperature in flaming combustion cases could be expected to be higher than the TC1 temperature, and a higher temperature leads to a higher combustion rate. Thus, the difference between the rates of combustion in smoldering and flaming combustion shown in Figure 16 could be a result of inaccuracies in the measurement of the fuel bed temperature and not necessarily a true difference in temperature-dependent kinetics. Interestingly, the evaluated activation energy for the smoldering combustion of radiata pine is similar to that of the flaming combustion (7.8−12.4 kJ·mol^{-1}). The activation energy was calculated on the basis of the mass loss rate and the temperature. Theoretically, the mass loss of the top layer of the fuel bed can be attributed to char combustion and pyrolysis of the virgin fuel. According to the proximate analysis of the fuel (Table 1), radiata pine contains a high percentage of volatile matter (80.02%). In other words, the rate of pyrolysis would be expected to have a much more significant effect on the mass loss rate than the rate of char combustion. It is likely that the rates of pyrolysis in the initiation of smoldering and flaming combustion were close, with any differences likely being caused by the accuracy of the fuel bed temperature measurements (as discussed previously). The evaluated activation energy for the smoldering combustion of radiata pine (2.9−11.0 kJ·mol^{-1}) is also similar to the reported activation energy for the smoldering combustion of softwoods (Table 5).

Table 5. Activation Energies (in kJ·mol^{-1}) of Wood in the Literature

	wood species	E_a (kJ·mol^{-1})	reference
smoldering combustion of sawdust	softwoods	13.7	Ohtani et.al. (1991)[40]
pyrolysis reaction of wood	pine sawdust	102.1	Biagini et.al. (2002)[41]

An energy balance analysis of the system during the ignition stage for smoldering and flaming combustion was calculated in order to determine the heat release rate per unit mass of fuel based on the temperature, mass change, and product gas concentration measurements. The energy balance analysis was based on a simplified energy balance equation in which the energy input equals the sum of the energy output into the gas phase and heat losses. The energy input includes the heat released by the combustion of the fuel and the enthalpy/sensible heat of the product gas at the beginning of the ignition stage. The heat output is the integral of the enthalpy/sensible heat of the product gas during the ignition stage. The heat losses include the radiative heat loss through the surface of the fuel bed, the convective heat loss through the reactor wall, and the conductive heat loss away from the top layer of the fuel bed. Further elaboration of the energy balance calculation is provided in the Supporting Information. The average heat release rate per unit mass of fuel for smoldering combustion (46.8 W·g^{-1}) is much smaller than that for flaming combustion (217.0 W·g^{-1}). According to Figure 15, the heat generated from smoldering combustion is mainly produced by char combustion, whereas the heat generated from flaming combustion is released by both the combustion of volatile matter and char combustion. Hence, the average heat release rate per unit mass of fuel is considerably higher during flaming combustion.

4. CONCLUSIONS

Smoldering combustion is a hazard in wildfires, but it is difficult to detect the initiation of smoldering combustion because it does not have any obvious indications, such as visible flame or high temperature. In addition to this, the lack of understanding of the required conditions for the initiation of smoldering combustion limits the ability to predict smoldering ignition in wildfires. The effects of air flow velocity and radiant heat flux on the initiation of different regimes of combustion processes of biomass were investigated. It was found that the different regimes of combustion, including no ignition, smoldering ignition, and flaming ignition can be achieved by varying the air flow velocity and radiant heat flux. The air flow velocity has little effect on the peak freeboard temperature of smoldering combustion but has a relatively large effect on the peak freeboard temperature of flaming combustion. Under the current experimental conditions, smoldering combustion could be initiated only when the air flow velocity was below 38.1 mm·s^{-1}, and flaming combustion could be achieved only at high air flow velocities (≥55.4 mm·s^{-1}). The regimes of combustion in biomass (no ignition, smoldering ignition, and flaming combustion) were also identified on the basis of measurements of temperature, gas emission, and mass change. The results indicate that temperature profiles can be used to distinguish smoldering and flaming ignition with the freeboard temperature. The peak CO/CO_2 ratio in smoldering combustion is approximately twice that in flaming combustion. The results on mass loss profiles show that the peak mass loss rate of flaming combustion is about twice that of smoldering combustion. However, as mass loss profiles have little real-world application, the measurement of freeboard temperature and gas emissions in the field should give a strong indication of smoldering and flaming combustion.

From combustion rate analyses (activation energy and pre-exponential factor), the activation energies for flaming and smoldering combustion were found to be similar during the ignition stage. A simplified energy balance equation was used to determine the heat release rate per unit mass of fuel. It was found that the heat release rate per unit mass of fuel for smoldering combustion (46.8 W·g^{-1}) is much smaller than that for flaming combustion (217.0 W·g^{-1}).

In this study, the initiation of smoldering combustion refers to self-sustained smoldering combustion, which is independent of external heating under the conditions investigated in the current study. As mentioned in the Introduction, there is

DOI: 10.1021/acs.energyfuels.6b00314
Energy Fuels 2016, 30, 7666−7677

another type of smoldering combustion called aided smoldering combustion, whose propagation relies on external heating. It is believed that each type of smoldering combustion requires different conditions to ignite. There is no comprehensive understanding of these two types of smoldering combustion other than their dependences on external heating. Hence, further studies will be needed to determine the required conditions for the two types of smoldering combustion and whether the same methods can be used to identify and distinguish the initiation of aided and self-sustained smoldering combustion.

■ ASSOCIATED CONTENT

Supporting Information

The Supporting Information is available free of charge on the ACS Publications website at DOI: 10.1021/acs.energyfuels.6b00314.

Description of the control volume for the kinetic parameter and energy balance analyses and simplified energy balance assumptions and analysis (PDF)

■ AUTHOR INFORMATION

Corresponding Author

*E-mail: houzhi.wang@adelaide.edu.au.

Notes

The authors declare no competing financial interest.

■ ACKNOWLEDGMENTS

The support of the University of Adelaide and the Bushfire and Natural Hazards CRC are gratefully acknowledged. The authors thank Mr. Marc Simpson for his assistance throughout the experimental campaign. We also thank three anonymous reviewers for their insightful comments and suggestions on the previous versions of the manuscript.

■ REFERENCES

(1) Murphy, B. F.; Timbal, B. A review of recent climate variability and climate change in southeastern Australia. *Int. J. Climatol.* **2008**, *28*, 859−879.

(2) Hennessy, K. J.; Lucas, C.; Nicholls, N.; Bathols, J.; Suppiah, R.; Ricketts, J. *Climate Change Impacts on Fire-weather in South-east Australia*; CSIRO Marine and Atmospheric Research: Aspendale, VIC, 2005.

(3) Poumadere, M.; Mays, C.; Le Mer, S.; Blong, R. The 2003 heat wave in France: dangerous climate change here and now. *Risk Anal.* **2005**, *25*, 1483−1494.

(4) Lucas, C.; Hennessy, K.; Mills, G.; Bathols, J. *Bushfire Weather in Southeast Australia: Recent Trends and Projected Climate Change Impacts*; Bushfire Cooperative Research Centre: East Melbourne, VIC, Australia, 2007.

(5) McKenzie, L. M.; Hao, W. M.; Richards, G. N.; Ward, D. E. Quantification of major components emitted from smoldering combustion of wood. *Atmos. Environ.* **1994**, *28*, 3285−3292.

(6) McKenzie, L. M.; Hao, W. M.; Richards, G. N.; Ward, D. E. Measurement and Modeling of Air Toxins from Smoldering Combustion of Biomass. *Environ. Sci. Technol.* **1995**, *29*, 2047−2054.

(7) Tissari, J.; Lyyränen, J.; Hytönen, K.; Sippula, O.; Tapper, U.; Frey, A.; Saarnio, K.; Pennanen, A.; Hillamo, R.; Salonen, R.; Hirvonen, M.-R.; Jokiniemi, J. Fine particle and gaseous emissions from normal and smouldering wood combustion in a conventional masonry heater. *Atmos. Environ.* **2008**, *42*, 7862−7873.

(8) Evtyugina, M.; Alves, C.; Calvo, A.; Nunes, T.; Tarelho, L.; Duarte, M.; Prozil, S. O.; Evtuguin, D. V.; Pio, C. VOC emissions from residential combustion of Southern and mid-European woods. *Atmos. Environ.* **2014**, *83*, 90−98.

(9) Prat, N.; Belcher, C.; Hadden, R.; Rein, G.; Yearsley, J. A laboratory study of the effect of moisture content on the spread of smouldering in peat fires. *Flamma* **2015**, *6*, 35−38.

(10) Ohlemiller, T. Smoldering combustion. In *SFPE Handbook of Fire Protection Engineering*, 3rd ed.; National Fire Protection Association: Quincy, MA, 2002; Chapter 9.

(11) Rein, G. Smouldering combustion phenomena in science and technology. *Int. Rev. Chem. Eng.* **2009**, *1*, 3−18.

(12) McAllister, S. Critical mass flux for flaming ignition of wet wood. *Fire Saf. J.* **2013**, *61*, 200−206.

(13) Pyne, S. J.; Andrews, P. L.; Laven, R. D. *Introduction to Wildland Fire*, 2nd ed.; John Wiley & Sons: New York, 1996.

(14) Babrauskas, V. *Ignition Handbook: Principles and Applications to Fire Safety Engineering, Fire Investigation, Risk Management and Forensic Science*; Fire Science Publishers: Issaquah WA, 2003.

(15) Anderson, M.; Sleight, R.; Torero, J. Downward smolder of polyurethane foam: Ignition signatures. *Fire Saf. J.* **2000**, *35*, 131−147.

(16) Anthenien, R.; Fernandez-Pello, A. A study of forward smolder ignition of polyurethane foam. *Symp. Combust., [Proc.]* **1998**, *27*, 2683−2690.

(17) Tsuchiya, Y. CO/CO2 Ratios In Fire. *Fire Saf. Sci.* **1994**, *4*, 515−526.

(18) Bilbao, R.; Mastral, J.; Aldea, M.; Ceamanos, J.; Betran, M.; Lana, J. Experimental and theoretical study of the ignition and smoldering of wood including convective effects. *Combust. Flame* **2001**, *126*, 1363−1372.

(19) Cruz, M. G.; Butler, B. W.; Viegas, D. X.; Palheiro, P. Characterization of flame radiosity in shrubland fires. *Combust. Flame* **2011**, *158*, 1970−1976.

(20) Silvani, X.; Morandini, F. Fire spread experiments in the field: temperature and heat fluxes measurements. *Fire Saf. J.* **2009**, *44*, 279−285.

(21) Sluiter, A.; Hames, B.; Hyman, D.; Payne, C.; Ruiz, R.; Scarlata, C.; Sluiter, J.; Templeton, D.; Wolfe, J. *Determination of Total Solids in Biomass and Total Dissolved Solids in Liquid Process Samples*; NREL Technical Report No. NREL/TP-510-42621; National Renewable Energy Laboratory: Golden, CO, 2008; pp 1−6.

(22) Rein, G.; Garcia, J.; Simeoni, A.; Tihay, V.; Ferrat, L. Smouldering natural fires: comparison of burning dynamics in boreal peat and Mediterranean humus. *WIT Trans. Ecol. Environ.* **2008**, *119*, 183−192.

(23) Hadden, R.; Rein, G. In *Coal and Peat Fires: A Global Perspective*; Stracher, G. B., Prakash, A., Sokol, E. V., Eds.; Elsevier: Amsterdam, 2011; pp 317−326.

(24) He, F.; Yi, W.; Li, Y.; Zha, J.; Luo, B. Effects of fuel properties on the natural downward smoldering of piled biomass powder: Experimental investigation. *Biomass Bioenergy* **2014**, *67*, 288−296.

(25) Anca-Couce, A. Reaction mechanisms and multi-scale modelling of lignocellulosic biomass pyrolysis. *Prog. Energy Combust. Sci.* **2016**, *53*, 41−79.

(26) Chen, H.; Rein, G.; Liu, N. Numerical investigation of downward smoldering combustion in an organic soil column. *Int. J. Heat Mass Transfer* **2015**, *84*, 253−261.

(27) He, F.; Yi, W.; Zha, J. Measurement of the heat of smoldering combustion in straws and stalks by means of simultaneous thermal analysis. *Biomass Bioenergy* **2009**, *33*, 130−136.

(28) Hadden, R. Smouldering and self-sustaining reactions in solids: an experimental approach. Ph.D. Thesis, The University of Edinburgh, Edinburgh, U.K., 2011.

(29) Christian, T. J.; Kleiss, B.; Yokelson, R. J.; Holzinger, R.; Crutzen, P.; Hao, W. M.; Saharjo, B.; Ward, D. E. Comprehensive laboratory measurements of biomass-burning emissions: 1. Emissions from Indonesian, African, and other fuels. *J. Geophys. Res.* **2003**, *108*, 4719.

(30) Yokelson, R. J.; Susott, R.; Ward, D. E.; Reardon, J.; Griffith, D. W. Emissions from smoldering combustion of biomass measured by

open-path Fourier transform infrared spectroscopy. *J. Geophys. Res. D: Atmos.* **1997**, *102*, 18865−18877.
(31) Akagi, S.; Yokelson, R. J.; Wiedinmyer, C.; Alvarado, M.; Reid, J.; Karl, T.; Crounse, J.; Wennberg, P. Emission factors for open and domestic biomass burning for use in atmospheric models. *Atmos. Chem. Phys.* **2011**, *11*, 4039−4072.
(32) Carvalho, E. R.; Veras, C. A. G.; Carvalho, J. A., Jr. Experimental investigation of smouldering in biomass. *Biomass Bioenergy* **2002**, *22*, 283−294.
(33) Rein, G.; Cohen, S.; Simeoni, A. Carbon emissions from smouldering peat in shallow and strong fronts. *Proc. Combust. Inst.* **2009**, *32*, 2489−2496.
(34) Jenkins, B.; Baxter, L.; Miles, T. R., Jr. Combustion properties of biomass. *Fuel Process. Technol.* **1998**, *54*, 17−46.
(35) Laurendeau, N. M. Heterogeneous kinetics of coal char gasification and combustion. *Prog. Energy Combust. Sci.* **1978**, *4*, 221−270.
(36) Kallonen, R.; von Wright, A.; Tikkanen, L.; Kaustia, K. The toxicity of fire effluents from textiles and upholstery materials. *J. Fire Sci.* **1985**, *3*, 145−160.
(37) Prager, F.; Einbrodt, H.; Hupfeld, J.; Muller, B.; Sand, H. Risk oriented evaluation of fire gas toxicity based on laboratory scale experiments-The DIN 53436 Method. *J. Fire Sci.* **1987**, *5*, 308−325.
(38) Tsuchiya, Y.; Mathieu, J. Heat, CO and Smoke Release Rates of Plywood under a Depleted Oxygen Atmosphere: An Experimental Study Using an OSU Heat Release Rate Apparatus. *Fire Saf. Sci.* **1991**, *3*, 605−614.
(39) Arpiainen, V.; Lappi, M. Products from the flash pyrolysis of peat and pine bark. *J. Anal. Appl. Pyrolysis* **1989**, *16*, 355−376.
(40) Ohtani, H.; Maejima, T.; Uehara, Y. In-situ Heat Release Measurement Of Smoldering Combustion Of Wood Sawdust. *Fire Saf. Sci.* **1991**, *3*, 557−564.
(41) Biagini, E.; Lippi, F.; Petarca, L.; Tognotti, L. Devolatilization rate of biomasses and coal-biomass blends: an experimental investigation. *Fuel* **2002**, *81*, 1041−1050.

DOI: 10.1021/acs.energyfuels.6b00314
Energy Fuels 2016, 30, 7666−7677

Chapter 5

Effects of Oxygen Concentration on Radiation-Aided and Self-sustained Smoldering Combustion of Radiata Pine

Statement of Authorship

Title of Paper	Effects of oxygen concentration on radiation-aided and self-sustained smouldering combustion of radiata pine.
Publication Status	☑ Published ☐ Accepted for Publication ☐ Submitted for Publication ☐ Unpublished and Unsubmitted w ork w ritten in manuscript style
Publication Details	Wang, H., van Eyk, P., Medwell, P., Birzer, C., Tian, Z., & Possell, M. (2017). Effects of oxygen concentration on radiation-aided and self-sustained smouldering combustion of radiata pine. *Energy & Fuels*, 31(8), 8619-8630.

Principal Author

Name of Principal Author (Candidate)	Houzhi Wang		
Contribution to the Paper	Based on a literature review conducted by me, and discussions with my supervisors, I identified the research gaps of the paper. I set up the experiments using the same testing rig I designed and built for the 'Identification and quantitative analysis of smoldering and flaming combustion of radiata pine' paper in *Energy & Fuels*. I conducted all the experiments and collected experimental data independently. I processed, analysed and interpreted all the experimental data. I performed an analysis of the experimental results, and the analysis was presented in text or figures by me. I interpreted data, wrote the manuscript. I also acted as the corresponding author, and responded to the reviewers' and the editor's comments and recommendations.		
Overall percentage (%)	75		
Certification:	This paper reports on original research I conducted during the period of my Higher Degree by Research candidature and is not subject to any obligations or contractual agreements with a third party that would constrain its inclusion in this thesis. I am the primary author of this paper.		
Signature		Date	15/Jan/2018

Co-Author Contributions

By signing the Statement of Authorship, each author certifies that:

i. the candidate's stated contribution to the publication is accurate (as detailed above);

ii. permission is granted for the candidate in include the publication in the thesis; and

iii. the sum of all co-author contributions is equal to 100% less the candidate's stated contribution.

Name of Co-Author	Philip van Eyk		
Contribution to the Paper	This co-author provided feedback, supervised development of work, helped in data interpretation and manuscript evaluation.		
Signature		Date	19/Jan/2018

Name of Co-Author	Paul Medwell		
Contribution to the Paper	This co-author provided feedback, supervised development of work, helped in data interpretation and manuscript evaluation.		
Signature		Date	18-JAN-2018

Name of Co-Author	Cristian Birzer		
Contribution to the Paper	This co-author provided feedback, supervised development of work, helped in data interpretation and manuscript evaluation.		
Signature		Date	19 Jan 2018

Name of Co-Author	Zhao Feng Tian		
Contribution to the Paper	This co-author provided feedback, supervised development of work, helped in data interpretation and manuscript evaluation.		
Signature		Date	18/01/2018

Name of Co-Author	Malcolm Possell		
Contribution to the Paper	This co-author provided feedback, supervised development of work, helped in data interpretation and manuscript evaluation.		
Signature		Date	19/01/2018

Please cut and paste additional co-author panels here as required.

energy&fuels

Article

pubs.acs.org/EF

Effects of Oxygen Concentration on Radiation-Aided and Self-sustained Smoldering Combustion of Radiata Pine

Houzhi Wang,*[,†,‡] Philip J. van Eyk,[§] Paul R. Medwell,[†] Cristian H. Birzer,[†] Zhao F. Tian,[†] and Malcolm Possell[‡,∥]

[†]School of Mechanical Engineering, The University of Adelaide, Adelaide, SA 5005, Australia

[‡]Bushfire and Natural Hazards CRC, Melbourne, VIC 3002, Australia

[§]School of Chemical Engineering, The University of Adelaide, Adelaide, SA 5005, Australia

[∥]School of Life and Environmental Sciences, The University of Sydney, Sydney, NSW 2006, Australia

Supporting Information

ABSTRACT: Smoldering combustion is an important form of combustion in wildfires and hazard reduction burning because it plays vital roles in pollutant emission, fire re-ignition, and ecological impact. Smoldering combustion can be classified as either radiation-aided or self-sustained, depending on the nature of the reactions. The latter is often considered a more hazardous type of smoldering combustion, because it can persist for a long period of time and can transition into flaming combustion. However, there is a lack of understanding of the differences between radiation-aided and self-sustained smoldering combustion processes, especially regarding characterization. The aim of this study is to investigate and quantify the differences between radiation-aided and self-sustained smoldering combustion in biomass. Experiments were conducted using an infrared heat lamp to heat pulverize fuel samples in a reactor. The external energy input and oxygen concentration were controlled in order to achieve radiation-aided and self-sustained smoldering combustion. Radiation-aided and self-sustained smoldering combustion were quantified based on temperature measurements in the reactor, the analyses of product gases, and the mass change of the testing samples. Under the current experimental conditions, self-sustained smoldering can only be initiated when the oxygen concentration is between 10% and 21%; only radiation-aided smoldering combustion can be initiated in oxygen concentrations under 7.5%; and no ignition occurs when the oxygen concentration is equal to or less than 5%. From the temperature measurements, there is a linear relationship between oxygen concentration and smoldering velocity.

1. INTRODUCTION

Wildfires are uncontrolled, large-scale burning of vegetation. Annually, 464 million hectares of land are burned by wildfires, releasing the equivalent of 5−10 billion tonnes of CO_2 into the atmosphere globally.[1−3] While wildfires are often stereotyped with large flames, smoldering combustion (a slow and low-temperature form of heterogeneous combustion) is also important to wildfires. Smoldering combustion is particularly problematic because it can be started with low energy,[4] and occur under limited oxygen conditions associated with forest fuel beds.[5] Smoldering combustion produces large quantities of emissions which can cause harmful environmental impacts.[6,7] Once ignited, smoldering combustion can persist for long periods of time, up to the order of several months.[8] Moreover, it may reignite flaming fires that have been deemed controlled or extinguished.[9−12] However, despite the significance of smoldering combustion, particularly in the context of wildfires, understanding of its initiation, identification, and quantification is lacking.

Smoldering combustion is often self-sustained, such that the net exothermic heat release is sufficient for the reaction to continue without an external energy source. However, in a wildfire situation, the radiant heat from the fire may be sufficient to promote a smoldering reaction, but one that may not generate sufficient heat for it to be self-sustained. This so-called radiation-aided smoldering combustion regime requires an external heat source to drive the reactions. This is a precursory process that occurs within wildfires, prior to the smoldering combustion becoming self-sustained (and in turn flaming combustion). In many previous studies, aided smoldering combustion has been considered the same as no ignition, even though it does still generate heat and releases emissions.[13−15] Furthermore, in some previous studies, self-sustained smoldering combustion was initiated with continuous exposure to an external heating;[16,17] hence, there is no evidence that the combustion processes were self-sustained in those cases. Despite the contributions of these previous studies, it is not clear how important the radiation-aided smoldering regime is, nor how to identify and quantify radiation-aided smoldering from self-sustained smoldering.

In wildland fires, radiation-aided smoldering combustion can be a standalone phenomenon under certain conditions, or it can transition to self-sustained smoldering (and subsequently flaming combustion). For example, self-sustained smoldering combustion can be achieved by further heating a fuel bed which is already in the radiation-aided smoldering combustion stage. In other cases, radiation-aided smoldering combustion will never turn into self-sustained smoldering, no matter how long it

Received: March 3, 2017
Revised: June 9, 2017
Published: June 28, 2017

DOI: 10.1021/acs.energyfuels.7b00646
Energy Fuels 2017, 31, 8619−8630

is heated. On this basis, radiation-aided smoldering combustion could be treated as no ignition; however, while the fuel is irradiated, the combustion process continues, and in doing so still consumes fuel and releases emissions. In other words, under certain conditions, the fuel bed is limited to the radiation-aided smoldering stage: in these cases, it is considered a standalone process, not a transitional stage. A better understanding of these phenomena will provide a foundation for more accurate assessment of the risks of smoldering combustion and better control of smoldering in wildfires.

Radiation-aided smoldering combustion of biomass in wildfires has received very little attention in the scientific literature, especially with respect to identification and quantification. It has previously been demonstrated that smoldering and flaming combustion can be characterized using temperature, gas concentrations, and mass loss profiles.[18] In an effort to reconcile the differences between radiation-aided and self-sustained smoldering combustion, the present study will follow a similar methodology to Wang et al.[18] with a view of identifying the conditions (in terms of heating time and oxygen concentration) required for each combustion regime.

Smoldering requires lower energy to initiate, compared with flaming combustion.[8] The energy required for the initiation of smoldering combustion can come from either an external heat source or self-heating.[19] The total external heat input is a function of the heating rates and the heating time: both of these parameters have been commonly used to control the external heat input in previous studies.[20] In particular, it has been demonstrated that the heating time can be used to achieve various combustion regimes.[20] The aforementioned research has predominantly been carried out with polyurethane foam and plywood because they are important materials to residential fires; however, there is a lack of data in the behavior of the smoldering combustion in biomass fuel with varying heating time.[4,15,21]

Smoldering combustion can occur in a low oxygen concentration environment, as low as 10%.[22,23] Consequently, smoldering combustion can propagate deep in a fuel bed, such as in the duff layer in a forest, where the oxygen availability is limited.[24] This increases the difficulties of detecting and smothering smoldering combustion in a fuel bed. There have been a few studies on the oxygen concentration required to extinguish smoldering combustion in peat;[23,25,26] however, the minimum oxygen concentration required for self-sustained smoldering combustion in biomass is still not clear. Similar research has previously been conducted by Hadden et al.[23,25] on the effects of oxygen concentration on the smoldering combustion in peat. It has been experimentally demonstrated that smoldering combustion of peat can only be initiated when the oxygen concentration is above a critical value (10% for peat).[23,25] However, there is a lack of understanding of the effects of oxygen concentration on the initiation of smoldering combustion in biomass. It was found that oxygen concentration does not have a significant effect on the minimum heating time for radiation-aided smoldering.[27] However, the effect of oxygen concentration on the minimum heating times for self-sustained smoldering combustion is still unclear. Furthermore, past research on these phenomena is based on polyurethane foam and peat.[25,27,28] The current study investigates the effect of oxygen concentration on the initiation of radiation-aided and self-sustained smoldering specifically of biomass.

Smoldering combustion is an important combustion regime in wildfires, because it has close links with wildfire re-ignition and the carbon emissions from wildfires.[29,30] It is difficult to detect or predict smoldering combustion in a wildfire due to the limited understanding of smoldering combustion in biomass fuel, especially the initiation of smoldering combustion in biomass fuel. In order to better understand smoldering combustion, it is important to understand the fundamental differences between the two smoldering combustion regimes. The experiments reported in this study are designed to initiate both radiation-aided and self-sustained smoldering combustion in a biomass fuel bed by varying the heating time and the oxygen concentration of the input oxidizer, to quantitatively characterize the two types of smoldering combustion using temporal/spatial temperature profiles, gas analysis, and mass loss profiles. A regime map to illustrate the effects of heating time and oxygen concentration on the initiation of different combustion regimes is presented.

2. METHODS

2.1. Experimental Apparatus. A schematic diagram of the experimental apparatus is shown in Figure 1. It consists of four main components: an infrared heater, a smoldering reactor, thermocouples, and a laboratory balance. The infrared heat lamp is used to heat the fuel sample in the smoldering reactor. Five thermocouples installed in the reactor measure the temperature: one above the fuel bed (the freeboard, FB) and four embedded in the fuel (TC1−4). The reactor has a square cross-sectional area of 1444 mm^2 (38 mm × 38 mm) and a height of 120 mm. The smoldering reactor has one oxidizer inlet at the bottom of the reactor, and one output connected to a gas analyzer (VARIOplus, MRU Instrument Inc., Neckarsulm, Germany). A scrubber (described in the Supporting Information) is installed between the smoldering reactor and the gas analyzer to remove heavy hydrocarbons and tars, in order to avoid contamination within the gas analyzer. The gas analyzer measures the gas concentration of five gases, namely, O_2, CO, CO_2, H_2, and CH_4 (on a dry basis). In the current study, the oxygen concentration of the input oxidizer was modified by adding nitrogen to the air stream, to investigate the effects of oxygen concentration on the initiation of radiation-aided and self-sustained smoldering combustion. The bulk volumetric flow rate was constant for all experiments. Further details related to the experimental apparatus and setup have been presented previously.[18]

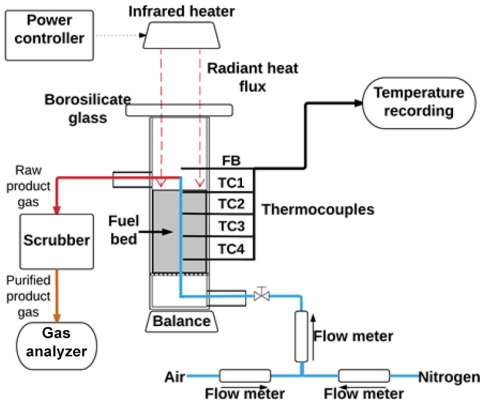

Figure 1. Schematic diagram of the experimental testing apparatus (the reactor is of 38 mm square cross section, 120 mm high, and thermocouples are 10 mm apart).

2.2. Experimental Setup. The radiant heat flux generated by the infrared heater was controlled through a Variac. The radiant heat flux, 40 $kW \cdot m^{-2}$, was selected based on the Australian Standard for Construction of buildings in bushfire-prone areas (AS 3959-2009).[31] The input oxidizer flow velocity was constant for all cases and set to 15 $mm \cdot s^{-1}$ for two reasons. First, it is known that the input oxidizer flow

DOI: 10.1021/acs.energyfuels.7b00646
Energy Fuels 2017, 31, 8619−8630

velocity in the current testing rig needs to be less than 38 mm·s^{-1} in order to initiate smoldering combustion.[18] Second, the input oxidizer velocity also needs to provide enough flow for the gas analyzer to function correctly, and if too low, it will draw in ambient air and thus interfere with the measurements.

There are two main reasons for choosing the current reactor. First, a small area enables a more uniformly distributed heat flux profile. Second, smoldering combustion is a slow form of combustion. Hence, a laboratory scale experiment with high precision was chosen to measure the mass change of the fuel bed. However, the measuring capacity of the laboratory balance is limited, so the reactor is necessarily small. The heat loss from the reactor walls was calculated using the model presented in Wang et al.[18] The heat loss to the reactor walls is approximately 13% of the heat generated by exothermic reactions. This amount of heat loss will reduce the temperatures near the walls, but is sufficiently low to consider the reactor close to one-dimensional. In addition, the focus of this study is to distinguish the different combustion regimes based on thermocouples placed along the centerline of the reactor, where the effects of the heat loss are minimal.

The freeboard temperature (FB) was used as an indicator to help distinguish smoldering and flaming combustion in a previous study.[18] On the basis of the measurements of the FB temperature, the cases presented in this study are either smoldering or no ignition cases. By definition, smoldering combustion is solid-phase combustion. Hence, the highest temperatures only occur in the reaction zone, which is in the fuel bed. Only the highest temperature measurements of each thermocouple in the fuel bed (TC1−4) are presented, which therefore correspond to the smolder front.

2.3. Fuel Preparation. Pulverized and dried radiata pine chips were used as fuel in this study, as it is widely planted in many wildfire-prone countries, such as Australia, Canada, and the United States. To reduce variability between samples, the pine chips were milled, sieved (2 mm < d < 3 mm, where d is the sieve mesh size), and then dried in an oven at 105 °C for 24 h. The mass of the sample used in each run was 10 g. Proximate and ultimate analyses of the fuel used are reported in Wang et al.[18]

2.4. Experimental Procedure. Prior to each experiment, the predried fuel samples were weighed and loaded into the reactor. The input oxidizer flow velocity and oxygen concentration were set, and an aluminum shutter was placed above the reactor to initially isolate the sample from the radiation. The corresponding radiant heat flux levels from the infrared heater were controlled using a Variac transformer. After the heat flux levels were adjusted to the predetermined value, temperature, product gas concentration, and mass change recordings commenced. Then, the aluminum shutter was removed, so that the fuel bed was directly exposed to the radiation. The experiments were performed at various oxygen levels ranging from 5% to 21% by volume and heating times from 200 to 1200 s. In all cases, the radiative heating flux level and the oxidizer bulk mean flow velocity were fixed at 40 kW·m^{-2} and 15 mm·s^{-1}, respectively. In each experiment, only one variable (either heating time or oxygen concentration) was varied at a time. After the samples were heated for predetermined times, the infrared heater was turned off, and the oxidizer setting remained unchanged. The experiments were considered complete when all thermocouple measurements were below 100 °C. A summary of the experimental cases is shown in the Supporting Information.

The experiment was also conducted under a 0% oxygen condition, and the fuel bed was heated for 1200 s. At the end of the experiment, only the surface of the fuel bed was charred, which indicates that the heat from the external heater is not enough to drive the pyrolysis front through the fuel bed. There is no mechanism for the propagation of the pyrolysis front, and it therefore represents a different combustion regime, where not all of the fuel bed reacts. Therefore, direct comparison with the propagating cases is not appropriate. Hence, the 0% oxygen case is not included in this paper. Furthermore, the 0% oxygen condition is not applicable to wildland fires.

Multiple experiments were conducted under the same conditions to examine the reproducibility of the measurements. On the basis of the experiment results, the reproducibility of the peak temperature, the peak product gas concentration, and the average mass change rate for self-sustained smoldering combustion were 91%, 87%, and 81%, respectively.

3. RESULTS

3.1. Self-sustained Smoldering. Figure 2 shows an example of the temporal and spatial temperature profiles of a self-sustained smoldering combustion case (Case 3 in the Supporting Information). In this case, the fuel bed was heated for 300 s, and the oxygen concentration of the input oxidizer is 21%. The freeboard (FB) thermocouple gives the temporal temperature profile measured above the fuel bed, whereas TC1−4 are temporal temperature profiles at increasing depth beneath the top of the fuel bed. The vertical dashed line (LO*) in Figure 2 represents the time when the infrared heat lamp was turned off. The reason for choosing Case 3 to represent self-sustained smoldering is that this case has the shortest heating time among all the self-sustained smoldering cases. Self-sustained smoldering combustion is defined as the smoldering combustion that can propagate without the aid of any external heating. Hence, the case with the shortest heating time would be a typical example of self-sustained smoldering.

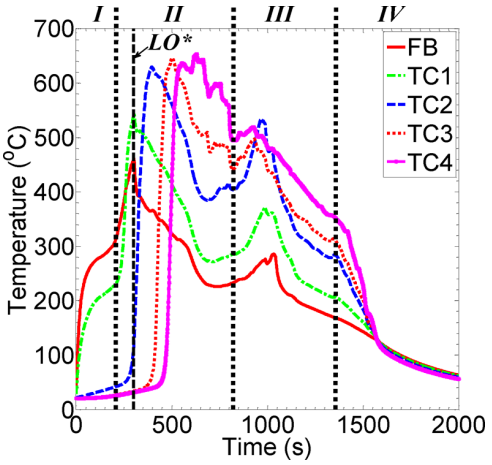

Figure 2. Temporal and spatial temperature profiles for self-sustained smoldering combustion (Case 3: oxygen concentration: 21%, heat flux level: 40 kW·m^{-2}, heating time: 300 s, flow velocity: 15.0 mm·s^{-1}, LO*: lamp off, FB: freeboard, TC: thermocouple). The vertical dashed line delineates the four stages of the reaction zone through the fuel bed: heating stage (I), devolatilization-dominated stage (II), char combustion dominated stage (III), and cool down stage (IV).

The temporal-spatial temperature (Figure 2) and the rate of temperature change profiles (Figure B1 in the Supporting Information) in the present study are consistent with the results of self-sustained smoldering combustion in Wang et al.[18] In Figure 2, the peak temperature is approximately 650 °C, which is slightly lower than the peak temperature (around 700 °C) reported previously. The minor variation is expected, as the air flow velocity in the previous study (20.8 mm·s^{-1}) is higher than the air velocity used in the current study (15.0 mm·s^{-1}). The effect of increased air velocity is known to lead to higher temperatures, because the greater oxygen availability facilitates more char oxidation.[32] Nevertheless, despite the minor difference in flow rate, the temperature profiles show the same features that have been reported previously. Hence, there

DOI: 10.1021/acs.energyfuels.7b00646
Energy Fuels 2017, 31, 8619−8630

is confidence that the cases shown in the current study are smoldering combustion, according to the temperature profiles.

The measurements of the freeboard temperature and the TC1 temperature shown in Figure 2 decrease at 300 s, as the external heating was eliminated at 300 s (lamp off, LO*). The measurements of TC2, TC3, and TC4 after LO* indicate that a strong exothermic reaction wave propagates through the fuel bed. Hence, it is evident that the smoldering combustion is self-sustained in this case.

The temperature measurements of thermocouples in the fuel bed (TC1−4) presented in Figure 2 all follow a similar trend, namely, a rapid temperature increase until a peak value and then a gradual decrease. This finding has been reported in other previous studies.[33,34] The smolder front can be divided into three layers: devolatilization layer, oxidation layer, and residue layer.[33,35] When the devolatilization layer approaches a thermocouple, the temperature measurement starts to increase, reaching a peak temperature when the oxidation layer reaches the thermocouple. As the oxidation layer propagates further toward the air supply, the temperature decreases, but the thermocouple is still exposed to the heat release from the upstream oxidation layer and therefore the temperature measurement decays slowly. The spatial and temporal information from the temperature measurements can be used to indicate the location of the smolder front and determine the propagation velocity (discussed further in section 3.4).

There are four stages of temporal evolution of the reaction zone through the fuel bed. These are heating stage (I), devolatilization-dominated (II), char combustion dominated (III), and cool down (IV). The transition from I to II is evident at approximately 210 s in Figure 2, where the freeboard and TC1 temperatures increase dramatically. The transition from II to III starts when the thermocouple measurements (Figure 2) start to increase again. This transition (II to III) is also evident from the temporal evolution of the gas profiles of the CO, CO_2, H_2, and CH_4 in the product gas, as shown in Figure 3. The thermocouple measurements decrease dramatically in the fourth stage (IV), which is evident in the temperature data presented in Figure 2.

In the first stage (heating stage), the concentrations of CO, CO_2, H_2, and CH_4 are minimal. In this stage, the temperature of the fuel bed is not high enough to start devolatilization. If the external heating is eliminated in this stage, no ignition will occur.

The second stage is devolatilization-dominated, in which the concentrations of CO, H_2, and CH_4 increase to their peak values. In this stage, the temperature of the fuel bed is high enough to start devolatilization. The majority of CO, H_2, and CH_4 are released during devolatilization; hence, the concentrations of CO, H_2, and CH_4 drop dramatically at the end of this stage (end of devolatilization). The concentrations of CH_4 and H_2 are the key measurements that distinguish the devolatilization-dominated stage from the char combustion dominated stage. This is because CH_4 and H_2 can only be produced by devolatilization, not char combustion. Noteworthy is that the oxygen concentration at the outlet of the reactor reaches its lowest concentration during stage II, indicating that the devolatilization products are partially oxidized during this stage and in doing so consumes the oxygen. This in turn limits oxidation of the char downstream of the devolatilization layer.

The third stage is the char combustion dominated stage. In this stage, the biomass fuel has already been converted to char by devolatilization and char oxidation becomes the dominant

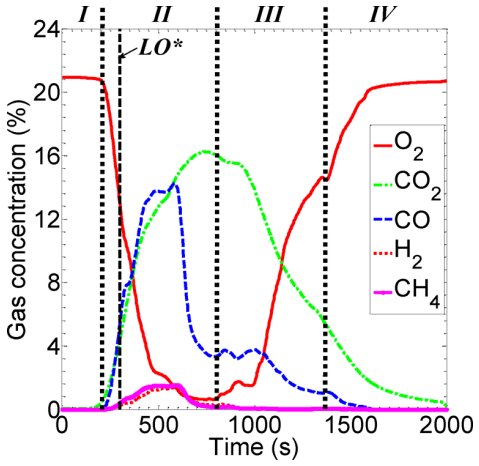

Figure 3. Temporal gas concentration profiles for self-sustained smoldering combustion (Case 3: oxygen concentration: 21%, heat flux level: 40 $kW{\cdot}m^{-2}$, heating time: 300 s, flow velocity: 15.0 $mm{\cdot}s^{-1}$, LO*: lamp off, FB: freeboard, TC: thermocouple). The vertical dashed line delineates the four stages of the reaction zone through the fuel bed: heating stage (I), devolatilization-dominated stage (II), char combustion dominated stage (III), and cool down stage (IV).

exothermic reaction. In the devolatilization stage, CO and CO_2 are at a similar concentration, whereas, during char combustion, the CO concentration is approximately one-quarter of the CO_2 concentration. The CO/CO_2 ratio is in good agreement with Tsuchiya.[36] Wang et al.[18] hypothesized that the dramatic drop of the CO level could be used to indicate the completion of the devolatilization stage; however, no further evidence was provided in that study because the major devolatilization products, H_2 and CH_4, were not measured. However, the hypothesis on the high yield of CO in the devolatilization-dominated stage is supported by the current study, as the concentrations of CO, H_2, and CH_4 are all measured and found to have a very similar trend, providing a stronger support of the hypothesis of the decrease in CO emission marking the end of devolatilization and commencement of char oxidation.

The fourth stage is the cool down stage, in which char combustion starts to decay. The cool down stage could occur under two circumstances. First, there is not sufficient char for char combustion to continue, and this circumstance normally occurs in self-sustained smoldering combustion cases. Second, the heat generated by char combustion is insufficient to overcome heat losses, and this circumstance occurs in radiation-aided and no ignition cases. The cool down stage is evident from the temperature measurements and the temporal evolution of the gas profiles of the O_2, CO, and CO_2.

Figure 4 shows the temporal mass change and mass loss rate profile for the same case presented in Figures 2 and 3 (viz. Case 3). In the first stage (heating stage), the mass change is minimal, as only physical changes occur during this stage (typically water evaporation, which is minimal in this case as the fuel was predried). In the devolatilization-dominated stage, the mass of the fuel bed dramatically drops because a large quantity of volatile matter is released. In the char combustion dominated stage, the absolute mass loss rate is approximately 2 times smaller than in the devolatilization-dominated stage. However, the total mass lost in the devolatilization-dominated stage is approximately 3 times more than that in the char combustion dominated stage. Hence, the mass loss rate was

DOI: 10.1021/acs.energyfuels.7b00646
Energy Fuels 2017, 31, 8619−8630

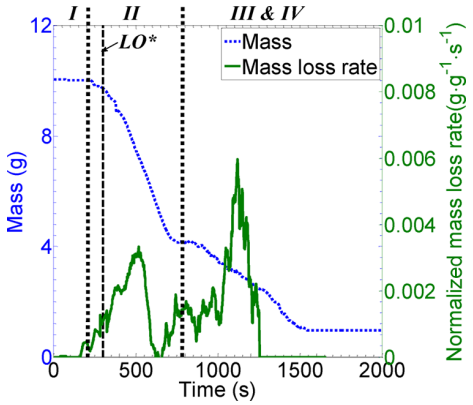

Figure 4. Temporal profiles of the mass loss and the normalized mass loss rate for self-sustained combustion (Case 3: oxygen concentration: 21%, heat flux level: 40 kW·m^{-2}, heating time: 300 s, flow velocity: 15.0 mm·s^{-1}, LO*: lamp off, FB: freeboard, TC: thermocouple). The vertical dashed line delineates the four stages of the reaction zone through the fuel bed: heating stage (I), devolatilization-dominated stage (II), char combustion dominated stage (III), and cool down stage (IV).

normalized based on the instantaneous mass of fuel remaining in the bed. From the results of the normalized mass loss rate, the peak mass loss rate relative to the instantaneous mass of remaining fuel is higher in the char combustion dominated stage than that in the devolatilization-dominated stage. The difference in the normalized mass loss rate indicates that the reaction rate in the char combustion dominated stage is faster than that in the devolatilization-dominated stage.

In the devolatilization-dominated stage (Figure 5), the devolatilization layer released a large amount of volatile matter.

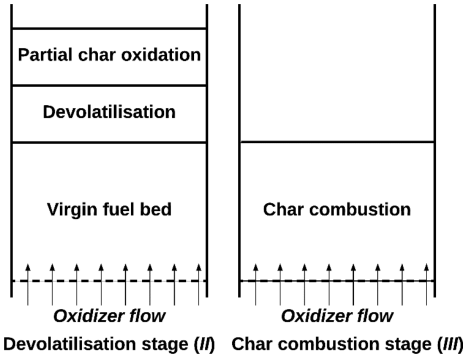

Figure 5. Combustion progress structure for self-sustained smoldering during the devolatilization-dominated stage (II) and the char combustion dominated stage (III) in a fuel bed (note that the thickness of each layer is not to scale).

The volatile matter mixed with the oxidizer before passing through the partial char oxidation layer. The mixture was then partially oxidized and then passed through the char combustion layer. The oxidization of volatile matter consumes oxygen, reducing the oxygen concentration to the point that it limited char combustion. Once the devolatilization layer reached the bottom of the reactor (at the end of the devolatilization-dominated stage), the oxygen concentration in the char combustion later increased, increasing the rate of char oxidation and releasing heat. The char combustion layer then propagated upward, back through the fuel bed in the direction of the oxidizer flow. At the beginning of the char combustion stage (Figure 5), all of the virgin fuel bed had been turned into char, and the fresh oxidizer flow directly interacted with the char combustion layer. With the sudden increase in oxygen concentration, char combustion released a large amount of heat, which then led to the second temperature peak seen at around 1000 s in Figure 2.

In summary, self-sustained smoldering combustion can be defined as a propagating exothermic reaction wave deriving its principal heat from heterogeneous oxidation of a solid fuel.[31] In this case (Case 3), smoldering combustion continued to propagate after the external heating input was turned off, so it is evident that the case presented here is self-sustained smoldering. From the combination of the temporal temperature profiles, gas and mass change profiles, self-sustained smoldering combustion can be divided into four stages: heating stage (I), devolatilization-dominated stage (II), char combustion dominated stage (III), and cool down stage (IV).

3.2. Self-sustained Smoldering under Limited Oxygen Concentration. Figure 6 shows an example of the temporal and spatial temperature profiles of a self-sustained smoldering combustion case (Case 23 in the Supporting Information). In this case, the fuel bed was heated for 600 s, and oxygen-depleted air (10% oxygen concentration) was introduced into the reactor (i.e., lower oxygen level, but longer heating time compared with Case 3 presented in section 3.1).

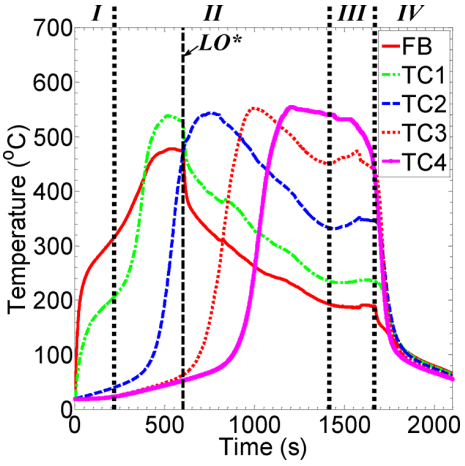

Figure 6. Temporal and spatial temperature profiles for self-sustained smoldering combustion (Case 23: oxygen concentration: 10%, heat flux level: 40 kW·m^{-2}, heating time: 600 s, flow velocity: 15.0 mm·s^{-1}, LO*: lamp off, FB: freeboard, TC: thermocouple). The vertical dashed line delineates the four stages of the reaction zone through the fuel bed: heating stage (I), devolatilization-dominated stage (II), char combustion dominated stage (III), and cool down stage (IV).

The trend of the temperature profiles, in this case, is similar to the temperature profiles for self-sustained smoldering combustion (Figure 2). From Figure 6, the combustion process continues for approximately 1100 s after the elimination of the external heater (at 600 s). Hence, this case is also a self-sustained smoldering combustion case. It is also noticed that there is a second temperature peak that occurred at approximately 1420 s. As discussed in the 21% oxygen case (section 3.1), the second temperature peak indicates the initiation of the char combustion dominated stage. Hence, it is

DOI: 10.1021/acs.energyfuels.7b00646
Energy Fuels 2017, 31, 8619−8630

apparent that the 10% oxygen case is self-sustained smoldering combustion based on the temperature measurements.

Four stages of temporal evolution of the reaction zone have been defined through the fuel bed. The transition from stage I to II is evident at approximately 210 s in Figure 7, where the

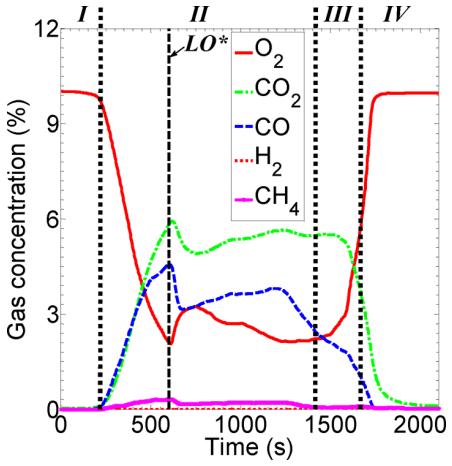

Figure 7. Temporal gas concentration profiles for self-sustained smoldering combustion (Case 23: oxygen concentration: 10%, heat flux level: 40 kW·m^{-2}, heating time: 600 s, flow velocity: 15.0 mm·s^{-1}, LO*: lamp off, FB: freeboard, TC: thermocouple). The vertical dashed line delineates the four stages of the reaction zone through the fuel bed: heating stage (I), devolatilization-dominated stage (II), char combustion dominated stage (III), and cool down stage (IV).

oxygen concentration drops and the concentrations of CO, CO_2, and CH_4 increase. The transition from stage I to II in Case 23 starts at a similar time (~210 s) as in Case 3. This shows that the change in oxygen concentration does not have a significant effect on the onset of the transition from stage I to II. As shown in Figure 7, the oxygen concentration increases and the concentrations of CO, CO_2, and CH_4 decrease for a short period of time after the elimination of the external heater. This indicates that the elimination of the external heater has effects on the combustion process. This observation is different from that shown in section 3.1. The transition from II to III can be defined based on the decrease in the CH_4 concentration, as well as the increase in oxygen concentration. The increase in oxygen concentration occurs at the same time as the onset of the second temperature peak (~1420 s), which indicates the initiation of the char dominated stage.

Figure 8 shows the temporal mass change and mass loss rate profiles for the same case presented in Figures 6 and 7 (viz. Case 23). The results in Figure 8 present that the elimination of the external heater has an effect on the mass change. This observation is consistent with that shown in Figures 6 and 7.

3.3. Radiation-Aided Smoldering. Figure 9 shows an example of the temporal-spatial temperature profiles of radiation-aided smoldering combustion (Case 28 in the Supporting Information). In this case, the fuel bed was heated by the infrared heat lamp for 1200 s, and oxygen-depleted air (7.5% oxygen concentration) was introduced into the reactor (i.e., lower oxygen level, but longer heating time, compared with Case 3 presented in section 3.1 or Case 23 in section 3.2).

The trend of the temperature profiles for self-sustained smoldering (Figure 2) and radiation-aided smoldering (Figure 9) are similar. However, radiation-aided smoldering has lower

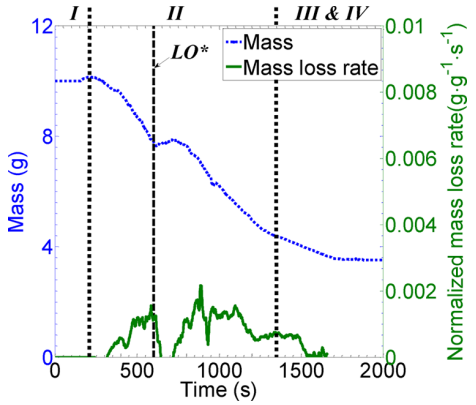

Figure 8. Temporal profiles of the mass loss and the normalized mass loss rate for self-sustained smoldering combustion (Case 23: oxygen concentration: 10%, heat flux level: 40 kW·m^{-2}, heating time: 600 s, flow velocity: 15.0 mm·s^{-1}, LO*: lamp off, FB: freeboard, TC: thermocouple). The vertical dashed line delineates the four stages of the reaction zone through the fuel bed: heating stage (I), devolatilization-dominated stage (II), char combustion dominated stage (III), and cool down stage (IV).

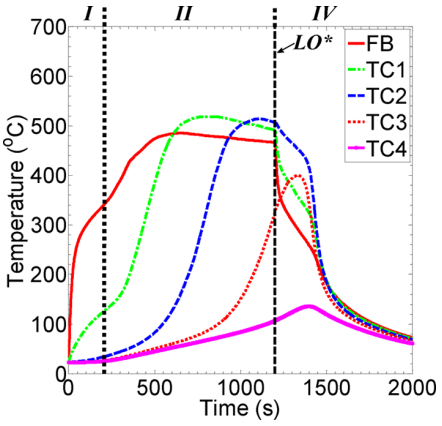

Figure 9. Temporal and spatial temperature profiles for radiation-aided smoldering combustion (Case 28: oxygen concentration: 7.5%, heat flux level: 40 kW·m^{-2}, heating time: 1200 s, flow velocity: 15.0 mm·s^{-1}, LO*: lamp off, FB: freeboard, TC: thermocouple). The vertical dashed line delineates three stages of the reaction zone through the fuel bed: heating stage (I), devolatilization-dominated stage (II), and cool down stage (IV).

peak temperatures and a slower rate of temperature increase. On the basis of the time between the temperature peaks, it is deduced that the combustion front propagates through the fuel bed slower than for radiation-aided smoldering compared with self-sustained smoldering. Interestingly, even though the heat source is directed at the top of the fuel bed, it has an impact on the propagation through the remainder of the fuel bed.

Standalone radiation-aided smoldering combustion, by definition, is a propagating exothermic wave which is dependent on the external heating: the elimination of the external heating leads to extinction. From Figure 9, the temperature profile (hence combustion process) starts to decay and extinguish after the lamp was turned off. Also, the peak rate of temperature change (Figure B2 in the Supporting Information) is approximately 1.4 °C·s^{-1}, which is much lower than that of the self-sustained smoldering combustion

DOI: 10.1021/acs.energyfuels.7b00646
Energy Fuels 2017, 31, 8619−8630

cases, namely, ~13 °C·s^{-1} as shown in Figure B1 in the Supporting Information. Further evidence that Case 28 is radiation-aided is that, when the lamp is switched off, the freeboard thermocouple measurement rapidly drops: indicating the majority of the heating is due to the lamp rather than the combustion reaction. This is in contrast to the self-sustained smoldering combustion case where the maximum freeboard temperature is recorded 148 s after the lamp is switched off.

Aided smoldering combustion is not a phenomenon with a clear definition and is often treated as no ignition in the literature. In this study, radiation-aided smoldering combustion and no ignition are distinguished by the onset of exothermic oxidation reactions (as evident by a temperature increase). Hence, radiation-aided smoldering combustion is defined as a transitional stage before self-sustained smoldering combustion has occurred, or a standalone combustion process in a solid fuel bed which requires an external source of heat to drive the reactions. The example shown in Figure 9 is a standalone radiation-aided smoldering combustion case.

As described in section 3.1, there are four stages in the temporal evolution of the reaction zone. In Figure 9, only the heating stage, the devolatilization-dominated stage, and the cool down stage can be observed. The transition from I to II occurs at approximately 210 s, whereas the transition from II to IV occurs at approximately 1200 s. From the results of Figure 2, the temperature measurements start to gradually drop to below 100 °C in the char combustion dominated stage due to the exothermicity of char combustion. The results in Figure 9 show that the temperature measurements rapidly drop to below 100 °C. Hence, the char combustion dominated stage (III) is not apparent in Figure 9. This indicates that the propagating reaction wave was controlled by the external heat source rather than the heat released by char combustion, so the smoldering front cannot propagate through the whole fuel bed without the external heater. Once the heater is turned off, radiation-aided smoldering combustion will decay and extinguish; then the fuel bed underneath the smoldering front will still be virgin fuel as the temperature there is not high enough to start devolatilization. For these reasons, the devolatilization process in the radiation-aided smoldering case did not completely convert all the fuel to char.

In the devolatilization-dominated stage of the radiation-aided smoldering case, the peak concentrations of CO to CO_2 are 2.9% and 4.4%, respectively, and the peak concentrations ratio of H_2 and CH_4 to CO_2 are close to zero. Compared to self-sustained smoldering combustion, the peak CO concentration yield in radiation-aided smoldering combustion (2.9%) is approximately one-fifth of the value in self-sustained smoldering combustion, viz. 14.3%. This indicates that the amount of volatile matter released during the devolatilization-dominated stage in radiation-aided smoldering combustion is significantly less than that in the case of self-sustained smoldering combustion.

Figure 10 shows that the O_2 concentration in the product gas increases, and the CO and CO_2 concentration decreases, after switching off the external heating. This is because a major part of the driving force of the reactions for combustion in this radiation-aided smoldering case is from the external heating. The elimination of the external heating suppresses the oxidation reactions that consume the O_2.

Figure 11 presents the mass profiles for the radiation-aided smoldering case presented in this section (Case 28). The vertical dashed line indicates the end of the heating stage (I),

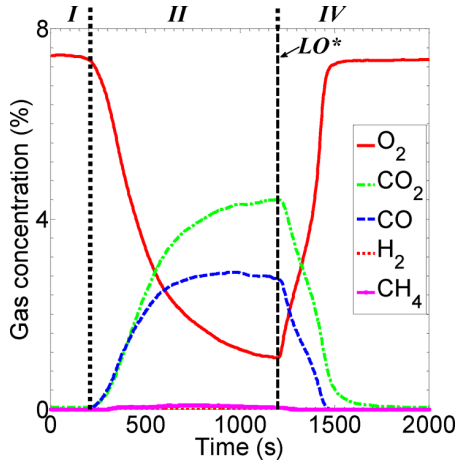

Figure 10. Temporal gas concentration profiles for radiation-aided smoldering combustion (Case 28: oxygen concentration: 7.5%, heat flux level: 40 kW·m^{-2}, heating time: 1200 s, flow velocity: 15.0 mm·s^{-1}, LO*: lamp off, FB: freeboard, TC: thermocouple). The vertical dashed line delineates three stages of the reaction zone through the fuel bed: heating stage (I), devolatilization-dominated stage (II), and cool down stage (IV).

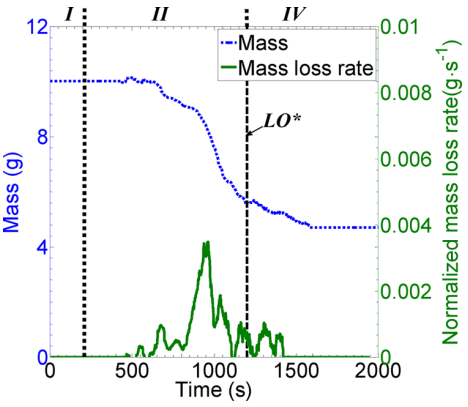

Figure 11. Temporal profiles of the mass loss and the normalized mass loss rate for radiation-aided smoldering combustion (Case 28: oxygen concentration: 7.5%, heat flux level: 40 kW·m^{-2}, heating time: 1200 s, flow velocity: 15.0 mm·s^{-1}, LO*: lamp off, FB: freeboard, TC: thermocouple). The vertical dashed line delineates three stages of the reaction zone through the fuel bed: heating stage (I), devolatilization-dominated stage (II), and cool down stage (IV).

based on the onset of the exothermic reactions from the rate of temperature change profile (Figure 9). It is noted that the mass of the sample starts to decrease 120 s later than the end of the heating stage. The delay in mass change indicates that it took a longer time to release enough volatile matter from the fuel bed for it to be detected by the scale after the onset of exothermic reactions. The onset of exothermic reactions mainly depends on the temperature of the fuel bed surface, and the fuel bed surface temperature is controlled by the external heat source. The temperature of the fuel bed under the surface must reach the devolatilization temperature (~250 °C) in order to release volatile matter in the fuel bed.[37] In the experiment, the energy that increases the temperature under the fuel bed surface is from the external heat source and exothermic reactions. At the beginning of the devolatilization-dominated stage in this radiation-aided smoldering case, the heat released by

DOI: 10.1021/acs.energyfuels.7b00646
Energy Fuels 2017, 31, 8619−8630

exothermic reactions on the surface is insufficient to drive the devolatilization under the fuel bed surface. Figure 9 also shows that the temperature of TC1 (2−3 mm below the fuel bed surface) reaches the devolatilization temperature (~250 °C) at approximately 400 s: this time is consistent with the time when the mass of sample starts dropping. The mass loss rate starts to decrease when the external heat source is removed at 1200 s. From Figure 10, the concentrations of CO and CO_2 also dramatically drop after the elimination of the external heat source. These facts all indicate that the combustion process strongly depends on the external heat source in the radiation-aided smoldering combustion, in contrast to self-sustained smoldering which derives its principal energy from exothermic combustion reactions.

3.4. Discussion. Figure 12 presents the effects of oxygen concentration on the peak temperature measurement of the

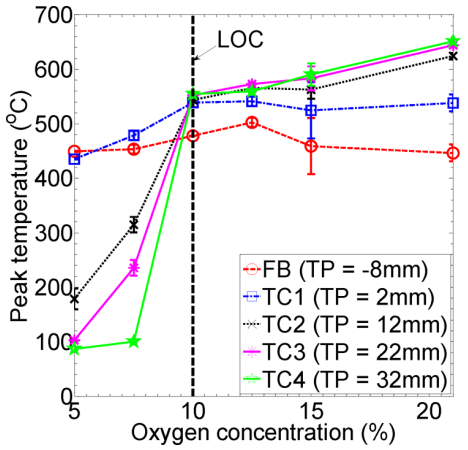

Figure 12. Effects of oxygen concentration (5−21% O_2) on peak temperature throughout the depth of the reactor (LOC: limiting oxygen concentration for self-sustained smoldering; TP: thermocouple position [the surface of fuel bed is located at 0 mm]).

thermocouples at the different positions. The temperatures in the fuel bed were measured by TC1−4, corresponding to depths below the top of the fuel bed of 2, 12, 22, and 32 mm, respectively. The freeboard temperature is at −8 mm. The error bars indicate the repeatability of the measurements. At each oxygen level, the results are presented for the minimum heating time to achieve self-sustained smoldering (the heating times are 300, 300, 450, and 600 s, corresponding to 21%, 15%, 12.5%, and 10% O_2, respectively). Below 10% oxygen, self-sustained smoldering is not possible: this is termed the limited oxygen concentration, LOC. To compare self-sustained with radiation-aided smoldering, the oxygen level is reduced but the heating time is kept constant. The lowest oxygen case where self-sustained is possible is 10%: lowering the oxygen to 7.5% gives a radiation-aided smoldering case—these two cases share a heating time of 600 s. When the oxygen level is further reduced to 5%, no ignition occurs, even with a heating time of 1200 s.

From Figure 12, it can be seen that, for each of the self-sustained smoldering cases, the peak temperatures are similar within the fuel bed (TC2−4). It is apparent that, the higher the oxygen concentration, the higher the peak temperatures (TC2−4), despite shorter heating times. However, the peak TC1 temperatures in the self-sustained smoldering cases are similar (approximately 550 °C), even though the heating time for these cases varies from 300 to 600 s. The heating times of the cases (10−21% oxygen concentration) presented in Figure 12 are based on the minimum heating time for the occurrence of self-sustained smoldering combustion. From the temperature and the rate of temperature change profiles, the onset of exothermic reactions caused a dramatic increase in TC1 temperature. It is likely that the peak TC1 temperatures are mainly caused by the exothermic reactions of the fuel bed surface, as evident by the marked temperature increase that occurs at the point of ignition (refer to Figure B1 in the Supporting Information). The peak TC1 temperatures for the radiation-aided smoldering and no ignition cases are much lower than those for the self-sustained smoldering cases. It is hypothesized that the smoldering front will become self-sustained once an energy, hence temperature, threshold is reached. Therefore, the peak TC1 temperature can act as an indicator to evaluate the heat released by the fuel bed surface, and the type of smoldering combustion can then be determined based on the peak TC1 temperature.

Figure 13 represents the time when the peak temperature occurs at different locations in different oxygen concentrations,

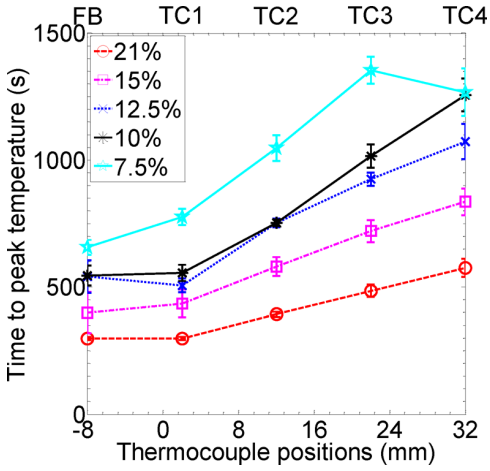

Figure 13. Effects of oxygen concentration (7.5−21%) on the time to peak temperature at different locations (flow velocity: 15.0 mm·s^{-1}; heat flux level: 40 kW·m^{-2}; 0 mm is the fuel bed surface, negative number denotes the distance above the fuel bed surface and positive number denotes the distance below the fuel bed surface). Error bars denote ±1 standard deviation.

for the reacting cases (the heating times are 300, 300, 450, 600, and 1200 s corresponding to 21%, 15%, 12.5%, 10%, and 7.5% O_2, respectively). The cases between 10% and 21% oxygen (inclusive) are self-sustained smoldering, whereas 7.5% oxygen is radiation-aided smoldering combustion. At 5% oxygen, no ignition occurs, and therefore, the results are not presented.

The results presented in Figure 13 show that the FB and TC1 temperatures peak at approximately the same time. The peak TC1 temperature occurs at the time of ignition, corresponding to the commencement of the exothermic reactions near the fuel bed surface in self-sustained smoldering combustion. The TC2 temperature was still too low for the initiation of combustion process at that time. Therefore, this indicates that the peak FB temperature is also caused by the exothermic reactions of the fuel bed surface. The time to the peak temperatures along the fuel bed is close to a linear progression in the self-sustained smoldering cases. This indicates that the smoldering propagation velocity is constant

DOI: 10.1021/acs.energyfuels.7b00646
Energy Fuels 2017, 31, 8619−8630

in these cases. In contrast, the radiation-aided smoldering case only shows a linear relationship between TC1−3. This is because the smoldering combustion did not actually reach the bottom of the fuel bed (TC4) in the radiation-aided smoldering case.

From Figure 13, the results in the self-sustained smoldering case indicate that the self-sustained smoldering front propagates at a constant velocity in the different oxygen concentrations. Figure 14 shows the average smoldering propagation velocity

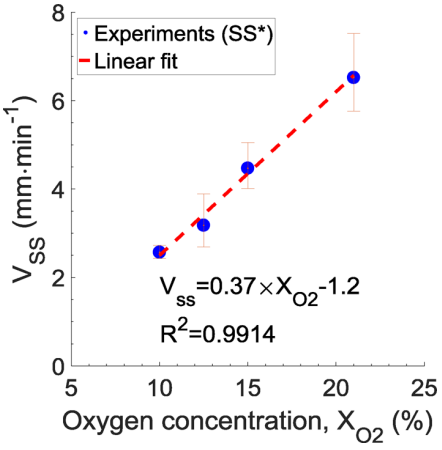

Figure 14. Effects of oxygen concentration on the smoldering propagation velocity (V_{ss}: average smoldering velocity; SS*: self-sustained smoldering).

for the self-sustained smoldering cases. The propagation velocity was calculated from the time between the arrival of the smolder front (peak temperature) at TC1 and TC4 and the known distance between the thermocouples.

From Figure 14, the minimum propagating velocity of the self-sustained smoldering front under the current experimental setup is approximately 2.6 mm·min^{-1} (which occurs at 10% oxygen concentration). The propagating velocity increases linearly with increasing oxygen concentration, which is consistent with the findings of the effect of oxygen concentration on the smoldering velocity in moss peat.[38] The self-sustained smoldering velocity is indicative of the amount of heat released by exothermic reactions, as the propagation of the reaction front in self-sustained smoldering combustion is driven by the heat from exothermic reactions. In self-sustained smoldering combustion, the heat released by exothermic reactions alone is sufficient to drive the reaction front. It is hypothesized that a critical heat flux is required for the smoldering front to start propagating. The critical heat flux needs to be sufficient to overcome the heat losses and thereby increase the temperature enough to drive the devolatilization and char oxidization reactions. The critical heat flux is dependent on oxygen concentration and the oxidizer flow velocity. The minimum smoldering velocity occurs when the heat input is equal to that minimum energy input. Conversely, it is possible that the smoldering velocity could be used to identify whether the smoldering combustion is radiation-aided or self-sustained. For example, if the propagating velocity of a smoldering front is below the minimum smoldering velocity, then this smoldering front is unlikely to be self-sustained. Under the current experimental setup, the minimum smoldering velocity for self-sustained smoldering is close to 2.6 mm·min^{-1}.

Figure 15 represents the total gas emissions in mass and the total CO-to-CO_2 emission ratio under different oxygen

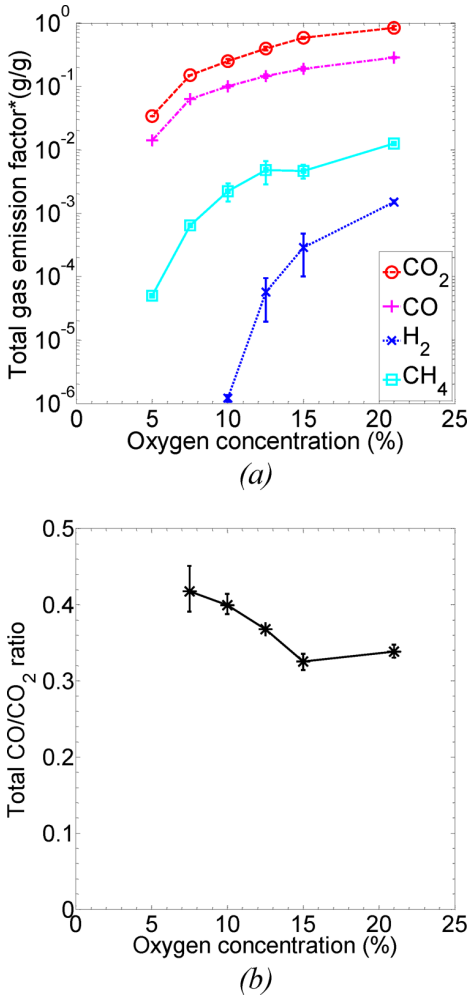

Figure 15. Effects of oxygen concentration on (a) the gas emission by mass in logarithm scale and (b) CO/CO_2 ratio (flow velocity: 15.0 mm·s^{-1}; heat flux level: 40 kW·m^{-2}; error bars denote ±1 standard deviation; total gas emission factor: total gas emission in mass/mass of fuel loaded).

concentrations. The total gas concentrations were calculated based on the gas concentration profiles and mass change profile. The mass flow rate of gases in the product gas was calculated through a mass balance equation based on the gases concentration in product gas. In the mass balance equation, the mass flow rates of the reactants (fuel and oxidizer) were determined based on the mass profile of the fuel sample, and the flow rate and composition of the oxidizer. The total mass flow rate of products was assumed to be equal to the mass flow rate of the reactants in the mass balance equation. The products of the reaction were assumed to be completely gaseous, including only CO, CO_2, CH_4, and H_2. The mass flow rate of CO, CO_2, CH_4, and H_2 was calculated from the mass loss of the sample, the mass flow rate of the oxidizer, and the volumetric concentration measurements. The cases in different oxygen concentrations presented in Figure 15 are the same as the cases

DOI: 10.1021/acs.energyfuels.7b00646
Energy Fuels 2017, 31, 8619−8630

in Figures 12 and 13 (self-sustained smoldering combustion between 10% and 21% oxygen, radiation-aided smoldering in 7.5% oxygen, and no ignition in 5% oxygen).

The results in Figure 15a show that a decrease in oxygen concentration significantly decreases the gas emissions of CO, CO_2, CH_4, and H_2 in radiation-aided and self-sustained smoldering cases. This finding is consistent with the temperature measurements (Figure 12) and the assertion that reducing the oxygen level impedes the reaction rates. It was also found that a decrease in oxygen concentration has a more significant effect on the CO_2 emissions than those of the other gases. This is because a large portion of CO_2 emission was produced in the char combustion dominated stage, while a decrease in oxygen concentration suppresses char combustion, which reduces the CO_2 emission. From Figure 3, it was found that the peak gas concentration of CO, CH_4, and H_2 all occur in the devolatilization-dominated stage (II), indicating that the CO, CH_4, and H_2 emissions were primarily produced in the devolatilization-dominated stage. Hence, the oxygen concentration has more effects on the char combustion dominated stage than that on the devolatilization-dominated stage. The results in Figure 15 show that self-sustained smoldering (10−21% oxygen concentration) produces approximately 3 times more CO_2 than CO, whereas radiation-aided smoldering combustion (7.5%) produces approximately 2 times more CO_2 than CO. Hence, the proportion of the CO emission is higher in the radiation-aided smoldering case than those in the self-sustained smoldering cases. The change in the proportion of the CO emission is possibly caused by the effect of oxygen concentration on char combustion.

Three combustion regimes of biomass combustion, including no ignition, radiation-aided smoldering, and self-sustained smoldering, can be achieved by varying the heating time and oxygen concentration. Figure 16 shows all the results from the current study, not just the cases presented in detail, compiled on a regime diagram. Radiation-aided smoldering can be achieved with a narrow heating time range (~250 to 300 s) when the oxygen concentration is between 15% and 21%. The range of the heating time required for radiation-aided smoldering combustion is much wider when the oxygen concentration is between 7.5% and 15% than when the oxygen concentration is between 15% and 21%.

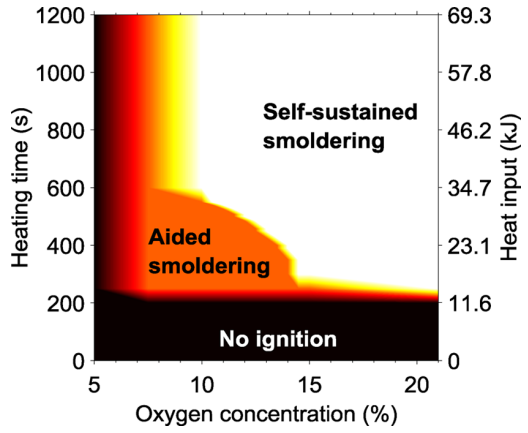

Figure 16. Interactive effects of oxygen concentration and heating time on the initiation of different smoldering combustion (flow velocity: 15.0 mm s^{-1}; heat flux level: 40 kW m^{-2}; heat input was calculated based on the heat flux and the area of the reactor opening).

The results in Figure 16 indicate that the oxygen concentration does not have a significant effect on the minimum heating time required to start radiation-aided smoldering combustion, when the oxygen concentration is between 7.5% and 21%. This finding agrees with the previous finding on the effects of oxygen concentration on polyurethane foam and peat.[9,10,23,39] When the oxygen concentration is below 5%, there is no indication of char oxidation, based on the change of temperature profiles. Only radiation-aided smoldering combustion can be achieved when the oxygen concentration is between 7.5% and 10%.

4. CONCLUSIONS

Smoldering combustion is an important process in wildfires because of its roles in fire safety and environmental impact. However, it is difficult to detect or predict smoldering combustion due to a lack of understanding of the initiation of smoldering combustion. Smoldering combustion can be radiation-aided or self-sustained, based on its dependence on the external heating. Radiation-aided and self-sustained smoldering combustion were characterized using measurements of temperatures in the reactor, the concentration of the gases in product gas, and the mass change of the sample. The main differences between radiation-aided and self-sustained smoldering can be summarized into the following four categories:

(1) The average peak temperature in radiation-aided smoldering is lower than that in self-sustained smoldering. The average peak temperature in the self-sustained smoldering combustion cases is in the range 550−650 °C and is mostly dependent on oxygen concentration. In comparison, the average peak temperature in the standalone radiation-aided smoldering cases is approximately 500 °C, and this temperature is predominantly dependent on the external heat source.

(2) The average propagation velocity of self-sustained smoldering combustion showed that a decrease in oxygen concentration significantly slows the propagation of the smoldering front. The relationship between oxygen concentration and the smoldering velocity is approximately a positive linear dependence between 10% and 21% oxygen concentration. It was also found that the minimum smoldering velocity under the current experimental setup is approximately 2.6 mm·min^{-1}, below which the smoldering was no longer self-sustained. Hence, the smoldering velocity can possibly be used as an indicator of radiation-aided and self-sustained smoldering combustion.

(3) From the gas emission profiles, the CO_2 emission is much higher than the CO, CH_4, and H_2 emissions. It was found that the CO-to-CO_2 emission ratio in the self-sustained smoldering cases is lower than that in the radiation-aided smoldering cases.

(4) The heating stage, the devolatilization-dominated stage, and the transition from the devolatilization-dominated stage to the char combustion dominated stage or the cool down stage can be identified based on the mass loss profile. From the mass loss rate profile, the peak mass loss rate in the radiation-aided smoldering case is similar to that in the self-sustained smoldering case under the current experimental setup. However, the peak mass loss

DOI: 10.1021/acs.energyfuels.7b00646
Energy Fuels 2017, 31, 8619−8630

rate in the radiation-aided smoldering combustion case occurred when the external heater was on, and the mass loss rate dramatically decreased to zero after the external heater was turned off. The peak mass loss rate in the self-sustained smoldering case occurred when the external heater was already off.

Apart from the differences between radiation-aided and self-sustained smoldering combustion, the conditions that lead to different combustion regimes were also investigated.

(5) The heating time and the oxygen concentration of the input oxidizer flow were controlled to achieve radiation-aided and self-sustained smoldering. Radiation-aided smoldering normally requires less energy to initiate compared to self-sustained smoldering, under the same oxygen concentration. The minimum energy (heating time) for the initiation of radiation-aided smoldering combustion is constant, whereas the minimum energy for the initiation of self-sustained smoldering combustion increases with decreasing oxygen concentration.

In this study, it has been experimentally demonstrated that radiation-aided and self-sustained in pulverized radiata pine chips can be identified and characterized based on the temperature, product gases concentration, and mass loss profiles. The heating time and oxygen concentration that lead to different combustion regimes were investigated. From the results of the required conditions for radiation-aided and self-sustained smoldering, critical oxygen concentrations for different combustion regimes were determined under the current experimental setup. By knowing the critical oxygen concentrations, smoldering combustion can be better predicted and controlled.

■ ASSOCIATED CONTENT

Supporting Information

The Supporting Information is available free of charge on the ACS Publications website at DOI: 10.1021/acs.energyfuels.7b00646.

Schematic diagram of gas washing system, temporal and spatial rate of temperature change for self-sustained and radiation-aided smoldering combustion, and table of summary of experimental runs (PDF)

■ AUTHOR INFORMATION

Corresponding Author

*E-mail: houzhi.wang@adelaide.edu.au.

ORCID

Houzhi Wang: 0000-0002-9814-6387

Notes

The authors declare no competing financial interest.

■ ACKNOWLEDGMENTS

The support of the University of Adelaide, Australian Government Research Training Program Scholarship and the Bushfire and Natural Hazards CRC are gratefully acknowledged. The authors thank Mr. Marc Simpson for his assistance throughout the experimental campaign. We also thank the anonymous reviewers for their constructive feedback which helped improved the quality of this manuscript.

■ REFERENCES

(1) Ito, A.; Penner, J. E. Global estimates of biomass burning emissions based on satellite imagery for the year 2000. *J. Geophys. Res.* **2004**, *109* (D14), D14S05.

(2) Randerson, J.; Chen, Y.; van der Werf, G.; Rogers, B.; Morton, D. Global burned area and biomass burning emissions from small fires. *J. Geophys. Res.* **2012**, *117* (G4), G04012.

(3) Seiler, W.; Crutzen, P. J. Estimates of gross and net fluxes of carbon between the biosphere and the atmosphere from biomass burning. *Clim. Change* **1980**, *2* (3), 207−247.

(4) Anderson, M. K.; Sleight, R. T.; Torero, J. L. Ignition signatures of a downward smolder reaction. *Exp. Therm. Fluid Sci.* **2000**, *21* (1), 33−40.

(5) Radojevic, M. Chemistry of Forest Fires and Regional Haze with Emphasis on Southeast Asia. In *Air Quality*; Rao, G. V., Raman, S., Singh, M. P., Eds.; Birkhäuser Basel: Basel, Switzerland, 2003; pp 157−187.

(6) Tissari, J.; Lyyränen, J.; Hytönen, K.; Sippula, O.; Tapper, U.; Frey, A.; Saarnio, K.; Pennanen, A.; Hillamo, R.; Salonen, R.; Hirvonen, M.-R.; Jokiniemi, J. Fine particle and gaseous emissions from normal and smouldering wood combustion in a conventional masonry heater. *Atmos. Environ.* **2008**, *42* (34), 7862−7873.

(7) Yokelson, R. J.; Susott, R.; Ward, D. E.; Reardon, J.; Griffith, D. W. Emissions from smoldering combustion of biomass measured by open-path Fourier transform infrared spectroscopy. *J. Geophys. Res. Atmos.* **1997**, *102* (D15), 18865−18877.

(8) Rein, G. Smouldering Combustion Phenomena in Science and Technology. *Int. Rev. Chem. Eng.* **2009**, *1*, 3−18.

(9) Putzeys, O.; Rein, G.; Fernandez-Pello, A.; Urban, D. Piloted Ignition to Flaming in Smoldering Polyurethane Foam. In *44th AIAA Aerospace Sciences Meeting and Exhibit*, Reno, NV, Jan 9, 2006; AAIA: Reston, VA, 2006; p 1131.

(10) Putzeys, O. M.; Fernandez-Pello, A. C.; Rein, G.; Urban, D. L. The piloted transition to flaming in smoldering fire retarded and non-fire retarded polyurethane foam. *Fire Mater.* **2008**, *32* (8), 485−499.

(11) Valdivieso, J. P.; de Dios Rivera, J. Effect of wind on smoldering combustion limits of moist pine needle beds. *Fire Technol.* **2014**, *50* (6), 1589−1605.

(12) Wang, S.; Huang, X.; Chen, H.; Liu, N. Interaction between flaming and smouldering in hot-particle ignition of forest fuels and effects of moisture and wind. *Int. J. Wildland Fire* **2017**, *26* (1), 71−81.

(13) Bilbao, R.; Mastral, J.; Aldea, M.; Ceamanos, J.; Betran, M.; Lana, J. Experimental and theoretical study of the ignition and smoldering of wood including convective effects. *Combust. Flame* **2001**, *126* (1), 1363−1372.

(14) El-Sayed, S.; Khass, T. Smoldering combustion of rice husk dusts on a hot surface. *Combust., Explos. Shock Waves* **2013**, *49* (2), 159−166.

(15) Gratkowski, M. T.; Dembsey, N.; Beyler, C. Radiant smoldering ignition of plywood. *Fire Saf. J.* **2006**, *41* (6), 427−443.

(16) Anez, N. F.; Torrent, J. G.; Pejic, L. M.; Olmedo, C. G. Detection of incipient self-ignition process in solid fuels through gas emissions methodology. *J. Loss Prev. Process Ind.* **2015**, *36*, 343−351.

(17) Carvalho, E. R.; Veras, C. A. G.; Carvalho, J. A., Jr. Experimental investigation of smouldering in biomass. *Biomass Bioenergy* **2002**, *22* (4), 283−294.

(18) Wang, H.; van Eyk, P. J.; Medwell, P. R.; Birzer, C. H.; Tian, Z. F.; Possell, M. Identification and Quantitative Analysis of Smoldering and Flaming Combustion of Radiata Pine. *Energy Fuels* **2016**, *30* (9), 7666−7677.

(19) Wu, D.; Huang, X.; Norman, F.; Verplaetsen, F.; Berghmans, J.; Van den Bulck, E. Experimental investigation on the self-ignition behaviour of coal dust accumulations in oxy-fuel combustion system. *Fuel* **2015**, *160*, 245−254.

(20) He, F.; Behrendt, F. Experimental investigation of natural smoldering of char granules in a packed bed. *Fire Saf. J.* **2011**, *46* (7), 406−413.

DOI: 10.1021/acs.energyfuels.7b00646
Energy Fuels 2017, 31, 8619−8630

(21) Swann, J.; Hartman, J.; Beyler, C. Study of radiant smoldering ignition of plywood subjected to prolonged heating using the cone calorimeter, TGA, and DSC. *Fire Saf. Sci.* **2008**, *9*, 155−166.
(22) Belcher, C.; McElwain, J. Limits for combustion in low O2 redefine paleoatmospheric predictions for the Mesozoic. *Science* **2008**, *321* (5893), 1197−1200.
(23) Hadden, R. M.; Rein, G.; Belcher, C. M. Study of the competing chemical reactions in the initiation and spread of smouldering combustion in peat. *Proc. Combust. Inst.* **2013**, *34* (2), 2547−2553.
(24) Hardy, C. C.; Ottmar, R. D.; Peterson, J. L.; Core, J. E. *Smoke Management Guide for Prescribed and Wildland Fire 2001 Edition*; National Wildfire Coordination Group, 2001.
(25) Hadden, R. Smouldering and self-sustaining reactions in solids: An experimental approach. Ph.D. Thesis, The University of Edinburgh, Edinburgh, U.K., 2011.
(26) Huang, X.; Rein, G. Interactions of Earth's atmospheric oxygen and fuel moisture in smouldering wildfires. *Sci. Total Environ.* **2016**, *572*, 1440−1446.
(27) Walther, D. C.; Anthenien, R. A.; Fernandez-Pello, A. Smolder ignition of polyurethane foam: effect of oxygen concentration. *Fire Saf. J.* **2000**, *34* (4), 343−359.
(28) Ortiz-Molina, M. G.; Toong, T.-Y.; Moussa, N. A.; Tesoro, G. C. Smoldering combustion of flexible polyurethane foams and its transition to flaming or extinguishment. *Symp. Combust., [Proc.]* **1979**, *17* (1), 1191−1200.
(29) Hollis, J.; Matthews, S.; Anderson, W.; Cruz, M.; Burrows, N. Behind the flaming zone: predicting woody fuel consumption in eucalypt forest fires in southern Australia. *For. Ecol. Manage.* **2011**, *261* (11), 2049−2067.
(30) Watts, A. C.; Kobziar, L. N. Smoldering combustion and ground fires: ecological effects and multi-scale significance. *Fire Ecol.* **2013**, *9* (1), 124−32.
(31) *AS 3959-2009: Construction of buildings in bushfire prone areas*; Standards Australia: Sydney, Australia, 2009.
(32) Ohlemiller, T. J. *NBSIR 85-3294: Smoldering Combustion*; U.S. Department of Commerce: Washington, DC, 1986.
(33) Moussa, N. A.; Toong, T.; Garris, C. Mechanism of smoldering of cellulosic materials. *Symp. Combust., [Proc.]* **1977**, *16* (1), 1447−1457.
(34) Zammarano, M.; Matko, S.; Pitts, W. M.; Fox, D. M.; Davis, R. D. Towards a reference polyurethane foam and bench scale test for assessing smoldering in upholstered furniture. *Polym. Degrad. Stab.* **2014**, *106*, 97−107.
(35) Rein, G. Smoldering Combustion Phenomena and Coal Fires. In *Coal and Peat Fires: A Global Perspective*; Elsevier: Amsterdam, 2011; Chapter 17, pp 307−315.
(36) Tsuchiya, Y. CO/CO_2 ratios in fire. *Fire Saf. Sci.* **1994**, *4*, 515−526.
(37) Klass, D. L. *Biomass for Renewable Energy, Fuels, and Chemicals*; Academic Press: San Diego, CA, 1998.
(38) Huang, X.; Rein, G. Thermochemical conversion of biomass in smouldering combustion across scales: The roles of heterogeneous kinetics, oxygen and transport phenomena. *Bioresour. Technol.* **2016**, *207*, 409−421.
(39) Hadden, R. M.; Scott, S.; Lautenberger, C.; Fernandez-Pello, A. C. Ignition of combustible fuel beds by hot particles: an experimental and theoretical study. *Fire Technol.* **2011**, *47* (2), 341−355.

DOI: 10.1021/acs.energyfuels.7b00646
Energy Fuels 2017, 31, 8619−8630

Chapter 6

Air Permeability of the Litter Layer in Temperate Forests of South-East Australia

Statement of Authorship

Title of Paper	Air permeability of the litter layer in temperate forests of South-East Australia.
Publication Status	☐ Published ☐ Accepted for Publication ☑ Submitted for Publication ☐ Unpublished and Unsubmitted w ork w ritten in manuscript style
Publication Details	Wang, H., Van Eyk, P., Medwell, P., Birzer, C., Tian, Z., & Possell, M. (Submitted). Air Permeability of The Litter Layer in Temperate Forests of South-East Australia. *International Journal of Wildland Fire*

Principal Author

Name of Principal Author (Candidate)	Houzhi Wang		
Contribution to the Paper	I conducted a thorough literature review, and identified the research gaps of the paper. After discussion with my supervisors, a detailed research methodology and experimental plan were decided. According to the plan, I designed and developed an experiment testing rig. I tested and calibrated the testing rig. The fuels used in this study were collected by one co-author, Malcolm Possell. I prepared the fuel samples for the experiments. I did preliminary experiments using the testing rig. I discussed the preliminary experiments with my supervisors; then, I modified the testing rig based on feedback from my supervisors. I set up the experiments. I conducted all the experiments and collected experimental data independently. I processed, analysed and interpreted all the experimental data. I performed an analysis of the experimental results, and the analysis was presented in text or figures by me. I interpreted data, wrote the manuscript. I also acted as the corresponding author, and responded to the reviewers' and the editor's comments and recommendations.		
Overall percentage (%)	75		
Certification:	This paper reports on original research I conducted during the period of my Higher Degree by Research candidature and is not subject to any obligations or contractual agreements with a third party that would constrain its inclusion in this thesis. I am the primary author of this paper.		
Signature		Date	15/Jan/2018

Co-Author Contributions

By signing the Statement of Authorship, each author certifies that:

i. the candidate's stated contribution to the publication is accurate (as detailed above);

ii. permission is granted for the candidate in include the publication in the thesis; and

iii. the sum of all co-author contributions is equal to 100% less the candidate's stated contribution.

Name of Co-Author	Philip van Eyk		
Contribution to the Paper	This co-author provided feedback, supervised development of work, helped in data interpretation and manuscript evaluation.		
Signature		Date	19/Jan/2018

Name of Co-Author	Paul Medwell		
Contribution to the Paper	This co-author provided feedback, supervised development of work, helped in data interpretation and manuscript evaluation.		
Signature		Date	18-JAN-2018

Name of Co-Author	Cristian Birzer		
Contribution to the Paper	This co-author provided feedback, supervised development of work, helped in data interpretation and manuscript evaluation.		
Signature		Date	19 Jan 2018

Name of Co-Author	Zhao Feng Tian		
Contribution to the Paper	This co-author provided feedback, supervised development of work, helped in data interpretation and manuscript evaluation.		
Signature		Date	18/01/2018

Name of Co-Author	Malcolm Possell		
Contribution to the Paper	This co-author provided feedback, supervised development of work, helped in data interpretation and manuscript evaluation. This co-author collected the fuel samples used in this study.		
Signature		Date	19/01/2018

Please cut and paste additional co-author panels here as required.

Air permeability of the litter layer in temperate forests of south-east Australia

Houzhi Wang,[*, †, ‡] *Philip J. van Eyk,*[§] *Paul R. Medwell,*[†] *Cristian H. Birzer,*[†] *Zhao F. Tian,*[†] *and Malcolm Possell*[‖, ‡]

[†]School of Mechanical Engineering, The University of Adelaide, Adelaide, SA 5005, Australia.

[‡]Bushfire and Natural Hazards CRC, Melbourne, VIC 3002, Australia.

[§]School of Chemical Engineering, The University of Adelaide, Adelaide, SA 5005, Australia.

[‖]School of Life and Environmental Sciences, The University of Sydney, Sydney, NSW 2006, Australia.

KEYWORDS: wildfires; hazard reduction burning; air permeability; natural forest fuel bed.

ABSTRACT: Fuel on the ground, such as leaves, twigs and decomposing matter, accumulate over time and account for a large percentage of the total fuel load in forests. In fire events, material on the ground is often referred to as a fuel bed. The air permeability of a fuel bed is a critical factor that influences fire behaviour because it controls the amount of air (oxygen) available for combustion within the fuel bed. The aim of this study is to provide a better understanding of the air permeability of the fuel beds in forests. The air permeability for different fuel beds were determined using experimental and theoretical methods. The pressure drop across the fuel bed

samples were experimentally measured using a verified permeability testing rig. The air permeability was then calculated using Darcy's Law (Darcian flow) or the Forchheimer equation (non-Darcian flow) from the pressure drop measurements. The particles in the fuel beds were characterised in terms of particle size and shape. Based on the particle characterisation, the air permeability of the fuel beds was also calculated using the Kozeny-Carman equation. The results show that the experimental method is preferred when determining the air permeability for natural forest fuel beds due to the variability in the size and shape of the particles. The results also show that both particle size and particle type are influential on the air permeability of the fuel bed. The significance of this study is that it increases the ability to predict the air permeability of fuel beds in forests, which is essential for modelling the combustion behaviour within the fuel beds.

Nomenclature

d = Glass bead diameter [mm]

d_t = Twig diameter [mm] (subscript t indicates twig)

k_D = Air permeability of the fuel bed [m^2] (subscript D indicates Darcian flows)

k_F = Air permeability of the fuel bed [m^2] (subscript F indicates non-Darcian flows)

K = Kozeny constant (K is typically 5) [1]

ℓ = Length of the fuel particle [mm]

L = Length of the fuel bed [m]

R = Drag force on the particle surface [N] (refer Equation 4)

Nomenclature (cont'd)

Re_l = Modified Reynolds number, determined from Equation 5

S_V = Specific surface area per unit volume [m^{-1}]

t = Thickness of the fuel particle [mm]

t_{DM} = Thickness of the decomposing matter particle [mm] (subscript DM indicates decomposing matter).

U_0 = Superficial velocity [$m \cdot s^{-1}$]

U = Interstitial velocity [$m \cdot s^{-1}$]

w = Width of the fuel particle [mm]

β = Forchheimer coefficient [m^{-1}]

ΔP = Total pressure drop across the fuel bed [Pa]

ε = Porosity of fuel bed [-]

μ = Dynamic viscosity [$Pa \cdot s$]

ρ = density of air [$kg \cdot m^{-3}$]

---

1. INTRODUCTION

Wildfires are a recurring issue throughout summer and the drier months in many parts of the world. In addition to potential loss of life, wildfires cause tremendous economic loss. For example,

the cost of the 2009 Victorian Black Saturday disaster in Australia is conservatively estimated at A$4.4 billion [2]. Climate change is increasing the risk and impact of wildfires [3], hence greater economic impact can be expected without improved methods of wildfire mitigation. Amongst the multiple measures to mitigate the risks of wildfires, hazard reduction burning (HRB) is one of the most effective and economical methods. As with any other technique, HRB has some drawbacks. For instance, the control of HRB is still challenging, especially in large-scale burning, where uncontrolled fire spread can occur. There is still room for improvement in the management and predictability of HRB; however, to do so, a more comprehensive understanding of hazard reduction burning is needed. Hence, the overall aim of this study is to develop a better understanding of HRB.

Ideally, the purpose of HRB is to apply controlled fires to a predetermined area in order to reduce the fuel load in that area. However, to achieve that, many specific conditions have to be met, such as weather conditions and the conditions of the fuel bed. Therefore, the success of HRB is influenced by many factors, such as the characteristics of the fuel, the weather and the topography [4]. These factors are so diverse that it is challenging to understand and effectively control HRB. At the moment, many decisions about HRB are made based on experience, and that is why trained personnel are essential for conducting HRB. Furthermore, there is a lack of detailed understanding of the effects of these factors on HRB. To better control and understand HRB, modelling is a critical approach. It is necessary to develop robust models which can provide a comprehensive understanding of HRB. Furthermore, these models can later be used as tools to predict and manage the HRB activities. However, to develop accurate models, reliably measured data such as air permeability of fuel beds are required as model inputs.

Fuel beds account for a large percentage of fuel in forests [4] and are especially important for HRB, as most of the fuel reduction is from them [5]. Modelling of their combustion needs to consider two different combustion regimes: smouldering and flaming. The combustion regime of a fuel bed can be controlled by oxygen availability [6-10], which is affected by the fuel bed's air permeability. The air permeability of a fuel bed, which can be considered a porous medium, characterises the ease with which air can pass through it. Determining the air permeability of a fuel bed is challenging because of the diversity of the material in fuel beds. In the literature, fuel beds are often characterised based on particle size [11, 12]. Previous studies of the air permeability of biomass have been only performed on regular-shaped particles, such as pine needles and soy straw; which reveals a strong dependence of particle shape on the air permeability[8, 13]. However, the fuel particles in forest fuel beds are diverse in size and shape, and therefore no such data are available in literature. Hence, there is a need to investigate the effects of the size and type of the forest fuel bed particles on the air permeability.

The permeability of a porous medium can be determined using either Darcy's Law, or the Forchheimer equation, depending on the flow regime. The fundamental principle in determining the air permeability is based on the pressure gradient, for a particular flow velocity [14]. The air permeability in fuel beds can also be calculated using the Kozeny-Carman equation, based on the physical properties of the porous medium. The Kozeny-Carman equation has been widely applied to flow through soils, sands, and synthetic materials [15-17]. However, the validity of the Kozeny-Carman equation has not been demonstrated for particles in natural forest fuel beds. The natural forest fuel beds are highly variable, which means that rather than relying on simple correlations, experimental methods are needed to determine characteristics of fuel beds. The results may subsequently be used as an input data for models.

A considerable number of studies have focused on water and oil permeability of porous media, such as rocks and soil, which is relevant to the field of geology [15, 18, 19]. The testing rigs presented in the literature use water as the working fluid to determine the permeability of porous media. However, these testing rigs can only be used to determine the permeability of a porous medium which is not water-sensitive. For instance, these water permeability testing rigs are not suitable for many materials, such as biomass, coal and clay, in which the absorption of water will lead to changes in particle volume and the fuel bed structure. Therefore, the determination of permeability by gaseous fluids, such as air, is needed for these materials. However, there are only a few studies that determine the permeability of a porous medium by air [8, 20]. The focus of the current study is on natural forest fuel beds, and as these materials are water-sensitive this study determines their permeability by air.

The overall aim of this study is to provide a better understanding of the air permeability of fuel beds, in the context of HRB; since the air permeability has significant effects on the combustion of fuel beds. First of all, it is important to find a robust method of determining the air permeability of fuel beds. It is also necessary to examine whether the fuel bed material can be characterised in a way that is suitable for providing input data into models. The experiments described in this study were designed to investigate the air permeability of natural forest litter layer, and the effects of particle size and particle type on the air permeability. Due to the lack of data in the literature, the air permeability of natural forest fuel beds will be reported.

2. METHODOLOGY

2.1 Experimental apparatus

The experimental testing rig was designed to determine the air permeability of a fuel bed by measuring the pressure drop across the fuel bed. The experimental testing rig consisted of three parts: a permeability testing rig, an air supply system and a manometer (Model 9565, TSI Inc., Shoreview, United States).

The air permeability testing rig shown in Figure 1 has top and bottom sections. There is a dual air inlet and a bed of ceramic beads in the bottom section to obtain uniform flow through the fuel bed. Fuel bed samples were loaded in the top section of the air permeability testing rig.

The input air flow in this study was supplied by an air compressor, and the moisture in the input air flow was removed by a dehumidifier before introducing into the air permeability testing rig. By removing the moisture in the air, the accuracy of the input flowrate and the pressure drop measurements can be improved, and the uncertainties caused by the moisture in the ambient air can be minimised.

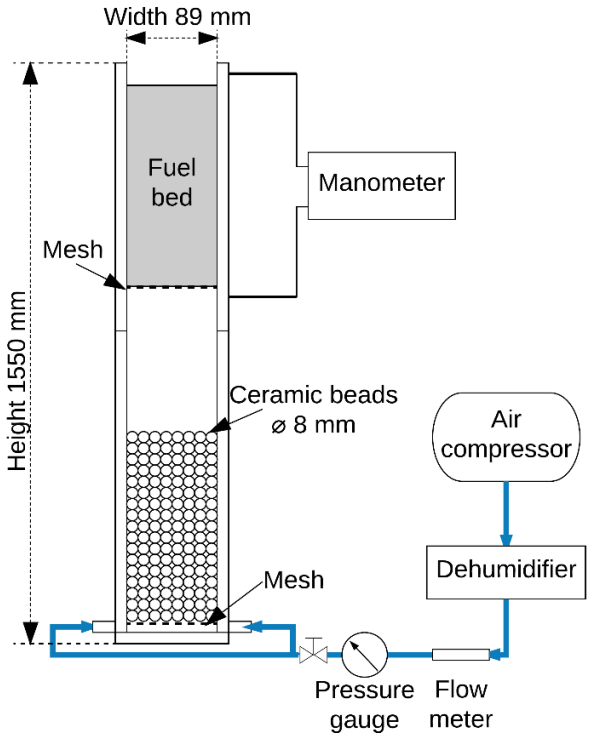

Figure 1. *Schematic diagram of the experimental testing apparatus for the air permeability experiments.*

2.2 Experimental setup and procedure

The input air flow rate was varied from 50.5 to 404 $g \cdot m^{-2} \cdot s^{-1}$ (42 to 337 $mm \cdot s^{-1}$), with a 50.5 $g \cdot m^{-2} \cdot s^{-1}$ increment. Below the lower limit (50.5 $g \cdot m^{-2} \cdot s^{-1}$), the error in the pressure drop measurement significantly increases due to the range of the manometer. Above the upper limit (404 $g \cdot m^{-2} \cdot s^{-1}$), the bed becomes fluidised. The pressure before and after the fuel bed (Figure 1) was measured using the manometer through holes in the rig.

Prior to each experiment, fuel material was weighed and loaded into the rig. The fuel material was carefully loaded to create an unconsolidated fuel bed; this is to ensure the consistency

throughout the fuel bed. The pressure drop across the fuel bed was based on a 60-second averaging period, with a 1 Hz sampling frequency.

2.3 Fuel bed samples collection and preparation

Three categories of fuel bed samples are used in this study: glass beads, milled biomass particles and natural forest fuel particles. For the milled biomass particles, pulverised and dried pine chips, gum bark and gum leaves were used to represent the three common fuel types in forests. The pine chips samples are from *Pinus* radiata, and the bark and twig samples are from *Eucalyptus* camaldulensis. To reduce variability between samples, the pine chips, gum bark and gum leaves were milled and sieved into three size ranges (1–2 mm; 2–3 mm; 3–4 mm).

All the forest fuel bed samples used in this study were collected from a forest in East Gippsland, Victoria (for more details about the collecting site, refer to[21]). This forest is located in one of the wildfire-prone areas of Victoria, Australia. Within the collecting site, three permanent circular plots with a radius of 5 m were established, at least 500 m apart, within similar vegetation types. The fuel samples were collected from these three plots, respectively. When collecting the fuel bed samples, especially the decomposing matter layer, attention was paid to ensure that inorganic matter, such as soils and sands, were not collected. After collecting the natural forest fuel bed, the samples were separated into three types: twig, leaf and decomposing matter. Then, the twig samples were sieved into three size ranges (> 10 mm, 5–10 mm, < 5 mm); and the decomposing matter samples were sieved into four size ranges (4–5 mm, 3–4 mm, 2–3 mm; 1–2 mm). To reduce uncertainty variability, and ensure experimental repeatability, the moisture of all fuel samples were reduced to zero by drying in an oven at 105 ^{o}C for 24 hours prior to experiments.

2.4 Fuel characterisation

Fuel material was sieved and the fuel bed samples within each range were characterised based on physical size and projected area. The physical size of particles was measured using a micrometer and repeated for 20 samples of each fuel type. For milled biomass particles, the particle shape was assumed to be cuboid according to their apparent shapes. Hence, the length, width and thickness of particles were measured to calculate the specific area. For twigs, the samples were assumed to be cylindrical; so, the diameter and the length of twigs were measured. In the natural forest fuel particles, the projected areas of 20 randomly selected leaves were measured in order to determine the specific area, rather than assuming a regular shape. The leaf litter was not sieved due to its shape. The specific area of the decomposing matter was calculated based on the sieve aperture rather than measurements of the individual particles. The details of these measurements are listed in Table 1, 2 and 3. The particle size grouping is based on the size of the sieve used to sort the material, apart from the glass beads which were monodisperse from the manufacturer.

The porosities of the different fuel beds were measured. For glass beads, the porosity was measured using the fluid saturation method, in which water was used to fill the void volume of the glass beads bed. Then, the porosity was calculated through the ratio of the void volume and the total volume of the glass beads bed ($\varepsilon = \frac{V_{void}}{V_{total}}$, where V_{void} is the void volume and V_{total} is the total volume of the glass beads bed). For the milled biomass and the natural forests fuel bed, the porosity was calculated based on the weight of the fuel bed and the particle density ($\varepsilon = 1 - \frac{W_{fuel\ bed}}{\rho_p \cdot V_{total}}$, where $W_{fuel\ bed}$ is the weight of the fuel bed and ρ_p is the particle density), as these fuel beds are all hygroscopic. The porosity measurements are included in Table 1, 2 and 3.

***Table 1**. Glass beads physical properties.*

Particle catalogue	Particle size (mm)	Diameter, d (mm)	Specific area, S_V (m^{-1})	Porosity, ε
Glass beads	6.1	6.07 ± 0.09	1012 ± 15	0.393
	5.1	5.11 ± 0.03	852 ± 5	0.389
	3.8	3.83 ± 0.07	638 ± 12	0.386
	2.2	2.16 ± 0.01	360 ± 2	0.362

***Table 2.** Milled and sieved fuel particles physical properties.*

Particle catalogue	Particle size (mm)	Length, ℓ (mm)	Width, w (mm)	Thickness, t (mm)	Specific area, S_V (m^{-1})	Porosity, ε
Pine chips	1-2	4.26 ± 1.58	1.47 ± 0.50	0.58 ± 0.18	5740 ± 908	0.457
	2-3	6.37 ± 1.78	2.50 ± 0.73	1.16 ± 0.43	3240 ± 1012	0.462
	3-4	9.68 ± 2.96	3.37 ± 1.04	1.63 ± 0.48	2260 ± 529	0.502
Gum bark	1-2	4.13 ± 1.28	1.20 ± 0.43	0.95 ± 0.35	4910 ± 1340	0.608
	2-3	8.05 ± 2.44	2.25 ± 0.51	1.50 ± 0.35	2630 ± 433	0.674
	3-4	8.90 ± 3.53	4.10 ± 0.70	1.83 ± 0.43	1940 ± 416	0.709
Gum leaf	1-2	2.73 ± 1.36	1.38 ± 0.54	0.3	9320 ± 1519	0.450
	2-3	5.55 ± 2.40	2.35 ± 0.76	0.3	7830 ± 424	0.508
	3-4	10.3 ± 4.40	3.53 ± 1.45	0.3	7420 ± 327	0.561

Table 3. *Natural forest fuel particles physical properties (DM*: decomposing matter).*

Particle catalogue	**Particle size (mm)**	**Length, L (mm)**	**Diameter for twig, d_t; Thickness for DM*, t_{DM} (mm)**	**Thickness, t (mm)**	**Specific area, S_V (m^{-1})**	**Porosity, ε**
Twig	>10mm	250	11.5	N/A	356 ± 89	0.800
	5-10mm	228.7 ± 57.23	6.49 ± 1.14	N/A	643 ± 104	0.828
	<5mm	199.5 ± 48.50	2.45 ± 0.92	N/A	1642 ± 235	0.942
Leaf	N/A	N/A	N/A	0.3	3550 ± 1023	0.955
Decomposing matter	4-5mm	19.36 ± 6.36	7.33 ± 2.12	1.07 ± 0.80	2250	0.550
	3-4mm	11.95 ± 4.26	4.07 ± 1.35	0.8 ± 0.61	3160	0.502
	2-3mm	7.17 ± 3.24	3.10 ± 2.09	0.79 ± 0.64	3460	0.462
	1-2mm	4.22 ± 2.52	1.62 ± 0.74	0.40 ± 0.35	6700	0.450

Figure 2 presents the mass distribution of the (a) twigs and (b) decomposing matter in the forest fuel bed. The results in Figure 2(a) imply that the thin twigs, with < 5 mm particle size, contribute approximately 50 % of the total mass in the twig litter. Similarly, the majority of the decomposing matter is smaller than 5 mm. Even though much of the forest fuel bed visually appears large, the size distribution presented in Figure 2 shows that the majority of the particles in the twigs and decomposing matter is smaller than 5 mm. From the point view of the air permeability, these small particles have significant effects on the air permeability of fuel bed.

Based on the results of Figure 2, the focus of this study is on the air permeability of small particles (< 5 mm) within the fuel bed that is an unconsolidated porous medium. To better understand the air permeability of the fuel bed, three common biomass samples, pine chips, gum bark and gum leaf were milled and sieved. By milling and sieving the particles the results can be

better controlled for repeatability, but the generality of the results still applies to the actual particles in the litter layer.

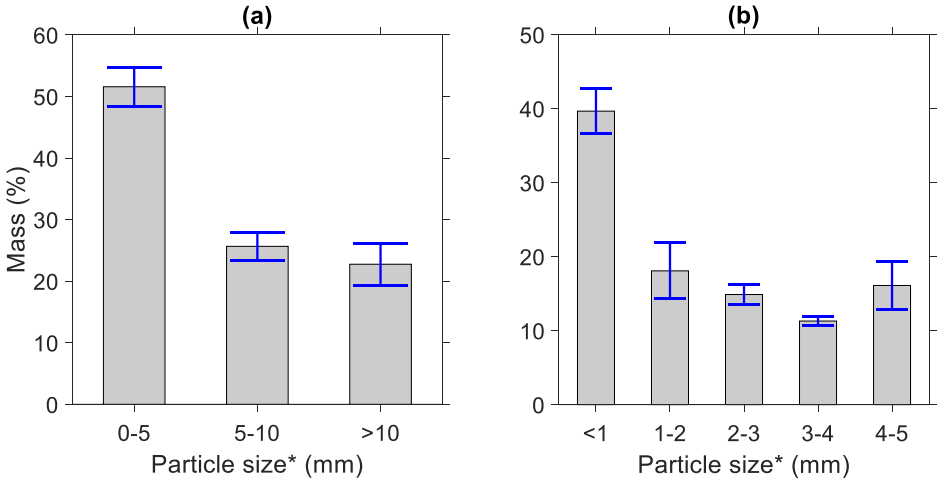

Figure 2. *Mass distribution as function of particle size for natural forest fuel bed. Particle size is based on sieve aperture. (a) Twigs, (b) Decomposing matter. Repeatability of measurements represented by ± 1 standard deviation error bars.*

2.5 Calculation of the fuel bed permeability

2.5.1 Determination of the air permeability

The air permeability of a porous medium particularly an unconsolidated fuel bed can be determined from pressure gradient measurements or from the fuel bed/particle properties. In this study, both methods are used to determine the air permeability of different porous media. A schematic diagram outlining how the air permeability was determined in this study is summarised in Figure 3.

The pressure gradient method is an empirical approach that does not need any information about the particle properties such as particle size. For the pressure gradient method, the air permeability was directly determined from the measured pressure gradient using Darcy's Law (Section 2.5.2) for Darcian flow regime, while the Forchheimer equation (Section 2.5.3) was used to determine the air permeability and the Forchheimer coefficient within the non-Darcian flow regime.

It should be noted that Darcy's Law is only applicable in the Darcian flow regime, namely when the Reynolds number, $Re_d < 10$ [22-24]. Here, $Re_d=\rho \cdot U_0 \cdot d/\mu$, where U_0 is superficial velocity and d is the average particle diameter [14]. For non-Darcian flow ($Re_d > 10$), the Forchheimer equation may be used.

For the fuel bed/particle properties method, the specific area of particle (S_v) and the porosity (ε) of fuel bed were measured to calculate the pressure gradient and the air permeability using the Kozeny-Carman equation (Section 2.5.4). The calculated pressure gradient was compared with the measured pressure gradient to validate the Kozeny-Carman equation.

Similar research has been conducted on the air permeability of pine needle fuel beds and the air permeability of fuel bed was calculated using Darcy's Law and the Kozeny-Carman equation [8]. However, both Darcy's Law and the Kozeny-Carman equation (Equation 3.a) can only be applied when $Re_d < 10$ [23]. This is because, as the air flow velocity increases, the experimental results do not agree with Darcy's law due to inertial effects [25].

To overcome the discrepancy between experimental results and Darcy's law, Forchheimer (1901) [25] suggested adding a kinetic energy term to Darcy's Law. In this study, for the cases with $Re_d>10$, the air permeability was calculated using the Forchheimer equation. To calculate the air permeability of fuel bed using the Forchheimer equation, the pressure drop across fuel bed is

required. The pressure drop can either be measured through experiment or calculated using the function of pressure gradient and the superficial air velocity. Similarly, the Kozeny-Carman equation can be modified to account for non-Darcian flow (Equation 3.b).

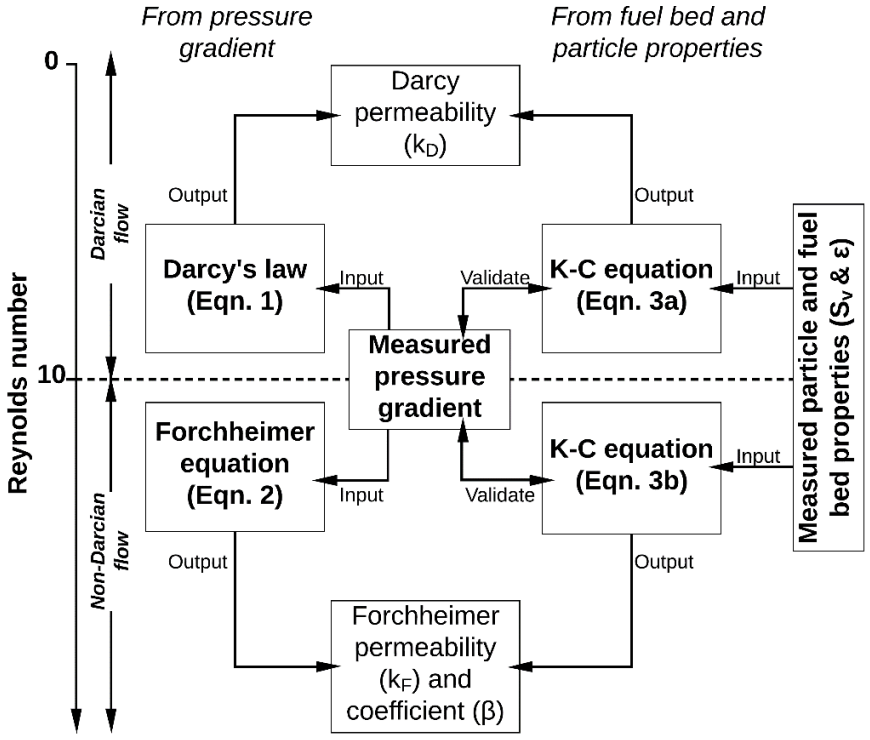

Figure 3. *Schematic diagram for determining the air permeability of a fuel bed.*

2.5.2 Darcy's Law

Permeability (isotropic permeability in this study) can be determined by using Darcy's Law (Equation 1) from the pressure gradient and the superficial velocity. Darcy's Law is only valid for Darcian flow, i.e. $Re_d < 10$.

$$\frac{\Delta P}{L} = \frac{\mu}{k_D} U_0 \ldots\ldots\ldots (1)$$

Equation 1 shows that the pressure drop of Darcian flows in the porous medium is proportional to the fluid dynamic viscosity and velocity. The pressure drop of Darcian flows in porous medium is mainly attributed to the skin friction of porous medium wall surface in porous voids (particle surfaces of the fuel bed in this study).

2.5.3 Forchheimer equation

The air permeability of a porous medium in a non-Darcian flow ($Re_d > 10$) can be determined based on the Forchheimer equation (Equation 2). The difference between the Forchheimer equation (Equation 2) and Darcy's Law (Equation 1) is that the Forchheimer equation includes an additional new term to incorporate the importance of kinetic energy loss due to inertial effects in non-Darcian flows. When the flow velocity increases, the pressure drop due to inertial effects (for example the change of flow cross section area in porous pores) increases and needs to be considered when Re_d is larger than 10. As a result, the relationship between the superficial velocity and the pressure gradient is a quadratic function in non-Darcian flows. The air permeability determined through the Forchheimer equation in this paper is referred to as the Forchheimer permeability (k_F), to distinguish it from the permeability from Darcy's Law (k_D). To characterise a porous medium in non-Darcian flow, the Forchheimer permeability and the Forchheimer coefficient are required.

$$\frac{\Delta P}{L} = \frac{\mu}{k_F} U_0 + \beta \cdot \rho \cdot {U_0}^2 \quad \ldots\ldots\ldots (2)$$

The air permeability can be determined by either Darcy's Law or the Forchheimer equation, depending on the flow regime. These methods require the experimental data of the pressure

gradient and the superficial velocity, which means that a similar experiment (as stated in Section 2.1) has to be conducted before using Darcy's Law or the Forchheimer equation.

2.5.4 Kozeny-Carman equation

For flows through unconsolidated beds of fuel particles, the pressure gradient can be calculated from the particle and fuel bed properties using the Kozeny-Carman equation (Equation 3.a and 3.b) [1]. Equation 3.a is for Darcian flows, while Equation 3.b is for non-Darcian flows. In the non-Darcian flow condition, a modified Reynolds number, Re_1, (Equation 5) is required to calculate the friction factor term, $\frac{R}{\rho \cdot U^2}$ (Equation 4). Within the Darcian flow regime, the air permeability can be calculated by rearranging the Kozeny-Carman equation, i.e. Equation 3.a.i. In the non-Darcian flow condition, the air permeability and the Forchheimer coefficient can be calculated by Equation 3.c.i and 3.c.ii.

$$\frac{\Delta P}{L} = \mu\left(\frac{K(1-\varepsilon)^2 {S_V}^2}{\varepsilon^3}\right) U_0 \ldots\ldots\ldots \text{(3.a)}$$

From Equation 3.a, the air permeability can be calculated using the following equation based on Equation 1:

$$K_{KC} = K_D = \frac{\varepsilon^3}{K(1-\varepsilon)^2 {S_V}^2} \ldots\ldots\ldots \text{(3.a.i)}$$

For non-Darcian flows, the following equation can be used to calculate the pressure drop in the fuel bed.

$$\frac{\Delta P}{L} = \left(\frac{R}{\rho U^2}\right) \frac{S_V(1-\varepsilon)\rho {U_0}^2}{\varepsilon^3} \ldots\ldots\ldots \text{(3.b)}$$

By substituting the Carman correlation (Equation 4) into the friction factor, $\frac{R}{\rho \cdot U^2}$ in Equation 3.b, Equation 3.c shows Equation 3.b in Forchheimer form:

$$\frac{\Delta P}{L} = \frac{5(1-\varepsilon)^2 {S_V}^2}{\varepsilon^3}\mu U_0 + [\frac{0.4(1-\varepsilon)^{1.1} {S_V}^{1.1} \mu^{0.1}}{\rho^{0.1}\varepsilon^3 U_0}]\rho {U_0}^2 \ldots\ldots\ldots \text{(3.c)}$$

From Equation 3.c, the air permeability and the Forchheimer coefficient can be calculated using the following equations based on Equation 2:

$$k_{KC} = K_F = \frac{\varepsilon^3}{5(1-\varepsilon)^2 {S_V}^2} \ldots\ldots\ldots \text{(3.c.i)}$$

$$\beta = \frac{0.4(1-\varepsilon)^{1.1} {S_V}^{1.1} \mu^{0.1}}{\rho^{0.1}\varepsilon^3 U_0} \ldots\ldots\ldots \text{(3.c.ii)}$$

For non-Darcian flows, the friction factor can be represented using the Carman correlation (Equation 4) and the friction can be represented as a function of the modified Reynolds number [1, 26].

$$\frac{R}{\rho U^2} = \frac{5}{Re_1} + \frac{0.4}{{Re_1}^{0.1}} \ldots\ldots\ldots \text{(4)}$$

The modified Reynolds number is calculated using Equation 5.

$$Re_1 = \frac{\rho U_0}{(1-\varepsilon) S_V \mu} \ldots\ldots\ldots \text{(5)}$$

3. SPHERICAL PARTICLE RESULTS

Due to the diversity and complexity of natural forest particles, benchmarking experiments using well controlled particles are first presented. These not only verify the reliability of the experimental testing apparatus, but can also be used as a reference for the natural forest samples. Hence, a set

of experiments were conducted using the experimental testing apparatus for regular-shaped spherical glass beads.

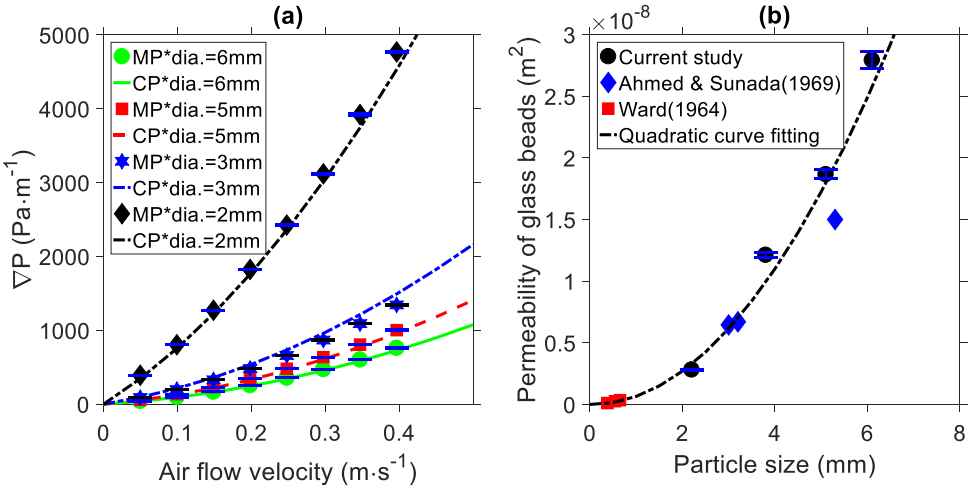

Figure 4. *Spherical glass bead particle results. (a) Pressure gradient as a function of air flow velocity for various sized particles. MP* is the measured pressure gradient and CP* is the calculated pressure gradient calculated using the Kozeny-Carman equation. (b) Air permeability measurement compared with previous studies [27, 28]. Repeatability of measurements represented by ± 1 standard deviation error bars.*

Figure 4(a) shows that, for spherical glass bead particles, the pressure gradient calculated using the Kozeny-Carman equation shows good agreement with the measured pressure drop. The results in Figure 4(a) demonstrate that the experimental testing apparatus is reliable and gives an approximate value for the pressure gradient that may be expected for forest fuels of a similar size.

The air permeability and the Forchheimer coefficient of glass beads were calculated using the Forchheimer equation, because at all of the measured flowrates in this study, the flow is non-

Darcian ($Re_d > 10$). The comparison in Figure 4(b) between the air permeability from the current results and previous studies [27, 28] gives further confidence in the experimental apparatus. Worth noting is that the permeability in the current study is with air as a working fluid, whereas the previous studies used water. Permeability is a fundamental property of a porous bed and ought to be independent of the fluid [29], which is demonstrated in Figure 4(b). Note that the pore sizes of the fuel beds in the study are much larger than the mean free path of air particles so the Klinkenberg effect can be safely neglected for air flows [30].

The air permeability can be calculated using the Kozeny-Carman equation (Equation 3.a.i or 3.c.i) if the specific area is known. In the case of a sphere of diameter D, the specific area, $S_V = \frac{6}{D}$. In both Equation 3.a.i and 3.c.i, the permeability is inversely proportional to the square of the specific area. On this basis, Figure 4(b) includes a quadratic curve fitting which shows a good agreement with the experimental results. Hence, this confirms that a quadratic relationship between the air permeability and particle size may be used for subsequent analysis.

The Forchheimer permeability and the Forchheimer coefficient of glass beads are listed in Table 4. The results of the Forchheimer coefficient show that an increase in the particle size of glass beads decreases the Forchheimer coefficient. According to the Forchheimer equation, the increase in the Forchheimer coefficient implies that the kinetic energy loss of air is higher in small particles than that in large particles.

Table 4 also includes measured air permeability of soy straw [13] and pine needles [8], which are other fuel beds reported in the literature. Although the size of soy straw was not reported in the paper [13], the size of soy straw particles is typically smaller than 6 mm. Despite the particle size of the fuels being in the same range as the glass beads, the permeability was much higher. Hence,

the results imply that particle shape has an effect on the air permeability and therefore will need to be determined for the irregular-shaped particles encountered within the fuel bed.

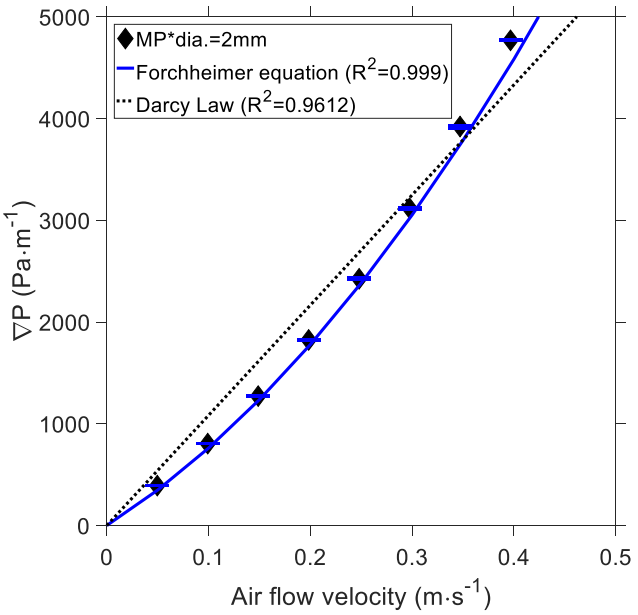

Figure 5. *A comparison between the Darcy law and Forchheimer equation on 2 mm spherical particles. Repeatability of measurements represented by ± 1 standard deviation error bars.*

A comparison between the Darcy law and Forchheimer equation on 2 mm spherical particles is shown in Figure 5. The Forchheimer fitting (R^2=0.999) in Figure 5, shows a better agreement with the experimental data than the Darcy fitting (R^2=0.9612). This is because the Darcy law is only valid under Darcian flow (Re<10); while most of the flows in this study are not in the Darcian flow regime. Hence, the Forchheimer equation should be used to determine the permeability of fuel beds.

Table 4. *Natural forest fuel particles physical properties.*

Spherical particles	**Particle size**	**Forchheimer permeability, k_F ($\times 10^{-9}$ m^2)**	**Forchheimer coefficient, β (m^{-1})**	**Darcy permeability, k_D ($\times 10^{-9}$ m^2)**
Glass beads	2.2 mm	2.8	11630	2.3 (by exp.)

	3.8 mm	12.1	3960	12.7 (by calc.)
	5.1 mm	18.7	3250	22.9 (by calc.)
	6.1 mm	27.9	2630	33.7 (by calc.)
Soy Straw*	Estimated (< 6 mm)	181-646	1200-4270	N/A
Pine needles+	0.5-1.85mm	40-314	N/A	N/A

*(Eric 2011) +(Santoni 2014)

4. MILLED FUEL PARTICLE RESULTS

4.1 Effects of fuel bed depth on the pressure drop across fuel bed

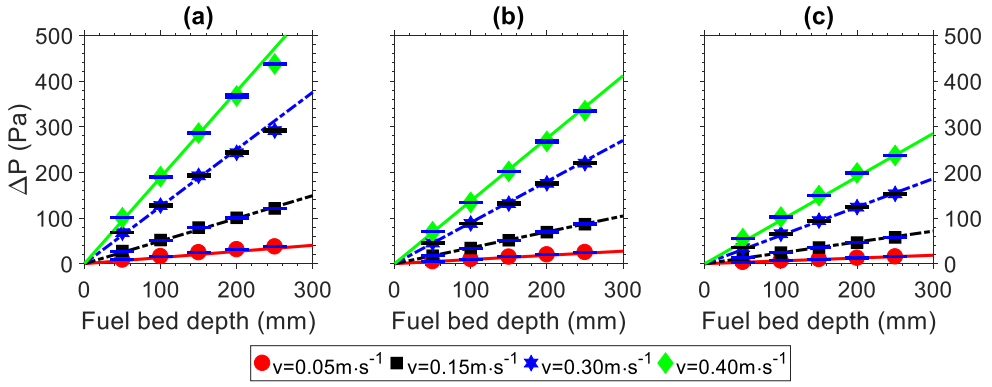

Figure 6. *Measured pressure drop as a function of the fuel bed depth for (a) 1–2 mm (b) 2–3 mm (c) 3–4 mm milled pine chip particles across a range of air flow velocities. Repeatability of measurements represented by ± 1 standard deviation error bars.*

After verifying the reliability of the experimental testing apparatus using regular-shaped particles (Section 3), a set of similar experiments were conducted for milled and sieved pine chips. Compared with glass beads, the milled biomass particles are more irregular in shape, and the behaviour of a porous medium made from them is expected to be more complex than that of the glass beads. In the case of spherical particles, it is accepted that the pressure gradient is independent of the bed depth. In the case of the irregular biomass fuel particles, this independence has not yet

been confirmed in the literature. Hence, Figure 6 assesses the linearity of the pressure drop measurements, as a function of bed depth, for a range of different particle size milled pine chips.

Overlaid on the experimental data points in Figure 6 are lines of best fit. It is apparent that the pressure drop across fuel bed is indeed linear with the fuel bed depth, which means that the pressure gradient of fuel bed is constant with a specific superficial velocity. In other words, the pressure gradient of fuel bed is dependent of fuel type, particle size and superficial air velocity. Hence, the pressure drop only needs to be measured at a single fuel bed depth, and can be inferred for other depths. For the remainder of the tests, only the deepest fuel bed was used, so as to maximise the pressure drop and thus minimise the uncertainty in the pressure gradient.

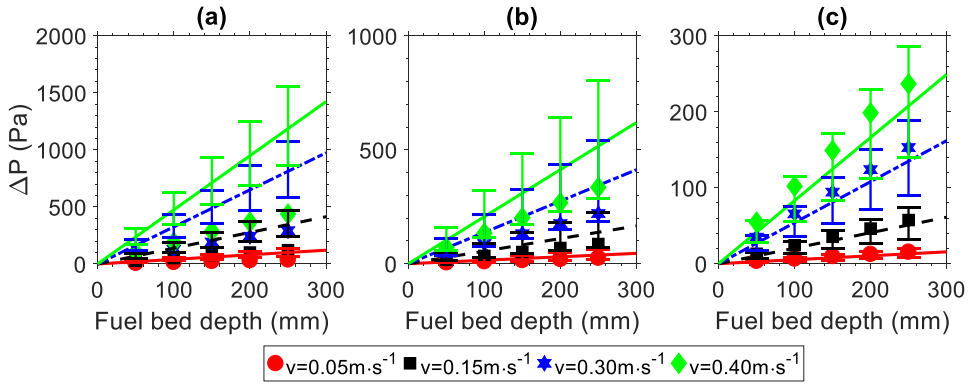

Figure 7. *Pressure gradient measured directly (markers) and calculated from the direct measured specific area (lines) as a function of fuel bed depth for pine chips over a range of air flow velocities. Error bars denote the calculated pressure drop based on the measure specific area through the Kozeny-Carman equation. Particle size ranges: (a) 1–2 mm (b) 2–3 mm (c) 3–4 mm.*

In Figure 7, the experimentally measured pressure drop is plotted (as per Figure 7) and overlaid with the calculated pressure drop using the Kozeny-Carman equation based on the direct measured

specific area of the particles and porosity (Table 2). The error-bars on the lines are determined from the resultant variability in the specific area, i.e. one standard deviation of the mean. Even accounting for the large error-bars, the calculated pressure drop based on the Kozeny-Carman equation is consistently higher than the measured values. The discrepancy between the calculated and measured pressure drop implies that the direct measured specific area is not the actual specific area of particle. This is because the direct measured specific area assumes a regular shape, which is unlikely to be the case for the biomass fuel. The specific area and the pore structure of the actual fuel bed are different from that of the bed of regular spheres, leading to different energy losses therefore different pressure drops shown in Figure 7.

Based on the results of Figure 7 it is deduced that the Kozeny-Carman equation is not able to accurately predict the pressure drop of the actual fuel bed. This is attributed to the errors in the assumptions used to determine the specific area. Instead, based on the measured pressure drop, the Kozeny-Carman equation (Equation 3.c) has been used to back-calculate the specific area. The results of this deduced specific area are compared to the direct measurements in Figure 7 for the various particle types and sizes.

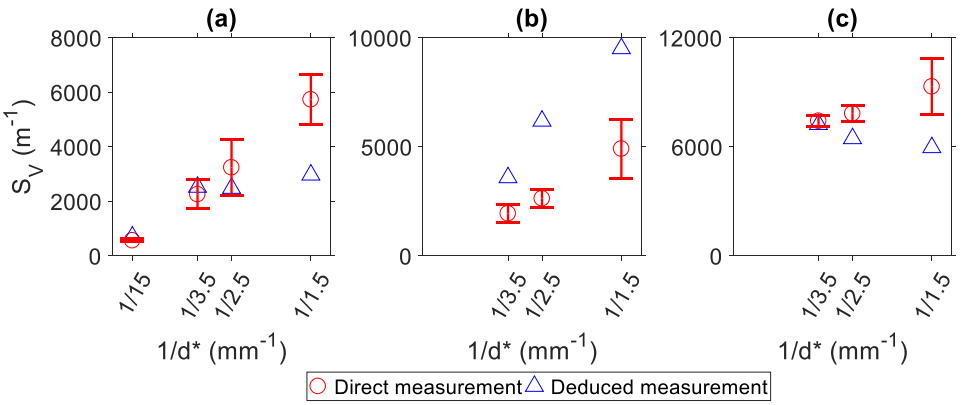

Figure 8. *Comparison of the direct measurement and the measurement through pressure gradient of the specific area under the different particle size (*Average sieve opening size). (a) pine chips (b) gum bark (c) gum leaves. Repeatability of measurements represented by ± 1 standard deviation error bars.*

Figures 8 shows the comparison between the direct measurement of the specific area and the deduced specific area, based on the Kozeny-Carman equation and pressure drop measurement, for the milled particles. The deduced measured specific area in Figure 8 is the average of the specific area calculated at the different superficial velocities. Hence, the specific area cannot accurately be determined for small particles, which are also the ones responsible for the majority of the pressure drop (Figure 4) and mass distribution (Figure 2) in a forest fuel bed. Therefore, to determine pressure gradient using the Kozeny-Carman equation first requires a correction of the direct measured specific area of the particles.

4.2 Effect of input air velocity on the pressure gradient

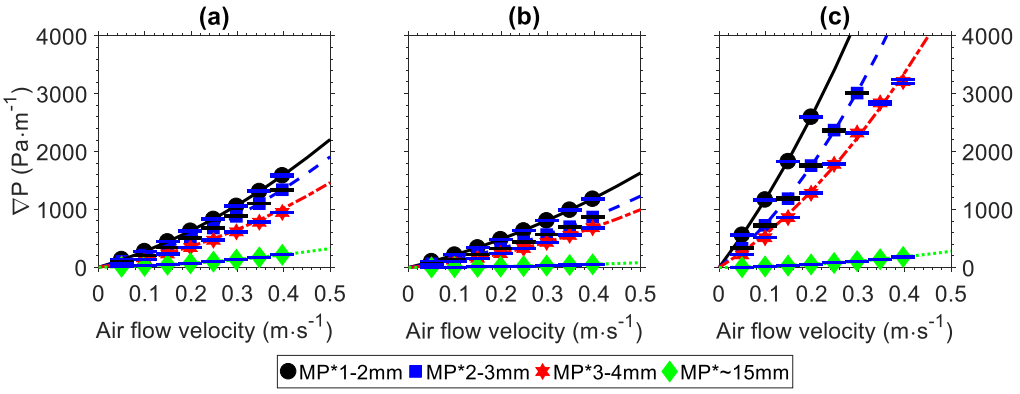

Figure 9. *Pressure gradient as a function of air flow velocity for particles: (a) pine chips (b) gum bark (c) gum leaves (Marker: measured pressure gradient; Line: calculated pressure gradient based on deduced measured specific area). Repeatability of measurements represented by ± 1 standard deviation error bars.*

Figure 9 presents the measured pressure gradient (markers) and the calculated pressure gradient (lines) against the superficial velocity. The consistency between the measured and calculated pressure gradients show that the relationship between the pressure gradient and the superficial velocity is quadratic for the milled biomass fuel beds, as the pressure gradient in the Kozeny-Carman equation is a function of the square of the superficial velocity. The results in Figure 9 also show that for the same particle size and superficial air velocity, milled gum leaf particles have the highest pressure gradient; the milled gum bark has the lowest pressure gradient. The difference in pressure gradient implies that fuel type has significant effects on the pressure gradient of a fuel bed, as different fuel type results in different shapes of milled particles.

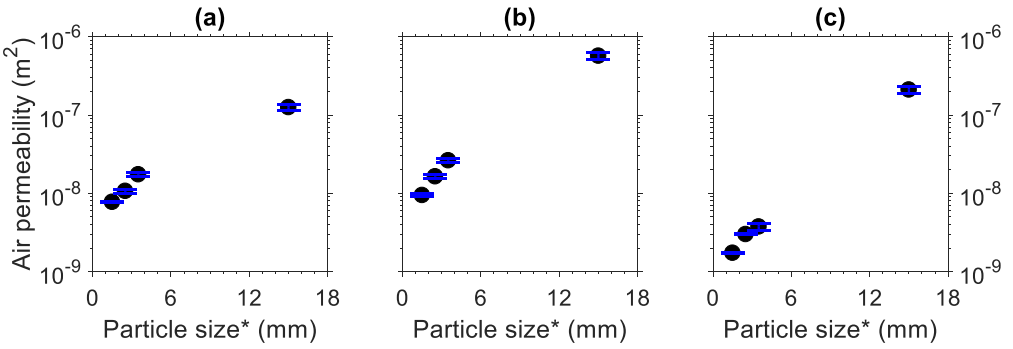

Figure 10. *Permeability (k) as a function of particle size for the milled particles (*Average sieve opening size) (a) pine chips, (b) gum bark, (c) gum leaves. Repeatability of measurements represented by ± 1 standard deviation error bars.*

The results in Figure 10 show that the air permeability of the fuel bed with small particles (<4 mm) is much less than that of the fuel bed with large particles (~15 mm). Furthermore, small particles contribute much more mass in natural forest fuel beds (Figure 2). Hence, small particles are expected to dominate the permeability.

As discussed in Section 3.1, the relationship between the air permeability and particle size is quadratic according to the Kozeny-Carman equation. The results shown in Figure 9 imply that the Kozeny-Carman equation is applicable for the milled biomass particles. Hence, theoretically the air permeability of the milled biomass fuel beds can be presented in a function of the square of particle size. The air permeability can be calculated from either pressure gradient or the particle/fuel bed properties. However, the pressure gradient needs to be obtained by conducting the experiments because the measured specific area of particles is not robust enough for the Kozeny-Carman equation. Hence, the air permeability of the milled biomass fuel beds can be alternatively estimated based on the average particle size, as it is much easier to measure the particle size.

The Forchheimer permeability and the Forchheimer coefficient of milled biomass fuel are listed in Table 5. The results in Table 5 show that for the same particle size, the air permeability of the pine chips beds is similar to that of the gum bark beds. The similar air permeability between the pine chips and gum bark beds is because the shape of these two fuel particles is also quite similar. The air permeability of the gum leaf beds is much lower (approximately one fifth) than those of the pine chips and gum bark beds for the same particle size. The shape of the milled leaf particle is flaky, which makes it easier for the leaf particles to create a more compact fuel bed compared to the milled pine chips and gum bark. Hence, these data imply that the particle shape has a significant effect on the air permeability, and this effect could be much higher than the effect of particle size on the air permeability.

Table 5. *Permeability (k) and Forchheimer coefficient (β) of the pulverised and sieved fuel material.*

Milled fuel material	**Particle size**	**Forchheimer permeability, k_F ($\times 10^{-9}$ m^2)**	**Forchheimer coefficient, β (m^{-1})**	**Darcy permeability, k_D ($\times 10^{-9}$ m^2)**
Pine chips	1-2mm	7.7	3450	6.6 (by exp.)
	2-3mm	10.7	3530	8.9 (by exp.)
	3-4mm	17.4	2840	16.0 (by calc.)
	~15mm	126	835	144 (by calc.)
Gum bark	1-2mm	9.5	2240	8.3 (by exp.)
	2-3mm	16.4	2260	13.9 (by exp.)
	3-4mm	26.3	2180	22.8 (by calc.)
	~15mm	570	228	461 (by calc.)
Gum leaf	1-2mm	1.7	10880	1.6 (by exp.)
	2-3mm	3.0	11520	2.7 (by exp.)

	3-4mm	3.8	7410	3.6 (by calc.)
	~15mm	211	787	227 (by calc.)

5. NATURAL FOREST FUEL BED PARTICLES

The results of the three milled biomass particles are shown in Section 4, where the fuel particles were broken down into small sizes using a mill. However, the fuel particles in the real world are broken down through the natural decomposition process. Hence, the shape of the particles in forests may be quite different from the milled fuel particles. As discussed in Section 4, the particle shape has a significant effect on the air permeability. Hence, it is also important to determine the air permeability of the natural forest fuel particles.

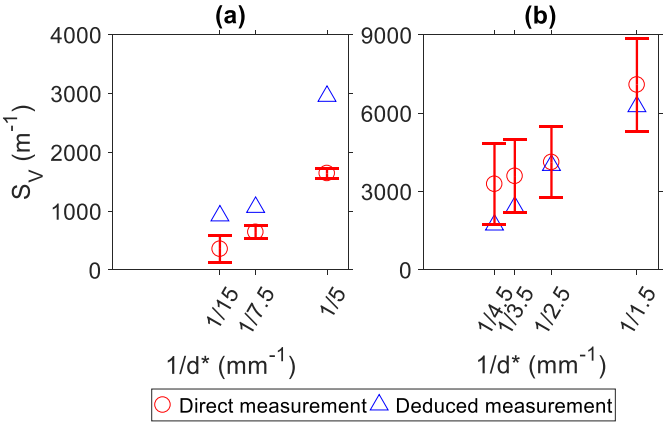

Figure 11. *Comparison of the direct measurement and the measurement through pressure gradient of the specific area under the different particle size (*Average sieve opening size) (a) twig, (b) decomposing matter (DM). Repeatability of measurements represented by ± 1 standard deviation error bars.*

The results in Figure 11(a) suggest that it is necessary to calculate the specific area for the twig particle no matter the size of the twig particle, as the deduced specific areas do not agree with the measured specific areas. The twig samples were assumed to be cylindrical when calculating their specific area; while the twig samples are so diverse that they cannot be represented by a cylindrical particle. For the decomposing matter particles (Figure 11(b)), the deduced specific areas are in good agreement with the measured specific areas.

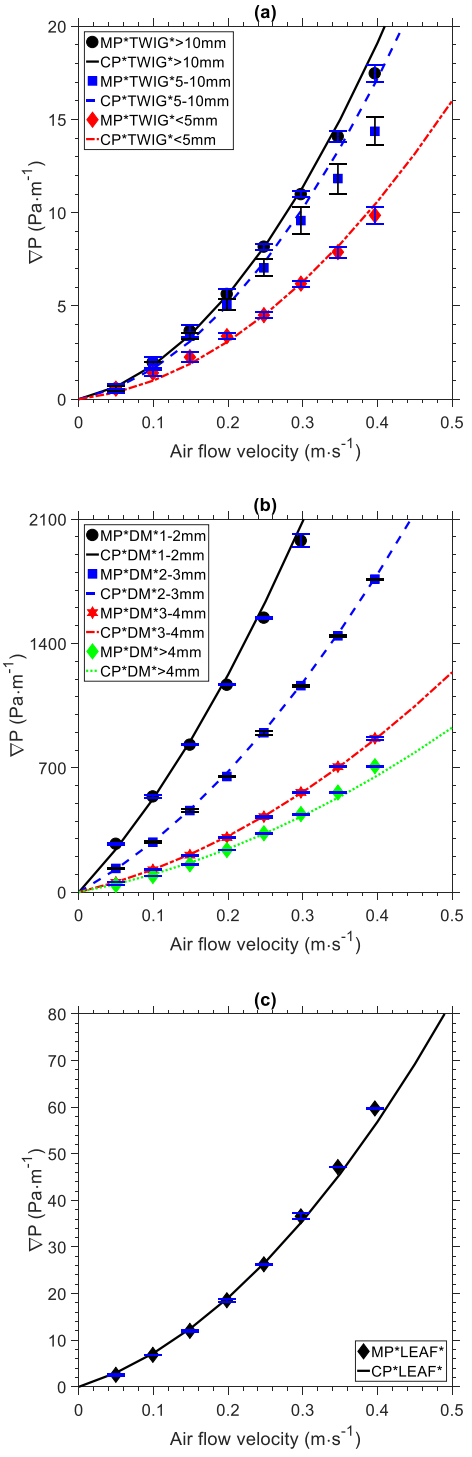

Figure 12. *Pressure gradient as a function of air flow velocity for particles: (a) twig (b) decomposing matter (DM) (c) leaf. (MP*: measured pressure gradient; CP*: calculated*

pressure gradient based on the deduced measured specific area). Repeatability of measurements represented by ± 1 standard deviation error bars.

Figure 12 shows the measured pressure gradients (markers) and the calculated pressure gradients (lines) against the superficial velocity for the natural forest fuel particles. The calculated pressure gradient was calculated using the Kozeny-Carman equation (Equation 3.c) based on the deduced measured specific area. The results in Figure 12 show that the measured and calculated pressure gradients are in good agreement, and this implies that the fuel bed made of the natural forest fuel material can be represented using the Forchheimer equation and the Kozeny-Carman equation. In comparison with the milled biomass, for the same particle size, the pressure gradient versus the superficial velocity curves of the decomposing matter beds are similar to those of the pine chips beds.

Based on the quadratic function of the pressure gradient and the superficial air velocity, the pressure gradient for each natural forest fuel bed particle size at a given superficial air velocity can be calculated. Similarly, the Forchheimer permeability was calculated based on the Forchheimer equation and the function of the pressure gradient versus the superficial velocity. However, similar to the milled biomass fuel particles, it is also difficult to measure the specific area of the natural forest fuel particles.

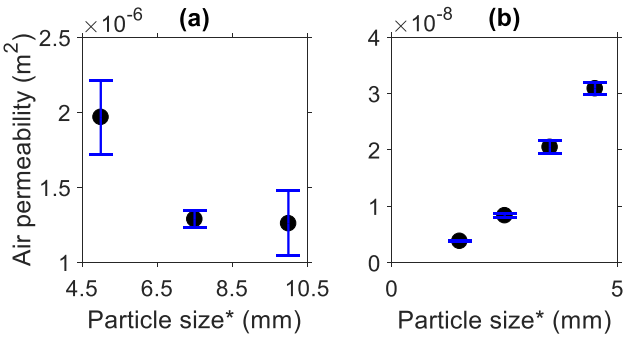

Figure 13. *Permeability (k) as a function of particle size (*Average sieve opening size) (a) twig (b) decomposing matter (DM). Repeatability of measurements represented by ± 1 standard deviation error bars.*

Figure 13 (a) shows that the particle size does not have a significant effect on the air permeability for the twig particles in the range of particle sizes investigated in the current study. Figure 13 (b) shows that decomposing matter shows a similar trend to the milled particles, i.e. a decrease in particle size decreases the air permeability. This is because the porosity of the twig fuel bed is much larger than that of the decomposing matter fuel bed. As shown in Figure 12 (b), the Kozeny-Carman equation is validated for the decomposing matter. Hence, the relationship between the air permeability of the decomposing matter beds and particle size is quadratic.

The Forchheimer permeability and Forchheimer coefficient of the natural forest material are listed in Table 6. The results in Table 6 show that the Forchheimer permeability of the twig and leaf samples are much higher than that of decomposing matter, which are up to 512 times and 123 times higher for the twig and leaf samples, respectively. In comparison with the results of the milled biomass particles (Table 5), it was found that for the same fuel type, the change in particle size has less effect on the air permeability than the fuel type. In the natural forest material, different fuel types have different particle shapes; hence, it implies that the particle shape has a significant

effect on the air permeability. Therefore, it is expected that the fire behaviour will be different within the different fuel beds in the natural forest fuel beds due to the difference in the air permeability.

Table 6. *Permeability (k) and Forchheimer coefficient (β) of the forest fuel bed material.*

Forest fuel material	**Particle size**	**Forchheimer permeability, k_F ($\times 10^{-9}$ m^2)**	**Forchheimer coefficient, β (m^{-1})**	**Darcy permeability, k_D ($\times 10^{-9}$ m^2)**
Twig/Bark	Small (0-5 mm)	1968±247	30±2	4809 (by calc.)
	Medium (5-10 mm)	1288±55	42±3	3368 (by calc.)
	Large (> 10 mm)	1259±217	60±7	3023 (by calc.)
Leaf	N/A	505±14	235±2	407 (by calc.)
Decomposing matter	1-2 mm	3.8±0.1	4957±465	3.3 (by exp.)
	2-3 mm	8.4±0.3	4786±169	6.7 (by exp.)
	3-4 mm	20.5±1.1	2741±117	19.2 (by calc.)
	> 4 mm	30.9±1.1	2480±36	30.0 (by calc.)

6. DISCUSSION

Darcy's Law and the Forchheimer equation are the two basic equations used to determine the air permeability of a porous medium, depending on flow regime. The Darcy permeability is not always equal to the Forchheimer permeability. Theoretically, the Darcy permeability can only be used to characterise a porous medium in Darcian flow; while the Forchheimer permeability is to characterise a porous medium in non-Darcian flow. In Darcian flows the superficial velocity is very low, leading to a small pressure drop which is difficult to measure accurately. Furthermore, the transition from Darcian to non-Darcian flow in a porous medium is vague. For example, the

transition from Darcian to non-Darcian flow can occur over a range of Reynolds number from 1 to 10 [22, 23, 31, 32].

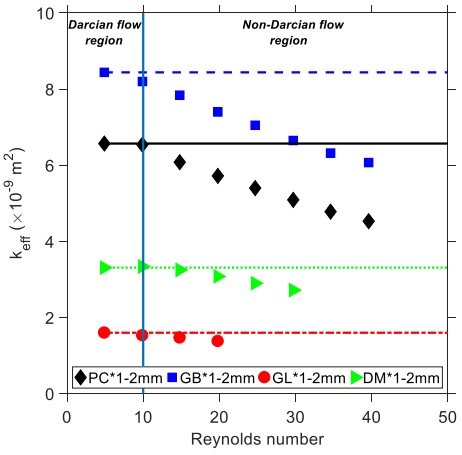

Figure 14. *Effective permeability (k_{eff}) as a function of Reynolds number. PC, pine chips; GB, gum bark; GL, gum leaf; DM, decomposing matter.*

The effective permeability was calculated using Darcy's law. The effective permeability (markers) and the Darcy's permeability (lines) are presented in Figure 14. The results in Figure 14 show that the effective permeability starts to decrease when Reynolds number is over 10, which is the upper limit of Darcy's law. This is because when Reynolds number is equal to, or below 10, the effective permeability is equal to the Darcy permeability of fuel bed. For the samples with low air permeability (gum leaf and decomposing matter), the upper limit of Darcy's law is slightly higher than 10. This finding is also reported by Sobieski (2014) [14]. For these cases, the Darcy permeability is equal to the effective permeability within the Darcian flow regime.

As mentioned previously, it is difficult to measure the pressure drop across the fuel bed in Darcian flow, as the pressure drop is too low to measure. Darcy's law requires the pressure gradient to determine the Darcy permeability. Hence, a different method is needed to determine the Darcy

permeability. A method is to calculate the Darcy permeability using the Kozeny-Carman equation. In this way, the Darcy permeability of a porous medium is calculated based on the specific area of particles and the porosity of the porous medium (Equation 3.c). The measured and calculated Darcy permeability for all samples is listed in Table 6. Comparing the Darcy permeability in Table 6 with the Forchheimer permeability in Table 4, 5 and 6, the Darcy permeability of the decomposing matter particles is close (with a maximum difference of 25 % at3-4mm) to the Forchheimer permeability for the same size, which means that the Darcy permeability can be assumed to be the same as the Forchheimer permeability for the decomposing matter particles.

7. CONCLUSIONS

This paper investigated the air permeability of fuel beds in forests, from the perspective of its effect on the combustion of fuel beds. An experimental testing apparatus was designed and developed to investigate the effects of particle size and type on the air permeability. The efficacy of the experimental testing apparatus was verified using spherical particles in different sizes. The air permeability of the porous medium made of glass beads were determined by experiment and calculation (Equation 3.c). The results show that the calculated pressure drop showed excellent agreement with the measured pressure drop, which implies that it is capable of calculating the air permeability for spherical particles. It was also found that the relationship between the air permeability and particle size is quadratic for spherical particles.

Three common biomass fuel types: pine chips, gum bark and gum leaf were milled and sieved into three sizes (1–2 mm; 2–3 mm; 3–4 mm). The air permeability of milled biomass fuel was also determined by experiment and calculation. The results show that the calculated pressure drop (Equation 3.c) is not in good agreement with the measured pressure drop. This is because it is

difficult to accurately measure the specific area of particles due to their irregular shape. Hence, the air permeability of the porous medium made of the milled biomass particles can only be determined by experiment. For the same particle size, the air permeability of milled gum leaves has the lowest air permeability, while the milled gum bark has the highest air permeability. These results suggest that the biomass fuel type has a significant effect on the air permeability. This can be attributed to the different porous pore structures of different fuel types. The results also imply that the relationship between the air permeability and particle size is quadratic for the milled biomass particles.

A natural forest fuel bed was separated into three categories: twig, leaf and decomposing matter; and the twig and decomposing matter were sieved into three (0–5 mm; 5–10 mm; > 10 mm) and four sizes (1–2 mm; 2–3 mm; 3–4 mm; > 4 mm), respectively. The air permeability of natural forest fuel bed was determined by experiment and calculation. Similar to the milled biomass fuel particles, the results show that the calculated pressure drop (Equation 3.c) does not match with the measured pressure drop due to the inaccuracy of the specific area estimations. The air permeability in natural forest fuel varies in different fuel types. For example, the air permeability of the twig layer is much larger (approximately 500 times) than that of the decomposing matter layer. Particle size does not have a significant effect for twigs, and the relationship between the air permeability and particle size is quadratic for decomposing matter.

In most of the cases, it is difficult to run the experiments with a Darcian air flow because the pressure drop is too low to reliably measure. By determining the effective permeability, the results show that the upper limit of Darcy's law for the low air permeability fuel bed is slightly higher than 10. The Darcy permeability was calculated using the Kozeny-Carman equation and the results show that the Darcy permeability is similar to the Forchheimer permeability. More research is

needed to better understand the relationship between the air permeability and the combustion of the forest fuel beds. The data presented in this paper is intended to be used for validation of subsequent models. The model can then be used to model the air flow in forest fuel beds.

AUTHOR INFORMATION

Corresponding Author

*E-mail: houzhi.wang@adelaide.edu.au.

ACKNOWLEDGMENTS

The support of the University of Adelaide, Australian Government Research Training Program Scholarship and the Bushfire and Natural Hazards CRC are gratefully acknowledged. The authors thank Mr Marc Simpson for his assistance throughout the experimental campaign.

REFERENCES

[1] R.G. Holdich, Fundamentals of particle technology, Midland Information Technology and Publishing, 2002.
[2] B. Teague, R. McLeod, S. Pascoe, Final report, 2009 Victorian bushfires royal commission, Parliament of Victoria, Melbourne Victoria, Australia, (2010).
[3] W. Steffen, L. Hughes, The critical decade 2013, Climate Change Science, Risks and Responses. Climate Commission, Department of Industry, Innovation, Climate Change, Science, Research and Tertiary Education, Commonwealth of Australia, (2013).
[4] H.H. Biswell, Prescribed burning in California wildlands vegetation management, Univ of California Press, 1989.
[5] E.E. Knapp, J.E. Keeley, E.A. Ballenger, T.J. Brennan, Fuel reduction and coarse woody debris dynamics with early season and late season prescribed fire in a Sierra Nevada mixed conifer forest, Forest Ecology and Management, 208(1) (2005) 383-397.
[6] R.M. Hadden, S. Scott, C. Lautenberger, A.C. Fernandez-Pello, Ignition of combustible fuel beds by hot particles: an experimental and theoretical study, Fire technology, 47(2) (2011) 341-355.
[7] X. Huang, G. Rein, Interactions of Earth's atmospheric oxygen and fuel moisture in smouldering wildfires, Science of The Total Environment, 572 (2016) 1440-1446.
[8] P. Santoni, P. Bartoli, A. Simeoni, J. Torero, Bulk and particle properties of pine needle fuel beds–influence on combustion, International Journal of Wildland Fire, 23(8) (2014) 1076-1086.

[9] H. Wang, P.J. van Eyk, P.R. Medwell, C.H. Birzer, Z.F. Tian, M. Possell, Identification and Quantitative Analysis of Smoldering and Flaming Combustion of Radiata Pine, Energy & Fuels, 30(9) (2016) 7666-7677.
[10] H. Wang, P.J. van Eyk, P.R. Medwell, C.H. Birzer, Z.F. Tian, M. Possell, Effects of Oxygen Concentration on Radiation-Aided and Self-sustained Smoldering Combustion of Radiata Pine, Energy & Fuels, (2017).
[11] H.E. Anderson, Aids to determining fuel models for estimating fire behavior, The Bark Beetles, Fuels, and Fire Bibliography, (1982) 143.
[12] S. El-Sayed, T. Khass, Smoldering combustion of rice husk dusts on a hot surface, Combustion, Explosion, and Shock Waves, 49(2) (2013) 159-166.
[13] A. Erić, D. Dakić, S. Nemoda, M. Komatina, B. Repić, Experimental method for determining Forchheimer equation coefficients related to flow of air through the bales of soy straw, International Journal of heat and mass transfer, 54(19) (2011) 4300-4306.
[14] W. Sobieski, A. Trykozko, Darcy's and Forchheimer's laws in practice. Part 1. The experiment, Technical Sciences/University of Warmia and Mazury in Olsztyn, (17 (4)) (2014) 321--335.
[15] R.P. Chapuis, M. Aubertin, Predicting the coefficient of permeability of soils using the Kozeny-Carman equation, École polytechnique de Montréal, 2003.
[16] C.P. Kyan, D. Wasan, R. Kintner, Flow of single-phase fluids through fibrous beds, Industrial & Engineering Chemistry Fundamentals, 9(4) (1970) 596-603.
[17] F. Mavis, E. Wilsey, Filter sand permeability studies, Eng. News Rec, 118 (1937) 299-300.
[18] R.P. Chapuis, D.E. Gill, K. Baass, Laboratory permeability tests on sand: influence of the compaction method on anisotropy, Canadian Geotechnical Journal, 26(4) (1989) 614-622.
[19] J. Kamath, E. de Zabala, R. Boyer, Water/oil relative permeability endpoints of intermediate-wet, low-permeability rocks, SPE Formation Evaluation, 10(01) (1995) 4-10.
[20] H. Shimizu, Air permeability of deposited snow, Contributions from the Institute of Low Temperature Science, 22 (1970) 1-32.
[21] M. Possell, M. Jenkins, T. Bell, M. Adams, Emissions from prescribed fire in temperate forest in south-east Australia: implications for carbon accounting, Biogeosciences Discussions, 11(9) (2014).
[22] R.E. Chapman, Geology and water: an introduction to fluid mechanics for geologists, Springer Science & Business Media, 2012.
[23] S.M. Hassanizadeh, W.G. Gray, High velocity flow in porous media, Transport in porous media, 2(6) (1987) 521-531.
[24] M.C. Sukop, H. Huang, P.F. Alvarez, E.A. Variano, K.J. Cunningham, Evaluation of permeability and non‐Darcy flow in vuggy macroporous limestone aquifer samples with lattice Boltzmann methods, Water Resources Research, 49(1) (2013) 216-230.
[25] P. Forchheimer, Wasserbewegung durch boden, Zeitz. Ver. Duetch Ing., 45 (1901) 1782-1788.
[26] P.C. Carman, Flow of gases through porous media, Academic press, 1956.
[27] N. Ahmed, D.K. Sunada, Nonlinear flow in porous media, journal of the Hydraulics Division, 95(6) (1969) 1847-1858.
[28] J. Ward, Turbulent flow in porous media, Journal of the Hydraulics Division, 90(5) (1964) 1-12.
[29] W.H. Green, G. Ampt, Studies on Soil Phyics, The Journal of Agricultural Science, 4(1) (1911) 1-24.

Chapter 7

Effects of *Eucalyptus* Species and Plant Parts on Smoldering Combustion

Statement of Authorship

Title of Paper	Effects of *Eucalyptus* species and plant parts on smouldering combustion
Publication Status	☐ Published ☐ Accepted for Publication ☑ Submitted for Publication ☐ Unpublished and Unsubmitted w ork w ritten in manuscript style
Publication Details	Wang, H., Van Eyk, P., Medwell, P., Birzer, C., Tian, Z., & Possell, M. (Submitted). Effects of *Eucalyptus* Species and Plant Parts on Smouldering Combustion. *Biomass & Bioenergy*

Principal Author

Name of Principal Author (Candidate)	Houzhi Wang		
Contribution to the Paper	I conducted a thorough literature review, and identified the research gaps of the paper. After discussion with my supervisors, a detailed research methodology and experimental plan were decided. I selected the fuels for this study. I collected and prepared the fuel samples for the experiments. I set up the experiments. I conducted all the experiments and collected experimental data independently. I processed, analysed and interpreted all the experimental data. I performed an analysis of the experimental results, and the analysis was presented in text or figures by me. I interpreted data, wrote the manuscript. I also acted as the corresponding author, and responded to the reviewers' and the editor's comments and recommendations.		
Overall percentage (%)	75		
Certification:	This paper reports on original research I conducted during the period of my Higher Degree by Research candidature and is not subject to any obligations or contractual agreements with a third party that would constrain its inclusion in this thesis. I am the primary author of this paper.		
Signature		Date	15/Jan/2018

Co-Author Contributions

By signing the Statement of Authorship, each author certifies that:

i. the candidate's stated contribution to the publication is accurate (as detailed above);

ii. permission is granted for the candidate in include the publication in the thesis; and

iii. the sum of all co-author contributions is equal to 100% less the candidate's stated contribution.

Name of Co-Author	Philip van Eyk		
Contribution to the Paper	This co-author provided feedback, supervised development of work, helped in data interpretation and manuscript evaluation.		
Signature		Date	19/Jan/2018

Name of Co-Author	Paul Medwell		
Contribution to the Paper	This co-author provided feedback, supervised development of work, helped in data interpretation and manuscript evaluation.		
Signature		Date	18-JAN-2018

Name of Co-Author	Cristian Birzer		
Contribution to the Paper	This co-author provided feedback, supervised development of work, helped in data interpretation and manuscript evaluation.		
Signature		Date	19 Jan 2018

Name of Co-Author	Zhao Feng Tian		
Contribution to the Paper	This co-author provided feedback, supervised development of work, helped in data interpretation and manuscript evaluation.		
Signature		Date	18/01/2018

Name of Co-Author	Malcolm Possell		
Contribution to the Paper	This co-author provided feedback, supervised development of work, helped in data interpretation and manuscript evaluation.		
Signature		Date	19/01/2018

Please cut and paste additional co-author panels here as required.

Effects of *Eucalyptus* species and plant parts on smouldering combustion

Houzhi Wang,[*, †, ‡] *Philip J. van Eyk,*[§] *Paul R. Medwell,*[†] *Cristian H. Birzer,*[†] *Zhao F. Tian,*[†] *and Malcolm Possell*[∥, ‡]

[†]School of Mechanical Engineering, The University of Adelaide, Adelaide, SA 5005, Australia.

[‡]Bushfire and Natural Hazards CRC, Melbourne, VIC 3002, Australia.

[§]School of Chemical Engineering, The University of Adelaide, Adelaide, SA 5005, Australia.

[∥]School of Life and Environmental Sciences, The University of Sydney, Sydney, NSW 2006, Australia.

KEYWORDS: wildfires; hazard reduction burning; smouldering combustion; *Eucalyptus*.

Abstract:

Eucalyptus is one of the most widespread plants in Australia, and there are more than 800 different *Eucalyptus* species in Australia. In a *Eucalyptus* forest, the accumulation of fuel, such as leaves, barks and twigs, builds up a fuel bed for fire events. The different plant parts (bark, leaf and twig) behave differently in a fire event because of their different physical and chemical properties. In light of the variety of different fuel

load scenarios, it is not clear what effects different *Eucalyptus* species and the plant parts have on smouldering combustion. Smouldering combustion is a slow and low-temperature form of combustion, which shows no flame. This study aims to develop a better understanding of the effects of *Eucalyptus* species and the plant parts on smouldering combustion. Smouldering combustion was investigated for the three plant parts (leaf, bark and twig) of four south-eastern Australian *Eucalyptus* species (*E*. *camaldulensis*, *E*. *fasciculosa*, *E*. *baxteri* and *E. obliqua*). It was found that the *Eucalyptus* species and plant parts have effects on smouldering combustion in terms of peak temperatures and product gases concentration. For example, the bark of stringybark samples have lower peak temperatures and higher CO/CO_2 ratio than those of the bark of smoothbark samples. Similarly, the leaf samples also have lower peak temperatures and CO/CO_2 ratio than those of the twig and bark samples. As a result, *Eucalyptus* species and plant parts should be taken into account as important factors in wildfires modelling and planning for hazard reduction burning.

1. Introduction

Wildfires are a global issue, and are becoming worse due to climate change. A recent study found that the frequency of large wildfires is increasing [1]. At the same time, wildfires are one of the major contributors to climate change, as wildfires emit large amounts of greenhouse gases [2] furthermore, extreme wildfires may slow down the natural regeneration of vegetation, which reduces the net carbon sink [3]. A vicious

circle between climate change and wildfires is gradually forming. Hence, it is crucial to develop a better understanding of wildfires to help mitigate their impacts.

Vegetation plays important roles in wildfires, as it determines the size and amount of fuel available for wildfires. In Australia, *Eucalyptus* is an iconic native tree genera, with more than 800 species present in the country [4]. It plays an important role in Australian wildfires due to its highly combustible oil. *Eucalyptus* has been introduced and widely planted all around the world, because of its high environmental and economic benefits. For example, *Eucalyptus* is one of the most common sources for pulpwood [5]. *Eucalyptus* is also often used to reduce soil erosion [6]. There are approximately 20 million hectares of *Eucalyptus* forest planted on the Earth, and the majority of them were planted outside Australia [7, 8]. Although the planting of *Eucalyptus* trees can bring many benefits to people, it also greatly increases the risk of wildfires. For example, *Eucalyptus* was introduced to Portugal to prevent soil erosion and has since become a widely distributed species across the country. *Eucalyptus* trees were a predominant factor in the 2017 Portuguese wildfires, which were the country's worst wildfires to-date [9]. As *Eucalyptus* wildfires are an increasingly important issue more research on this type of fire is urgently needed to better understand the associated combustion processes.

One of the most common ways to identify *Eucalyptus* species is from the bark, and can be broadly divided into either smoothbark or stringybark. A previous study has also shown that the leaf oils from different *Eucalyptus* species have different chemical

compositions [10], and the difference in chemical compositions could have effects on combustion processes. Hence, it is important to know the effects of different *Eucalyptus* species on smouldering combustion. In a *Eucalyptus* forest, the accumulation of fuel, such as leaves, bark and twigs, builds up a fuel bed for fire events. The different plant parts (leaf, bark and twig) behave differently in a fire event because of their different physical and chemical properties. However, understanding of the effects of different *Eucalyptus* species and their plant parts on the combustion process is still lacking, and this knowledge is essential for a better understanding of *Eucalyptus* wildfires.

To investigate the effects of *Eucalyptus* species and their plant parts on the combustion process, it is necessary to characterise different fuel samples as the fuel properties have critical effects on the combustion process. The fuel properties include both the physical and chemical properties. It is known that the chemical composition of leaves is qualitatively different from that of barks or twigs [11]. However, there is a lack of quantitative analysis of the chemical composition of leaf, bark and twig; not to mention the chemical properties that are relevant to combustion. The chemical and physical properties of the fuel samples were determined to investigate the effects of these properties on smouldering combustion. The chemical properties include proximate and ultimate analyses, while air permeability is the chosen physical property. Air permeability has significant effects on the combustion of a fuel bed. Hence, the physical and chemical characterisations of the different plant parts from different *Eucalyptus* species are essential to understand their effects on the combustion process.

There are two types of combustion processes involved in wildfires, namely, smouldering and flaming combustion. Previous research on wildfires has mainly focused on flaming combustion, as it is often considered a more dangerous and destructive type of combustion regime than smouldering combustion. However, smouldering combustion has negative impacts on ecosystems because it can kill seeds and roots which greatly prolong the plant restoration process [12]. The delay of the plant restoration process also reduces the carbon offset capability of a forest after a wildfire [13]. Furthermore, smouldering combustion itself poses a safety issue in wildfires and hazard reduction burning, as it is difficult to detect or predict the initiation of smouldering combustion. Previous studies on smouldering combustion have investigated radiata pine [14-16], which is another important tree species to wildfires, however, there is a paucity of research on the smouldering combustion of *Eucalyptus*.

The primary research aim of this study is to investigate the effects of different *Eucalyptus* species on smouldering combustion. More specifically, to determine if there are any differences between smooth-bark and stringybark *Eucalyptus* trees. The secondary research aim is to investigate the effects the different plant parts have on the combustion process. This study also aims to provide quantitative analyses of the chemical and physical properties of the different plant parts from different *Eucalyptus* species.

2. Methodology

2.1 Fuel selection, collection and preparation

Eucalyptus species can be divided into two types: smooth-bark and stringybark [17]. In the present study, four *Eucalyptus* species are investigated, namely, two smooth barks: *E. camaldulensis* and E*. fasciculosa*, and two stringybarks: *E. baxteri* and *E. obliqua*. These four species were collected from Black Hill Conservation Park, South Australia, and are all native to south-eastern Australia. For each species, three plant parts (bark, leaves and twigs) were collected. Among the four species and three plant parts, a total of 12 unique fuels were considered.

For the leaf samples, the fresh adult leaves were picked directly from trees for consistency. For the twig samples, twigs were cut from trees. The bark samples were collected from the trunk. To reduce variability between samples, all the fuel samples were milled, and sieved (1 mm < d < 2 mm, where d is the sieve mesh size) and then dried in an oven at 105°C for 24 hours, consistent with the drying method presented in a previous study [18]. The reason for milling and sieving the fuel samples is to reduce variability between samples. It is important to note that the pulverised fuel samples are different from the fuel particles in a forest fuel beds in terms of particle size and shape. This is because the effects of particle shape and size are not in the scope of this study.

2.2 Fuel characterisation

All the fuel samples were characterised based on their physical and chemical properties. Although all of the fuel samples were milled and sieved into the same particle size range, the different fuel samples have different particle shapes. Hence, the air permeability of the fuel bed was determined, as it has a significant effect on the air flow and the combustion of the fuel.

For the air permeability experiments, the sieved pulverised fuel samples were loaded into an air permeability testing rig [16], and the pressure drop across the fuel bed recorded under different inlet air flow velocities. The air permeability of the fuel beds was determined using the Forchheimer equation (Equation 1).

$$-\frac{dP}{dx} = \frac{\mu}{k_F} U_0 + \beta \rho U_0^2 \cdots\cdots (1)$$

where $\frac{dP}{dx}$ is the pressure gradient across the fuel sample; μ is the dynamic viscosity of air; ρ is the air density; k_F is the Forchheimer permeability; and β is the Forchheimer coefficient.

The chemical characterisation of the fuel samples was based on thermogravimetric and ultimate analyses. The proximate analysis was conducted on a thermogravimetric analyser (TGA/DSC 2, Mettler Toledo, Greifensee, Switzerland) according to previous studies and the relevant standard [18-20]. The heating rate in the thermogravimetric analysis was set at $2K \cdot min^{-1}$. One of the main purposes of the thermogravimetric analysis is to investigate the pyrolysis rate under different temperatures. Hence, the

heating rate was kept low in order to provide accurate and detailed information of the pyrolysis rate at various temperatures. The thermogravimetric analysis was repeated three times for each of the fuel samples to ensure verifiable repeatability.

Ultimate analysis was conducted to determine the elemental composition, including carbon, hydrogen, nitrogen and oxygen of the fuel samples. The ultimate analysis was conducted in an elemental analyser (2400 CHNS/O Series II System, Perkin Elmer, Waltham, Massachusetts, United States). For the ultimate analysis, three repeats were completed for each fuel samples.

The higher heating value (HHV) was measured using an oxygen bomb calorimeter (6400 Automatic Isoperibol Calorimeter; Parr Instrument Company, Moline IL) and also determined based on the results of ultimate analysis and Equation 2 [21]. A comparison between the experimentally determined and theoretical higher heating values were made to cross check the higher heating values of the fuel samples.

$$HHV = 0.3491 \cdot Y_C + 1.1783 \cdot Y_H - 0.0151 \cdot Y_N - 0.1034 \cdot Y_O - 0.0211 \cdot Y_{ash} \ldots\ldots (2)$$

Where Y_C is the mass fraction of carbon; Y_H of hydrogen; Y_N of nitrogen; Y_O of oxygen; Y_{ash} of ash, and HHV reported in $MJ \cdot kg^{-1}$.

Carbohydrate and lignin composition analysis was used to determine the percentage of the three major components, namely, cellulose, hemicellulose and lignin, in each fuel sample. These three components are the main constituents of plants [21, 22]. The

theory of the carbohydrates and lignin composition analysis is based on the assumption that a mechanical mixture of materials would give a thermogram that would be the arithmetic sum of the proportional quantities of each component [22].

Cellulose (CAS-No.: 9004-34-6), xylan (CAS-No.: 9014-63-5) and lignin (CAS-No.: 8068-05-1) were obtained from Sigma-Aldrich Co., Ltd (St. Louis, Missouri, United States). Xylan was selected to represent hemicellulose, as it is one of the most common types of hemicellulose [23, 24]. Thermogravimetric analyses of cellulose, hemicellulose and lignin were conducted in the same thermogravimetric analyser using the same method as for the fuel samples. Then, it is assumed that the fuel sample is composed of five components, namely, cellulose, hemicellulose, lignin, protein and ash (Equation 3):

$$\boldsymbol{Cellulose}(\%) + \boldsymbol{Hemicellulose}(\%) + \boldsymbol{Lignin}(\%) + \boldsymbol{Protein}(\%) + \boldsymbol{Ash}(\%) = \mathbf{100}(\%) \ldots\ldots (\mathbf{3})$$

The percentage of protein was estimated based on the nitrogen content from the ultimate analysis using the Kjeldahl method [25]. The ash content is based on the results of the proximate analysis. Protein and ash were assumed constant across the temperature range of the thermogravimetric analysis. Protein is assumed constant due to two reasons. Firstly, protein is not a major chemical component in the fuel samples. Secondly, unlike cellulose, hemicellulose and lignin, it is difficult to find a reference protein which can be used to present the protein the fuel samples. Hence, the method of the carbohydrates and lignin composition analysis is to find mixtures of cellulose,

hemicellulose and lignin, whose derivative thermogravimetric curves match with those of the fuel samples. Figure 1 illustrates how a three components mixture can be simplified and represented by an arithmetic sum of the three components' thermograms. The proportions of the three components were determined from curve-fitting to the thermogram of each of the *Eucalyptus* fuel samples.

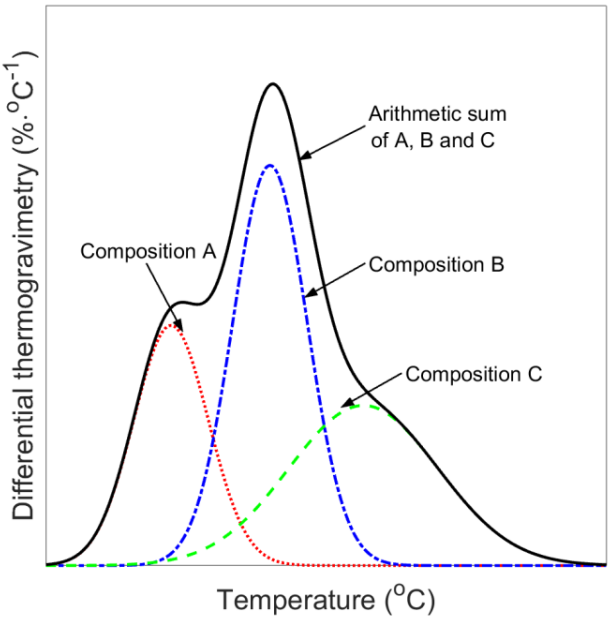

Figure 1. An illustration of the arithmetic sum of three compositions

2.3 Combustion experiment

The combustion experiment was designed to investigate the effects of the *Eucalyptus* species and the plant parts on combustion. The combustion was conducted using the same testing rig as in previous studies [15, 16].

2.3.1 Experimental apparatus

The experimental apparatus consists of six main components: an infrared heat lamp, a smouldering reactor, thermocouples, a laboratory balance, a scrubber and a gas analyser. The infrared heat lamp is used to heat the fuel sample in the smouldering reactor. Five thermocouples installed in the reactor measure the temperature: one above the fuel bed (the freeboard, FB) and four embedded in the fuel (TC1−4). The reactor has a square cross-sectional area of 1444 mm^2 (38 mm × 38 mm) and a height of 120 mm. The smouldering reactor has one oxidizer inlet at the bottom of the reactor, and one output connected to a gas analyser (VARIOplus, MRU Instrument Inc., Neckarsulm, Germany). A scrubber (described in the Supporting Information of Wang (2017)[16]) is installed between the smouldering reactor and the gas analyser to remove heavy hydrocarbons and tars, in order to avoid contamination within the gas analyser. The gas analyser measures the dry-basis volumetric concentration of five gases, namely, O_2, CO, CO_2, H_2, and CH_4.

2.3.2 Experimental setup

The combustion of fuel samples was initiated by the radiant heat flux generated by an infrared heat lamp. The level of the radiant heat flux was controlled using a Variac. The radiant heat flux level was set at 40 $kW \cdot m^{-2}$ based on the Australian Standard (AS 3959–2009) for Construction of buildings in bushfire-prone areas [26].

The combustion experiment in this study focused on smouldering combustion, a slow form of combustion which shows no flame. Hence, the input oxidizer flow velocity was set to 15 $mm \cdot s^{-1}$, as smouldering combustion generally requires a lower air flow velocity than for flaming combustion [15]. The oxidizer used in this study is air.

The combustion experiment was conducted for the 12 fuel samples. As the fuel samples have various densities, the volume of the testing samples was kept constant to reduce variability between fuel samples. The mass of the sample used in each run was 6 grams for the *E. baxteri* and *E. obliqua* bark samples, and 12 grams for the other fuel samples. The reason that the mass of the *E. baxteri* and *E. obliqua* bark samples was less than that of the other fuel samples is because the bark of the stringybark *Eucalyptus* species (*E. baxteri* and *E. obliqua*) is fibrous and less dense than the other fuel samples.

2.3.3 Experimental procedure

Before each experiment, the predetermined amount of the pre-dried fuel samples was carefully loaded into the combustion reactor and the air permeability reactor to create an unconsolidated fuel bed; this is to ensure the consistency throughout the fuel bed. The input oxidizer flow velocity was set, and an aluminium shutter was placed above the reactor to initially isolate the fuel sample from the radiant heat flux. After the heat flux levels were adjusted to the predetermined value, temperature, product gas concentration, and mass change recordings commenced. Then, the aluminium shutter was removed, so that the fuel bed was directly exposed to the radiation. The heat lamp was kept on for 900 seconds. The completion of the combustion process was

determined based on the measurements of temperature, gas analysis and mass change.

Multiple experiments under the same conditions were conducted to examine the reproducibility of the measurements. According to the results, the reproducibilities of the temperature measurement, and gas analyses were 91 % and 87 %, respectively. Although care needs to be taken in extrapolating the results of a single experiment, it is inevitable that very detailed measurements can be performed only for a limited number of cases. Also, there is substantial value in identifying what does happen in at least one case and in demonstrating an approach by which such details can be provided for other assessments.

3. Results/Discussion

3.1 Fuel characterisation

3.1.1 Chemical characterisation

The chemical characteristics of the fuel samples were determined based on the results of proximate and ultimate analyses. The chemical characteristics also include the differences in the peak pyrolysis rates and the temperatures at which the peak pyrolysis occurred among the fuel samples.

3.1.1.1 Proximate analysis

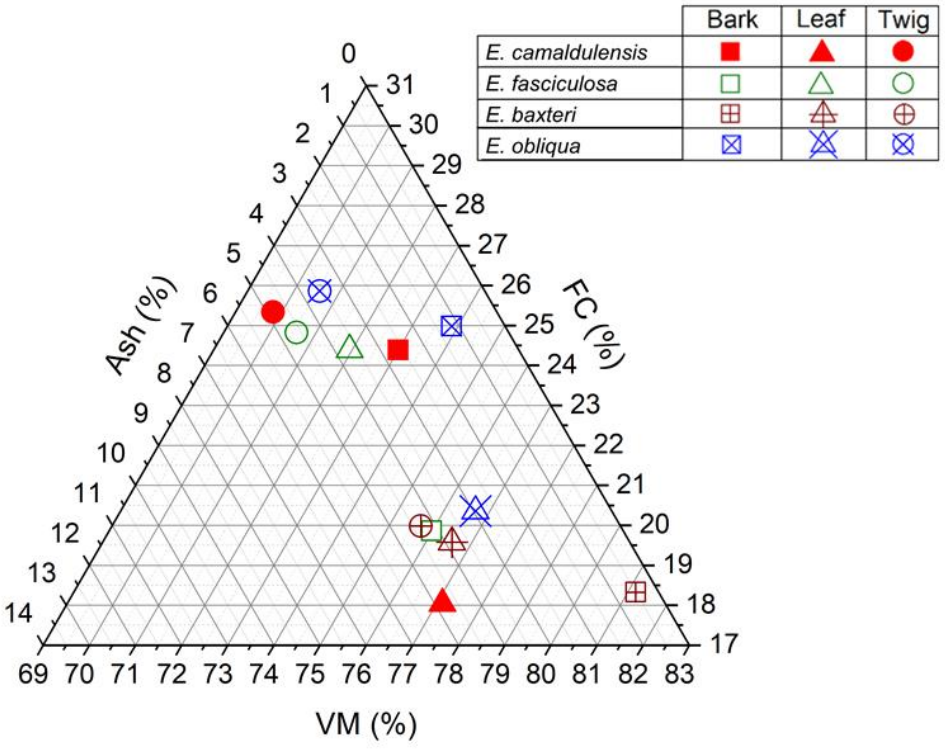

Figure 2. Ternary plot of volatile matter (VM), fixed carbon (FC) and ash. Species: *E. camaldulensis* = solid, *E. fasciculosa* = hollow, *E. baxteri* = square cross, and *E. obliqua* = diagonal cross. Plant parts: bark = square, leaf = triangle, and twig = circle.

Figure 2 shows the average percentages of volatile matter (VM), fixed carbon (FC) and ash (more details are presented in Table A1 of Supplementary Information). The results in Figure 2 show that most of the twig and leaf samples have similarities in the contents of volatile matter, fixed carbon and ash; while the bark samples are generally more diverse. For example, most of the twig samples have a relatively high content of fixed

carbon (~24.5-26 %), but a low content of volatile matter (~69-71 %). Theoretically, smouldering combustion would occur preferentially in the twig samples, as they have more fixed carbon. This is because, in self-sustained smouldering combustion, the majority of heat is from the oxidation of carbon [27]. Most of the leaf samples have a higher content of volatile matter (~76-77.5 %), a low content of fixed carbon (~18-20.5 %). Hence, the leaf samples could potentially produce more volatile matter, which is essential for flaming combustion [28].

From the results of proximate analysis (Figure 2), there is no significant correlation between the *Eucalyptus* species and the contents of volatile matter, fixed carbon and ash. For the bark samples, the *Eucalyptus* species do not have significant effect on the contents of volatile matter, fixed carbon. However, the barks of the stringybark *Eucalyptuses* (*E. baxteri* and *E. obliqua)* have a lower content of ash (~0.5-1.5 %) than those (2.5~4.5 %) of the smooth-bark *Eucalyptus* (*E. camaldulensis* and *E. fasciculosa*).

The results of the proximate analysis present that the leaf samples generally have higher volatile matter contents and lower fixed carbon than those of the bark and twig samples; and the high content of volatile matter is favoured by flaming combustion. The diversity in the contents of volatile matter and fixed carbon of the bark samples indicates that the combustion process of the barks of different *Eucalyptus* species could also be diverse. The proximate analysis results also show that ash content in the bark changes most significantly between the smooth and stringybark *Eucalyptus*, and therefore this is

anticipated to be a contributor to differences in the combustion results later presented in Section 3.2.

3.1.1.2 Ultimate analysis

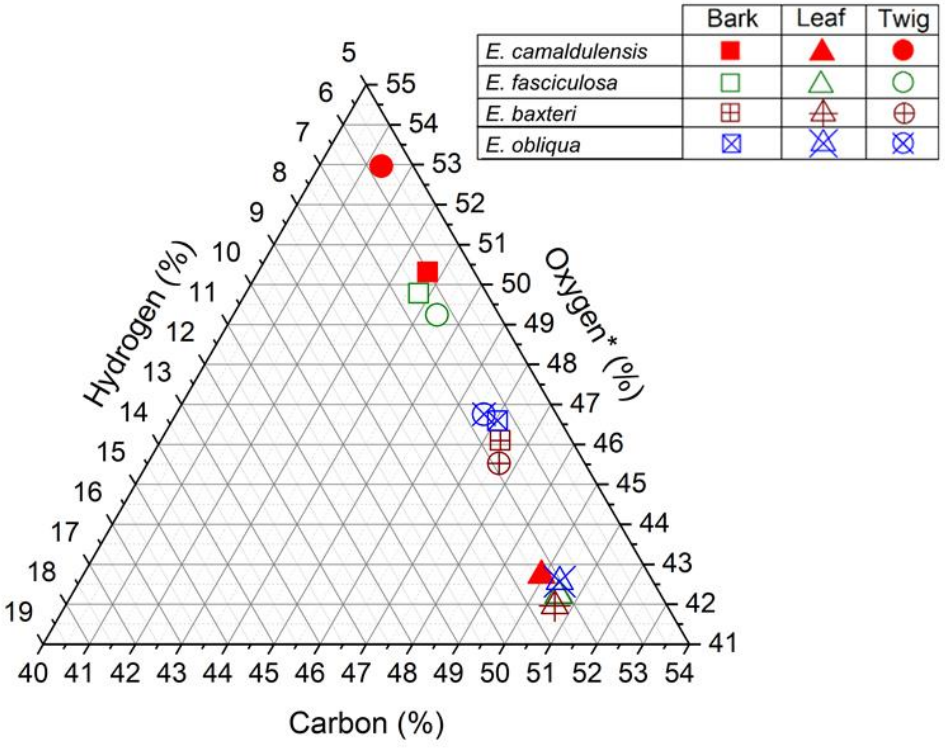

Figure 3. Ternary plot of ultimate analysis. Mass-based concentration excludes the nitrogen content. Oxygen was calculated by difference. Species: *E. camaldulensis* = solid, *E. fasciculosa* = hollow, *E. baxteri* = square cross, and *E. obliqua* = diagonal cross. Plant parts: bark = square, leaf = triangle, and twig = circle.

Figure 3 shows the results of ultimate analysis (further details in Table A1 of Supplementary Information), excluding the nitrogen contents to more clearly elucidate the results. The reason that the nitrogen content was not included in the figure is the nitrogen content (<1.65 %) of the fuel samples is much lower than the carbon, oxygen and hydrogen contents. Nevertheless, according to the Kjeldahl method [25], the nitrogen content indicates the protein content in the fuel samples. For example, the results in Table A2 show that the nitrogen content of the bark (0.13~0.58 %) and twig (0.35~0.44 %) samples is much lower than that of the leaf (0.90~1.65 %) samples. The high content of nitrogen in the leaf samples suggests that the leaf samples contain more protein. The high carbon and hydrogen contents of the leaf samples imply that the leaf samples have higher heating values than the twig and bark samples.

The results in Figure 3 show that the leaf samples have similarities in the carbon, hydrogen and oxygen contents. Furthermore, the carbon content of the leaf (50~51 %) samples are higher than that of the twig (41~48 %) and bark (43.5~47.5 %) samples; and the hydrogen content of the leaf (7~7.5 %) samples is also slightly higher than that of the twig (5.5~7 %) and bark (6~6.5 %) samples. The elemental composition is closely related to the heat of combustion [21, 29]; hence, the complete combustion of the leaf samples could release more energy per unit mass of the fuel than that of the twig and bark samples. Table 1 presents the estimated and measured higher heating value of the fuel samples. The estimated higher heating values were determined using the results of ultimate analysis (Section 2.1). From Table 1, it can be seen that the smooth-bark samples have slightly lower heating values than that of the stringybark samples. This is

because the stringybark samples normally have higher carbon contents than that of the smooth-bark samples (Figure 3). The results in Table 1 also show that the estimated higher heating values are very close to the measured higher heating values, which further indicate the effects that the *Eucalyptus* species and the plant parts have on the higher heating values.

Table 1. Estimated and measured higher heating value.

Fuel sample (Fuel species)	**Estimated higher heating value ($MJ \cdot kg^{-1}$, dry basis)**			**Measured higher heating value ($MJ \cdot kg^{-1}$, dry basis)**		
	Bark	**Leaf**	**Twig**	**Bark**	**Leaf**	**Twig**
E. camaldulensis	17.1	21.3	15.6	16.2	20.0	14.9
E. fasciculosa	17.7	21.5	17.8	16.6	20.2	16.6
E. baxteri	19.3	21.8	19.8	18.0	20.4	18.5
E. obliqua	18.8	20.7	18.8	17.8	19.5	17.6

Figure 3 shows that the *Eucalyptus* species do not have significant effects on the carbon, hydrogen and oxygen contents of the leaf samples. However, there is a significant correlation between the *Eucalyptus* species and the carbon content of the twig and bark samples. The results in Figure 3 show that the bark samples from the

stringybark *Eucalyptus* (*E. Baxteri* and *E. Obliqua)* have a lower carbon content than that of the smooth-bark *Eucalyptus* (*E. Camaldulensis* and *E. Fasciculosa*).

From the results of ultimate analysis, the leaf samples have distinctive carbon, hydrogen, nitrogen contents from the bark and twig samples. The results also show that the carbon content can be used to distinguish the bark and twig samples between the smooth and stringybark *Eucalyptus*.

3.1.1.3 Pyrolysis reaction

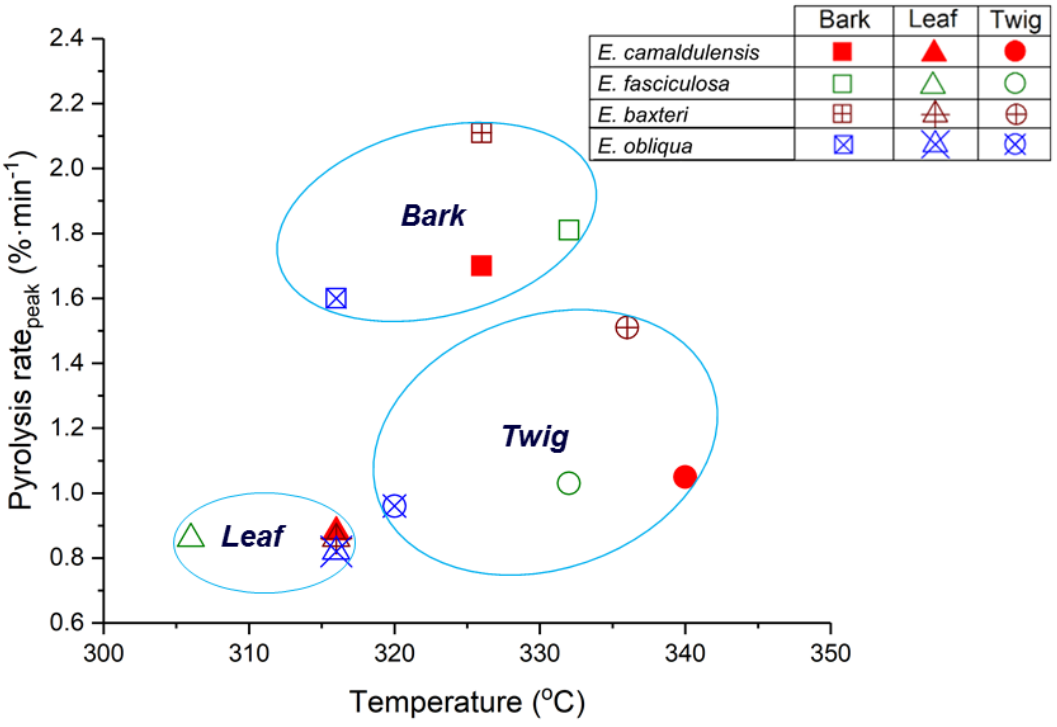

Figure 4. Plot of average peak pyrolysis rate value and the temperature at which the peak pyrolysis rate occurred, at a heating rate of 2 K·min^{-1}. Species: *E. camaldulensis* = solid, *E. fasciculosa* = hollow, *E. baxteri* = square cross, and *E. obliqua* = diagonal cross. Plant parts: bark = square, leaf = triangle, and twig = circle.

The thermogram of the pyrolysis of the fuel samples is heavily dependent on the chemical components of the fuel samples. Hence, the thermogram of the pyrolysis is one of the ways to understand the differences in chemical components among all the fuel samples. For example, the peak pyrolysis rate represents the reaction rate of

pyrolysis, and the temperature at which the peak pyrolysis rate occurred, is affected by the chemical components of the fuel samples. Figure 4 shows the peak pyrolysis rate and the temperature at which the peak pyrolysis rate occurred, for all the fuel samples.

The results in Figure 4 show that the bark, leaf and twig samples have different peak pyrolysis rate and the temperature at which the peak pyrolysis rate occurred. For example, the leaf samples have lower peak pyrolysis rate and the temperature at which the peak pyrolysis rate occurred compared with the twig and bark samples. The low pyrolysis rates suggest that the chemical components of the leaf sample are more complex than those of the twig and bark samples. As different chemical components normally have different pyrolysis temperature and peak pyrolysis rate; a fuel sample, which has more chemical components, will generally have a lower peak pyrolysis rate. This implies that the bark samples have fewer chemical components than the leaf samples. For example, cotton has a simple chemical composition, in which more than 90 % of cotton is constituted by cellulose [30] while, bagasse has a more diverse chemical compositions. Under the same heating rate, the peak pyrolysis rate of cotton (16.13 %•min^{-1}) is higher than that of bagasse (11.95 %•min^{-1}) [22].

For the bark and twig samples, the different *Eucalyptus* species does have some effects on the peak pyrolysis rates and the temperature at which the peak pyrolysis rate occurred. For instance, the bark and twig samples of *E. baxteri* have higher peak pyrolysis rates compared to the other *Eucalyptus* species, while the bark and twig samples of *E. obliqua* have the lowest temperature at which the peak pyrolysis rates

occur. For the leaf samples, the different *Eucalyptus* species do not appear to have a significant effect on the pyrolysis rates.

From Figure 4, the pyrolysis reactions of the same plant parts are similar. In each plant part, the *Eucalyptus* species that have the lowest temperature at which the peak pyrolysis rate occurred, e.g. *E. fasciculosa* for leaf, and *E. obliqua* for bark and twig, generally have a lower content of volatile matter and a higher content of fixed carbon than those of the other *Eucalyptus* species. In the bark and twig samples, it was also found that the samples with the highest peak pyrolysis rate have the highest volatile matter among all the *Eucalyptus* species. This result shows that for the same plant part, the samples that have a low content of volatile matter and a high content of fixed carbon, leads to a low temperature at which the peak pyrolysis rate occurred. For the bark and twig samples, the samples that have a high content of volatile matter leads to a high peak pyrolysis rate. This implies that there is a chemical component in the fuel samples which has a low volatile matter/high fixed carbon and pyrolyses at a low temperature. It is also noted that the leaf samples generally have a high content of volatile matter; however, the results in Figure 4 show that the leaf samples have the lowest peak pyrolysis rate. This is because the leaf samples have a high content of oils, and these oils evaporate at low temperatures (105~250 ^{o}C) [31]. The results in Figure 4 also suggest that the chemical components in the leaf samples are more complex than the twig and bark sample. These chemical components could have effects on the combustion process. Hence, it is necessary to determine the contents of the major

chemical components of the fuel samples, as this information could help better understand the differences in the combustion process among the fuel samples.

3.1.2 Carbohydrates and lignin composition analysis

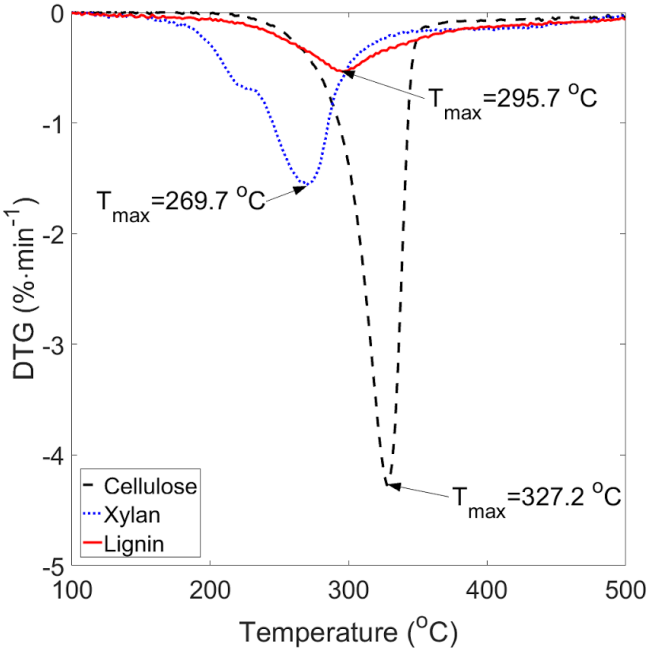

Figure 5. Derivative thermogravimetric analyses (DTG) of the devolatilisation of cellulose, hemicellulose (xylan) and lignin at a heating rate of 2 K·min^{-1}.

Vegetation is composed primarily of carbohydrates (cellulose and hemicellulose), and lignin. To better characterise the fuel samples, the components of the fuel samples were estimated based on the derivative thermogravimetric analysis results through curve fitting. The derivative thermogravimetric analyses of the devolatilisation of cellulose, hemicellulose (xylan) and lignin is shown in Figure 5.

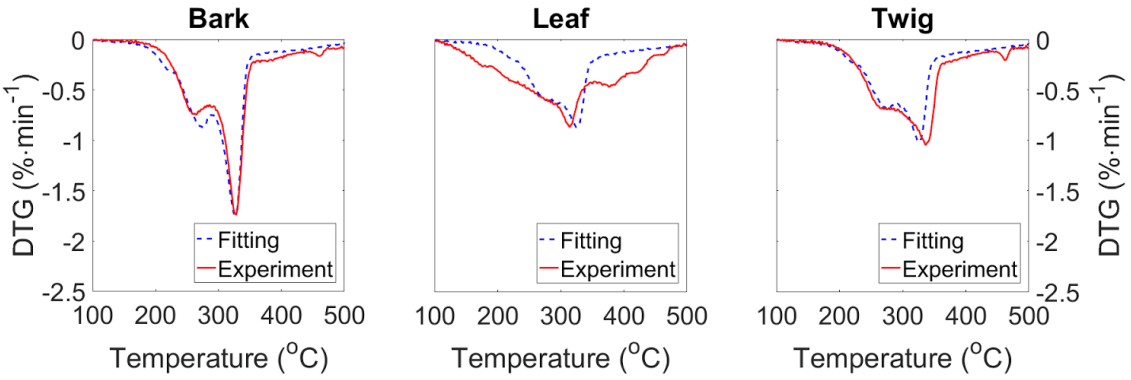

Figure 6. Derivative thermogravimetric analyses and three-component fittings of *E. camaldulensis* bark, leaf and twig, at a heating rate of 2 K·min^{-1}.

A curve-fitting approach was used to determine the percentages of cellulose, hemicellulose and lignin. Examples of the three-component fitting results are shown in Figure 6. The results in Figure 6 show that the three three-component curves fit the experimental curves of the bark and twig samples well. These results indicate that the actual chemical components of the bark and twig samples are closely approximated to the three-component curve. In other words, the major chemical components in the bark and twig samples can accurately be represented by cellulose, hemicellulose and lignin. However, the three three-component curve does not fit as well with the experimental curve of the leaf sample. This implies that other components may also be significant in the leaf sample, consistent with the findings from the pyrolysis rate.

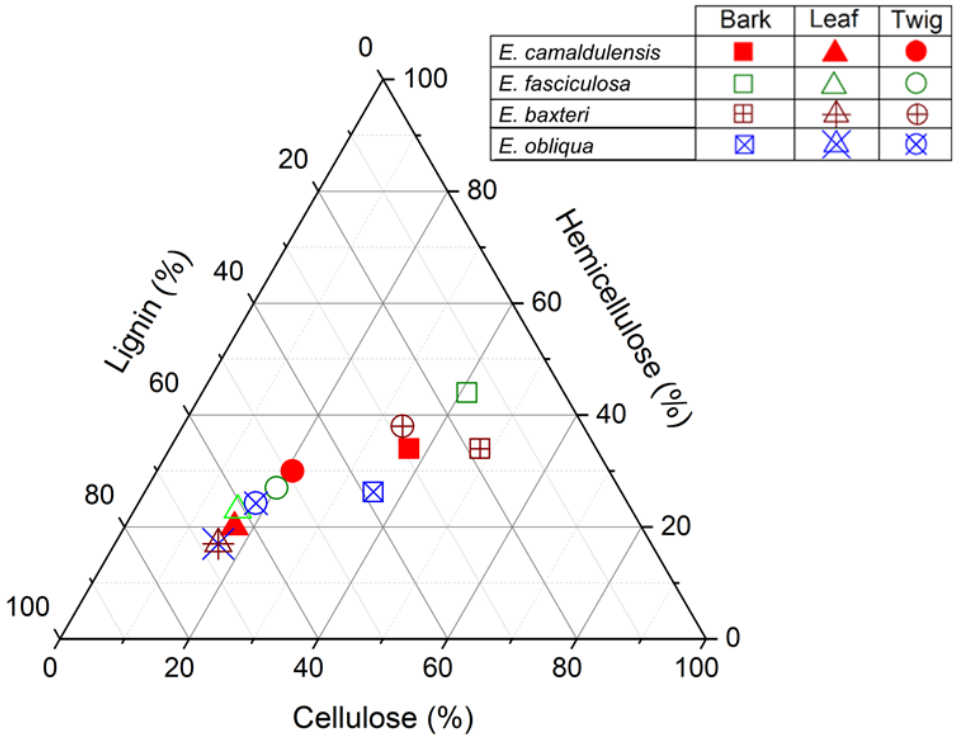

Figure 7. Cellulose, hemicellulose (xylan) and lignin composition analyses of the fuel samples. Species: *E. camaldulensis* = solid, *E. fasciculosa* = hollow, *E. baxteri* = square cross, and *E. obliqua* = diagonal cross. Plant parts: bark = square, leaf = triangle, and twig = circle.

Figure 7 shows the percentages of cellulose, hemicellulose and lignin of all the fuel samples. The results in Figure 7 show that there is no significant correlation between the *Eucalyptus* species and the percentages of cellulose, hemicellulose and lignin. From the results of proximate analysis (Figure 2) and the cellulose, hemicellulose and lignin composition analyses (Figure 7), it was found that there is a correlation between the

volatile matter content and the cellulose and hemicellulose contents in the bark and twig samples. For example, the *E. baxteri* bark, *E. fasciculosa* bark and *E. baxteri* twig are the top three samples on the volatile contents in the bark and twig samples. The results in Figure 7 show that the cellulose and hemicellulose contents of these three fuel samples are higher than those of the other samples. This is because cellulose and hemicellulose have a higher content of volatile matter than lignin.

Unlike the bark and twig samples, there is no correlation between the volatile matter content and the cellulose and hemicellulose contents in the leaf samples. This is because the volatile matter of the leaf samples include an amount of oils, which were not studied in the current study. The oils in the leaf samples can also been seen in Figure 4 and Figure 6, where Figure 4 indicates that the chemical compositions of the leaf samples are more complex than those of the bark and twig samples; and Figure 6 show that three-component fitting provides a poor fitting mainly due to the oils and protein in the leaf samples.

The carbohydrates and lignin composition analysis of the different fuel samples has been demonstrated. The results show that the carbohydrates and lignin composition analysis can be used to qualitatively identify the contents of cellulose, hemicellulose and lignin in the bark and twig samples.

3.1.3 Air permeability

The milled and sieved fuel sample was loaded into the air permeability testing rig. The pressure drop across the fuel sample was measured under different inlet air flow velocities. Then, the air permeability and Forchheimer coefficient were calculated using the Forchheimer equation (Equation 3).

Table 2. Permeability (k_F) and coefficient (β) of the pulverised and sieved fuel material of 1-2 mm particle size.

Fuel sample (Fuel species)	**Forchheimer permeability, k_F ($\times 10^{-9}$ m^2)**			**Forchheimer coefficient, β (-)**		
	Bark	**Twig**	**Leaf**	**Bark**	**Twig**	**Leaf**
E. camaldulensis	5.82 ± 0.21	5.87 ± 0.26	1.45 ± 0.07	3414 ± 102	3749 ± 157	6975 ± 146
E. fasciculosa	4.87 ± 0.12	4.68 ± 0.09	1.76 ± 0.09	3110 ± 124	4231 ± 131	6774 ± 203
E. baxteri	5.33 ± 0.19	5.35 ± 0.23	2.87 ± 0.07	457 ± 20	4017 ± 189	3622 ± 76
E. obliqua	5.8 ± 0.13	4.02 ± 0.16	2.08 ± 0.04	650 ± 18	5052 ± 182	901 ± 36

The results in Table 2 show that the air permeability of the bark and twig samples is similar for all the *Eucalyptus* species and the leaf samples have the lowest air permeability. This is because the leaf samples create a more compact fuel bed than that of the bark and twig samples due to their flaky shape. In comparison with the plant parts, the *Eucalyptus* species does not have significant effect on the air permeability.

3.2 Combustion experiment

3.2.1 Temporal profile results

The results of the combustion experiments include the temporal and spatial temperature profiles and the temporal gas concentrations profile. Experiments were performed for all species, however, the trends of the temperature and gas concentration profiles are similar. Hence, only one species is presented in this section — *E. camaldulensis*.

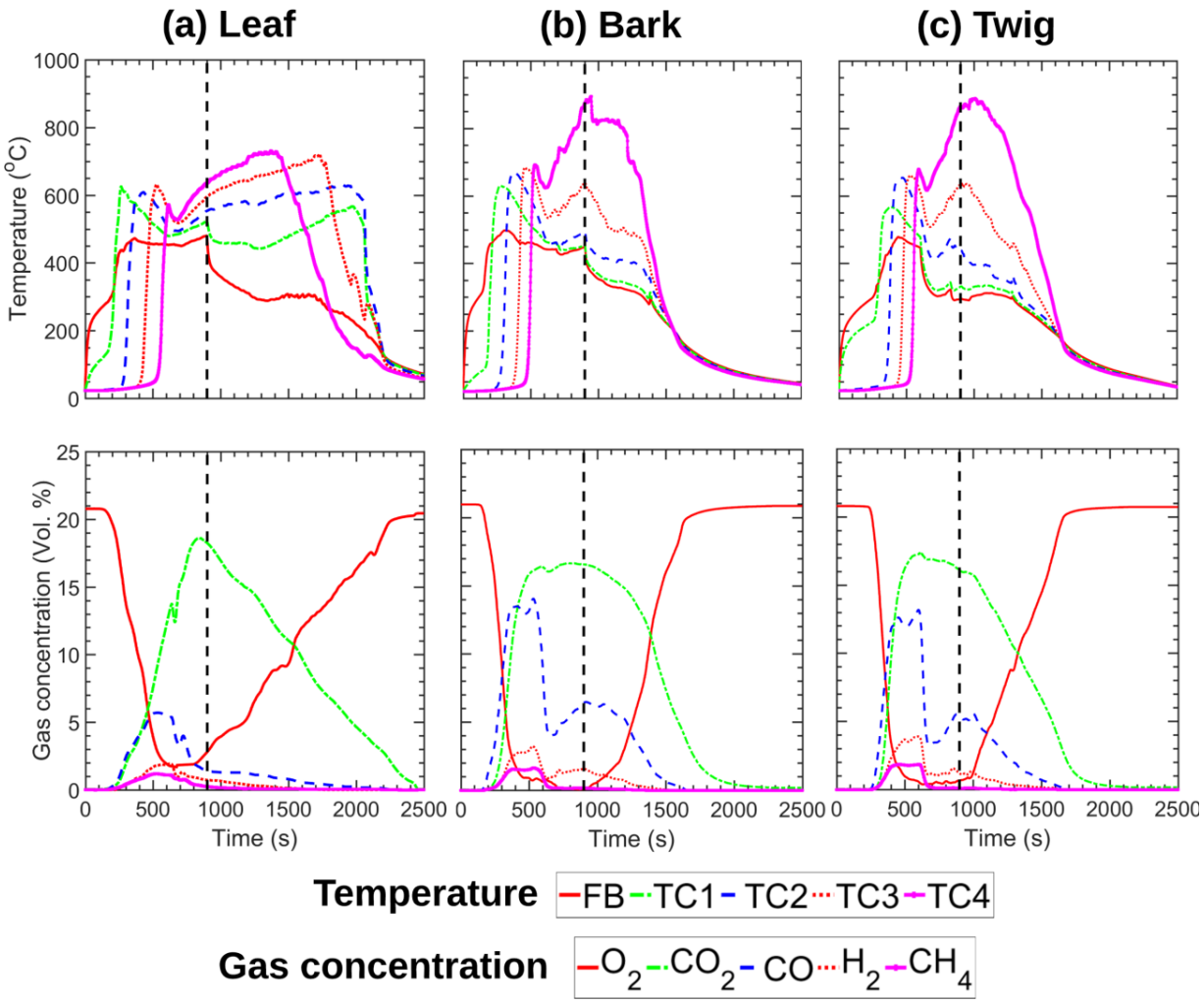

Figure 8. Temporal and spatial temperature profiles (Top) and temporal gas concentration profiles (Bottom) for the combustion of the leaf, bark and twig of *E. camaldulensis.* Heat flux level: 40 kW·m^{-2}, heating time: 900 s (lamp off indicated by vertical dashed line), flow velocity: 15.0 mm·s^{-1}, FB: freeboard, TC: thermocouple, vertical dash line: lamp off.

Figure 8 shows an example of the temporal and spatial temperature profiles of the various plant parts of E. *camaldulensis*. The freeboard (FB) thermocouple gives the temporal temperature profile measured above the fuel bed, whereas TC1−4 are

temporal temperature profiles at increasing depth beneath the top of the fuel bed. The vertical dashed line at 900 s in Figure 8 represents the time when the infrared heat lamp was turned off.

The combustion process was divided into two stages: radiation-aided and self-sustained smouldering combustion. In the radiation-aided smouldering stage (first 900 s), the external heat lamp is on and provides heat to drive the reactions. Self-sustained smouldering combustion is defined as the smouldering combustion that can propagate without the aid of any external heating [16]. In the self-sustained smouldering stage, the combustion process continues for about 700 seconds with no external heat source. As evident from the temperature profiles which continues to increase after the lamp is switched off.

The temporal-spatial temperature profiles (Figure 8) and the rate of temperature change profiles in the present study are consistent with the results of smouldering combustion presented previously [15, 16]. The peak temperature in the radiation-aided smouldering stage is approximately 650 ^{o}C, which is very close to the peak temperature of the smouldering combustion of radiata pine chips reported previously. The second temperature peak can also be seen in the self-sustained smouldering stage in Figure 8. The second temperature peak is caused by the initiation of the char combustion dominated stage [16]. However, the second temperature peak in the present study is stronger than the second temperature peak in the previous study. This is because the radiative heating time in the current study (900 s) is much longer than in the previous

study (300 s). The longer heating time increased the net heat gain in the reactor and the average fuel bed temperature, which promoted the char combustion. A stronger char combustion in the char combustion dominated stage led to higher temperatures.

Figure 8a shows an example of the temporal and spatial temperature profiles of the leaf sample of *E.* camaldulensis. The trend of the temperature profile of this leaf sample is dissimilar to that of the bark and twig sample (Figure 8b). Firstly, the peak temperature (~635 ^{o}C) in the radiation-aided smouldering stage is slightly lower than that of the bark sample (~650 ^{o}C). This is mainly because the evaporation of the oil in the leaf sample absorbs heat and decreases temperature. The self-sustained smouldering combustion of the leaf sample lasted for about 1300 seconds, which is much longer than that of the bark sample (~700 s). This is because the flaky shape of the leaf sample create a more compact fuel bed, which slows down the smouldering propagation velocity. The decrease in temperature indicates that the net heat released by exothermic reactions decreased due to the removal of the heat input. The product gas concentration profile demonstrates that the yield of CO and CO_2 continues after the lamp is switched off. The yield of CO and CO_2 are the main products of char oxidation. Hence, it is evident that exothermic reaction (char oxidation) continues after the lamp is switched off. As the mass of the fuels loaded into the reactor were the same for the bark and leaf samples; this indicates that the reaction rate of smouldering combustion is slower in the leaf sample than that in the bark sample. Figure 8a shows that the emission of CO in the radiation-aided and self-sustained smouldering stages of the leaf sample is much lower compared with the bark sample. As stated in Section 3.1.1.1, the leaf samples have a

high content of volatile matter and elemental carbon; but a low content of fixed carbon. This means that a large amount of the elemental carbon is released through the volatile matter of the leaf sample. The low content of fixed carbon suppresses smouldering combustion; hence; the emission of CO was quite low in the self-sustained smouldering combustion stage. Furthermore, the leaf samples have a high content of volatile matter; the release of volatile matter, the devolatilisation and evaporation processes are endothermic, which leads to a lower temperature than that of the bark and twig samples.

The temporal evolution of the gas profiles of the CO, CO_2, H_2 and CH_4 in the product gas for the bark of *E. camaldulensis* are shown in Figure 8b. The trend of the temporal gas profiles is similar to the temporal gas profiles of the smouldering combustion of the radiata pine sample reported in Wang et al. (2016). However, the concentration of CO during the char combustion dominated stage (600–1600 s) of the bark of *E. camaldulensis* is higher than that of the radiata pine sample. It is also noticed that the elimination of the radiative heating did not have great effects on the concentration of CO and CO_2 downstream the fuel bed.

The results in Figure 8c show the temporal and spatial temperature profiles of the twig of *E. camaldulensis*. The temperature profiles of the twig sample is similar to that of the bark sample. The results in Figure 2 show that the content of fixed carbon is similar for the bark and twig sample of *E. camaldulensis*. Hence, it implies that there is a positive correlation between the content of fixed carbon and the temperature of the combustion

process. Figure 8c shows the temporal gas concentration profiles of the twig of *E. camaldulensis*. The temporal gas concentration profiles of the twig sample is also similar to that of the bark sample. Hence, there is no significant effect on the combustion of the bark and twig samples of *E. camaldulensis*.

From the results in Figure 8, the leaf of *E. camaldulensis* combusted differently from the bark and the twig samples; and the combustion of the bark and twig of *E. camaldulensis* is similar based on the temperature and gas concentrations measurements. This could be because the particle shape has significant effects on the combustion process. The results in Section 3.1.3 show that the air permeability of the leaf samples are different from the bark and twig samples due to the particle shape; and the results also show that the air permeability of the bark and twig samples are similar. Hence, this could explain the similarity between the bark and twig samples.

3.2.2 Peak temperature

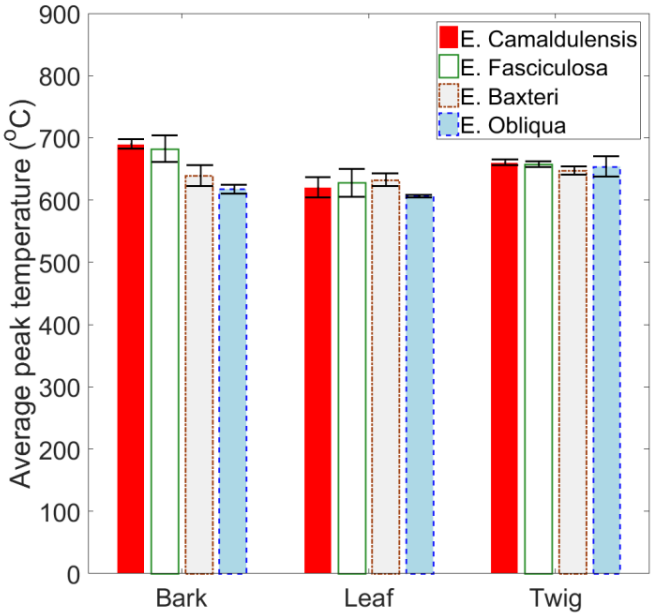

Figure 9. Effects of the *Eucalyptus* species on the average peak temperature measurements. Error bars represent the standard deviation of the peak temperature measurements of the thermocouples (TC 1–4) between multiple repeated experiments for each fuel sample.

Figure 9 presents the effects of the *Eucalyptus* species and plant parts on the average peak temperature measurements. The average peak temperatures were calculated based on the average peak temperatures of TC 1–4. The results in Figure 9 show that the peak temperature measurements of the fuel samples vary from approximately 600 to 710 ^{o}C.

For the bark samples of the different *Eucalyptus* species, the peak temperatures of the smooth-bark *Eucalyptus* (*E. camaldulensis* and *E. fasciculosa*) are higher than those of the stringybark *Eucalyptus* (*E. baxteri* and *E. obliqua*). This may be because the bark of the stringybark *Eucalyptus* is fibrous, which increases the surface to volume ratio. A high surface to volume ratio increases the convectional heat loss, which causes lower temperatures.

For the leaf samples of the different *Eucalyptus* species, there is no significant correlation between the peak temperature and the *Eucalyptus* species. The average peak temperatures of the leaf samples are lower (~60 ^{o}C) than those of the bark samples of the smooth-bark *Eucalyptus*, and close to the bark samples of the stringybark *Eucalyptus*. The lower peak temperatures of the leaf samples may be because the shape of the leaf particles. The leaf particles are flaky, and its surface to volume ratio is large; which results in high convectional heat loss. Same for the twig samples, no significant correlation can be seen between the peak temperature and the *Eucalyptus* species.

3.2.3 Smouldering propagation velocity

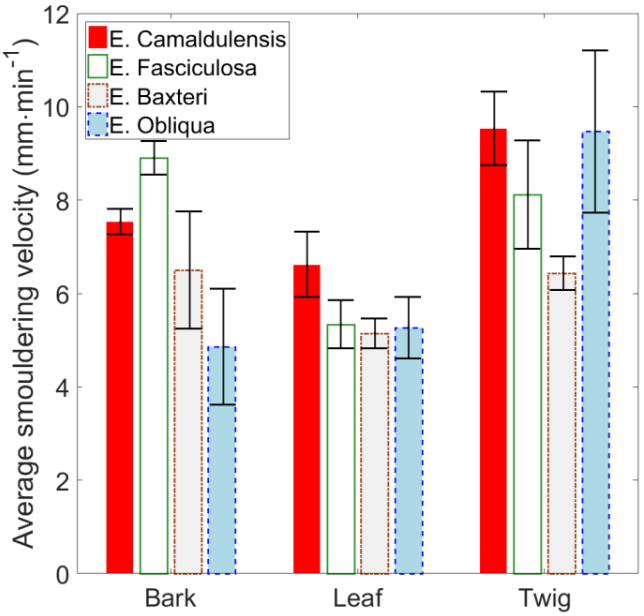

Figure 10. Effects of the *Eucalyptus* species on the average smouldering propagation velocity in the radiation-aided smouldering stage. Error bars represent the standard deviation of the smouldering velocity between multiple repeated experiments for each fuel samples.

Figure 10 shows the effects of the Eucalyptus species on the average smouldering propagation velocity in the radiation-aided smouldering stage. The propagation velocity was calculated from the time between the arrival of the smoulder front (peak temperature) at TC1 and TC4 and the known distance between the thermocouples. The average smouldering propagation velocity varies from approximately 5 to 11.5 mm·min^{-1}.

For the bark samples of the different *Eucalyptus* species, the average smouldering propagation velocity of the smooth-bark *Eucalyptus* (*E. camaldulensis* and *E. fasciculosa*) are faster than those of the stringybark *Eucalyptus* (*E. baxteri* and *E. obliqua*). As observed from Figure 9, the bark of the smooth-bark *Eucalyptus* have higher peak temperatures than those of the stringybark *Eucalyptus*.

For the leaf samples of the different *Eucalyptus* species, there is no significant correlation between the average smouldering propagation velocity and the *Eucalyptus* species. Overall, the average smouldering propagation velocity of the leaf samples are the lowest compared to the bark and twig samples. This finding is consistent with the finding in Figure 8, where the temperature and gas concentrations results show that for the same experimental conditions, the combustion of the leaf samples lasted longer than that of the bark and twig samples. The longer combustion time reveals that the combustion of the leaf samples is slower than the bark and twig samples. The leaf samples have the highest content of volatile matter amongst the three plant parts (Figure 2). However, the results in Figure 6 suggest that the volatile matter of the leaf samples include a quantity of oils. These oils release at low temperatures (105~250 ^{o}C), the evaporation of the oils absorbs heat. Similarly, the other devolatilisation reactions are also endothermic. Therefore, a high content of volatile matter leads to high heat absorption and hence a low temperature. In this study, the focus is on smouldering combustion, so conditions were set to initiate smouldering combustion. Under these conditions, the majority of the volatile matter is not oxidised, which can be seen from the temperature and gas concentrations (Figure 8) profiles. As the strong oxidisation of

volatile matter will lead to a high temperature and low contents of H_2 and CH_4. The particle shapes also have effects on the heat transfer, which eventually slows down the combustion process. For the twig samples of the different *Eucalyptus* species, there is also no significant correlation between the average smouldering propagation velocity and the *Eucalyptus* species.

3.2.4 Gas concentration

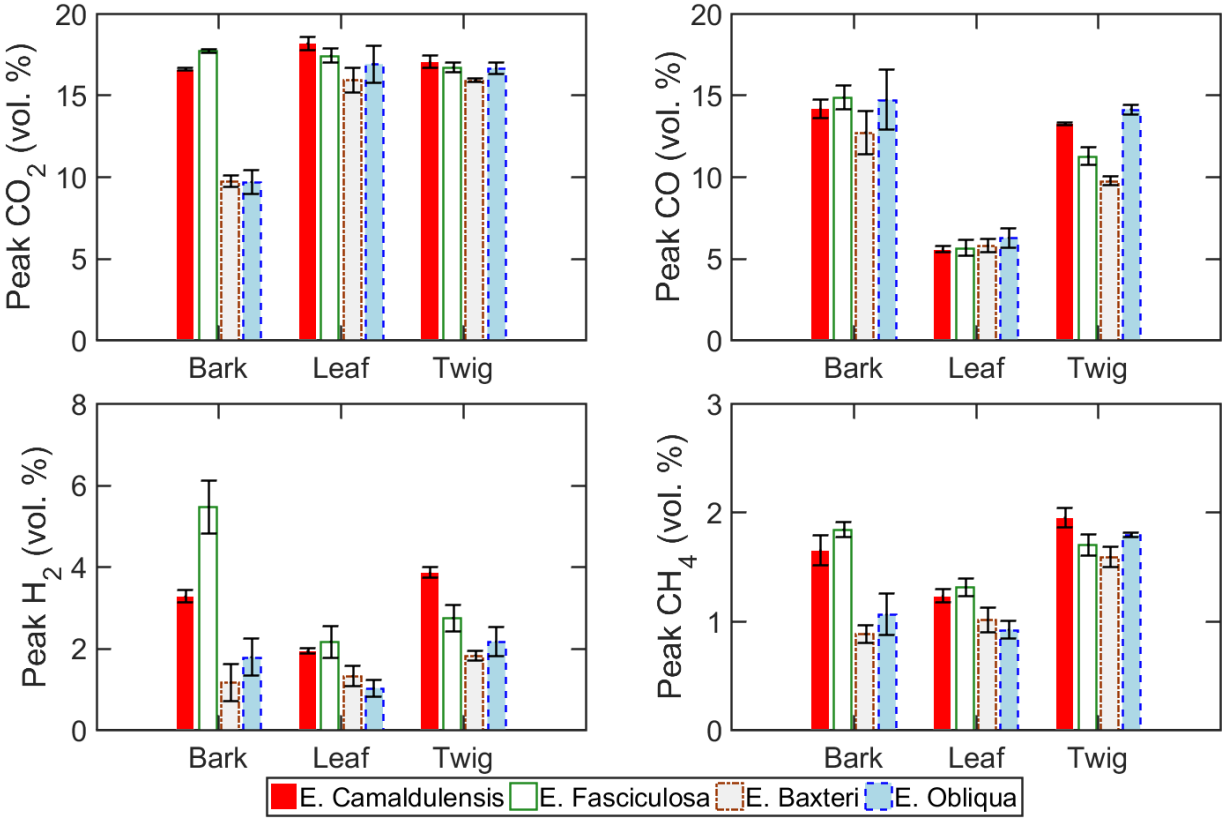

Figure 11. Effects of the *Eucalyptus* species and plant parts on the peak value of CO_2, CO, H_2 and CH_4 measurements. Error bars represent the standard deviation of the peak values between multiple repeated experiments for each fuel samples.

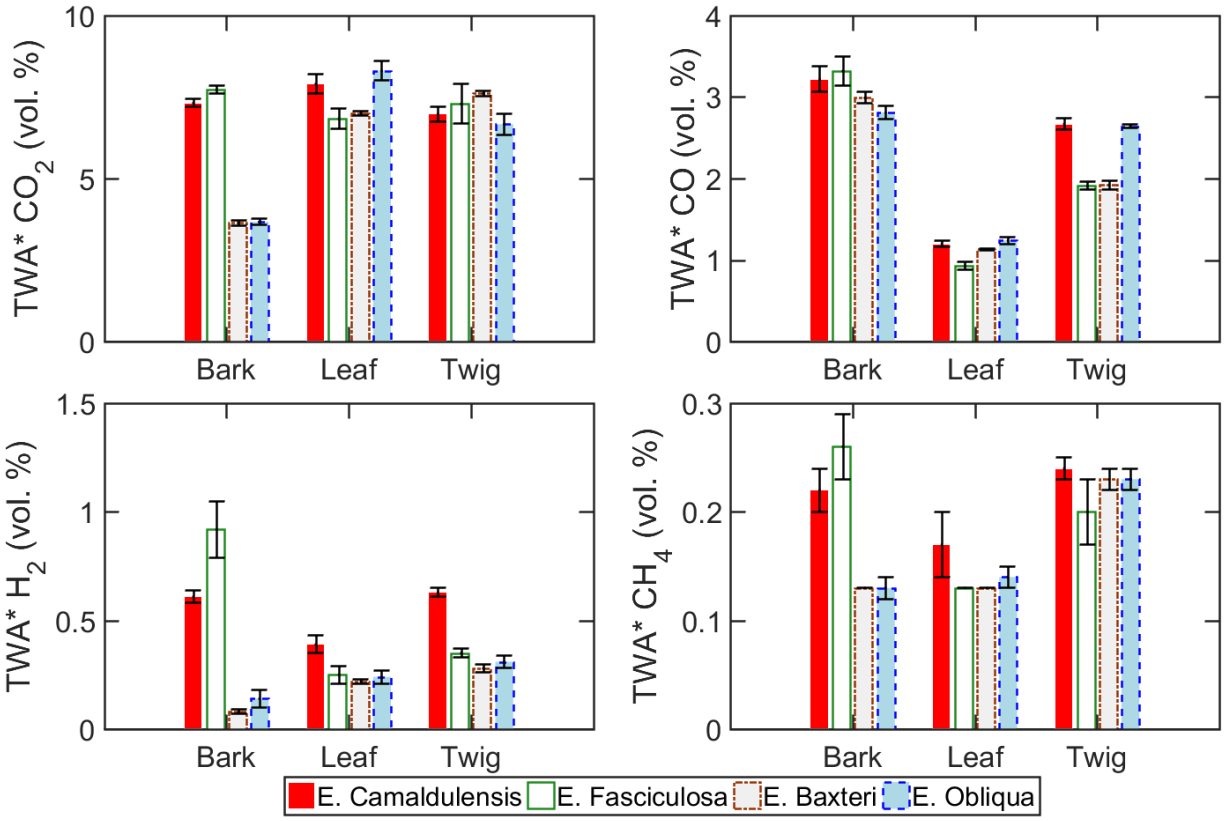

Figure 12. Effects of the *Eucalyptus* species and plant parts on the time-weighted average (TWA) of CO_2, CO, H_2 and CH_4 measurements. Error bars represent the standard deviation of the time-weighted average between multiple repeated experiments for each fuel samples.

For the bark samples of the smooth-bark *Eucalyptus* (Figure 11), the peak CO_2 measurements (16.5~18 %) is higher than the peak CO measurements (14~15 %). However, the bark samples of the stringybark *Eucalyptus* showed the peak CO_2 measurements (~9.5 %) is lower than the peak CO measurements (13~15 %). It is also noticed that the peak H_2 and CH_4 measurements follow the same trend as the CO and CO_2 measurements. As H_2 and CH_4 are from the pyrolysis of the fuel samples, this implies that the differences in the gases emission between the bark samples is due to

the pyrolysis of the fuel samples. The time-weighted average gas measurements are not shown for brevity, but show a similar trend as the peak values shown in Figure 11.

From the proximate analysis (Figure 2) and the cellulose, hemicellulose and lignin analysis (Figure 7), it was found that there is a correlation between the content of volatile matter and the contents of cellulose/hemicellulose. The bark of *E. fasciculosa* has the highest content of hemicellulose. From the molecular formula of cellulose ($C_6H_{10}O_5$), hemicellulose ($C_5H_{10}O_6$) and lignin ($C_9H_{10}O_2$), hemicellulose has the highest H/C ratio (2), which means for the same amount of each sample, hemicellulose releases more hydrogen than cellulose and lignin. Therefore, the fuel sample which has a high content of hemicellulose, will produce more hydrogen. From the results of gas concentration (Figure 11 and 12), it can be seen that the bark of *E. fasciculosa* produces the most hydrogen among all the samples.

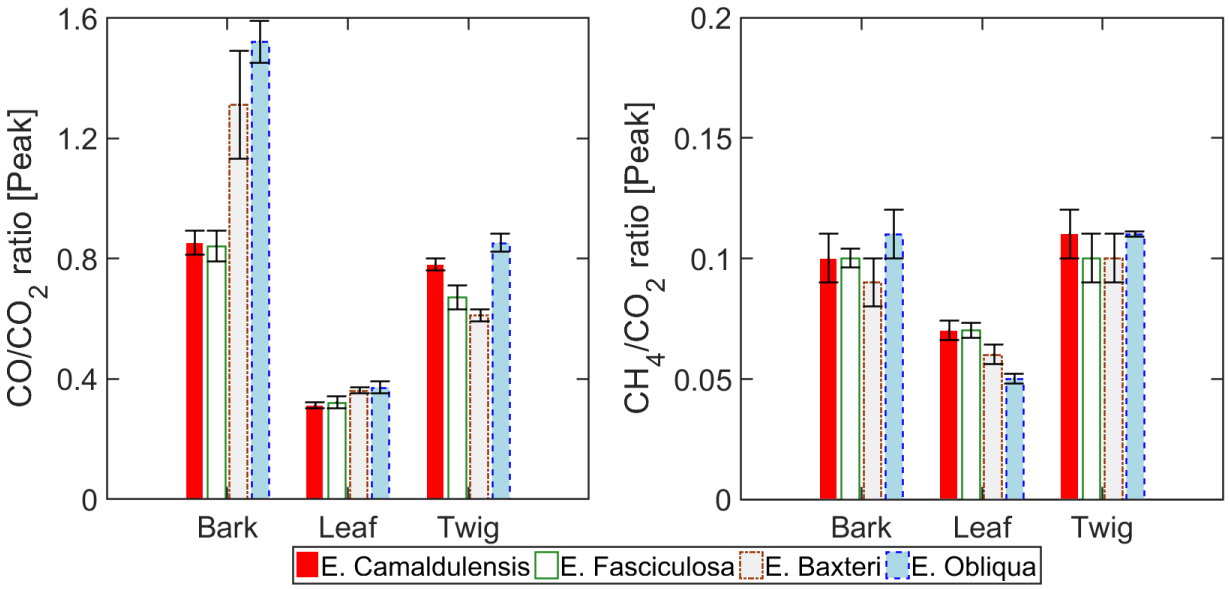

Figure 13. Effects of the *Eucalyptus* species and plant parts on the ratio of peak CO and CH_4 to CO_2. Error bars represent the standard deviation of the peak values between multiple repeated experiments for each fuel samples.

To better interpret the results of gas concentration, the ratios of peak CO and CH_4 to CO_2 are shown in Figure 13. The high CO/CO_2 ratio indicates incomplete combustion. The results in Figure 13 present that the ratios of CO to CO_2 are less than 1 (~0.8) for the bark of smooth barks, and larger than 1 (~1.4) for the bark of stringybarks. Hence, the combustion of the bark of stringybarks is more incomplete than that of the bark of smooth barks. This could be because the bark of stringy barks is fibrous, which does not allow the fuel bed to form an insulation layer. The heat losses of smouldering combustion are high without this insulation layer. The high heat losses lead to a more incomplete combustion. The CO/CO_2 ratio of the leaf samples are the lowest among the all fuel samples, which implies a more complete combustion.

4. Conclusions

Eucalyptus wildfires are becoming a global issue, as it is now widely cultivated across the world. Hence, the motivation of the current study is to develop a better understanding of the fires in *Eucalyptus* forests. In this work, a laboratory-scale study was conducted to help better understand the fundamental aspects of smouldering combustion. This study investigated the effects of *Eucalyptus* species and the plant parts on smouldering combustion; and quantitatively characterised the differences. Overall, the *Eucalyptus* species and the plant parts have significant effects on the combustion process. This can be seen from the measurements of temperatures in the reactor and the concentration of the gases in product gas. The effects of the *Eucalyptus* species and the plant parts on the combustion process can be summarised into the following three categories:

1) The *Eucalyptus* species have significant effects on the smouldering combustion of the bark samples. The peak temperatures of the bark (~650-700 ^{o}C) of smooth bark (*E. camaldulensis* and *E. fasciculosa*) are higher than those (~610-650 ^{o}C) of the bark of stringybark (*E. baxteri* and *E. obliqua*). The smouldering front also propagates faster in the bark of smooth bark (~7.2-9.3 mm·min^{-1}) than in that of stringybark (~3.8-7.7 mm·min^{-1}). The differences in the peak temperature and the smouldering propagation velocity indicate that the reaction rate of smouldering combustion is lower in the bark of stringybark than in the bark of smooth bark. However, the results of heating value show that the bark of stringybark (17.8-18 MJ•kg^{-1}) has a higher heating value than that of smooth bark (16.2-

16.6 MJ•kg^{-1}). This inconsistency reflects that the higher heating of a fuel bed influences the peak temperature of smouldering combustion, as well as the smouldering propagation velocity. The CO/CO_2 ratio of the bark of smooth bark (~0.8) and stringybark (~1.1-1.6) show that the combustion in the bark of stringybark is more incomplete than in the bark of smooth bark.

2) Smouldering combustion of the leaf samples is different from that of the bark and twig samples. The average peak temperature of the leaf samples (~600-650 ^oC) is lower than those of the twig samples (~660 ^oC) and the bark of smooth bark (~650-700 ^oC). Similarly, the smouldering propagating velocity of the leaf samples (~4.6-7.2 mm·min^{-1}) is lower than those of the twig samples (~6-11.2 mm·min^{-1}) and the bark of smooth bark (~7.2-9.3 mm·min^{-1}). This is because the leaf samples contain a high content of oils and volatile matter, the release of oils and volatile matter absorbs heat which leads to lower temperatures and slower propagation. While, the CO/CO_2 ratio of the leaf samples (~0.38) is much lower than the bark samples (~0.8-1.6) and twig samples (~0.6-0.85). This is because the leaf particles have a high surface to volume ratio which promotes the surface reaction.
3) The smouldering combustion of the twig samples is similar to the bark of smooth bark in terms of peak temperature and CH_4/CO_2 ratio

In this study, the smouldering combustion of different *Eucalyptus* species and their different plant parts were investigated. It was found that the *Eucalyptus* species and their different plant parts have effects on smouldering combustion. This is mainly because the difference in the physical and chemical properties of fuel. Therefore, the

Eucalyptus species and their different plant parts should be considered as an important factor in wildfires and hazard reduction burning. This study investigated the effects of four Eucalyptus species and their plant parts on smouldering combustion. These plant parts are the main components of forest fuel beds. However, forest fuel beds are composed of mixtures of different plant parts with different particle sizes. Hence, future work should consider the effects of different particle sizes, shapes and the mixture of different plant parts on the combustion process of fuel beds in order to better understand the combustion of natural forest fuel beds. One of the purposes of this study is to investigate the effects of the *Eucalyptus* species on smouldering combustion. There are more than 800 *Eucalyptus* species in Australia. To start with, four common *Eucalyptus* species were chosen. *Eucalyptus* species can normally be divided into smooth bark and stringybark. Hence, two common smooth bark and two common stringybark species were selected. As an early study, it is too early to translate the results of this study to the genus *Eucalyptus*. Hence, more studies on the effects of different *Eucalyptus* species on smouldering combustion are still needed.

Chapter 8

Conclusions

8.1 Discussion

In this thesis, smouldering combustion of biomass has been studied in a series of small-scale laboratory experiments with an emphasis on wildfires. The experimental studies investigated the initiation of smouldering combustion in a biomass fuel bed. These studies aimed to provide a better understanding of the ignition of smouldering of biomass fuels, which is essential to locate and predict the initiation of smouldering combustion in wildfires and hazard reduction burning. The research outcomes from these studies are summarised in this chapter.

The initiation of smouldering combustion in a biomass fuel bed has been studied in Chapter 4, 5 and 7. Smouldering combustion was initiated using radiation, as radiant heat is a primary heat transfer mechanism in wildfires and hazard reduction burning. It is critical to develop a better understanding of the radiant ignition of smouldering in biomass. This is because the initiation of smouldering combustion requires much less energy than flaming combustion. In a wildfire, the radiation generated by fire fronts could lead to smouldering ignition, which could be far away from the fire fronts. This smouldering combustion could later transition to flaming combustion, and develop into a new fire front. The focus is on smouldering combustion in wildfires and hazard reduction burning; hence,

smouldering combustion of a *Pinus* species (Chapter 4 and 5) and four *Eucalyptus* species (Chapter 7) were studied. *Pinus* and *Eucalyptus* trees are planted widely around the world due to their environmental and economic benefits. Both *Pinus* and *Eucalyptus* trees are important to wildfires, as they are highly combustible trees. In a real-world scenario, smouldering combustion often occurs in natural forest fuel beds during a wildfire or hazard reduction burn. From the research outcomes of Chapter 4 and 5, it was found that oxygen availability has significant effects on the initiation of smouldering combustion in a biomass fuel bed. The air permeability of a fuel bed determines the oxygen availability in that fuel bed. Hence, the air permeability of natural forest fuel beds was studied in Chapter 6.

As stated in the research gaps (Section 2.7), there is currently no effective way to identify the initiation of smouldering of biomass. Because of this, smouldering combustion is often described based on its related phenomena, such as the release of smoke and heat. Hence, the first part of this thesis is to answer the question of what metrics are appropriate for identifying the initiation of smouldering combustion of biomass. To answer this question, the initiation of smouldering and flaming combustion in radiata pine chips were firstly studied in the combustion testing rig. In the experiments, temperature, product gas concentration and mass change were selected to characterise and quantify the differences between smouldering and flaming combustion of radiata pine. The results show that apparent differences can be identified between smouldering and flaming combustion from the measurements of temperature, product gas concentration and the fuel sample mass change. These results imply that smouldering combustion can be identified based on the measurements of temperature, product gas concentration and the fuel sample mass change. This study also investigated the required conditions of radiant heat flux and air flow rate for the initiation of smouldering and flaming combustion of radiata pine. It was found that smouldering combustion can only be initiated under a low air flow rate; for the experimental apparatus used, this corresponded to a flow velocity of $\leq$38.1 mm$\cdot$s^{-1}. This result indicates that oxygen availability has a significant effect on the initiation of smouldering and flaming

combustion of radiata pine. Furthermore, the stages of smouldering, including preheating, aided smouldering and self-sustained smouldering are identified.

It was found in the first part of the experiments that oxygen availability has significant effects on the initiation of smouldering combustion. In that part of the study, oxygen availability was changed by adjusting air flow rate. It is also known that smouldering combustion can occur in a low oxygen concentration condition. In wildfires and hazard reduction burning, smouldering combustion often propagates deep in natural forest fuel beds, where oxygen availability is limited. Hence, a further study on the effects of oxygen availability on the initiation of smouldering combustion of radiata pine was studied using the same combustion testing rig. A better understanding of the effects of oxygen availability on smouldering is also beneficial to the prediction and suppression of smouldering combustion. In this part of the study, oxygen concentration was changed by modifying the oxygen concentration in the oxidizer.

Smouldering combustion can be divided into aided and self-sustained based on the dependence of the external heating. However, the understanding of the difference between aided and self-sustained smouldering combustion is lacking. Hence, this study also investigated the effects of heating time and oxygen concentration on radiation-aided and self-sustained smouldering, as well as the differences between radiation-aided and self-sustained smouldering combustion. The initiation of radiation-aided and self-sustained smouldering combustion in radiata pine chips were studied in the combustion testing rig. The results show that the difference between radiation-aided and self-sustained smouldering can be characterised and quantified based on the measurements of temperature, gas concentration and the fuel sample mass change. Four stages, including heating stage, devolatilisation-dominated stage, char combustion dominated stage and cool down stage were identified in self-sustained smouldering combustion based on the measurements of temperature and product gas concentration. The results of the experiments indicate that a decrease in oxygen concentration increases the required heating time for initiating self-sustained smouldering combustion; and 10 % is the critical oxygen concentration for self-sustained smouldering combustion, as self-sustained

smouldering could not be initiated when the oxygen concentration is $\leq$10 %. It was also found that a decrease in oxygen concentration significantly slows the propagation of the smouldering front.

The experimental studies show that oxygen availability has significant effects on smouldering combustion. Fuel on the ground, such as leaves, twigs and decomposing matter, accumulate over time and account for a large percentage of the total fuel load in forests. In fire events, material on the ground is often referred to as the fuel bed. Fuel beds in a forest can be considered porous media, and their air permeability determines the ease with which air flow passes through them. Therefore, the air permeability of a fuel bed can have a significant effect on the oxygen availability in that fuel bed. The air permeability of a fuel bed is a critical factor that influences fire behaviour because it controls the amount of air (oxygen) available for combustion within the fuel bed. However, there are only a few studies on the air permeability of biomass fuel beds. The air permeability of natural forest fuel beds and milled gum bark, leaf and chips were determined using the air permeability testing rig. This study investigated the effects of particle size and type on the air permeability. The natural forest fuel beds were firstly divided into three fuel types: twig, leaf and decomposing matter. The results of the mass distribution of the twig and decomposing matter show that the majority of the fuel particles in the twigs and decomposing matter beds is small than 5 mm. The results show that for the same particle size, the air permeability of milled gum leaves has the lowest air permeability, while the milled gum bark has the highest air permeability. These results suggest that the biomass fuel type has a significant effect on the air permeability. This can be attributed to the different porous pore structures of different fuel types. It was also found that for the natural forest fuel beds, the air permeability of the twig and leaf samples are much higher (up to 500 times) than that of the decomposing matter sample. This indicates that smouldering combustion is more likely in the decomposing matter due to the low air permeability (oxygen availability).

From the study of the air permeability of natural forest fuel beds, it was found that the fuel types, such as twig, leaf, bark and decomposing matter, have

a significant effect on the air permeability. Therefore, the fuel types have an influence on the physical property of fuel beds. A research question was then raised on whether fuel types will have effects on chemical properties, and if so, will these differences in chemical properties affect smouldering combustion. *Eucalyptus*, one of the most widespread genera of native plants in Australia, has always played a central part in Australian wildfires. Not only does it contribute the majority of fuel for the wildfires, but it is also highly combustible due to its high content of volatile oil. Furthermore, there are more than 800 different *Eucalyptus* species in Australia. In a *Eucalyptus* forest, the accumulation of fuel, such as leaves, barks and twigs, builds up a fuel bed for fire events. *Eucalyptus* species may also have influences on the chemical and physical properties of fuel beds. Hence, fuel types were expanded to *Eucalyptus* species and plant parts. The differences among the different plant parts from the different *Eucalyptus* species were studied. It was found that most of the leaf and twig samples and the difference between the bark of the smooth and stringybark *Eucalyptus* can be distinguished based on the proximate analysis results. The leaf samples and the difference between the twig and bark of the smooth and stringybark *Eucalyptus* can be identified based on the ultimate analysis results. The bark and twig samples can be distinguished based on the results of the carbohydrates and lignin composition analysis. Effects of four common *Eucalyptus* species and their bark, leaf and twig on smouldering combustion were studied in the combustion testing rig. The results show that *Eucalyptus* species have significant effects on the combustion of the bark samples, and the combustion of the leaf samples is different from those of the bark and twig samples. Overall, *Eucalyptus* species and its plant parts have significant effects on smouldering combustion and should be considered as important factors related to the wildfire model and planning for hazard reduction burn.

8.2 Summary of Conclusions

This section includes summaries of the research findings which answer the research questions posed in Section 2.8, and an assessment of the significance of these

research findings.

Research Questions for Research Aim 1

- *What metrics are appropriate for identifying the initiation of smouldering combustion in biomass fuel?*

  The measurements of temperatures, product gas concentrations and the mass change of the fuel samples have been demonstrated to identify the initiation of smouldering combustion of biomass, as well as the difference between smouldering and flaming combustion. This finding provides a pathway to quantitatively analyse smouldering combustion of biomass. There is also a potential for applying the knowledge in practice. For example, the product gas composition could be used as a metric to help locate smouldering combustion in wildfires and hazard reduction burning.

- *What are the interactive effects of radiant heat flux and air flow rate on the initiation of smouldering and flaming combustion in biomass fuel beds?*

  It was found that smouldering and flaming combustion of biomass can be achieved by changing the combination of radiant heat flux and air flow rate. Smouldering combustion is more likely under a condition of low air flow rate. In this study (Chapter 4), smouldering combustion was only initiated when air flow velocity is below 38 $mm{\cdot}s^{-1}$. It was also found that an increase in air flow velocity increases the minimum required radiant heat flux for smouldering combustion. The finding of the required conditions for smouldering combustion of biomass could help predict the initiation of smouldering combustion in wildfires and hazard reduction burning.

Research Questions for Research Aim 2

- *What are the interactive effects of heating time and oxygen concentration on the initiation of radiation-aided and self-sustained smouldering*

combustion?

The study of radiation-aided and self-sustained smouldering combustion reveals that radiation-aided and self-sustained smouldering combustion of biomass can be achieved by varying heating time and oxygen concentration. The results presented in Chapter 5 indicate that a decrease in oxygen concentration increases the heating time required to initiate self-sustained smouldering combustion. It was also found that there was no indication of self-sustained smouldering combustion when the oxygen concentration is below 10 %, irrespective of the heat flux under the experimental conditions stated in Chapter 5. An implication of these findings of radiation-aided and self-sustained smouldering combustion is that the initiation of self-sustained smouldering combustion can be better predicted and assessed in practice, and the minimum oxygen concentration for self-sustained smouldering combustion of biomass provides the essential knowledge for the suppression of smouldering combustion in wildfires and hazard reduction burning.

- *What are the differences between radiation-aided and self-sustained smouldering combustion in terms of temperature, product gas concentration and mass change?*

  The differences between radiation-aided and self-sustained smouldering combustion can be distinguished based on the measurements of temperature, product gas concentration and mass change. For example, in this study (Chapter 5) the average peak temperature in the self-sustained smouldering combustion cases is in the range 550–650 °C; while, the average peak temperature in radiation-aided smouldering cases is approximately 500 °C. It was found that the propagation velocity of self-sustained smouldering combustion is higher than that of radiation-aided smouldering combustion, and under the current experimental setup the minimum propagation velocity of self-sustained smouldering combustion is approximately 2.6 mm·min^{-1}. It was also found that the CO/CO_2 ratio in the self-sustained smouldering cases is lower

than that in the radiation-aided smouldering cases.

Research Questions for Research Aim 3

- *How to determine the air permeability of natural forest fuel beds? What is the air permeability of natural forest fuel beds?*

  The air permeability of the natural forest fuel beds collected from temperate forests of south-east Australia were determined using experimental and theoretical methods. In the experimental method, the air permeability was determined based on the measured pressure drop across a fuel bed using the Forchheimer equation. In the theoretical method, the air permeability was determined based on the fuel bed properties, namely porosity and the specific area of fuel particles, using the Kozeny-Carman equation. The natural forest fuel beds are divided into different fuel types: leaf, twig/bark and decomposing matter. It was found in this study (Chapter 6) that both the fuel type and particle size have significant effects on the air permeability. For example, the air permeability of the decomposing matter samples ($\sim$3.8-30.9 $\times 10^{-9}$ m^2) is much lower than that of the leaf ($\sim$505 $\times 10^{-9}$ m^2) and twig/bark ($\sim$1259-1968 $\times 10^{-9}$ m^2) samples.

Research Questions for Research Aim 4

- *What are the effects of Eucalyptus species and plant parts on the initiation of smouldering combustion?*

  The effects of *Eucalyptus* species and plant parts on the measurements of temperature and product gas concentrations of smouldering combustion were investigated. The results show that *Eucalyptus* species have significant effects on smouldering combustion of the bark samples. For example, the bark of stringybark *Eucalyptus* undergoes more incomplete combustion than that of smooth-bark *Eucalyptus*. The leaf samples have the lowest smouldering propagation velocity, and CO/CO_2

ratio among the three plant parts. *Eucalyptus* species and plant parts have a little effect on the peak temperature.

- *Will Eucalyptus species and plant parts have effects on their physical and chemical properties? How will these differences in the properties have effects on smouldering combustion?*

  It was found in this study (Chapter 7) that most of the leaf and twig samples can be distinguished based on the volatile matter and fixed carbon content; while the smooth bark and stringybark can be distinguished based on the ash content. The volatile content of most the leaf samples (∼76-78 %) is higher than that of most the twig samples (∼69-71 %). The ash content of the bark of stringybark (∼0.5-1.5 %) is lower than that of the bark of smooth bark (∼2.5-4.5 %). The leaf samples and the difference between the twig and bark of the smooth and stringybark *Eucalyptus* can be identified based on carbon content from the ultimate analysis results. The carbon content of the leaf samples (∼50-51 %) are much higher than that of the bark and twig samples (∼41-48 %). The carbon content of the bark and twig of smooth bark (∼41-44.5 %) is higher than that of the bark and twig of stringybark (∼46.5-48 %). The bark, leaf and twig samples can be distinguished based on the peak pyrolysis rate and the temperature at which the peak pyrolysis rate occurred. The peak pyrolysis rate of the bark samples (∼1.6-2.1 %·min^{-1}) is higher than that of the leaf and twig samples (∼0.8-1.5 %·min^{-1}). The temperature at which the peak pyrolysis rate occurred is lower in the leaf samples (∼305-312 °C) than in the bark and twig samples (∼313-340 °C). The bark and twig samples can be distinguished based on the results of the carbohydrates and lignin composition analysis. The hemicellulose content of most of the bark samples (∼35-45 %) is higher than that of most of the twig samples (∼25-30 %). The cellulose content of most of the bark samples (∼35-50 %) is higher than that of most of the twig samples (∼20 %).

  It was found that the volatile matter content has significant effects on

the peak temperature and propagation velocity of smouldering combustion. The fuel samples with a high volatile content generally have low peak temperatures and slow propagation velocity. This is mainly because the release of volatile matter absorbs heat which decreases temperatures and slows down the smouldering propagation velocity. The particle shape determines the surface to volume ratio, which influences surface reactions. For example, the leaf particles have a high surface to volume ratio which promotes surface reactions, which leads to a low CO/CO_2 ratio. There is a correlation the hemicellulose content and the yield of hydrogen. The fuel samples with a high content of hemicellulose (e.g. *E. fasciculosa* bark) produce more hydrogen.

8.3 Future Work

This thesis presented a series of detailed investigations of smouldering combustion of biomass fuels in order to develop a better understanding of the initiation of smouldering combustion in wildfires and hazard reduction burning. Most of the previous work on smouldering combustion is for fire safety in buildings or industries. Over the past decade, smouldering combustion in wildfires, especially peat fires, has received more attention, as more people realise the importance of smouldering combustion in wildfires. Hence, more interdisciplinary research, for example between combustion science and fire ecology, is needed to better understand combustion processes in wildfires. The following recommendations are made to highlight a few research topics on which further research is necessary.

- The initiation of smouldering combustion has been identified based on the measurements of temperatures, product gas concentration and the fuel sample mass change. Although these indications of smouldering combustion of biomass have been demonstrated in a small-scale laboratory experiment reported in this thesis, the implication of these indications may not be directly applied in a real-world application. More studies on medium or large scale

combustion experiments may be necessary to create a link between laboratory work and wildfires. Secondly, the measurements of temperatures and the fuel sample mass change are intrusive measurement techniques, which may not be suitable in real-world applications for detecting smouldering combustion in wildfires. Hence, future research on the indications of smouldering combustion should focus more on non-intrusive measurement techniques, for example, the product gas concentration used in the current studies, which are more likely to be implemented.

- In wildfires and hazard reduction burning, smouldering combustion is considered as a potential hazard, as it can transition to flaming combustion. Not only that, it is also difficult to locate smouldering combustion, which makes it even harder to develop a better understanding of the transition from smouldering to flaming combustion in wildfires and hazard reduction burning. There is a paucity of research on the transition from smouldering to flaming combustion in wildfires. Hence, more studies are needed to investigate the conditions that lead to the transitions from smouldering to flaming combustion in a biomass fuel bed, as well as the indications of the transition.

- As highlighted in Chapter 7, it was found that *Eucalyptus* species and plant parts have significant effects on smouldering combustion. It would be interesting to investigate the effects of *Eucalyptus* species and plant parts on flaming combustion. There are more than 800 *Eucalyptus* species, and this thesis only covers four common *Eucalyptus* species in South-East Australia. However, similar studies on different *Eucalyptus* species would help gain a complete picture of smouldering combustion in different *Eucalyptus* species. The information on effects of *Eucalyptus* species would significantly enhance the ability to assess the risk of smouldering combustion in *Eucalyptus* forests. Furthermore, it is possible that the similar effects may occur in other tree genera, such as *Pinus* and *Abies*. Hence, future work should also be conducted for other tree genera.

Appendix A

Supplementary Information: Identification and Quantitative Analysis of Smoldering and Flaming Combustion of Radiata Pine

This page is intentionally left blank.

Supplementary Information: *Identification and Quantitative Analysis of Smoldering and Flaming Combustion of Radiata Pine*

H. Wang, P. J. van Eyk, P. R. Medwell, C. H. Birzer, Z. F. Tian, M. Possell

1 Description of control volume for the kinetics parameters analysis and energy balance analysis

The ignition stage is the reactions of the top layer of fuel bed (fixed control volume), which is around TC1 (Figure 1). The ignition stage of smouldering and flaming combustion were chosen according to the TC1 temperature increase rate and TC2 temperatures. The ignition stage starts when the TC1 temperature rapidly increases, and this indicates the onset of strong exothermic reactions at the surface of fuel bed. The TC1 temperature was used as the temperature of the top layer; and the mass loss is caused by the pyrolysis and char combustion of the top layer. The TC2 temperature was used to define the end of the ignition stage, as the thermocouple TC2 was located about 10 mm below the top layer of the fuel bed. So the TC2 temperature can be used to indicate the layer below the control volume. For example, if the TC2 temperature is high, then this indicates that the reacting layer is close to the thermocouple TC2; and the reactions are not limited to the top layer fuel bed (control volume). In this analysis, the ignition stage ends when the TC2 temperature reaches 100°C.

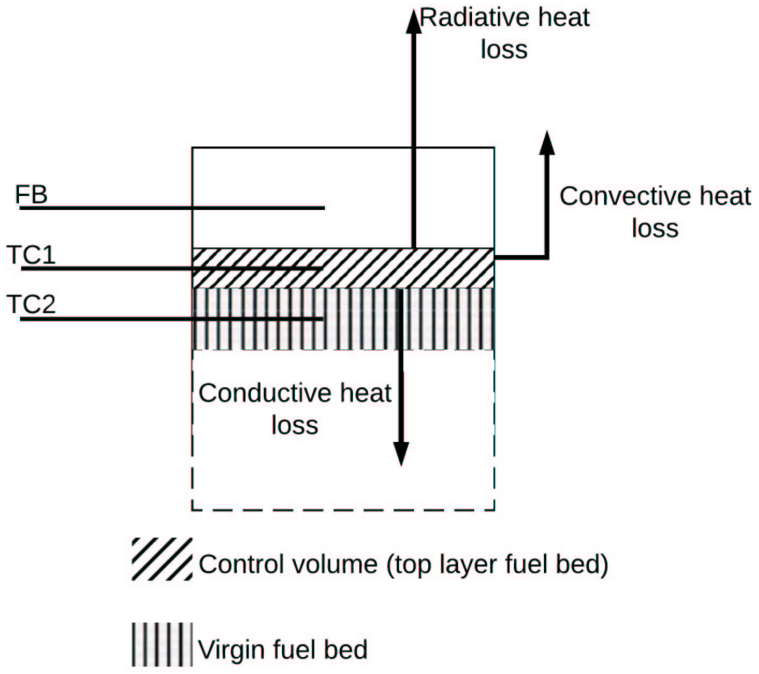

Figure 1: Schematic diagram of the reactor indicating the control volume

2 Simplified energy balance assumptions and analysis

The assumptions made for the simplified model are listed here:

1. The gas temperature was assumed to be uniform above the fuel bed, and the temperature of gas was equal to the freeboard(FB) temperature.

2. The compositions of the product gas include O_2, CO, CO_2, N_2. $C_xH_yO_z$ represents volatiles and H_2O in the product gas.
3. The emissivity of the fuel bed surface was assumed to be 0.924.[Lopez et al.(2013)Lopez, Basterra, Acuna, and Casado]
4. The temperature in the top layer of the fuel bed is equal to the TC1 temperature, as which is embedded in the the top layer of the fuel bed.
5. The heat loss through the reactor wall was assumed to be natural convective heat loss, and the temperature of the reactor wall around the top layer fuel bed is assumed to be the same as the top layer fuel temperature, *i.e.* TC1 temperature. The ambient air temperature was assumed to be 25°C.
6. The temperature of the fuel bed under the top layer is equal to the TC2 temperature, as TC2 was located below the top layer of the fuel bed.

A sensitivity analysis of the heat release rate to changes in emissivity and ambient temperature was performed. The heat release per unit mass of fuel reduces by 7.7% for smouldering combustion and 7.0% for flaming combustion, respectively, when the emissivity is decreased from 0.95 to 0.75. The heat release per unit mass of fuel reduces by 1.1% for smouldering combustion and 0.6% for flaming combustion, respectively, when the ambient temperature increases from 25°C to 40°C.

The energy balance analysis for the ignition stage was based on a simplified energy balance:

$$Energy_{fuel} + Heat_{initial,gas} = Heat_{final,gas} + Heat_{loss} \tag{1}$$

The heat input was calculated as:

$$Heat_{in} = HRR \times t_{ignition} + \int \sum_i \dot{m}_i(t) \left[\bar{h}_g^\circ + C_p(T_{gas} - T_{ref})\right] dt \tag{2}$$

The terms in Equation (2) are given below:

Term	**Comments**	**Units**
HRR	The average heat release rate during the ignition stage.	W
$t_{ignition}$	The duration of the ignition stage.	s
$\sum_i \dot{m}_i(t) \left[\bar{h}_g^\circ + C_p(T_{gas} - T_{ref})\right]$	This is the sum of the enthalpy of formation and the sensible heat of gases at the beginning of the ignition stage. The reference temperature was assumed to be 25°C.	W
$\dot{m}_i$	Mass flow rate of gases, *e.g.* O_2, CO, CO_2.	$g{\cdot}s^{-1}$
$\bar{h}_g^\circ$	Enthalpy of formation of gases at 25°C.	$J{\cdot}g^{-1}$
C_p	Specific heat capacity at 25°C.	$J{\cdot}g^{-1}{\cdot}K^{-1}$
T_{gas}	The product gas temperature. This term was obtained based on the freeboard temperature.	°C

The heat output was calculated as:

$$Heat_{out} = \int \sum_i \dot{m}_i(t) \left[\bar{h}_g^\circ + C_p(T_{gas} - T_{ref})\right] dt \tag{3}$$

The heat losses were calculated as:

$$Heat_{loss} = Q_{radiation} + Q_{reactor} + Q_{fuelbed} \tag{4}$$

The terms in Equation (4) are given below:

Term	**Comments**	**Units**
$Q_{radiation}$	The radiative heat loss through the surface of fuel bed.	J
$Q_{reactor}$	The convectional heat loss through the reactor wall to ambient.	J
$Q_{fuelbed}$	The conductive heat loss through the fuel bed below the control volume.	J

According to the ultimate analysis of the pine chips (Table 1 in the paper), the chemical formula for the pine chips sample can be represented as $CH_{1.446}O_{0.062}N_{0.003}$. The smouldering combustion process can be described by a single-step reaction as below:

$$CH_{1.446}O_{0.062}N_{0.003} + \alpha \cdot (0.21 \times O_2 + 0.79 \times N_2) \rightarrow \beta \cdot CO + \gamma \cdot CO_2 + \delta \cdot O_2 + \varepsilon \cdot N_2 + \zeta \cdot (C_xH_yO_z) \tag{5}$$

Coefficient	Comments
α	This value is based on the input air flow rate.
β	This value is based on the measurements of CO concentration.
γ	This value is based on the measurements of CO_2 concentration.
δ	This value is based on the measurements of O_2 concentration.
ε	This value is a constant, as it is assumed that the nitrogen in the input air does not participate in reactions.
ζ	$C_xH_yO_z$ is used to balance the single chemical reaction. The value of ζ is calculated by mass difference.

References

Lopez et al.(2013)Lopez, Basterra, Acuna, and Casado. Lopez, G.; Basterra, L.; Acuna, L.; Casado, M. *Journal of Nondestructive Evaluation* **2013**, *32*, 172–176.

Appendix B

Supplementary Information: Effects of Oxygen Concentration on Radiation-Aided and Selfsustained Smoldering Combustion of Radiata Pine

This page is intentionally left blank.

Supplementary Information:

Effects of oxygen concentration on radiation-aided and self-sustained smouldering combustion of radiata pine

H. Wang, P. J. van Eyk, P. R. Medwell, C. H. Birzer, Z. F. Tian, M. Possell

---

A. Scrubber

The product gas stream was directly sampled from the reactor. The product gas stream contains a large amount of heavy hydrocarbons, which must be scrubbed to prevent erroneous gas concentration measurements and to prevent damage to the gas analyser. A wet scrubber was implemented to remove the heavy hydrocarbons, as shown in Figure 1. The scrubber consists of a series of test tubes, containing either ethanol (labelled A-C) or activated carbon (labelled E & F), and submerged in a cold bath. The gases from the reactor pass through ethanol, which is sufficiently stable and an efficient hydrocarbon solvent [1]. Testing confirmed that the test gases were not dissolved in the ethanol, consistent with previous studies [2, 3]. Whilst the ethanol performed well at scrubbing the heavy hydrocarbons, a small amount of ethanol vapour was released into the gas stream, which was then captured by activated carbon [4, 5].

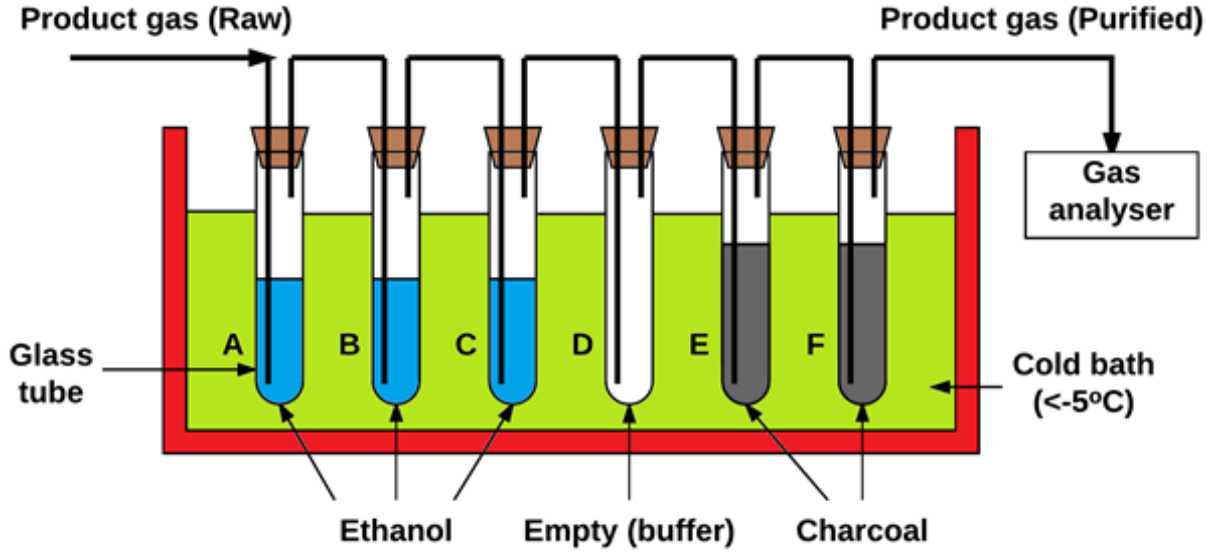

Figure A1. Schematic diagram of gas washing system used to remove heavy hydrocarbons from the product gas.

B. Temperature increase rate profiles

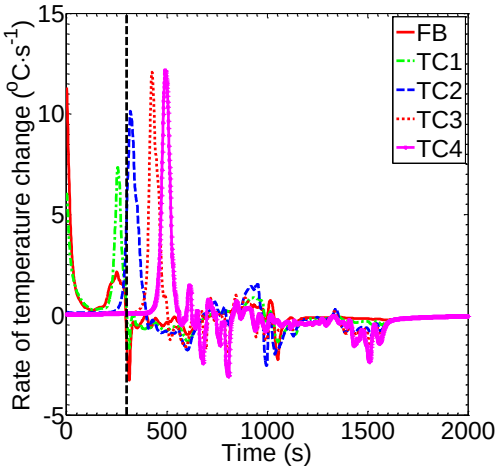

Figure B1. Temporal and spatial rate of temperature change for self-sustained smouldering combustion (Case 3: oxygen concentration: 21 %, heat flux level: 40 kW·m^{-2}, heating time: 300 s, flow velocity: 15.0 mm·s^{-1}, LO*: Lamp off, FB: Freeboard, TC: thermocouple). The vertical dashed line delineates the four stages of the reaction zone through the fuel bed: (I) heating stage, (II) devolatilisation, (III) char combustion, and (IV) cool down.

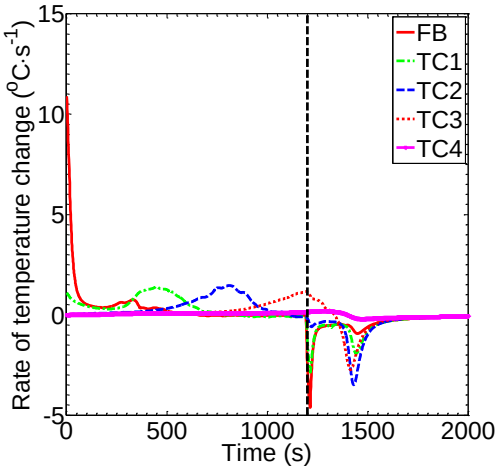

Figure B2. Temporal and spatial rate of temperature change for aided smouldering combustion in biomass fuel (Case 28: Oxygen concentration: 7.5 %, Heat flux level: 40 kW·m^{-2}, heating time: 1200 s, flow velocity: 15.0 mm·s^{-1}, LO*: Lamp off). The blue, vertical dashed line delineates two stages of the reaction zone through the fuel bed: (I) heating stage, (II) devolatilisation, and (IV) cool down.

C. Experimental runs

Table C1. Summary of experimental runs

Case	*Oxygen conc. (%)*	*Heating time (s)*	*Results*
1	21	200	*NI
2	21	250	*AS
3	21	300	*SS
4	21	350	*SS
5	21	400	*SS
6	15	250	*AS
7	15	300	*SS
8	15	350	*SS
9	15	400	*SS
10	15	500	*SS
11	15	600	*SS
12	15	900	*SS
13	13.5	400	*AS
14	13.5	450	*SS
15	12.5	300	*AS
16	12.5	350	*AS
17	12.5	400	*AS
18	12.5	450	*SS
19	10	350	*AS
20	10	400	*AS
21	10	500	*AS
22	10	550	*AS
23	10	600	*SS
24	7.5	600	*AS
25	7.5	700	*AS
26	7.5	800	*AS
27	7.5	900	*AS
28	7.5	1200	*AS
29	5	300	*NI
30	5	600	*NI
31	5	800	*NI
32	5	1000	*NI
33	5	1200	*NI

SS: Self-sustained smouldering; *AS: Aided smouldering combustion; *NI: No ignition.

References

1. Perez, L. B.; Cortez, L., Potential for the use of pyrolytic tar from bagasse in industry. *Biomass Bioenergy* **1997,** 12, (5), 363-366.
2. Tokunaga, J., Solubilities of oxygen, nitrogen, and carbon dioxide in aqueous alcohol solutions. *J. Chem. Eng. Data* **1975,** 20, (1), 41-46.
3. Abraham, M. H.; Whiting, G. S.; Shuely, W. J.; Doherty, R. M., The solubility of gases and vapours in ethanol-the connection between gaseous solubility and water-solvent partition. *Can. J. Chem* **1998,** 76, (6), 703-709.
4. Bansal, R. C.; Goyal, M., *Activated carbon adsorption*. CRC press: 2005.
5. El-Sharkawy, I.; Saha, B.; Koyama, S.; He, J.; Ng, K.; Yap, C., Experimental investigation on activated carbon–ethanol pair for solar powered adsorption cooling applications. *Int. J. Refrig* **2008,** 31, (8), 1407-1413.

Appendix C

Supplementary Information: Effects of *Eucalyptus* species and plant parts on smouldering combustion

This page is intentionally left blank.

Supplementary Information:

Effects of Eucalyptus species and plant parts on smouldering combustion

H. Wang, P. J. van Eyk, P. R. Medwell, C. H. Birzer, Z. F. Tian, M. Possell

---

A. Proximate analysis

The proximate analysis of all the fuel samples was determined according to ASTM-E1131 using a thermogravimetric analyser (TGA/DSC 2, Mettler Toledo, Greifensee, Switzerland): ~5 mg sample, heating rate of 10 $K \cdot min^{-1}$ for determination of moisture content, and 2 $K \cdot min^{-1}$ for determination of volatile content. One of the main purposes of the thermogravimetric analysis is to investigate the pyrolysis rate under different temperatures. Hence, the heating rate was set to 2 $K \cdot min^{-1}$ in order to provide accurate and detailed results of the pyrolysis rate at various temperatures. Fuel samples were placed in 30 μL Alumina crucibles (Mettler Toledo, Greifensee, Switzerland) and nitrogen was switched to air at 650 ^{o}C for determination of ash content.

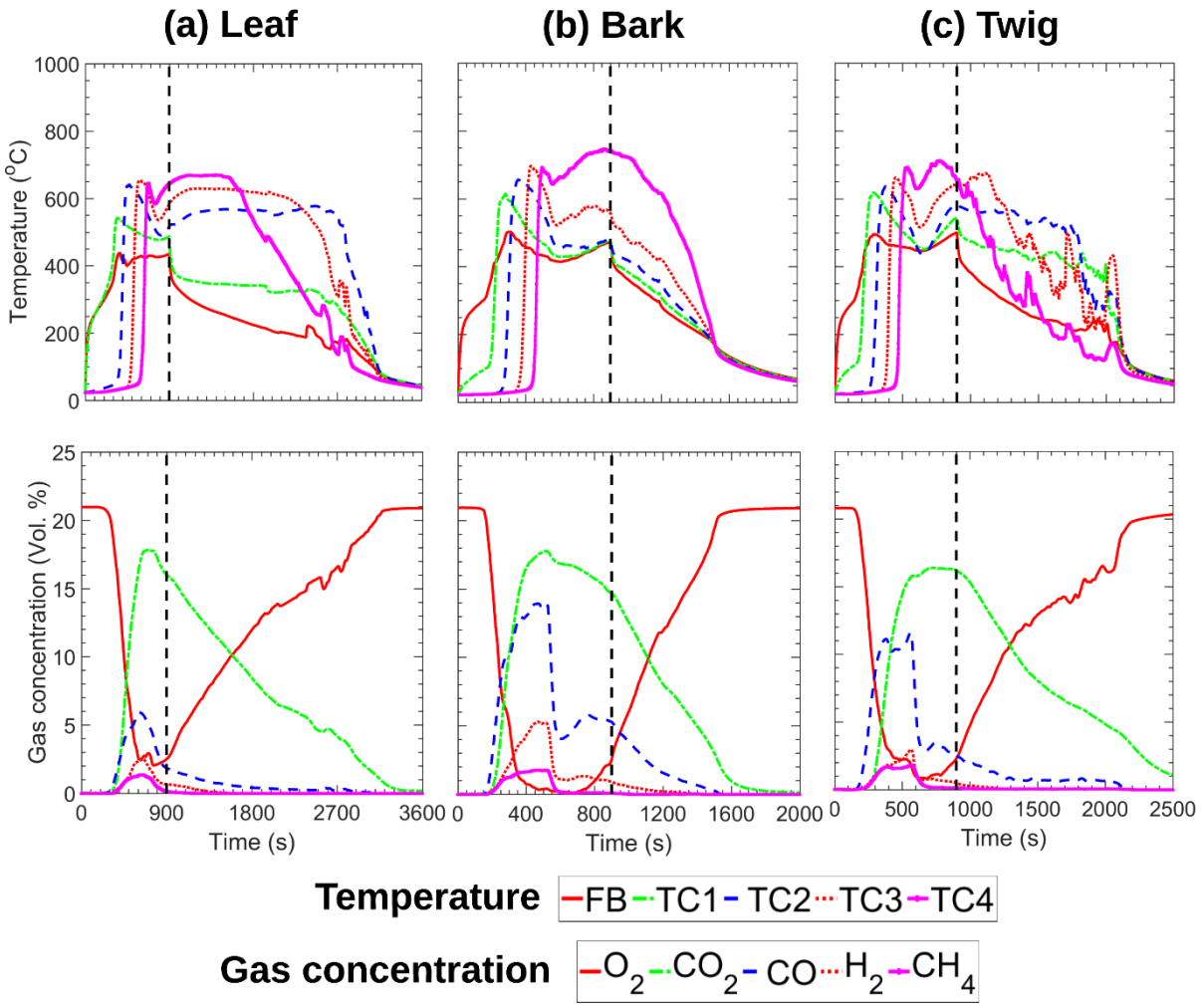

Figure A1. Temporal and spatial temperature profiles (Top) and temporal gas concentration profiles (Bottom) for the combustion of the leaf, bark and twig of *E.* fasciculosa. Heat flux level: 40 kW·m^{-2}, heating time: 900 s (lamp off indicated by vertical dashed line), flow velocity: 15.0 mm·s^{-1}, FB: freeboard, TC: thermocouple, vertical dash line: lamp off.

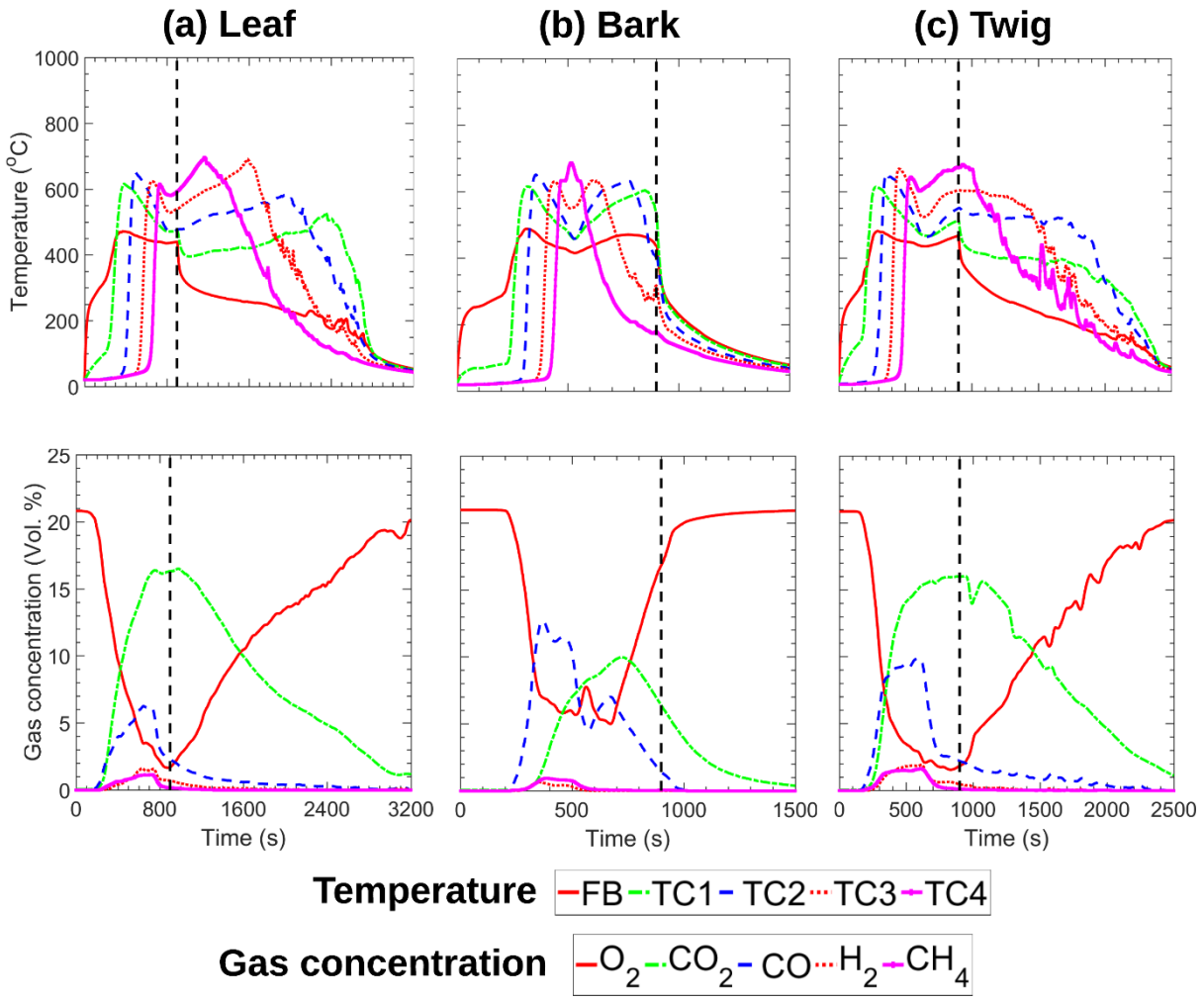

Figure A2. Temporal and spatial temperature profiles (Top) and temporal gas concentration profiles (Bottom) for the combustion of the leaf, bark and twig of *E.* baxteri. Heat flux level: 40 kW·m^{-2}, heating time: 900 s (lamp off indicated by vertical dashed line), flow velocity: 15.0 mm·s^{-1}, FB: freeboard, TC: thermocouple, vertical dash line: lamp off.

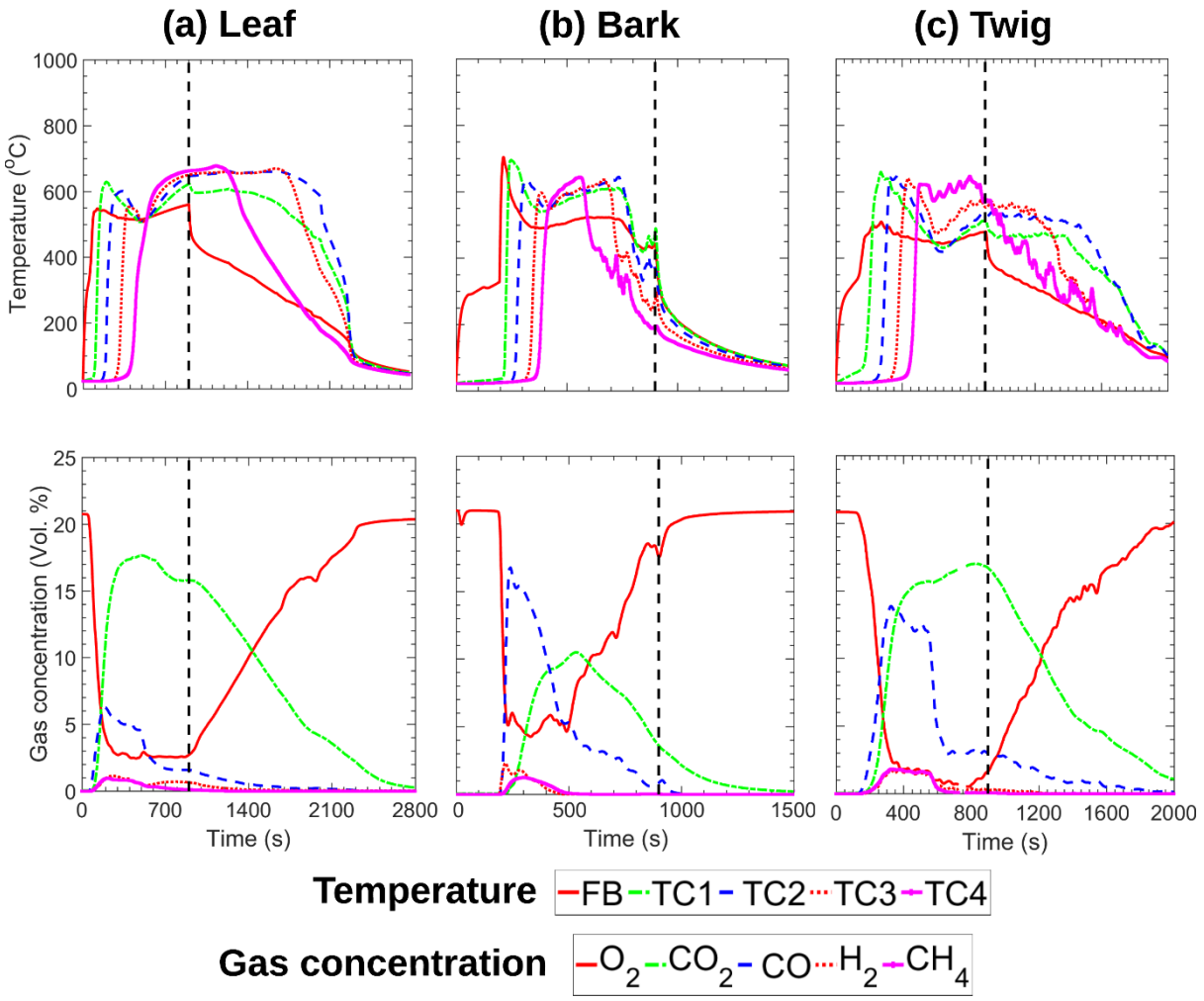

Figure A3. Temporal and spatial temperature profiles (Top) and temporal gas concentration profiles (Bottom) for the combustion of the leaf, bark and twig of *E.* obliqua. Heat flux level: 40 kW·m^{-2}, heating time: 900 s (lamp off indicated by vertical dashed line), flow velocity: 15.0 mm·s^{-1}, FB: freeboard, TC: thermocouple, vertical dash line: lamp off.

Table A1. Proximate and Ultimate Analyses of fuel samples

Fuel sample (Fuel species/ Fuel type)	Proximate analysis [wt %, dry basis]			Ultimate analysis [wt %,dry ash-free basis]			
	VM	FC	Ash	C	H	N	O (by diff.)
E. camaldulensis bark	73.00 ± 0.93	24.39 ± 0.78	2.61 ± 0.26	43.56 ± 0.22	6.00 ± 0.14	0.13 ± 0.01	50.31
E. camaldulensis leaf	77.20 ± 0.31	17.99 ± 0.06	4.81 ± 0.34	49.25 ± 0.10	7.24 ± 0.09	1.18 ± 0.02	42.33
E. camaldulensis twig	69.84 ± 0.32	25.32 ± 0.15	4.84 ± 0.19	41.14 ± 0.13	5.66 ± 0.08	0.35 ± 0.01	52.85
E. fasciculosa bark	76.00 ± 0.36	19.85 ± 0.11	4.15 ± 0.26	43.60 ± 0.18	6.45 ± 0.10	0.24 ± 0	49.71
E. fasciculosa leaf	71.97 ± 0.03	24.37 ± 0.26	3.66 ± 0.25	49.99 ± 0.38	7.14 ± 0.02	0.94 ± 0.01	41.93
E. fasciculosa twig	70.61 ± 0.41	24.86 ± 0.22	4.53 ± 0.45	44.15 ± 0.36	6.31 ± 0.02	0.42 ± 0.02	49.12
E. baxteri bark	81.17 ± 0.12	18.34 ± 0.38	0.49 ± 0.27	47.03 ± 0.53	6.50 ± 0.06	0.50 ± 0.02	45.97
E. baxteri leaf	76.80 ± 0.31	19.38 ± 0.08	3.82 ± 0.32	50.03 ± 0.54	7.35 ± 0.11	0.90 ± 0.01	41.72
E. baxteri twig	75.70 ± 0.68	19.98 ± 0.46	4.32 ± 0.30	47.25 ± 0.49	6.81 ± 0.18	0.44 ± 0.02	45.50
E. obliqua bark	73.86 ± 0.32	24.98 ± 0.25	1.16 ± 0.08	46.43 ± 0.48	6.28 ± 0.14	0.58 ± 0.04	46.71
E. obliqua leaf	76.74 ± 0.22	20.26 ± 0.09	3.00 ± 0.18	48.94 ± 0.30	6.82 ± 0.05	1.65 ± 0.02	42.59
E. obliqua twig	70.58 ± 0.25	25.84 ± 0.20	3.58 ± 0.14	45.94 ± 0.08	6.47 ± 0.07	0.40 ± 0.01	47.19